博士論文

Evaluation and Simulation of Passive Energy Efficiency Technology with an Experimental House in Hangzhou Rural Area, China

中国杭州市農村部における実験住宅を用いたパッシブ省エネルギー技術の評価とシミュレーションに関する研究

北九州市立大学国際環境工学研究科

2017 年 9 月
武 茜
Qian WU

Preface

This study focused on the energy situation and environment problem of China's rural residence. Hangzhou rural area was taken as a case. Through survey, experiment and further simulation, a passive design idea for rural house was finally realized and proved on an experimental building. In future, such a building is expected to be as a low-carbon and low-cost example for demonstration in Hangzhou rural area. Among the study, the experiment and simulation work were performed in Zhejiang University of Science and technology during 2015~2016.

ACKOWLEDGEMENT

First of all, I would like to express my gratitude to all those who helped me during the writing of this thesis. I gratefully acknowledge the help of my supervisor, Professor Weijun Gao, who has not only offered me valuable suggestions in the academic studies but also provided me with unselfish help and concern. I am deeply grateful of his help in the completion of this thesis.

Secondly, I would thanks to my colleagues in University of Kitakyushu and in University of Science and Technology for their direct and indirect help to me.

Also, I thanks to my friends who have put considerable time and effort into their comments on the draft.

Finally, I am indebted to my parents for their continuous support and encouragement. In addition, I express my deepest thanks to my husband and my children, for their understanding, encouragement and company.

Special thanks to my friend Meiyan Wang, who shared her part of research results with selflessness; special thanks to Zhengguang Li and Huacun Liu, who provided great support to me on experiment work; special thanks to Weiwei Fan and Bing Zhang, for their powerful support on simulation work; special thanks to Dr. Honghu Zhang, Dr. Jian Yang and Dr. Guoqing He, for their selfless guidance.

Content

Chapter Five: Field-measurement on thermal performance of experimental house in winter time

Chapter Six：Field-measurement on thermal performance of experimental house in summer time

Chapter Seven: Improvement on thermal performance of Trombe wall by simulation

Chapter One: Previous study and the purpose of the study

1-1 Introduction

As a developing country, China has experienced rapid economic growth in recent years and at the same time has great demand for energy. It was pointed in *Trends in Global CO_2 Emissions: 2015 Report* [1] that the largest CO_2 emitting country by far is China, whose share of 30% in 2014 was twice as large as the second-largest, the United States, at 15%. Third was the European Union, at almost 10%. This high ranking is mainly due to the size of its population and economy, but also because of the high share of coal in its energy mix, as it has much more coal reserves than oil and gas. In recent years, with the advancement of urbanization and the improvement of people's living standards, building energy consumption account for a significant portion in total energy consumption. In the Reference case[2], China's residential energy use per capita grows by 2.3% per year from 2012 to 2040，China will becomes the world's largest residential energy consumer.

China is a traditional agricultural country, and the proportion of rural population take up to 45% of all[3]. By 2020, it was estimated that the rural building area will be responsible for 62%[4] of the total gross floor area in China. Large rural population and increasing building areas lead to the remarkable energy consumption in rural houses. With higher income, more and more rural households are becoming interested in using commercial energy resource (coal, liquefied petroleum gas and electricity) instead of non-commercial one[5], but the energy efficiency is very low and the indoor thermal environment is still poor. At the same time, a lot of pollutants and greenhouse gas were released when using unclean energy, resulting in rural ecological environment damaged seriously.

In this decade, China's government has put forward the future development target, namely "No-coal Village" in north rural area and "Ecological Village" in south rural area[6]. Passive energy-efficient technology, is an appropriate and effective way to improve the energy situation and solve the environmental pollution in China's rural areas. Buildings that use passive energy efficient technologies can significantly reduce the energy consumption of the building while minimizing the dependence on active mechanical heating and cooling systems with significantly enhancing the comfort of the indoor environment. In 2008, China's government started to carry out the study on passive energy efficient technologies based on the "Passive House" standard of Germany, and to explore the feasibility of developing the demonstration projects in China. By the end of December in 2015, there has been more than 50 passive house projects that were built or planned[7], most of which were located in North China but less in the South.

Hangzhou city, located in hot/summer & cold/winter zone, was taken as a case study in this research, where the rural residences have higher electricity energy consumption by using more air-conditioners for heating and cooling in recent years. Conforming to the construction target of "Ecological Village" raised by China's government, and combining with the characteristics of Hangzhou's rural residence, an experimental building integrated with passive energy-efficient technologies was designed and constructed. Through the methods of experiment and simulation, the effectiveness of passive energy efficient technologies was evaluated under real climate

conditions of Hangzhou; otherwise, the thermal performance of passive energy technologies were investigated and improved. By this case study, the research results about passive energy-efficiency technology with this designed building can be applied and promoted in rural areas of Hangzhou, also can be used for reference by architects and engineers.

1-2 Research background and significance

1-2-1 Energy and environment situation in China

China has abundant energy resource, among which the coal reserves are rich accounting for as much as 13.3% of the world's total reserves. As can be seen in Fig.1-1, the component of China's energy consumption was dominated by coal in 2012, accounting for 67% of the total energy consumption, followed by oil and natural gas[8].

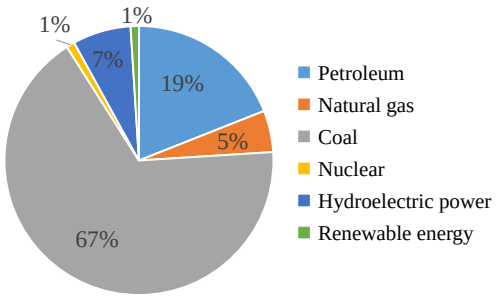

Fig.1-1 Portion of energy consumption in China, 2012
(Data source: Sustainability Review 2013)

China's CO_2 emissions have grown extraordinarily rapidly since it started on its fast industrialization path and after it joined the World Trade Organization (WTO) in 2003 (see Fig.1-2). As illustrated in the reference [1], in 1990, China's CO_2 emissions were exactly half of those of the United States that, at the time, was the largest emitter of all countries in the world. Fourteen years later, in 2004, it surpassed the United States as the largest emitting country, and after yet another 10 years, in 2013, China's emissions had increased by 80% and were twice the amount of those of the United States, whose emissions had decreased by 10% since 2004[1].

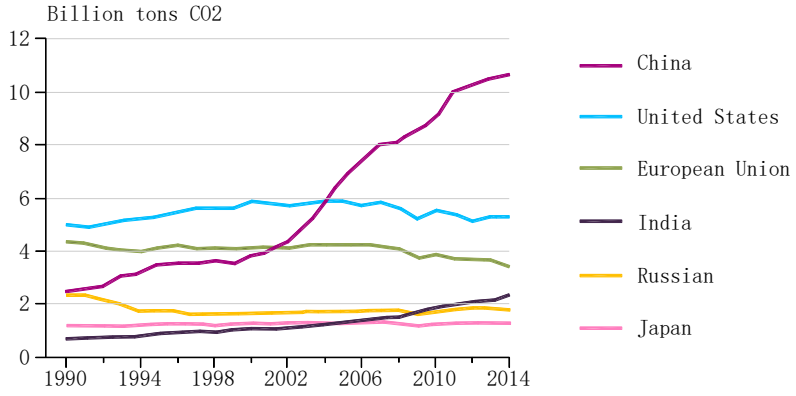

Fig.1-2 CO_2 emissions from fossil-fuel use and cement production in the main countries
(Data source: Trends in Global CO_2 Emissions, 2015 Report)

The rapid growth in China's residential sector energy consumption is mainly the result of strong economic growth and urbanization, as lifestyle and energy use patterns vary widely between urban and rural populations[9]. The advent of China's economic reform in the late 1970s has led to "the largest migration in human history", with more than 160 million people moving from farming communities to cities to seek employment in growing industries. According to the United Nations, nearly three-fourths of the Chinese population will live in urban areas by 2040[10]. China's demand for energy services increases as per capita income and quality of life improve, accompanied by an increase in urban population and increased access to nontraditional fuels in rural areas.

From 1998 to 2012, energy consumption in China's buildings increased by about 7.7% per year[2] (see Fig.1-), much faster than China's average annual population increase, which was less than 1% per year. Growing incomes and modernization contributed to the significant increase in consumption of electricity and other forms of energy. In the Reference case[2], China's residential energy use per capita grows by 2.3% per year from 2012 to 2040 (see Fig.1-)，China becomes the largest residential energy consumer in the world.

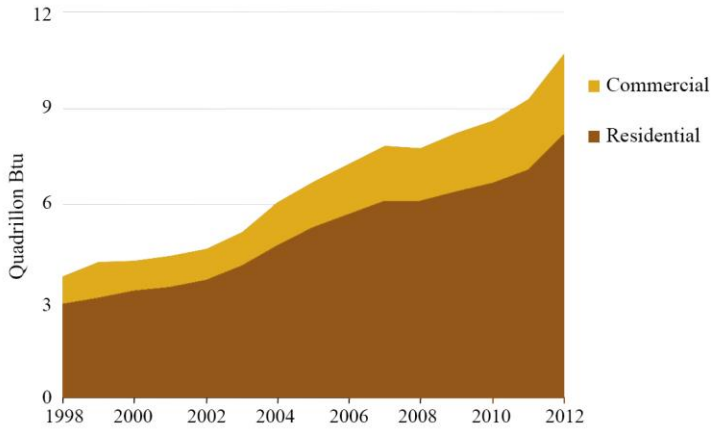

Fig.1-3. Buildings energy consumption in China, 1998–2012
(Data source: International Energy Outlook 2016)

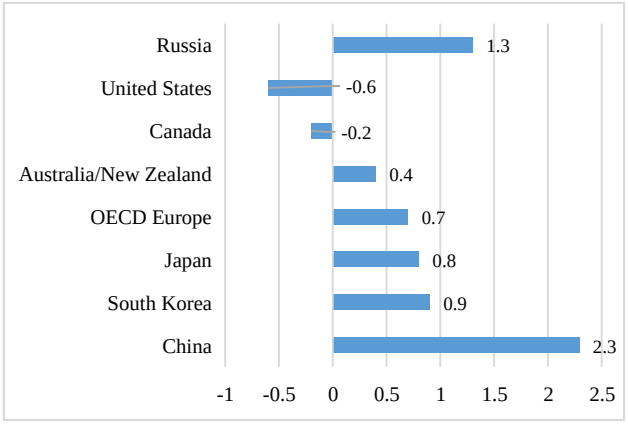

Fig.1-4. Average annual change in residential sector energy consumption per capita (%), 2012–2040. (Data source: International Energy Outlook 2016)

Thus, Large amounts of new buildings and energy used in construction procedure result in continuous growth of energy consumption and CO_2 emissions. According to the research conducted by the Building Energy Conservation Research Center of Tsinghua University[11], as is shown in Fig.1-5, from 2000 to 2010, the total energy consumption of buildings in China had increased from 2.89 × 10^2 million tce (tons of standard coal equivalent) to 6.77 × 10^2 million tce which was more than 2 times, and the building area had expanded from 277 × 10^2 million m^2 to 453 × 10^2 million m^2. And now, the gross building area reached 561 × 10^2 million m^2 in 2014, when the total energy consumption in buildings attained 8.19 × 10^2 million tce[11]. A large number of new buildings was completed after the year of 2000, accounting for nearly 40% of buildings that have been built.

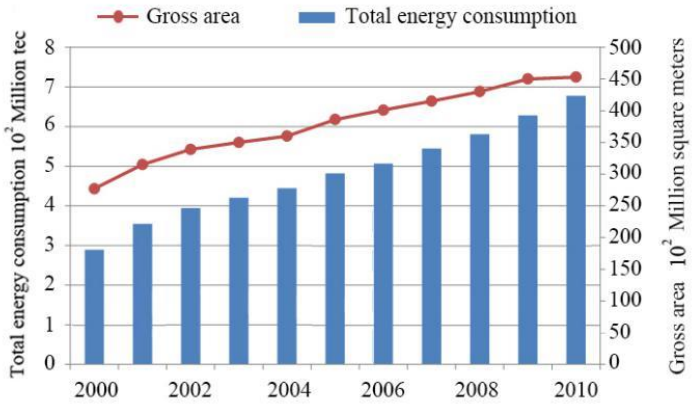

Fig.1-5 Growth of total energy consumption and gross building area of China, 2000-2010
(Data source: 2011 Annual Report on China Building Energy Efficiency)

1-2-2 Energy consumption in rural areas of China

China is a traditional agricultural country, and the proportion of rural population take up to 45% of all [3]. It has a significant difference in architectural form between rural residence and urban housing due to the characteristics on historical tradition, mode of production, lifestyle and natural environment in rural area, where the single house is the main style. Based on the report[12], the area of rural residences in 2010 reached 230 × 10^2 million m^2, about 50% of national total area in this year. By 2020, it was estimated that the rural building area will reach 425 × 10^2 million m^2, responsible for 62% of the total gross floor area in China. Due to the large rural population and increasing building areas, energy consumption in rural houses has become an important part in total building energy usage of China.

In this century, with higher incomes, more and more households are becoming interested in using quality energy sources, namely commercial energy instead of non-commercial one[5], seen in Fig.1-. Fig.1-7 shows the change of energy consumption per unit of building area from 2000 to 2010[5]: From the figure, the energy consumption of urban residence of north China decreased from 23.1 kgce/m^2 to 16.6 kgce/m^2 , which shows a great progress made on building energy-saving measures. With the improvement of rural living standard and the guidance of the new rural

construction policy, the energy consumption of rural buildings increased from 5.0 kgce/m² to 7.5 kgce/m², with an increase of 50%. What's more, the energy saving of rural buildings is becoming more and more important and caught more and more attention from all the sectors in the society.

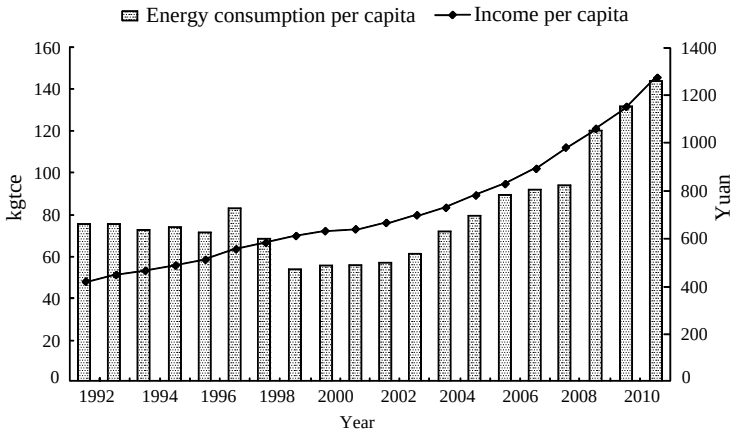

Fig.1-6. Rural residential commercial energy consumption per capita and rural net income per capita over the period 1991 - 2010[5].

(Data source: Analysis of rural residential commercial energy consumption in China)

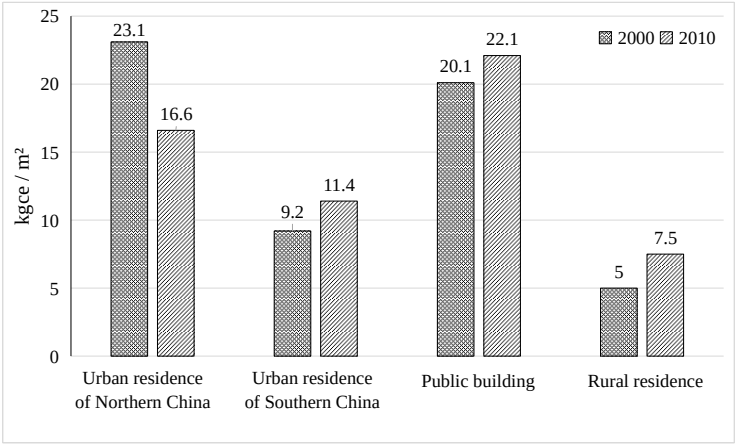

Fig.1-7 Variation of energy consumption per unit building area of China, 2000 & 2010[5].

(Data source: Analysis of rural residential commercial energy consumption in China)

1-2-2-1 Energy situation

The statistics by the team[6] showed that annul energy consumption in rural areas of China was 327 million tce in 2014, mainly including four aspects: heating, cooking, air conditioning, household electricity (lighting and appliances). The energy sources consist of commercial energy (coal, liquid petroleum gas, electricity) and non-commercial energy (wood and straw), and the quantity[6] of which are shown in Fig.1-8. It can be found that the energy consumption by rural residence was dominated by coal, and the total quantity of commercial energy (coal, liquid gas, electricity) was about 225 million tce, accounting for 68.8% of all the energy consumption in rural buildings, and 27% of all the building commercial energy in China.

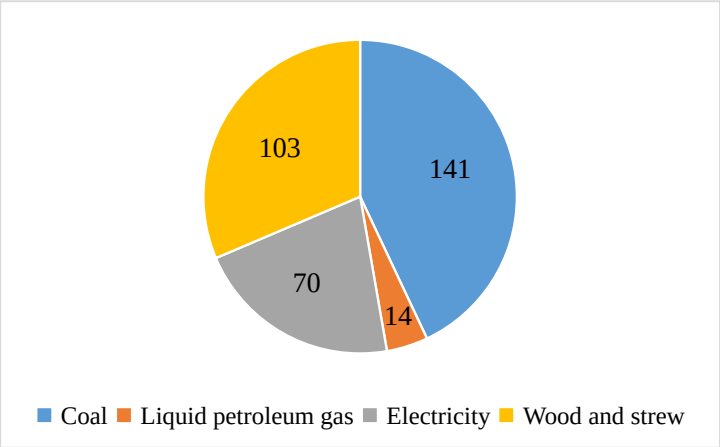

Fig.1-8 Energy consumption in rural area of China in 2014 (million tce).
(Data source: 2016 Annual Report on China Building Energy Efficiency.)

(1) Living energy consumption per household in China's rural area.

It could be found from surveyed results[6] that the annual energy consumption per household in rural area of North China was high due to the higher heating demand in winter. Among the provinces shown in Fig.1-9 (a), Qinghai, Heilongjiang, Ningxia and Neimenggu, being in sever cold zone, have more thermal load with about 4 tce per household a year than other provinces. Otherwise, more commercial energy, such as coal, liquid gas and electricity were consumed by the provinces of Gansu, Neimenggu, Shanxi, Xinjiang, Beijing, Hebei, and Tianjin.

In the provinces of South China (see Fig.1-9 (b)), more commercial energy were consumed by rural area of Hunan, Jiangsu, Zhejiang and Guizhou, with ratio of over 70%[6]. Compared with North China, non-commercial energy accounted for higher proportion in South China, where the rural residents commonly burn the strew for heating or cooking directly with lower efficiency, resulting in wasting of resources and environment pollution.

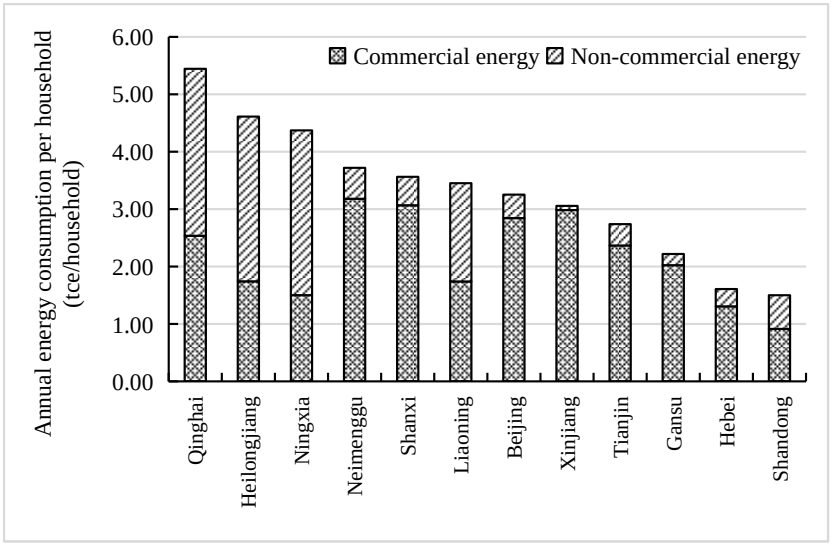

(a)

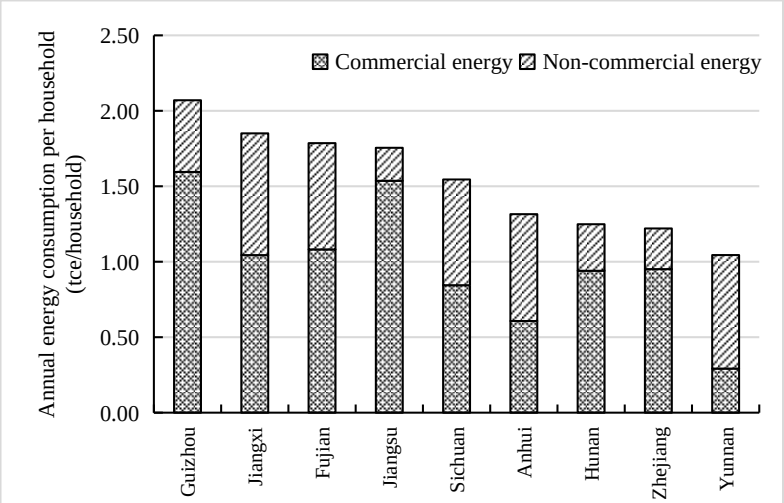

(b)

Fig.1-9 Annual energy consumption per household in rural area of China, 2014.

(a) North China; (b) South China

(Data source: 2016 Annual Report on China Building Energy Efficiency.)

Taking Zhejing province as example. In 2014, the total annual consumption of energy consumption, converted to standard coal for 7.84 million tce, among which, the commercial energy occupied 78%, and electricity energy accounted for 60% in the total commercial energy[6].

(2) Energy consumption for heating and cooling in rural areas of South China.

Fig.1-10 shows the heating energy consumption in the rural areas of South China in 2014. It was reported in the reference[6] that the amount of coal for heating in South China accounted for about 26.4% in total energy consumption, much lower than that in North China with 53.6%. In addition, when it comes to the heating consumption per floor area, the quantity was estimated to close or over 20 kgce/m^2·a in most of provinces of North China[6]. Although using distributed heating in rural house, the indoor temperature is still lower than urban residence. The main reasons are poor insulation of envelope and unreasonable single building design, causing excessive heat loss. For Jiangsu, Jiangxi and Zhejiang province, more rural households usually adopt electrical appliances for heating in winter time, thus the annual heating consumption per area by using coal were relatively lower than other provinces.

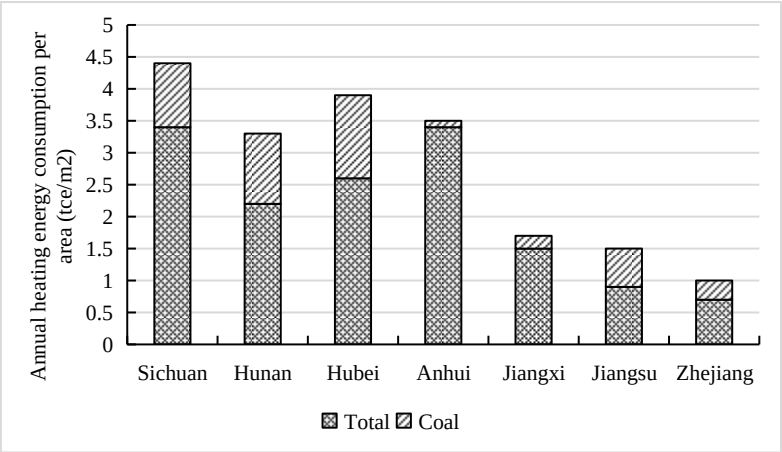

Fig.1-10 Annual heating energy consumption per building area in rural area of South China, 2014 (Data source: 2016 Annual Report on China Building Energy Efficiency.)

Fig.1-11 shows the cooling energy consumption in the rural area of South China in 2014. It can be seen that there was obvious difference in cooling energy consumption by air conditioners among the provinces due to the variable economical and climate conditions. The total electricity energy consumed for cooling in rural area of South China was about 30 billion kWh, accounting for 25% of all energy consumption[6].

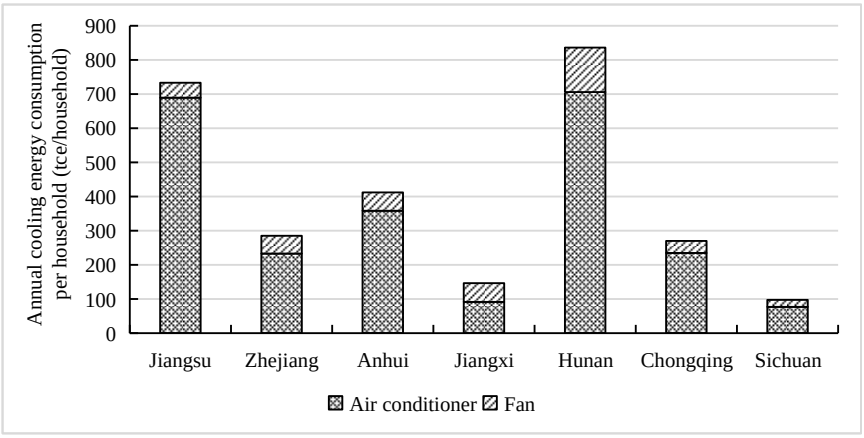

Fig.1-11 Annual cooling energy consumption per household in rural area of South China, 2014 (Data source: 2016 Annual Report on China Building Energy Efficiency.)

1-2-2-2 Environmental problems

According to the above energy situation in China's rural, the main energy and environmental problems are concluded in the following[6]:

(1) Significant total energy consumption in rural residences, low energy efficiency and poor indoor thermal environment.

With the rural economical development, the commercial energy consumption indicated an increasing trend, while the indoor thermal environment in rural houses were still poor. In North China, indoor temperature in winter only reached 5~10℃; in South China, it is universal hot in summer and cold in winter. Poor thermal performance of building construction and low energy

efficiency for cooking and heating are the main reasons

(2) Serious indoor air pollution by burning solid fuels.

Solid fuels such as coal and biologic materials were burnt incompletely when cooking and heating in rural areas, which would produce a lot of contaminants being harmful to people's health[错误!未定义书签。]. According to many measurement results, the indoor contaminant concentration of rural residences, such as CO、SO_2 and respirable particulate matter (PM2.5) are normally high. Reported by WHO (World Health Organization), there were 420 thousand deaths in rural areas caused by solid fuels burning, 40% more than the number of deaths caused by urban pollution. Thus, unclear energy usage has become the sixth largest health killer in China.

(3) A large number of emissions of greenhouse gases and pollutants, affecting the atmospheric environment.

Estimated by the reference[6], yearly emissions of CO_2 produce by living energy consumption could reach 800 million tons, accounting for 10% of total CO_2 emissions in China. In addition to the decreased indoor air quality, the large number of pollutants produced by burning coal would also influence the ambient environment. As the demand for comfortable indoor thermal environment increasing, the biomass is replaced by commercial energy gradually, the amount of emissions will grow further.

(4) A large number of solid waste affecting biological environment and water.

In addition to the large amount of harmful gases emitted into the air, the widespread use of small coal-fired furnaces can also produce pollution of ash and the pollution of coal. Especially the slag produced by small distributed coal stoves in rural areas were scattered everywhere, difficult to be cleared and reused, resulting in the rural living environment, water and farmland damaged greatly.

Thus, the issues about ecological environment in China's rural area caused by living energy consumption should be paid great attentions. It is quite necessary to carry out the studies on the appropriate and low-cost energy efficient technologies in rural residences, as well as the renewable energy usage, thereby reducing the fossil fuels consumption, improving the indoor and outdoor environment, and optimizing energy construction.

1-2-3 Advantage of passive energy efficiency in buildings

1-2-3-1 Characteristics of passive energy efficiency

Passive energy efficiency refers to the building itself collecting and storing energy by the natural ways, which forms a self-circulation system between the building and its surroundings so that it does not need mechanical equipment to provide support, instead it makes full use of natural resources to achieve comfortable indoor environment thereby saving traditional energy sources[13]. Passive energy efficiency and active energy efficiency are two opposite concepts. The active energy efficiency refers to the creation of a comfortable building environment through mechanical energy system, whereas passive energy efficiency can not only save resources, but reduce

construction funds. As low cost and high efficiency, it is necessary to promote the advantage idea of passive energy efficiency in building design.

Passive buildings originated from the rise of solar heating buildings in the late 1970s. With the developing of building industry, the significance of passive buildings was expanded. Now, in developed countries, the meaning of passive building is to achieve the winter heating and summer cooling without relying on external energy, such as “Passive House” put forward by Germany.

“Passive House” is a building, for which thermal comfort (ISO 7730) can be achieved solely by post-heating or post-cooling of the fresh air mass, which is required to full-fill sufficient indoor air quality conditions (DIN 1946) - without a need for recirculated air. The “Passive House” is not an energy performance standard, while is a concept to achieve highest thermal comfort conditions on low total costs. A passive house is a building in which a comfortable interior climate can be maintained without active cooling and heating systems.

The standard of “Passive House” was officially formulated in 1988 by Professors Bo Adamson of Lund University in Sweden, and Wolfgang Feist, German Institute of Construction and Environment. The first passive-house residences were built in Darmstadt, Germany in 1991 (see Fig.1-12). In this building, the total energy for heating was below 15 kWh/m^2 per year, and for cooling below 15 kWh/m^2 per year. Otherwise, there were less thermal energy to heat water and less electricity for air conditioning in a year. “Passive House” not only has ultra low energy, but also has High quality of indoor air environment. As shown in Fig.1-13, the CO_2 concentration monitored in a passive house was much lower than in a common building, due to the none-usage of fossil fuel[14]. It can be seen that passive energy efficient technology has great advantage in building energy-saving and creating excellent indoor air quality.

Fig.1-12 The first passive house in Darmstadt, Germany in 1991
（Data source: http://www.passiv.de/ ;https://en.wikipedia.org/wiki/Passive_house）

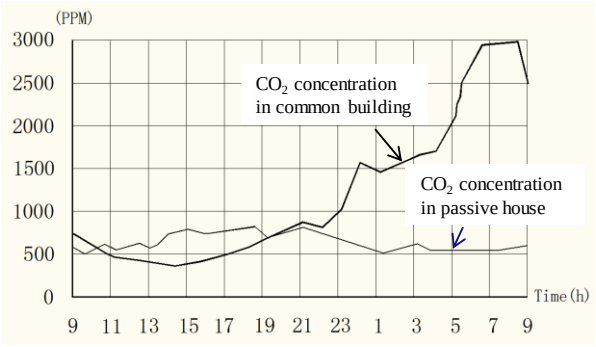

Fig. 1-13 CO_2 concentration (PPM) of indoor air[14].

By 2000, there were about 800 passive houses built in Germany, accounting for 30% of total construction of the country. In these decades, "Passive House" has been very popular in the world. In Europe, the number of passive houses is increasing at an annual rate of 8%. According to the European regulation, there has been 27 European Union countries to carry out Passive House standard in 2020[15]. In China, subject to economic development and technological level, the construction and energy efficiency standards were lower than developed countries (see Table.1-1). The introduction of passive energy efficient concept to China greatly enhanced the development on building energy conversation and environment protection.

Table.1-1 Comparison of U-values for envelope in different countries.

Country	U-Value ($W/m^2 \cdot k$)		
	Wall	Roof	Window
China-HSCW (JGJ 134-2010)	0.8~1.5	0.5~1.0	2.3~4.7
China-Zhejiang (DB 33/1015-2015)	0.8~1.5	0.5~0.8	1.9~2.8
America (IECC2015)	0.34~0.77	0.17	1.99
Germany (ENEV2001)	0.35	0.25	1.5
Germany (ENEV2009)	0.28	0.2	1.3
Passive House	0.15	0.15	1.3

(Data source: JGJ 134-2010, DB 33/1015-2015, BECS2013, IECC2015, ENEV2001, ENEV2009)

In 2008, China's government started to carry out the study on passive energy efficient technologies based on the "Passive House" standard of Germany, and to explore the feasibility of developing the demonstration projects in China. In 2010, China's first passive house—Hamburg House was finished in Shanghai World Expo (see Fig.1-14), which had been certificated by Passive House Institute (PHI) and as a gift to Shanghai city by Hamburg of Germany[16]. Three years later, a China-Germany cooperation project of passive house—"Zai Shui Yi Fang" was

completed in Qinhuangdao of Hebei province, as the first demonstration residence, obtaining the China - Germany Passive Low Energy Building Energy Identification. According to the statistic[7], there had been more than 50 passive house projects that were built or planned by the end of December, 2015. In Zhejiang province of China, the first passive house - Brooker Project (see Fig.1-15) designed by Landsea Group, German Passive House Institute and DENA (Deutsche Energy Agency) was finished in Huzhou city, and got certification of PHI.

Fig.1-14 Hamburg House in Shanghai
(Data source: Spengler · Wiescholek)

Fig.1-15 Brooker Project
(Data source: by the author)

Passive building energy-efficient technology is an effective way to improve the energy situation and solve the environmental pollution in China's rural areas. Combining with the exploration and practice in the process of new countryside construction, China's government put forward the future development target, namely "No-coal Village" in north rural area and "Ecological Village" in south rural area.

There are three characteristics for "No-coal Village"[6]:

(1) No coal. Most of energy demand in heating, cooking and hot water are from biomass fuel and renewable energy such as solar energy, replacing coal resources in rural residences. Electricity, liquefied petroleum gas and other clean energy are as supplement when renewable energy are insufficient, at the same time meeting the living demand for lighting, home appliances and others。

(2) Energy saving. The construction envelope has good thermal insulation performance for reducing energy demand greatly.

(3) Liveable environment. To create the comfortable environment in rural areas and avoid indoor and outdoor air pollution and environmental degradation caused by using non-clean energy.

The construction target of "Ecological Village"[6] is to take passive energy efficient technologies and renewable energy to create comfortable indoor and outdoor thermal environment, non-use of coal and less-consumption of commercial energy, for realizing low-carbon development mode in future.

1-3 Relative concept and field

1-3-1 Passive energy efficient technology

Passive energy conservation refers to the building itself collects and stores energy in a variety of natural ways. It forms a self-circulating system between the building and its surroundings so that it does not need energy-consuming mechanical equipment to provide support, instead it makes full use of natural resources to achieve the effect of saving traditional energy sources[17]. Passive energy-saving and active energy-saving is two relative concepts, among them the active energy-saving refers to the creation of a comfortable building environment through mechanical energy, whereas passive energy conservation can not only save resources, but save construction funds.

Building energy consumption is mainly concentrated on three aspects: the production of building materials, construction and building operation, among which energy consumed in building operation accounts for about 80% to 90% of the total. The building energy consumption is mainly focused on heating, ventilation, air conditioning, lighting and other aspects. The key technical points of passive energy-saving design are as follows:

(1) Thermal Insulation

To maintain a good indoor space environment, the building itself needs to possess excellent thermal insulation properties which reduces the impact of the thermal bridge, thus a closed environment with being interfered from outside will be formed.

(2) Natural Ventilation

A closed building environment is the environment where good ventilation takes away the indoor air and bring fresh air in so as to achieve good air exchange between the indoor and outdoor. While mechanical ventilation is able to achieve the purpose of ventilation, the operation of machinery needs to consume energy. Researches have shown that the spectrum between mechanical ventilation and natural ventilation is different as the former brings different level of comfort compared with that of human body. Natural ventilation is found easier to bring people comfort.

(3) Sun Shading

Too much or too little sunlight will affect the living environment inside the building room. It is cold in areas of high latitudes in winter, where the natural light needs to be accepted as much as possible and heating costs and energy consumption must be reduced. As a matter of fact, it is hot in areas of low latitude climate, the need for proper use of shading facilities is called for, and excessive sunlight should be reduced so a to create a comfortable indoor environment.

(4) Collection of Rainwater

The recycling of rainwater can reduce the use of freshwater resources and save freshwater resources. Reclaimed rainwater can not only be used to irrigate the garden meadows, but it can also be used to irrigate certain areas.

1-3-2 Hangzhou rural area of China

1-3-2-1 Overview of Hangzhou

Hangzhou is the capital city of Zhejiang province in China, which is located on the southeast coastal of china, and at latitude 29°11' ~ 30°34' N and longitude 118°20' ~ 120°37' E. Hangzhou features a perfect blending of hill and water, and lake and town, with rich water resources and a ubiquitous yet harmonious presence of rivers, canals, lakes, sea, creeks. Throughout its territory, hilly or mountains area account for 65.6% and are largely concentrated in the west, middle and south; Plains amount to 26.4%, mainly found in the northeast; surface area of rivers, lakes and reservoirs takes up 8.0%. Hangzhou boasts the largest reservoir in China's southern coast.

Under the jurisdiction of the City of Hangzhou are 9 districts, namely Shangcheng, Xiacheng, Jianggan, Xihu (West Lake), Binjiang, Xianshan, Yuhang, and Fuyang, two county-level cities of Jiande and Lin'an, and two counties of Tonglu, and Chun'an (see Fig.1-16). They are made up of a total of 190 towns (sub-districts), among which are 23 townships, 75 towns, 92 sub-districts, 1072 communities, 34 residential quarters and 2,043 administrative villages. The city covers a total area of 16,596 square kilometers, of which the urban area takes up 4,876 square kilometers.

As a well-developed city, it has experienced rapid economic growth and population explosion in recent decades. Statistics carried by Hangzhou Statistic Bureau indicated that at year-end of 2016, Hangzhou boasts a resident population of 9.19 million. Among the total population, 7 million are urban residents, accounting for 76.2%. It realized Gross Domestic Product (GDP) totaling 1.105 trillion RMB (Yuan), at a growth rate of 9.5%, ranking first among the China's sub-provincial level cities, and 2.8% and 2.0% respectively higher than the national and provincial average[18]. From 1995~2013, per capita income had remarkable increase, shown in Fig.1-17. It can be seen that in every five years, income of rural and urban residents all had a prominent rise of over 50%.

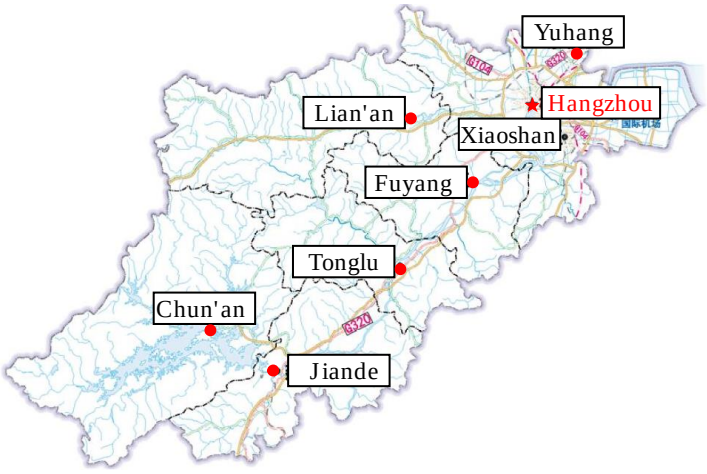

Fig.1-16 Administrative division of Hangzhou city.

(Data source: http://www.hzstats.gov.cn)

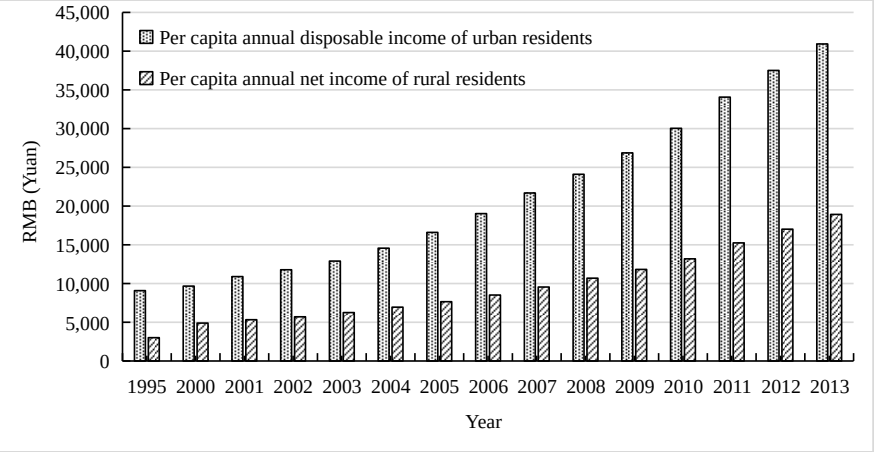

Fig.1-17. Incomes of urban and rural residents in Hangzhou area, 1995~2013

(Data source: http://www.hzstats.gov.cn)

1-3-2-2 Weather conditions and thermal environment

Hangzhou has typical climate feature of hot/summer & cold/winter zone (see Fig.1-1), which is one of five zones divided by *Thermal Design Code for Civil Building* (GB50176-93) of China with the main zoning index of the average temperature in the coldest month (January) and that in the hottest month (July), and the days of the average daily temperature ≤5℃ and ≥25℃ taken as auxiliary zoning indicators. In hot/summer & cold/winter zone, the average temperature in January is 0~10℃and 25~30℃in July, the days of daily temperature ≤5℃is 0-90 and ≤5℃is 40-110. Table.1-2 shows the climate conditions of Hangzhou.

Hangzhou enjoys a subtropical monsoon climate, featuring distinct seasons, ample, sunlight and rainfall, shorter in spring and autumn, and longer in winter and summer. In the summer of Hangzhou, the highest temperature in one day could be over 40℃ and the lowest over 30℃with no cooling hours in a whole day. What's more, during the hot days, the surface temperatures of every place are very high heated by ambient air and solar radiation; while at night, the heat could not be brought away due to lower wind speed. In winter, there is great difference between indoor and outdoor temperature, with the average temperature 8.5℃. Thus, if there is no heating facilities in the houses, people would feel cold even have chilblains on their feet and hands.

The year of 2016 registers an annual average temperature of 18.2℃; total rainfall of 1,797 mm; and total sunshine of 1,522 hours. An extreme high temperature of 40.3℃ is recorded on 24th July in downtown of Hangzhou, and a lowest temperature of -11.3℃ occurs in the city of Lin'an, on 25th January.

Table.1-2. Climate conditions of Hangzhou

Month	Temperature (℃)	Humidity
January	Min. = -5.4 Avg. = 4.7	Avg. ≈ 80%
July	Min. > 28, Max. = 38.4 Avg. = 28.1	Avg. ≈ 80%

(Data source: http://www.hzqx.com)

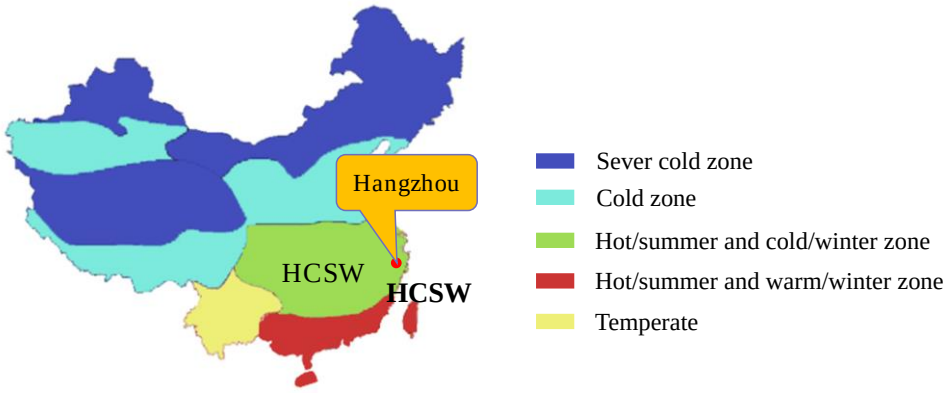

Fig.1-1. Climate zones for residential buildings in China's energy code.

1-3-2-3 Building energy consumption in Hangzhou area

Due to the sever climate conditions of hot summer & cold winter, more and more households with higher incomes has become interested in using air conditioners to obtain the comfortable indoor thermal environment, which resulting in huge electricity energy consumed (see Fig.1-19).

In 2012, a team[19] made a survey on electricity consumption in summer and winter of Hangzhou. The surveyed object was the common residence without energy-saving measures built after 2008, including 300 households whose electricity consumption generated from January to December in 2012 were collected and analyzed. The research results showed that the household electricity consumption accounted for 30% of the total electricity consumption in Hangzhou in 2012. The total residential electricity consumption was 59.17 billion kWh, among which there was 1.8 billion kWh electricity caused by air-conditioners.

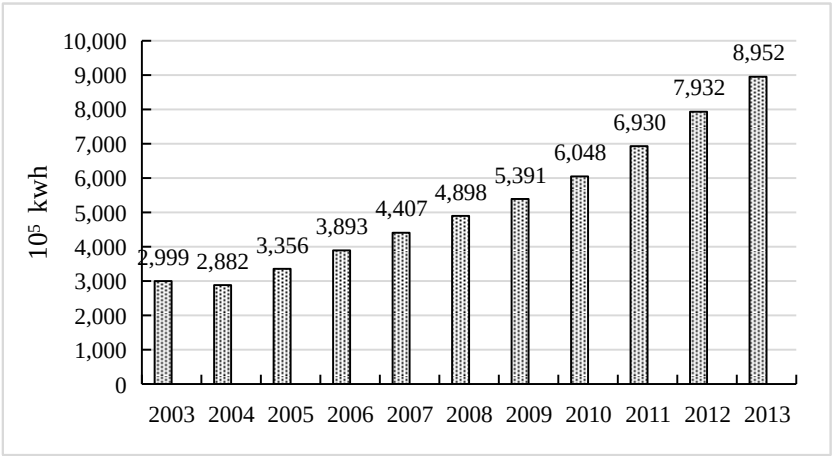

Fig.1-19. Annual electrical consumption in residential buildings of Hangzhou (2003~2013). (Data source: http://www.hzstats.gov.cn)

According to the statistical results[错误!未定义书签。] from Hangzhou government, the ownership of air conditioners per 100 urban and rural households of Hangzhou is shown in Fig.1-0. It can be seen that the ownership of air conditioners per household in rural area got sharply enhanced in 2010, turned several times than in 2005, then over 150 in 2016.

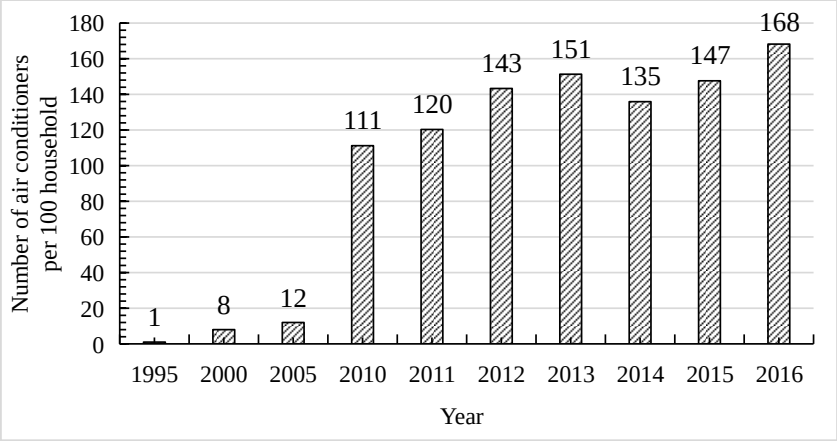

Fig.1-20. The ownership of air conditioners per 100 households of rural residence in Hangzhou, 1995~2016. (Data source: http://www.hzstats.gov.cn)

Based on the above background, energy shortage and huge energy consumption in buildings have been considered the crucial factors in economic growth and continuous development in Hangzhou area of China. Driven by the energy crisis and demand for sustainable development, advanced energy efficiency technology and sustainable strategies used in buildings must be put forward.

1-4 Previous study

1-4-1 Theory and practice research

From the point of view of architect, what they are concerned about are: how is the effect of the heating and ventilation of different passive ventilation forms and which form is more effective; how is the applicability of passive building technology under different climatic conditions; how is the regulation of the heating ventilation technology that the passive ventilation adopts on the indoor thermal environment; and what are the building designing factors that influence the heating ventilation technology of passive ventilation. At present, the researches carried out by domestic and foreign scholars are started with the mechanism of passive heating and cooling, and then are continued with study of the natural convection flow pattern of air and the coupling between the air and wall heating.

The history of the applications and research of modern solar energy in terms of architectural design can be traced back to the 1980s. In 1881, Edward S.Morse from Massachusetts, the United States built the first experimental device and succeeded. Later, France's Felix Trombe and an architect named Jacques Michel, by using this principle, built a number of solar homes in Ode illao in 1967, and made the efficiency of this heating method improved[20]. After the 1930s and 1940s, the design and research of the solar house have been carried out widely in Europe, the Americas and other places. Especially after the 1973 energy crisis, the way of solar heating for air conditioning has been gradually enhanced and gradually improved. In 1974, the first International Conference on Passive Solar Energy was held, which vigorously advocated the solar heating, including solar collector technology and the development and utilization of solar energy

greenhouse, reducing the reliance on non-renewable energy. On the basis of the development of solar energy residential, there has been residential buildings that further took energy efficiency into consideration, and the thermal insulation performance of building materials has been improved. In the 1980s there have been many modern casing construction, the majority of which are residential constructions and among them there are libraries, museums and other public buildings as well. Even with more mechanical ventilation and artificial lighting, there is still a significant saving in heating and cooling energy consumption[21].

The relevant literature on passive solar building research is quite abundant, the research aspects of which can be summed up as solar energy absorption, geometric structure, orientation and angle of inclination. The United States published the "*Manual of Passive Design for Sun Room*" and the relevant principles books, atlas based on a large number of solar building practice. Since 1970s, Japan's famous architect Kato Yifu has attempted to design many inducing solar buildings by using ecological design idea under the analysis of natural energy and the geographical characteristics of the environment. In 1988, Swedish architect Ademason and German architect Feste together put forward the concept of "*Passive House*". In 1990s, the world's first passive house hosted by Feste was constructed in Darmstadt City, Germany. Then later, in 1996, Dr. Feste firstly established Passive House Institute, where more than 10,000 "Passive House" has accept the certification by now, including residential, public, office, commercial, school, hotel and so on. During ten years development, Europe and the United States formed a consensus on the standards of passive architecture[22]. In 1990s, famous German architect and professor, Thomas Herzog, published an important works[23] in the history of ecological architecture and passive design, named *Solar energy in architecture and city planning*, which introduces the main strategies of relying on passive design of solar energy and the analysis of specific examples.

The United States is one of the most energy-consuming countries in the world, whose 70% of energy demand rely on import. In such situation, America carried out earlier study on passive buildings. Since 1970s, under the encouragement of government, America has have built a number of residential buildings such as Atasca De Cotto, Kelbusi, Santa Fe solar energy building, Davis house and many other passive buildings based solar heating, among which Atasca De Cotto house almost realized complete solar heating, and the heating rate of the others were more than 75%. In 2008, American architect Daniel D. Sheila[24] published *Solar Building-Passive Heating and Cooling*, analyzed the utilization of passive solar energy in buildings with examples.

Japan is an island country with a shortage of various nature resources, especially fossil fuel. Thus, Japan attached great importance to the study of passive energy efficiency in buildings. At present, the way of solar energy utilization in Japan is mainly to install the solar photo-voltaic panels and thermal collector onto the building roof or facade, providing heating, cooling and hot water for residential dwellings.

The research on passive buildings in China started relatively late, mainly in sever cold and cold zone. With the total amount of economic increasing, energy and environment has become a critical

issue in China. Enhanced by the world's development of passive house, the studies on passive buildings in different climate zones have got ambitious progress. At the end of 1970s, Tsinghua University as the representative of the university carried out the theoretical study of passive solar buildings in Northern China, and published the relevant design atlas, construction specifications and other technical documents. In 1985, Gao Yilan of Tsinghua University introduced the concept "Arcology" created by Italian architect Paul Soller to China, so that China had a theoretical understanding on ecological architecture for the first time. In 1988, Wu Liangyong creatively conduct "Integrated Architecture"[25], proposed to treat architecture as one factor of the integrated background, among which the urban planning, architecture and gardens design are taken as the core, combined with geography, ecology and other subjects. This concept breaks through the simple understanding about architecture, leading people to build "living environment science" system and improve our life quality. In 1999, Liu Jiaping[26] of Xian University of Architecture and Technology proposed a new ecological building made of rammed earth based on the climate conditions of Southern Shanxi and local residential space configuration. This housing style present the ecological idea integrated with passive solar energy design, constant temperature and humidity conducted by raw soil and natural ventilation. In 2003, Dr. Yang proposed the passive design strategies response to different climate zones of China[27]. In 2007, Yin[28] put forward to passive design strategies suited to Wuhan climate.

Since 1970s, China started to carry out the research on passive solar heating buildings in sever cold and cold area. In 1977, the first passive solar building was built in Minqin county of Gansu, China. From 1980s, passive demonstrating buildings of nearly 100,000 m^2 were completed in rural areas of North China. In 2004, a ecological office building[29] was built in Shanghai for demonstration, which is the first super low-energy consumption building in hot/summer and cold/winter zone of China. In 2005, the first ultra-low energy building of China designed by Jiang Yi was constructed in Tsinghua University, displaying more than 100 research results and technique products representing the scientific level of China. In 2013, a demonstration project of "passive low-energy residential housing" as an achievement of China - Germany cooperation successfully passed the joint acceptance hosted by German Energy Agency and Chinese Ministry of Housing and Urban. In 2014, the first passive house in hot/summer and cold/winter zone of China was built up in Changxing county of Zhejiang.

Based upon the above introduction, for China, the researchers and practice on passive building mainly focus on the cold area of Northern China, where is very cold with a long duration in winter, and has a short summer time. Thus, the energy consumption for heating in buildings would be much higher than cooling, as same as in Germany, who only focus on keeping warm inside, and the design strategies for passive design are not suitable for all the areas of China due to the variable climate conditions.

When it comes to hot/summer and cold/winter zone of China, architects and engineers were just beginning to explore in the field of passive design, and the theoretical and practical research are

still lacking. Moreover, it is not only to consider the heat insulation in winter, but also how to decrease the cooling load in summer. Researches on passive building design for hot/summer and cold/winter zone of China is very less, so it is necessary to carry out study on passive energy efficiency, taking Hangzhou rural area of Zhejiang province as a case.

1-4-2 Development of study method

1-4-2-1 Experimental study

There are many pieces of literature on the design of solar chimneys. The earliest record of using solar energy to enhance the chimney's effect of indoor ventilation appeared in the sixteenth century[30]. As early as the year of 1925, Mingle[31] has investigated the traditional chimney shape and heat capacity. Until the 1970s, due to the increasing popularity of air-conditioning, the new researches of the passive ventilation technology were barely seen. At the same time, there appeared the energy crisis, as a result, the scholars have re-explored both theory and practice of re-energy saving and natural ventilation technology. Determining the parameters of the air temperature, humidity, and flow rate in the room temperature by the way of experiment is to, by measuring heat flux density, air inter space and room air temperature under the experimental conditions, get the natural convection heat transfer in passive ventilation system characteristic parameters. Compared with the theoretical method, the main advantage of the experimental method is that it does not need to make assumptions on the wall structure and thermal properties, air flow and physical properties, outdoor weather conditions, etc., and is more suitable for getting the effect of the Ventilation cooling performance of the heating into effect and for researching the capacity that passive ventilation's adjustment to thermal environment[错误!未定义书签。].

(1) Small-scale experimental models

The small-scale experimental models use measuring techniques to predict or evaluate ventilation performance with a reduced scale of the buildings or rooms. It is much more economical to use a small-scale experimental model than a full-scale building or room. One can get realistic ventilation performance by directly measuring thermo-fluid conditions in a small-scale model if the flow in the model is similar to these in reality. In order to achieve flow similarity between a small-scale experimental model and real building or room, important dimensionless flow parameters in a small-scale experimental model such as Reynolds number, Grashof number, Prandtl number, etc. must remain the same as those in the actual building or room. When heat transfer is involved in a room with ventilation, it is difficult to obtain the same Reynolds and Grashof numbers. One possibility is to use liquid with different density, such as water or Freon to simulate thermal buoyancy. Otherwise, the small-scale model may not simulate the actual flow in buildings or rooms. Even though, the flow in the small-scale may not be the same as that in the actual room.

The small-scale experimental models are very effective and economical to study ventilation performance in buildings. However, in addition to scaling issues associated with thermo-fluid

dimensionless parameters, it can be rather challenging to scale down complex flow geometry, for example a complex diffuser. Our literature review found that instead of being used directly to study ventilation performance, the small-scale experimental models were mainly used to validate analytical, empirical, or numerical models. The validated analytical, empirical, or numerical models were then scaled up for studying the ventilation performance in real buildings.

(2) Full-scale experimental models

The full-scale experimental models have been widely used for predicting ventilation performance in buildings. The full-scale models were mainly used to generate data to validate numerical models, especially CFD models. Many well-known researchers started to switch their career to use numerical models.

The full-scale experimental models can be further classified into two categories: laboratory experiment and in-situ measurements.

Laboratory experiment often uses an environmental chamber to mimic a room or a single-deck building with several small rooms. If outdoor wind conditions have to be considered, the chamber should be placed in a wind tunnel, which would make the facility very expensive. In a chamber, the thermo-fluid boundary conditions can usually be controlled. In the past year, there were considerable amount of studies on predicting ventilation performance using full-scale models. Zhang et al.[32] used an environmental chamber to mimic a section of a twin-aisle airliner cabin.

It is documented that Bouchair studied the way how to reach ventilation and cooling to a full-scale experimental “chimney” in Southern Algerian region with the conditions in experiment[33]. In 1999, Hirunlabh studied the passive cooling and ventilation condition in a metal-type solar house with a thermal insulation on the side of the tropics. The experimental results show that the air flow rate can reach 0.01-0.02 kg / s when the air passage width is 14.5 cm and the surface area is $2m^2$[34].

The recent applications indicate that the full-scale models by laboratory experiment or in-situ measurements gave the most realistic prediction of ventilation performance for buildings. However, they were generally very expensive and time consuming. In addition, these experimental measurements were not free from errors. Current trend seems to use full-scale experimental models of laboratory experiment and in-situ measurements to obtain data for validating computer models, such as CFD models, and then use the validated computer models to conduct the predictions of ventilation performance or design ventilation systems. The in-situ measurements were more frequently used to evaluate the performance of existing buildings.

1-4-2-2 Numerical simulation

The numerical simulation method of the passive ventilation system is to make the physical model easy to deal with by making certain assumptions and simplifications to the wall structure and material, and then express the physical model by the governing equations. What’s more, the equation group shall be solved to reflect the air natural Convective flow and thermal

characteristics, and then use these parameters to predict the thermal performance of buildings[错误!未定义书签。]. The most popular method in the fields of numerical simulation was to use Computational Fluid Dynamics (CFD) model to numerically solve a set of partial differential equations for the conservation of mass, momentum (Navier–Stokes equations), energy, chemical-species concentrations, and turbulence quantities. The solution provides the field distributions of air pressure, air velocity, air temperature, the concentrations of water vapor (relative humidity) and contaminants, and turbulence parameters for both indoor and outdoor spaces. Despite having some uncertainties in the models, requiring sufficient knowledge on fluid mechanics from a user and demanding a high capacity computer, the CFD models have become more and more popular in predicting ventilation performance due to the rapid increase in computer capacity and the development of user-friendly CFD program interfaces.

The study[35] reviewed and presented the following subsections for predicting ventilation performance in human occupied buildings in the past year.

(1) CFD model validation

At present all the CFD models use approximations for predicting ventilation performance for buildings. The approximations inevitable bring some uncertainties in predicting the distributions of airflow, air velocity, air temperature, and chemical-species concentrations. Even CFD has been applied to ventilation studies for over 30 years; engineers are still seeking for more accurate, more reliable, and faster CFD models. Zhai et al.[36] reviewed popular turbulence models that could be used for indoor environment modeling. They identified the most promising models from eight different categories including eddy viscosity models, Reynolds stress models, LES, and detached eddy simulation. Detached eddy simulation is a hybrid model that use LES for main flow region and RANS for boundary layer flow. Zhang et al. [37] then further validated these eight models for force convection and mixed convection in ventilated spaces, natural convection with medium temperature gradient in a tall cavity, and natural convection with large temperature gradient in a model fire room. They found that the performance of the models was not always consistent for different flows. Among the RANS models tested, the v2f-dav and RNG $k-\varepsilon$ models had the best overall performance. Many other researchers[38][39] tested various RANS models for predicting ventilation performance in buildings. These studies also concluded that one model could perform well for one flow but poorly in another. The performance of the RNG $k-\varepsilon$ model was rather stable.

(2) Coupling CFD models with other building simulation models

CFD models have also been used to improve other building simulation tools so that ventilation performance can be more accurately predicted. This has become a trend in areas involving multi-scale flow and heat transfer. For example, researchers coupled energy simulation with CFD to improve the accuracy in natural ventilation prediction with reduced computing effort[40][41] and to study the performance of a double skin facade system. The trend is clear that the researchers

were satisfied with the coupling. The coupling did increase significantly the complexity, a price the researchers seemed rather willing to pay.

(3) Applications of CFD models for indoor air quality studies.

Applications of CFD models for predicting ventilation performance in buildings at present can be generally divided into three categories: for indoor air quality studies in spaces with non-uniform distributions of contaminant concentrations, for natural ventilation designs, and for investigations on stratified indoor environments. Zhang et al.[42] and Zhao et al.[43][44] used a CFD model to study particle transport in different environment with high health concerns. Similar applications can also be found for a dental clinic[45]. In addition to particulate matters, CFD has also been used to study indoor air quality caused by gaseous contaminants. Examples are to evaluate indoor air quality in a polyvinyl chloride chemical plant[46] and to develop ventilation efficiency indices for indoor environments in urban domains[47].

(4) Applications of CFD models for natural ventilation designs

Design of natural ventilation is very challenging due to the change of wind speed and direction over time as well as significant impacts of surrounding buildings on the ventilation rates through building openings. The multi - zone network models are often incapable to deal with such complicated scenarios of airflow. Due to the increasing interests in using natural ventilation to reduce energy demand and to improve indoor air quality, the applications of CFD models for natural ventilation design are popular at present[48].

(5) Applications of CFD models for investigations on satisfied indoor thermal environment

Simple models, such as analytical and empirical models, have great uncertainties when being used for stratified environments, including indoor spaces with displacement ventilation and under-floor air distribution. Therefore, CFD models have been widely used in such indoor environments for the investigations of ventilation effectiveness, indoor air quality, thermal comfort, etc. Wang Hanqing[49] applied computational fluid dynamics (CFD) to carry out research on numerical simulation under the winter heating. He proposed that this heating model is well applied in Zhuzhou, Hunan province where is the potential of improving indoor air temperature and improving indoor thermal environment even under weak solar radiation, which has a very significant effect in improving the indoor thermal environment.

1-5 Purpose and methods

Hangzhou city, located in hot/summer & cold/winter zone, was taken as a case study, where rural residences have higher electricity energy consumption by using more air-conditioners for heating and cooling in recent years. Combining with the characteristics of Hangzhou's rural residence, an experimental rural house integrated with passive energy-efficient technologies was designed and constructed. Through the methods of experiment and simulation, the research purpose are as follows:

- To evaluate the effectiveness of passive energy efficient technologies under real climate

conditions of Hangzhou;

- To investigate and improve the thermal performance of passive energy technologies.
- To provide a demonstration building to be further researched and promoted in rural areas of Hangzhou.

The research flow is illustrated in Fig.1- 1, and the research methods applied in this paper are as follows.

1-5-1 Reference reading

Before carrying out the study, I hope to have a whole grasp of this study by reading a lot of literature on low carbon building, passive solar architecture, heat transfer theory, hydrodynamics, computer simulation and so on, striving to ensure the forward-looking ideas of the methods and the innovation in contents.

1-5-2 Quantitative study

Qualitative research focuses on the attribute relations of things. Quantitative research focuses on the quantitative relationship of things. Without qualitative analysis and judgment, quantitative research may have only microscopic meanings. On the contrary, only by qualitative research can not make correct conclusions drawn, especially when several self-contradictory concepts occur at the same time. Therefore, the work of this paper will combine the logical qualitative research and experimental and empirical study so as to get through a reasonable method of relatively perfect research results.

1-5-3 Experimental study

The performance evaluation of "passive" building energy-saving technology can be said as the multi- variable and complex system. The heat transfer process is different due to objective factors such as climatic conditions in different seasons, different time periods and different sunshine intensities. In order to master objective laws, carrying out research is indispensable. In this study, two test methods were used:

One is to carry on the continuous and uninterrupted long-time data monitoring in a certain season in order to seek the law and characteristic of the dynamic change of the building thermal environment under the actual climatic condition of the monitoring place.

Second is a comparative test method. The data are monitored synchronously with other reference objects under the same design conditions. When the objective variables are the same, the differences between the two are found and the advantages and disadvantages of the design objects are evaluated.

1-5-4 Simulation study

The CFD-Fluent software was used to simulate the heat transfer characteristics of "passive" energy-saving technology system in order to comprehensively consider the complexity of objective factors, such as meteorological condition and surrounding environment of the building, and the physical model of the actual building was established. The simulation application of the

software can greatly save the working time and economic investment, and can also draw a series of design principles and key points about the passive energy saving technology, and draw the conclusion that there is reference value.

However, the use of any tool method has its premises and scope of application, the accuracy of the predictive results for indoor environmental performance usually rely on very precise input conditions and comprehensive control of the system parameters, so the pre-measured data for the simulation study provides a calibration basis to ensure that the simulation work of the scientific and reliability.

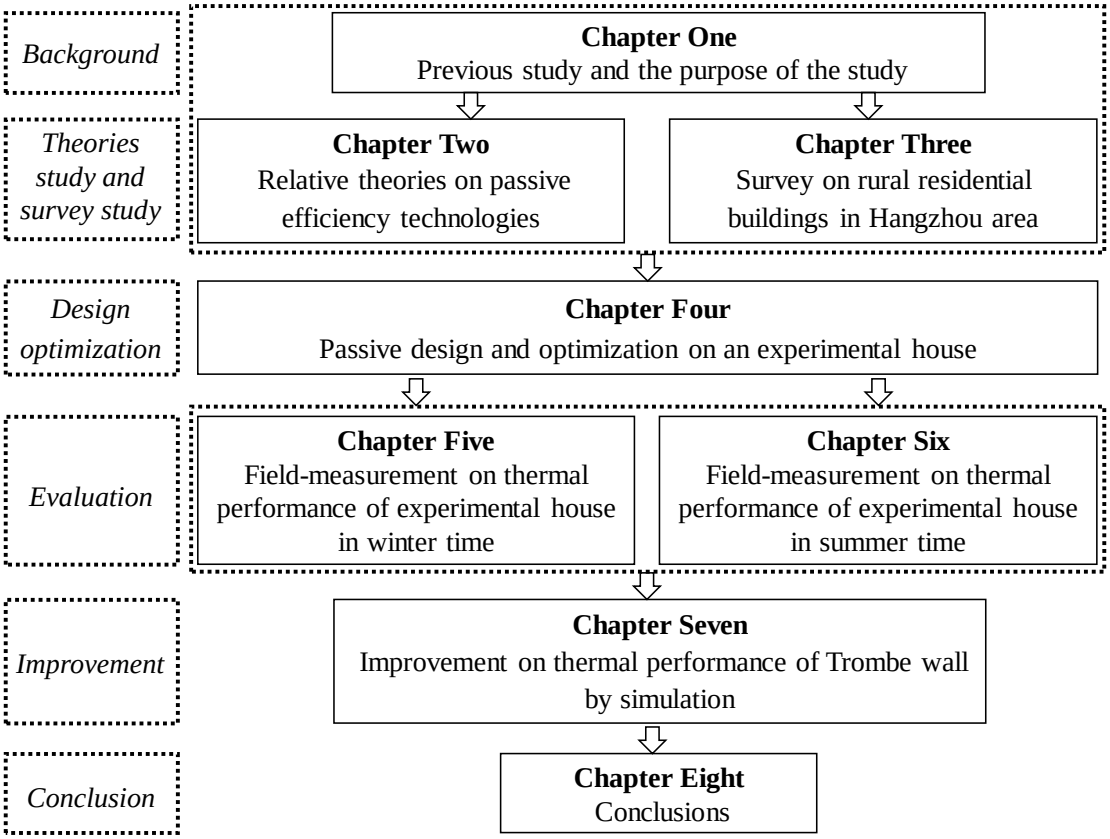

Fig.1- 21 Research flow.

Reference

[1] Olivier J, Janssens-Maenhout G, Muntean M, et al. Trends in Global CO2 emissions: 2015 report[J]. Maenhout, 2015.
[2] J Conti, P Holtberg, International Energy Outlook 2016, U.S.Energy Information Administration, 2016
[3] People's Republic of China. China Statistical Year Book 2014. China Statistics Press, 2014.
[4] Zhu, Y.M. and Liu, J.P. Exploration of Optimization Measures for Energy Saving Technology of Urban Residential Buildings. Industrial Construction, 2007(37): 1-4.
[5] Zhang M, Guo F. Analysis of rural residential commercial energy consumption in China[J]. Energy, 2013, 52(1):222-229.
[6] Building Energy Conservation Research Center of Tsinghua University. 2016 Annual Report on China Building Energy Efficiency [M]. Beijing:China Building Industry Press, 2016.
[7] Liu, W. Current Situation of Passive Building Development. Door and Window,2017(2):26-29.
[8] British Petroleum Company. Statistic Review of World Energy 2013[R]. 2013.6
[9] 4R. Vasudevan, K. Cherail, R. Bhatia, and N. Jayaram, Energy Efficiency in India: History and Overview (Alliance for an Energy Efficient Economy), New Delhi, India, December 2011: 16-17
[10] United Nations, Department of Economic and Social Affairs, Population Division, “World Urbanization Prospects: The 2014 Revision, CD-ROM Edition”, 2014.11
[11] Building Energy Conservation Research Center of Tsinghua University. 2011 Annual Report on China Building Energy Efficiency [M]. Beijing:China Building Industry Press, 2011.
[12] Building Energy Conservation Research Center of Tsinghua University. 2012 Annual Report on China Building Energy Efficiency [M]. Beijing:China Building Industry Press, 2012.
[13] Chen, H.J. Li, B.J. Dong, Z.F. Discussion on passive energy saving design of building. Building Energy Efficiency. 2007, 35(3): 29~31
[14] Liu, M. Passive House in Europe. Resources Inhabitant and Environment. 2005(9):34-36.
[15] Liu, W. Current Situation of Passive Building Development. Door and Window, 2017(2):26-29.
[16] Wiescholek, S. Hamburg House, Expo 2010 Shanghai, World Architecture, 2010(2):84-87.
[17] Chen, H.J. Li, B.J. Dong, Z.F. Discussion on passive energy saving design of building. Building Energy Efficiency. 2007, 35(3): 29~31
[18] http://www.hzstats.gov.cn
[19] Wang, Y.M. Study on the energy-consumption problem and energy-efficiency technologies of buildings in Hangzhou. Xi’an University of Architecture and Technology, 2015.
[20] Belinda Reeder. Passive solar buildings. University Press of the Pacific. 1992
[21] Christian Schittich.In Detail:Solar Architecture-Strategies Visions Concepts. Birkhauser.2003
[22] Zhang, N. Passive Solar Heating Strategy and Application Analysis in Northern Region：Master thesis. Beijing: Beijing Jiaotong University, 2011
[23] Herzog, T. Solar energy in architecture and city planning. München: Ludwig

Maximilians Universität München，2008
[24] Daniel D. Sheila. Solar building - Passive heating and cooling. Beijing：China Building Industry Press, 2008
[25] Wu, L.Y. Integrated Architecture[M]. Beijing, Tsinghua University Press, 2011
[26] Liu, J.P. Yang, L. Design Methods on Zero Auxiliary Energy Efficiency Kiln House. Journal of Solar Energy, 1999(3)
[27] Yang, L. Study on Architectural Climate Analysis and Design Strategy: Dr. thesis. Xian: Xian University of Architecture and Technology, 2003
[28] Yin, C.J. Research on Application of Passive Architectural Design Strategy in Hot Summer and Cold Winter Zone: Master thesis. Hubei; Huazhong University of Science and Technology, 2007
[29] Shanghai Academy of Buildings. Technical Demonstration of Shanghai Ecological Office Demonstration Building. Computer Knowledge and Technology, 2006(30)：101-105
[30] Spencer S. An experimental investigation of a solar chimney natural ventilation system. Master thesis, Department of Building, Civil and Environmental Engineering, Concordia University; 2001.
[31] Mingle J. Draft and capacity of chimneys. New York: Combustion Publishing Corporation; 1925.
[32] Zhang Z, Chen X, Mazumdar S, Zhang T, Chen Q. Experimental and numerical investigation of airflow and contaminant transport in an airliner cabin mockup. Building and Environment 2009; 44(1):85~94.
[33] Bouchair A. Solar chimney for promoting cooling ventilation in southern Algeria.Buildings Services Engineering Research and Technology 1994;15:81~ 93.
[34] J. Hirunlabh, W. Kongduang, P. Namprakai, J.Khedari. Study of natural ventilation of houses by a metallic solar wall under tropical climate, Renewable Energy, 1999;18(1):109~119
[35] Qingyan Chena,b,*Ventilation performance prediction for buildings: A method overview and recent applications,Building and Environment,44 (2009) 848~858
[36] Zhai Z, Zhang Z, Zhang W, Chen Q. Evaluation of various turbulence models in predicting airflow and turbulence in enclosed environments by CFD: part 1 –summary of prevalent turbulence models. HVAC&R Research 2007;13(6):853~70.
[37] Zhang Z, Zhang W, Zhai Z, Chen Q. Evaluation of various turbulence models in predicting airflow and turbulence in enclosed environments by CFD: part 2 – comparison with experimental data from literature. HVAC&R Research 2007;13(6):871~86.
[38] apsoba M, Moureh J, Flick D. Airflow patterns inside slotted obstacles in a ventilated enclosure. Computers and Fluids 2007;36(5):935~48.
[39] Rohdin P, Moshfegh B. Numerical predictions of indoor climate in large industrial premises. A comparison between different k–e models supported by field measurements. Building and Environment 2007;42(11):3872–82.

[40] Wang L, Wong NH. Coupled simulations for naturally ventilated residential buildings. Automation in Construction 2008;17(4):386–98.

[41] Fortmeyer R. Getting aggressive about passive design. ENR (Engineering News-Record) 2007 ;258(19):81–5.

[42] Zhang R, Tu G, Ling J. Study on biological contaminant control strategies under different ventilation models in hospital operating room. Building and Environment 2008; 43(5):793–803.

[43] Zhao B, Yang C, Yang X, Liu S. Particle dispersion and deposition in ventilated rooms: Testing and evaluation of different Eulerian and Lagrangian models. Building and Environment 2008; 43(4):388–97.

[44] Zhao B, Guan P. Modeling particle dispersion in personalized ventilated room. Building and Environment 2007; 42(3):1099–109.

[45] Helmis CG, Tzoutzas J, Flocas HA, Halios CH, Stathopoulou OI, Assimakopoulos VD, Panis V, Apostolatou M, Sgouros G, Adam E. Indoor air quality in a dentistry clinic. Science of the Total Environment 2007; 377 (2–3):349–65.

[46] Kassomenos P, Karayannis A, Panagopoulos I, Karakitsios S, Petrakis M. Modelling the dispersion of a toxic substance at a workplace. Environmental Modeling and Software 2008; 23(1):82–9.

[47] Bady M, Kato S, Huang H. Towards the application of indoor ventilation efficiency indices to evaluate the air quality of urban areas. Building and Environment 2008;43(12):1991–2004.

[48] Chen Q, Glicksman L, Lin J, Scott A. Sustainable urban housing in China.
Journal of Harbin Institute of Technology (New Series) 2007; 14:6–9.

[49] Wang, H.Q. Guo, J. Zhou, H.W. Numerical simulation analysis of Trombe wall which was used to improve indoor thermal environment, Building Energy & Environment, 2013;32(6): 74~77

Chapter Two: Relative theories on passive energy efficient technologies

2-1 Introduction

Before considering passive energy efficiency technology, the outer environmental conditions should be taken into account, including air, soil, water and solar energy. China has a vast territory and complex terrain. Because of the difference in latitude, terrain and geographical conditions, the climate in different areas of China vary widely, and different requirements for ventilation, shading, insulation, heating, and cooling were put forward according to various climatic conditions. In terms of thermal engineering design, there are five zones divided by *Thermal Design Code for Civil Building* (GB50176-93) of China, with the purpose of being adapting the local climate.

Compared to other areas in the same latitude, the climate conditions in hot/summer & cold / winter area of China are relatively harder with obvious characteristics of extremely high temperature in summer and very low temperature in humid winter. For improving the thermal environment and reducing heating and cooling energy consumption by using air conditioners, passive energy efficient technology is an effective way.

Passive energy conservation refers to the building itself collects and stores energy in a variety of natural ways. It forms a self-circulating system between the building and its surroundings so that it does not need energy-consuming mechanical equipment to provide support, instead it makes full use of natural resources to reduce the dependence on fossil fuels[1]. Passive energy-saving and active energy-saving is two relative concepts, among them the active energy-saving refers to the creation of a comfortable building environment through mechanical energy, whereas passive energy conservation can not only save resources, but save construction funds.

In this chapter, taking hot/summer & cold winter zone as a case, its external environment and resources are described, and the feasibility of the application of solar energy is evaluated. Then, according to the climate characteristics, the appropriate passive energy efficiency strategies are to be summarized.

2-2 Preconditions of passive energy efficient technologies

2-2-1 Climate zones of China

China has a vast territory and complex terrain. Because of the difference in latitude, terrain and geographical conditions, the climate in different areas of China vary widely, and different requirements for ventilation, shading, insulation, heating, and cooling were put forward according to various climatic conditions. In terms of thermal engineering design, there are five zones[2] divided by *Thermal Design Code for Civil Building* (GB50176-93) of China, with the purpose of being adapting the local climate, where the thermal design of civil buildings (including residential and public) must meet the mandatory standard for insulation and ventilation thereby reducing the energy demand. The five zones are shown in Fig.2-, respectively named sever cold zone, cold zone, hot/summer & cold/winter zone, hot/summer & warm/winter zone (HCSW), as well as temperate zone, with the main zoning index of the average temperature in the coldest month (January) and in the hottest month (July). By the way, the days of the average daily temperature ≤5℃ and ≥25℃ are taken as auxiliary zoning indicators. At the same time, the corresponding design requirements have been put forward.

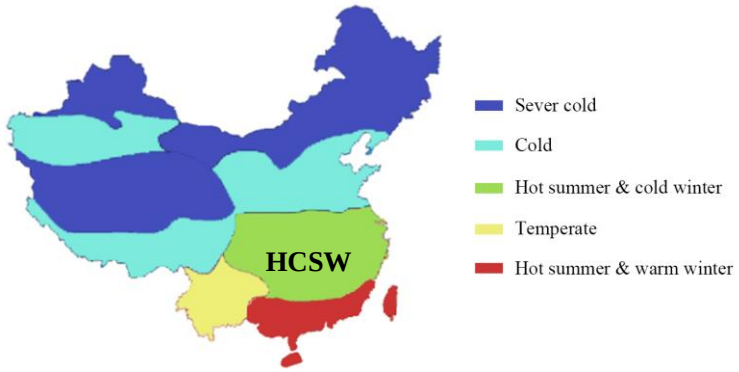

Fig.2-1. Climate zones for residential buildings in China's energy code.
(Data source: *Thermal Design Code for Civil Building* (GB50176-93), 1993)

Table.2-1 Zoning index with thermal engineering design of China[2].

Zone name	Main index		Auxiliary index	
	Average temperature in January	Average temperature in July	Days of average daily temperature ≤5℃	Days of average daily temperature ≥25℃
Sever cold	≤ -10℃	—	≥145	—
Cold	0~10℃	—	90~145	—
Hot/summer & cold/winter	0~10℃	25~30℃	0~90	40~110
Hot/summer & warm/winter	> 10℃	25~29℃	—	100~200
Temperate	0~13℃	18~25℃	0~90	—

(Data source: *Thermal Design Code for Civil Building* (GB50176-93), 1993)

Compared to other areas in the same latitude, the climate conditions in hot/summer & cold/ winter (HSCW) zone in China are more sever with extremely high temperatures in summer and low temperature in winter. This region is the most densely populated and fastest-growing economy area of China, covering a total of 550 million people in 16 provinces, autonomous regions and municipalities, and accounting for about 48% of China's total GDP. The climate of this area is characterized by: the average temperature being 25℃~30℃ in the hottest month (July) and sometimes the maximum temperature being 40℃ or more; higher average humidity being 70% ~ 80% of all year; cold in winter with coldest month's average temperature being 4℃ and the extreme low temperature being -10℃ occasionally.

2-2-2 External environment and resources

Before considering passive energy efficiency technology, the outer environmental conditions should be taken into account, including air, soil, water and solar energy. Victor Olgyar[3] considered that it is only by skillfully dealing with balance of the climate and the building construction, could the building be independent on mechanics and factories. Therefore, it could be known that the climatic resources are the key factor in the passive energy efficiency strategy.

Modern architectures are built for comfortable living space. The air-conditioners are normally used when the indoor temperatures are out of comfortable range. Passive design aims to reduce the use of air-conditioners by adjusting the environmental temperature to the comfortable zone, thus to lower the fossil fuel consumption of the appliances, and the primary investment in mechanic equipment are also decreased (see Fig.2-).

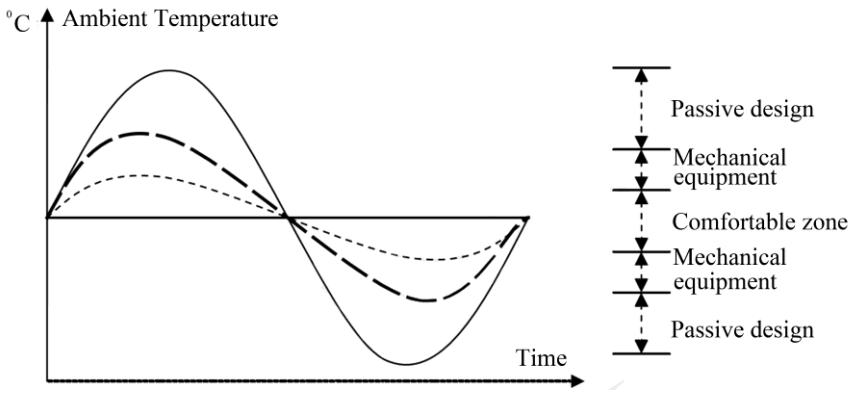

Fig.2-2. Design aim of passive technology of buildings.
(Data source: Design with Climate: Bioclimatic Approach to Architectural Regionalism, 1963)

According to the results by city research center of Cambridge, the micro indoor climate change could ease the physical and psychological pressure, which means that the dynamic changes of the indoor climate could promote the human body feelings of the comfortableness[4].

2-2-2-1 Solar energy resources in China

According to *Assessment Method for Solar Energy Resources*, there are total four ranks in China[5] (see Fig.2- & Table 2-2). Some parts of the hot/summer and cold/winter area are located at the Zone III with available sunshine, the others are located in Zone IV where Sichuan and Guizhou Province have the smallest solar energy. The sunshine percentage in Zone III / IV are no more than 50%, Chongqing enjoys 13%, Chengdu 21%, Changsha 27%, Nanjing 47%, and Shanghai 43%.

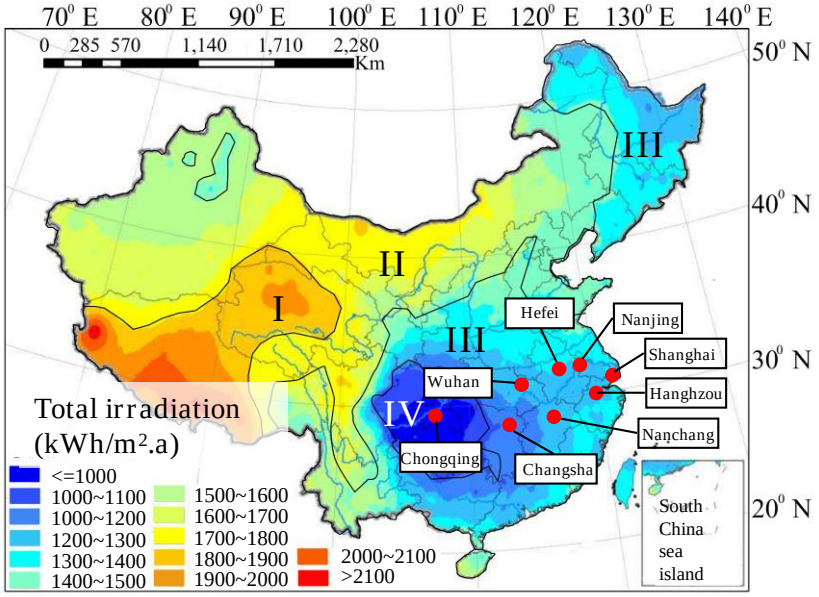

Fig.2-3 Solar energy resource distribution of China.
(Data source: Assessment Method for Solar Energy Resources, 2008)

Table.2-2 Rank of solar energy resources of China

Rank	Feature	Index [kw · h (m^2 · a)]
I	rich	□1750
II	abundant	1400~1750
III	available	1050~1400
IV	poor	< 1050

(Data source: Assessment Method for Solar Energy Resources, 2008)

To determine adequacy of the solar energy resources in a region, the main index are sunshine hours and percentage of sunshine。Six cities in hot/summer and cold/winter zone were compared with six cities in Northern China[错误!未定义书签。]. It can be seen in Fig.2-4 and Fig.2-5 that the sunshine radiation resources in hot/summer and cold/winter area in summer is basically the same as Northern and Western China, but in winter it is greatly lower than these areas.

Fig.2- shows the global irradiation distribution. Compared to many developed countries (especially European countries), the solar resources in hot/summer and cold/winter areas are obviously more abundant and are basically the same as Northern America.

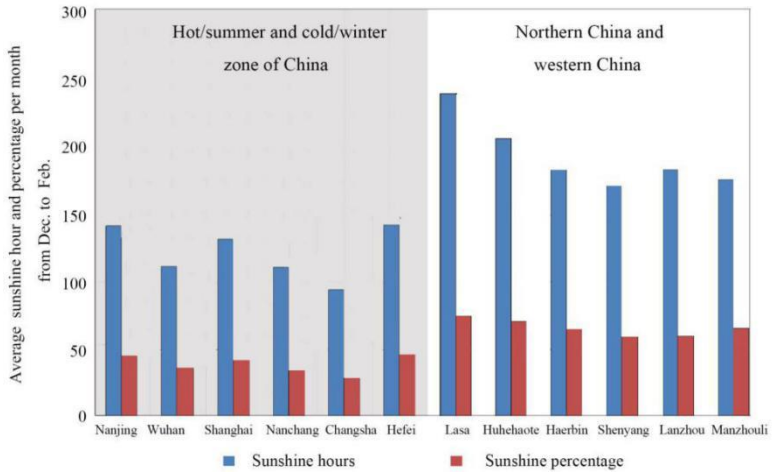

Fig.2-4 Comparison of sunshine hours and percentage in winter time between hot/summer and cold/winter area and Northern and Western China[8].

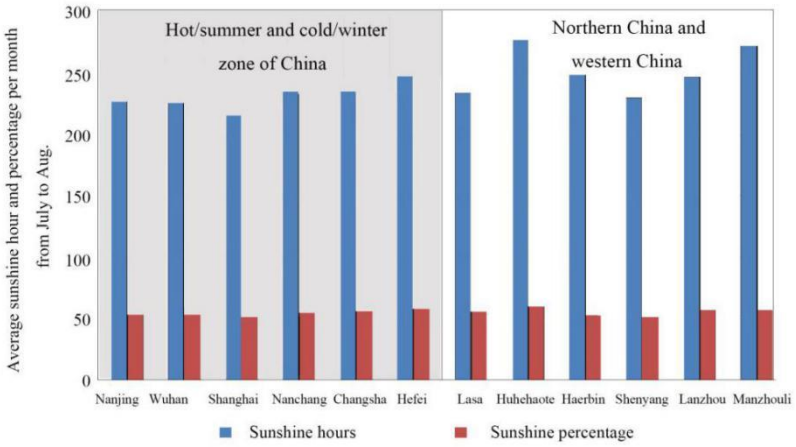

Fig.2-5 Comparison of sunshine hours and percentage in summer time between hot/summer and cold/winter area and Northern and Western China[8].

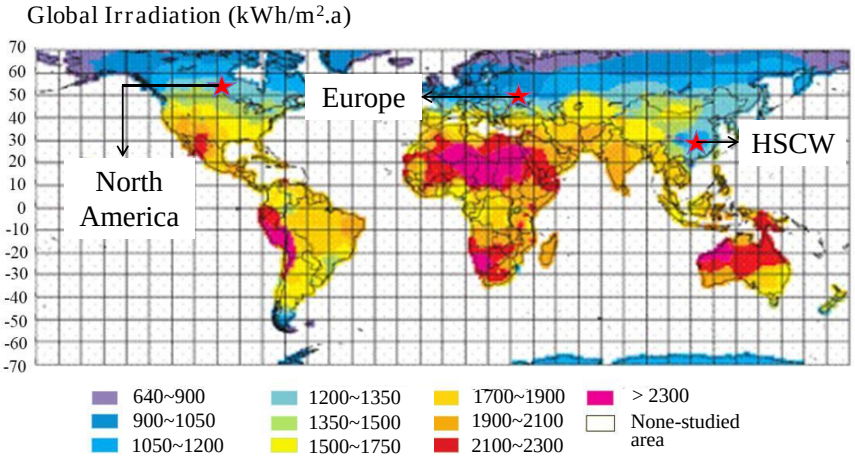

Fig.2-6 Global irradiation.
(Data source: http://blog.163.com/satan_lemon/blog/static/122051278200961865138170/)

Fig.2- shows the comparison of solar energy resources between China, Europe and North America. It can be seen that the average sunshine duration both in Northern America and China's hot summer and cold winter area are basically equal to about 115 hours and the percentage of sunshine of 39%[6]. However, in Europe where the solar energy is widely used, the average solar radiation resources are relatively poor which only accounts 50%[6] of the resources of China's hot summer and cold winter area (see Fig.2-8).

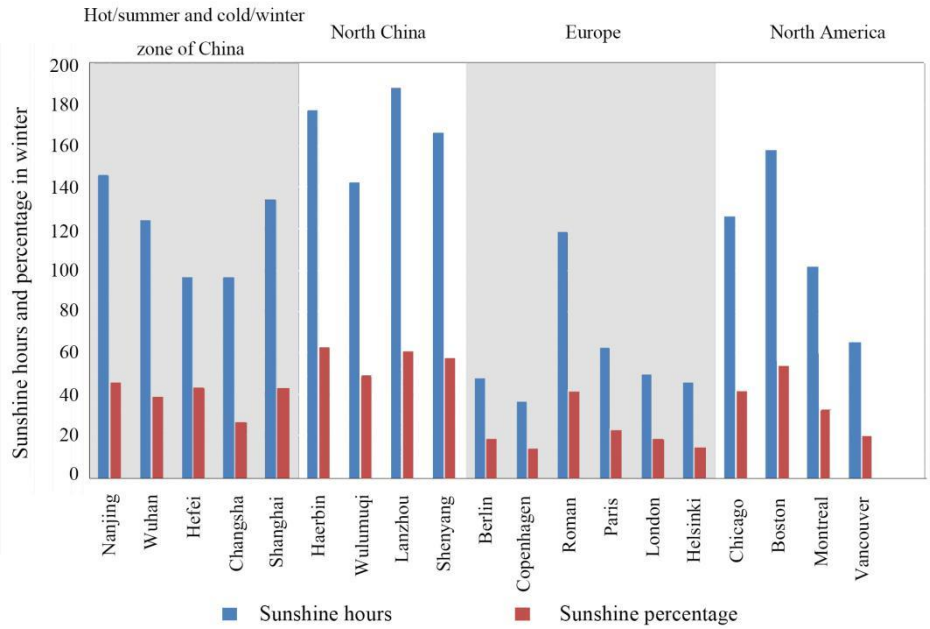

Fig.2- 7. Comparison of solar energy resources in different areas[8].

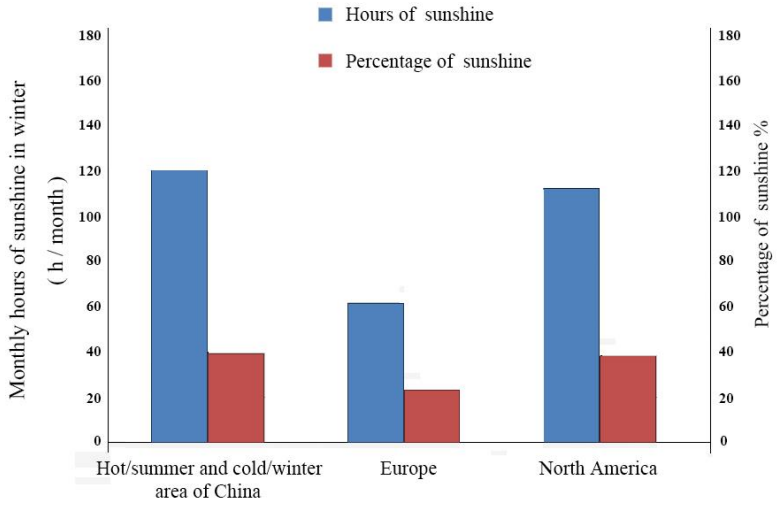

Fig.2-8. Comparison of average solar energy resources in different areas [8].

In summer, the solar energy resources in this area is more abundant than in winter（see Table.2-），which brings great difficulty to develop passive solar energy design. In summer, what we need is to isolate the solar radiation from the indoor place, and induce solar energy inside in winter.

Table.2-3. Solar radiation in heating season & cooling season in main cities of hot/summer &

cold/winter area in China [7]. (MJ/m^2.a)

City	Shanghai	Chongqing	Nanjing	Hangzhou	Hefei	Nanchang	Changsha	Wuhan
Heating season	945	1256	1040	1168	1192	1886	1595	1421
Cooling season	2155	1968	1999	2235	2150	1984	2176	2195

2-2-2-2 Solar energy application in hot/summer & cold/winter zone of China

In 2003, a measurement[8] was carried out on a six-floor brick-mixed flat in Wuhan, a typical city in hot/summer and cold/winter area (see Fig.2-). According to the comparison, due to the lack of sunshine spacing, the ground floor could not enjoy the sunshine in winter while the fifth floor could enjoy better. The test results showed that the temperature in southern bedroom on the fifth floor was always 3℃ higher than that on the ground floor. Due to the effect of the southern room, the northern living room on the fifth floor is also 1℃ higher than that on the ground floor. It meant that in Wuhan and other cities in hot/summer and cold/winter area, there still existed the possibility of passively using the solar energy although the sunshine in this area was not better than northern and western China.

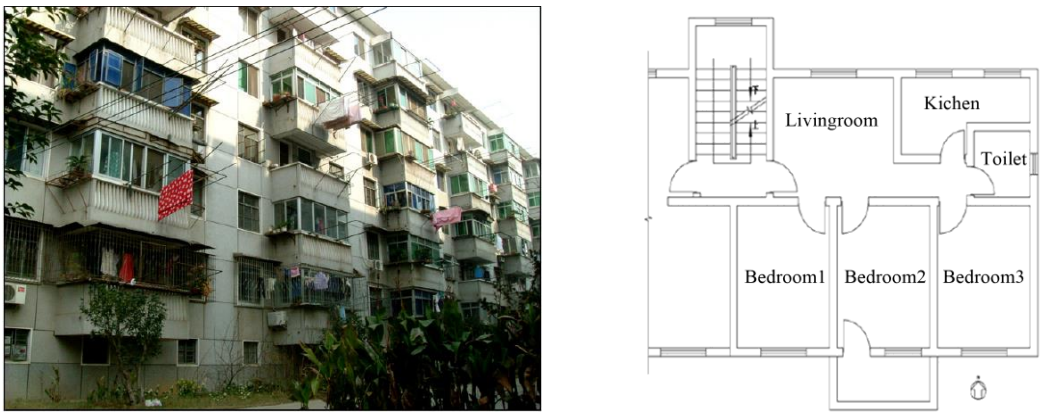

(a) (b)

Fig.2- 9 Overview and plan of the tested flat[8]

(a) Overview; (b) Plan

What's more, the southward balcony was closed with aluminum alloy windows in this household, that the room spaces could be enlarged and the balcony could become a sunlight room where the solar energy could be obtained indirectly and passively. According to the test[8], when the balcony was closed, the temperature in the balcony and the other rooms has been obviously improved. In the closed balcony space, the indoor temperature was 4℃ higher than that in the open balcony.

According to the references[9], there was a passive energy efficiency building in Hangzhou. The living room was designed to be a sunlight room with double glazing windows. In winter, when the temperature rises in the living room, the warm air would be naturally ventilated into the living

room, kitchen and dining room. In summer, the sunlight could be proofed with the sun shading. It would be better if there has a curtain indoor. According to the test results, the highest indoor temperature could reach to 18~20 ℃ when the outdoor temperature was 0℃（see Fig.2-0）.

Fig.2-10. Overview of the passive energy efficiency house[9].

Based upon the above introduction, in China's hot summer & cold winter areas, passive solar energy can be used with a possibility and potential, compared with some countries of Europe and North America.

2-3 Strategies on passive design in hot/summer & cold/winter zone

2-3-1 Appropriate form and orientation

(1) Appropriate form

Building form affects the energy consumption. From the point of view of energy-saving, the smaller the unit area corresponding to the outer surface is, the smaller the heat loss through the external envelope is. Form coefficient (FC) is an indicator used to control building shape, with the ratio F_0 / V_0 (F_0 refers to the outer surface area of buildings, V_0 refers to the volume of them) to be described. From the point of energy saving, internal volume of the building shall be enclosed with the external surface area as smaller as possible. The smaller FC means the less heat loss in winter and less thermal obtained in summer due to the small external surface area, accordingly reducing the heating and cooling load. But, too small FC will easily lead to poor lighting and ventilation, which can not make full use of natural ventilation and natural light cooling. In this case, the energy consumption for lighting and ventilating will be increased. In addition, the FC also affects the architectural style, layout, function and other aspects. The creativity of the architects will be seriously constrained for too tight shape. Therefore, there should be a comprehensive analysis and comparison, in regard to the relationship of energy consumption and building shape.

From perspective of energy-saving, the appropriate design should be based on the principle that the amount of solar heat shall be absorbed by the south wall as much as possible, more than what the building lost, so that the redundant part could improve indoor temperature. Based on this idea, when it come to the optimum building form in summer, it must be avoided excessive heat radiation. In other words, the solar radiation should be the primary consideration factor.

(2) Appropriate orientation

Orientation refers to the azimuth of the main facade of the building, generally determined by the relationship between the building and the surrounding roads. In the hot/summer and cold/winter area, the principle of choosing residential orientation is to get sufficient sunshine in winter but avoid the dominant winter wind direction for the bedrooms. In the summer, solar radiation must be prevented, and the hot cross-ventilation should be avoided. Therefore, it shall comprehensively consider the relationship of sunshine and the dominant wind direction, so as to select the best orientation of the building.

From the perspective of the use of solar energy, solar radiation at 9:00 am ~ 15:00 pm in winter normally accounted for about 90% of the solar heat all day. In this regard. It is very important to ensure that buildings in this period of time will get enough sunshine.

Fig.2--11 and Fig.2-1-12 show the daily solar radiation curves of different cities in winter and summer. The results show that the maximum sunrise intensity is from the south wall, followed by the southwest (and Southeast) to the wall. The west (east) to the wall is small in the amount, and the intensity of the North (N) to the wall is the lowest. In the summer, among the peaks of the solar radiation intensity of walls facing, the east to the west (east) to the wall ranked the highest, followed by the southwest (SE) to the SW (SE), the northwest (NE) to the second, South (S) to the wall and north (N) to the wall.

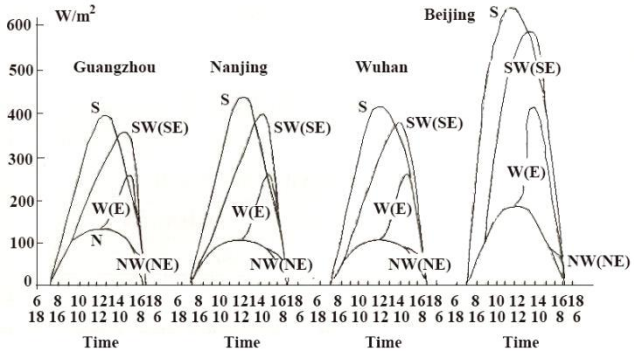

Fig.2-11. Diurnal change of solar radiation on different wall surfaces in winter[10].

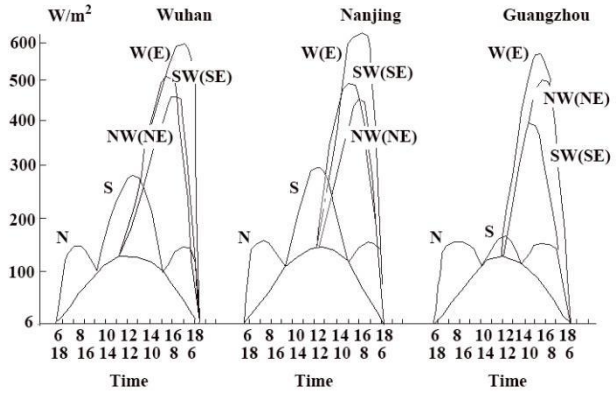

Fig.2-1. Diurnal change of solar radiation on different wall surfaces in summer[10].

From the above analysis, it can be seen that the southward vertical surface has the largest daily solar radiation in winter while is smaller in summer. The east-west vertical surface is the largest, which is consistent with the actual situation in the low-latitude area in hot/summer and cold/ winter zone. It is the reason for this region that prevents sunlight shining facing the east in the summer and the aims to get sunshine facing the south as much as possible in winter.

2-3-2 Principles and basic measures on thermal insulation

2-3-2-1 Characteristics of thermal transfer in hot/summer and cold/winter area.

In the condition of hot summer and cold winter climate, the building thermal process is an unsteady heat transferring effected by outdoor sol-air temperature. As shown in Fig.2-2 and Fig.2-3, the building enclosure is heated by solar radiation during the daytime of summer, when heat is transferred to the room. In the nighttime, the envelope is cooled due to the decreasing ambient air temperature. That is to say, there is an alternative heat transfer between the inner and outer surfaces of the building with day and night, resulting the two-way temperature fluctuation on the envelope under natural ventilation conditions. In winter, the heat only transfer from inside to outside through building envelope.

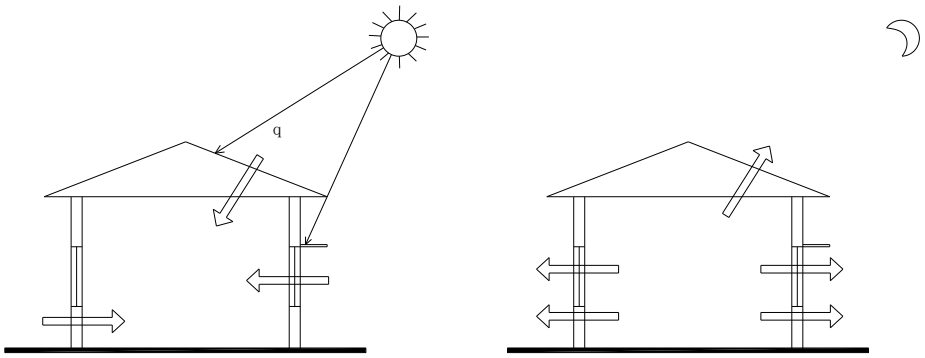

(a) (b)

Fig.2-2. Heat transfer in summer[10]: (a) daytime; (b) nighttime.

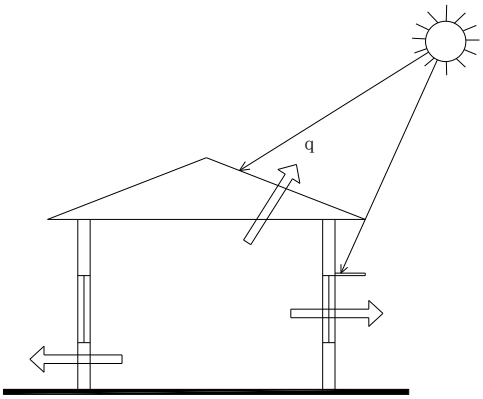

Fig.2-3. Thermal transfer in winter[10].

Therefore, the building envelope for energy saving in hot/summer and cold/winter should be designed with consideration of heat proof in summer and thermal conservation in winter.

2-3-2-2 Principles and measures

According to the characteristics of the thermal process in this area, the envelope design should be taken into account:

(1) Basic measures for thermal conservation in winter

- To take full advantage of solar energy

The solar radiation incident on the window directly supplies the heat to the room. The solar radiation falling on the wall or the roof help to raise the envelope temperature and reduce the room heat loss. At the same time, the structure can store the solar energy during the daytime contribute to the less reduction of temperatures at night.

- To prevent cold air penetration

Cold wind blowing on the surface of buildings will penetrate into the room through the door, window, hole and gap. Secondly, the convective heat transfer coefficient on the outer surface can be raised so as to accelerate the heat transfer there. Then, the temperature of inner room will become much lower with more cold air infiltration; while, the thermal energy will be further lost with more heat dissipation on the outer surface. Therefore, it should be avoided to make large area of the outer surface facing cold wind direction in winter.

- Appropriate form and plane

Reducing external surface areas of buildings, at same time meeting the functional requirements.

- Good thermal performance and appropriate heating system for rooms.

In terms of the buildings using intermittent heating mode in hot/summer & cold/winter zone, it is required that the room temperature can quickly rise to the required standard when heating at beginning.

(2) Basic measures on heat prevention in summer

- Reducing thermal effect outside

Reasonable arrangement for building orientation and layout to avoid sun radiation. At the same time, better greening environment help to decrease the radiation and air temperature. The outer envelope surface should be painted in light color for less absorption of solar radiation.

- Thermal insulation and dissipation for exterior envelope

The roof and the external walls (especially the west wall) should be insulated so as to meet the requirements of regulated thermal indicators in energy-saving standard. Structures with good thermal performance should be designed to settle thermal insulation during the day and heat dissipation at night.

- Well natural ventilation

Buildings should be as much as possible to face the wind direction at night in summer. Good natural ventilation can induce the outer flow enter into the room and take away the indoor heat, enhance body’s heat dissipation under certain wind speed. Thus, it is important to deal with the

layout of buildings properly, especially the plane, the profile, the location and size of openings. In addition, appropriate structures design for ventilation should also be considered.

- Shading design

The role of the shading devices is to prevent the direct sunlight from the window into the room, contribute to reducing radiation on the human bodies and temperature rising on the surface of the indoor walls, floors and furniture. There are many ways of shading, such as combining with building components, or using temporary tarpaulin and flexible louver, or special shading facilities. Vegetation can also be used to be planted as shade components.

- Preventing moisture for the ground

When it comes to the season between spring and summer in hot summer and cold winter zone, due to the tropical air mass, the wet air will be blown to the mainland and witness a sudden increase. The humid air will flow through the open window to the ground. When the ground temperature is lower than the indoor air dew point temperature, there will be condensation on the ground. In order to control and prevent the tide of the ground, indoor air humidity should not be too high and the surface temperature should not be too low. Increasing the ground heat resistance and using smaller heat storage coefficient of surface material can improve the surface temperature and prevent damp in hot and humid seasons.

2-3-3 Passive solar energy heating

The solar heating used in buildings can be divided into active systems and passive systems. Active solar heating system is composed of solar collectors, pipes, radiators, fans or pumps and heat storage devices such as forced circulation solar heating system (see Fig.2-4). When water is as the working fluid, pump is commonly used to provide cycle power; when air as the working fluid, the fan is often used to provide power cycle. The control and regulation of this system is more convenient and flexible with people in a proactive position. But with technical complexity and higher maintenance management cost, using active system would be a large investment. What's more, it still consumes a certain amount of conventional energy, thus it is not suitable to be operated simply for heating. For residential buildings as well as small and medium-sized, mainly use the passive solar heating system.

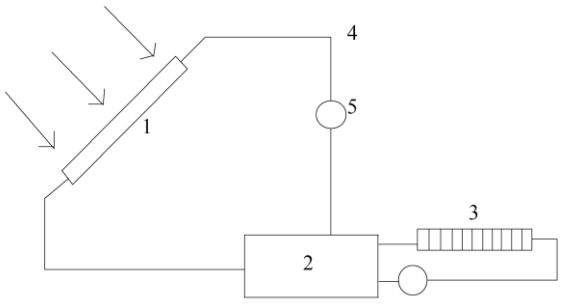

Fig.2-4. Schematic diagram of active solar energy heating system.
1-Collector; 2-Heat storage; 3-Radiator; 4-Pipe; 5-Pump or fan.

Passive solar heating relies on its building component to complete the solar collection, heat storage and cooling functions without pipes, pumps and other mechanical equipment. During the daytime, the solar energy serves as room heater when sunlight directly enters the room through the window, some of which are absorbed and stored in building components with large thermal capacity such as walls and floors, then slowly release to the room at night so that the air temperature in the room can be kept a certain high level. Passive solar heating technologies are relative simple and realized by using of local materials with none of conventional energy. They are very suitable to be promoted in rural areas. Its initial investment is mainly determined by the level of architectural design and the selection of building materials.

2-3-3-1 Gaining solar heat directly

This is the a simple form in the passive solar heating system featuring fast heating up, simple structure and no need of special heat collector. There is no much difference between it and other general building shape, and architecture design with this construction is also more flexible. In addition, its lower investment and more convenient management make it the most popular style in solar heating facilities.

Fig.2-5 shows the operation mode of gaining solar heat directly. In winter, the sun enters the interior of the room from the south window, and the floor board, the wall and the furniture facilities serve as the endothermic and heat storage. When the room temperature is lower than the surface temperature of them, these objects will be like a large low-temperature radiator to heat indoor spaces, and such radiation heating way is more effective and comfortable than air convection heating. In addition, in order to reduce heat loss, the windows must be covered with insulated curtains at night.

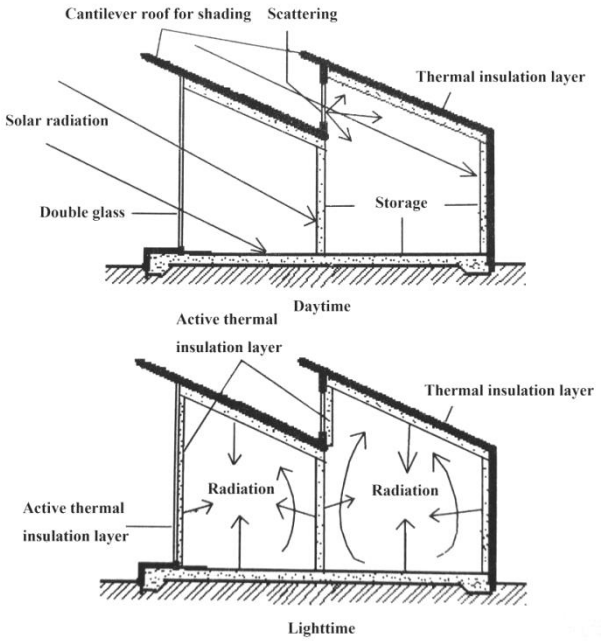

Fig.2-5. Operation mode of gaining solar heat directly.

2-3-3-2 Gaining solar heat indirectly

(1) Trombe wall system as heat storage devices

It is composed by the translucent glass cover and the thermal storage wall wit hits sunny surface coated with dark selective coating, leaving about 100mm in the middle of the air layers. Some set its outlet between the upper and lower part of the wall, such as Trumb thermal insulation wall (Trombe Wall).

This wall provide heat through two ways: 1) solar radiation is absorbed by the wall during the daytime and transfer to the inner surface by conduction, and then radiate to inner space; 2) when the air between the glass and thermal storage is heated, the hot air enters into the indoor through the upper vent of the wall, and the cold air enters into the lower vent, forming a continuous convection; at night, the upper and lower air vents are closed. (see Fig.2-6 and Fig.2-7).

Heat storage wall is usually made of concrete wall or solid brick wall, which are all heavy and have big heat capacity and thermal inertia, so it can store large thermal energy and release slowly, making it longer in the delay time of the temperature fluctuation and conducive to slow down the pace when the indoor temperatures drop at night. According to Trombe, the appropriate thickness of the concrete wall is 400 ~ 500mm. Balcomb, from the United States pointed out that, if the room temperature fluctuates among 18 ~ 24 ℃, the 300mm concrete wall is the best.

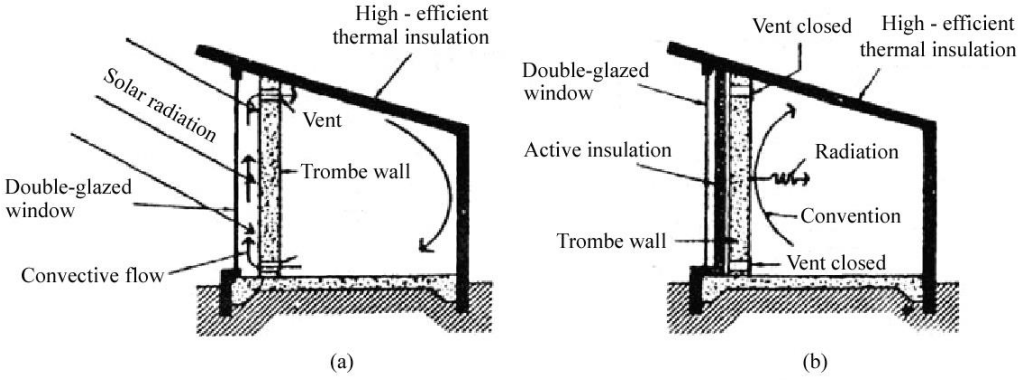

Fig.2-6. Operation mode of Trombe wall in winter：(a) Daytime；(b) Nighttime

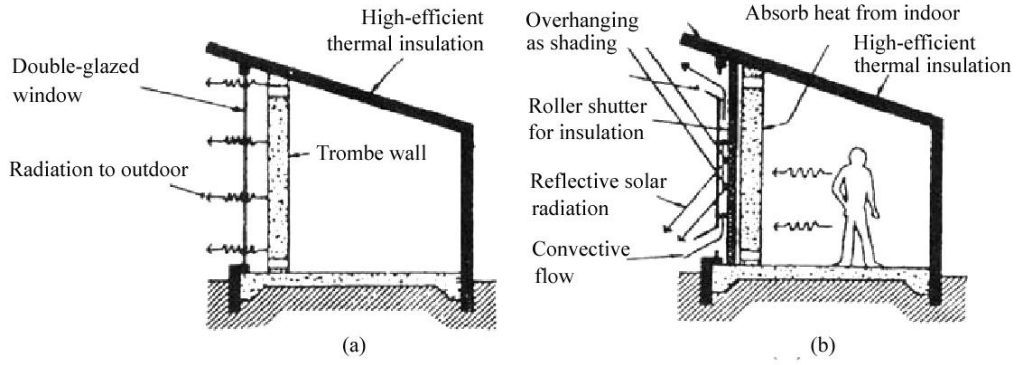

Fig.2-7. Operation mode of Trombe wall in summer：(a) Daytime; (b) Nighttime

(2) Attached sun-space in buildings

Attached sun-space in buildings is a special form that directly benefits from solar radiation through the transparent envelope on the south side of the main room which will create a n excellent indoor environment in the winter (See Fig.2- 8). In terms of the orientation of sun-space, it should be avoided from the surrounding terrain the objects in the range of south east 15° to south west 15°, as well as from the protrusion (eaves, prominent facades of the vertical column) covering the collector surface in the coldest month of January. In the summer, it should be taken into account that excessive solar radiation are prevented entering into the interior.

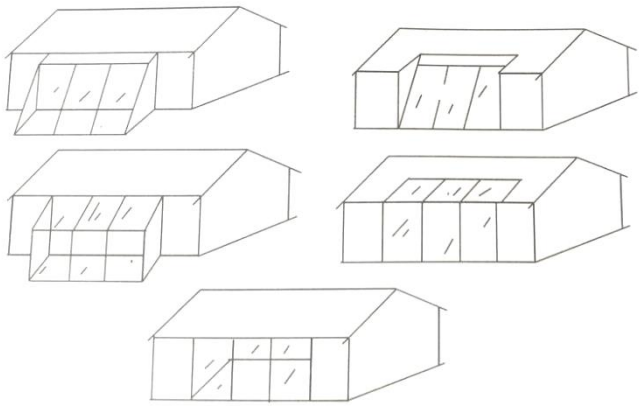

Fig.2- 8. Attached sun-spaces

Either by gaining solar radiation directly or indirectly, four basic principles must be satisfied for the passive solar heating technology as follows:

- Perfect thermal insulation is needed for the building envelope；
- The area of collecting heat surface is big enough;
- There are thermal storage structures as many as possible inside the room;
- Main heating rooms should be next to the collecting surface and storage structures, where the secondary rooms are located on the north, west or east.

2-3-4 Cooling by passive natural ventilation technologies

Natural ventilation is a popular way widely used in buildings to improve the indoor thermal environment and save the energy consumption of air conditioners. The purpose of using natural ventilation is to replace (or partially replace) air conditioning and refrigeration systems to achieve effective passive cooling. Its basic approach includes the following two points:

2-3-4-1 Restraining the hot air to flow into buildings

In areas with hot summer and cold winter, the outside temperature in the daytime is often higher than the human body skin. In this situation, it is need to suppress the convective heat into the room.

During the operation of the refrigeration unit, the cooling effect will be reduced if the windows and the entrances to the space with no-refrigeration unit are not closed. However, sometimes after the sunset, the decreased air temperature outside can be induced through the outlet or the entrance into inner space for ventilation and cooling. Absolutely, the openings designed only for ventilation are necessary.

2-3-4-2 Promoting heat dissipation

In order to make the outdoor low-temperature air enter into the room and to exhaust high-temperature air away from the room, it is an effective method by using the openings or gaps or air pressure difference between indoor and outdoor, namely wind pressure or hot pressure.

(1) Ventilation driven by wind pressure

Wind pressure is the static pressure generated when the airflow is blocked. When the wind blows through the building, due to the objects, the wind is blocked thereby producing the static pressure; side wind surface and leeward surface will produce local eddy current, then static pressure decreases. Thus, a pressure difference is formed between the windward side and the leeward side, and the indoor and outdoor air flows from the high-pressure side to the low-pressure side by the pressure difference. It is what often said the “Chimney”, whose principle is the air flow within the building. When the wind direction is certain, the wind pressure value at a certain point on the external structure of the building can be expressed by the following formula (1):

$$P = kv^2 / \rho^{14} \tag{1}$$

v - air velocity flowing through the vent;

ρ - air density;

k - air-dynamical coefficient.

If the wind pressure is to be used to achieve the natural ventilation of the building, it is first required to have an ideal external wind environment (the average wind speed is generally not less than 3~4 m/s). Secondly, the building should face the dominant wind direction in summer. Measures such as suitable structure, windows or louvers that can be opened and closed are to be taken to adjust the indoor wind air-flows with different wind speed and direction. In order to take advantage of natural wind, the building can be built in places prone to wind. In the surrounding sea, lake, river and other large water, in the daytime and night there will be a breeze from land to sea (see Fig.2-20). In terms of the terrain conditions, the buildings are best to be built on the top of the mountain, ridge or valley, where the wind is relative strong and the ventilated tunnel can be formed. The higher buildings are off the ground, the less obstructions are around them, thus the the wind speed is greater as the position of the buildings higher (see Fig.2-20). In order to reduce the absorption of solar radiation heat, the inlets can be set in large buildings so as to let the wind

enter into the buildings to cool the inner space (see Fig.2-21); In principle, the inlet has both natural ventilation and induced ventilation (Fig.2-22).

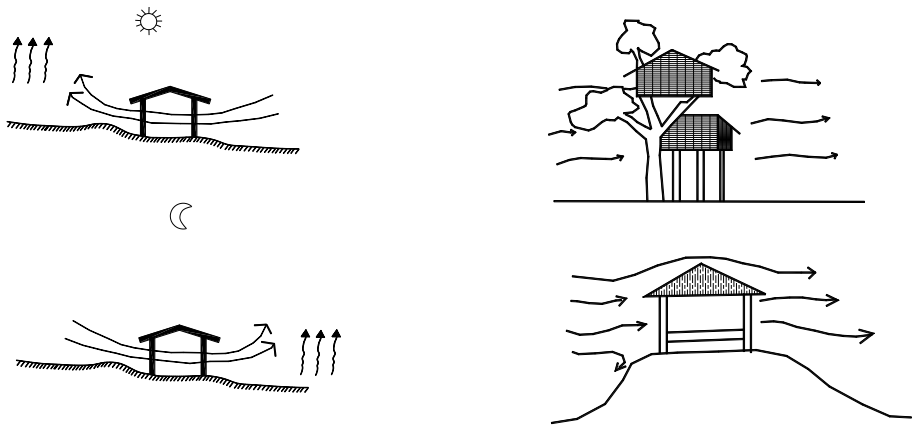

(a) (b)

Fig.2-20. Wind blow over the water surface

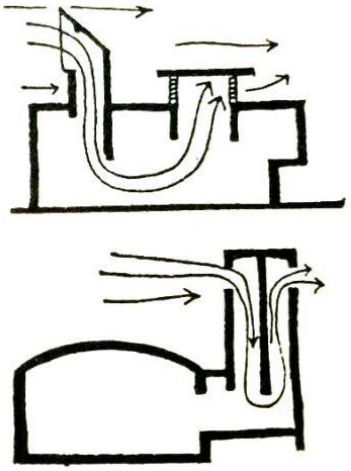

Fig.2-9. Cooling down interior by natural ventilation

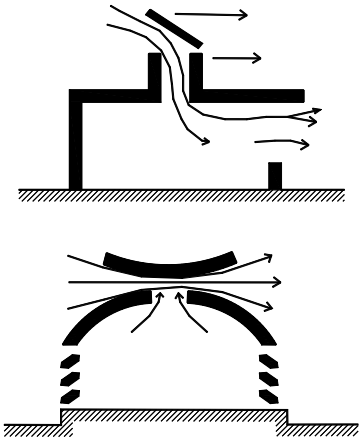

Fig.2-10. Natural ventilation and induced ventilation

(2) Ventilation driven by thermal pressure

Natural ventilation is not to be achieved because of the instability of the natural wind, or due to the influence of surrounding tall buildings and vegetation. Besides, in many cases, there will be insufficient wind pressure around the building, then needs to use hot-press to achieve natural ventilation.

Natural ventilation under the hot press is formed due to the principle that the temperature difference between the air inside and outside the building produces a difference in air density, which can drive the air flow. The indoor air temperature is higher and rise up with its density decreasing, then exhausted from the upper vent of the building driven by a negative pressure due to the low-density air. As a result, the outside low- temperature fresh air is sucked and pass through the bottom of vent in the building into the room. The air between the indoor and outdoor

flows continuously. People described the natural ventilation caused by hot press as the “stack effect”. The temperature difference between the air and the height difference among the window holes is a necessary condition for the realization of hot-press ventilation. It can be described in equation (2) as:

$$\Delta p = \beta \cdot \rho \cdot g \cdot \Delta H \cdot \Delta t^{15} \quad (2)$$

β -thermal expansion coefficient; ρ -air density; g -gravitational acceleration

Δp - pressure difference; ΔH - height difference; Δt -temperature difference

That is to say, the greater the air temperature difference between the indoor and outdoor is and the difference between inlet and outlet height is, the stronger the effectiveness of hot press is. In order to discharge high-temperature air from the entire building or a room, it is necessary to provide a vent at the highest point of the building. Because the higher it is, the strong the wind is. There is a lot of spaces or devices in the buildings to form a blowing space, while the role of hot press is more significant in the solar radiation stimulation, such as:

● Using the atrium space and sun-space for enhancing “stack effect” in buildings (see Fig.2-23).

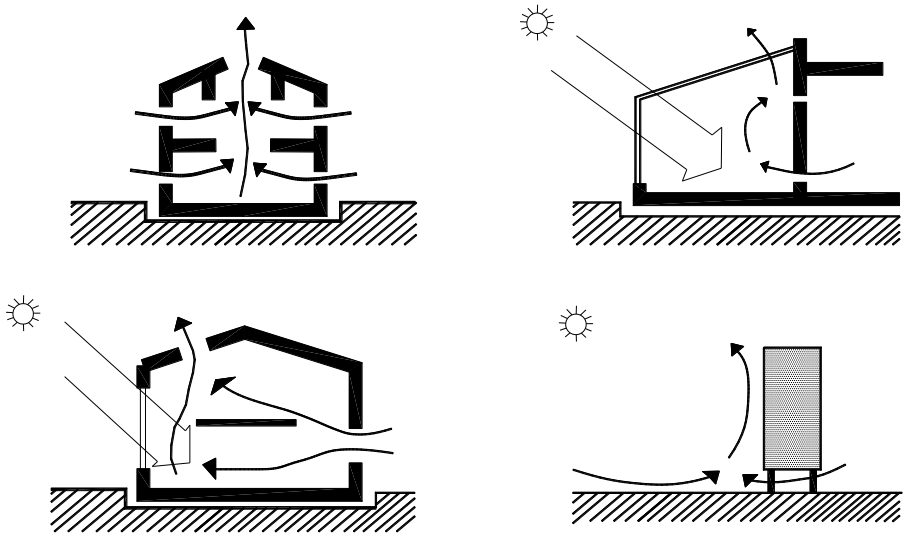

Fig.2- 11. Devices used for enhancing stack ventilation in buildings.

● Using the solar chimney for enhancing stack ventilation in buildings (see Fig.2-24).

Solar chimney, as a structure to enhance the natural ventilation in buildings (see Fig.2-24), reflect the basic principle of the “stack effect”. Solar radiation passing through the transparent glass into the chimney channel is absorbed by the heat storage material. Then the heated air around, has a smaller density than the air outside, thereby rising up, driving the outside flow to pass through the channel up to the top.

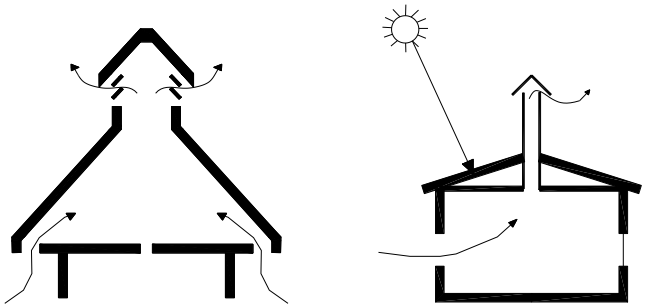

Fig.2- 12. Schematic of solar chimney devices.

2-4 Summaries

In this chapter, the external environment and resources in hot/summer & cold/winter zone were described, and the feasibility of the application of solar energy was evaluated. Then the appropriate passive energy efficiency strategies adapted to the hot summer and cold winter area were summarized as follows:

(1) Appropriate form.

From the perspective of energy-saving, the rational design should be based on the principle that the maximum amount of solar radiation shall be absorbed in the south wall, so the thermal energy should be greater than that dissipated by wall as large as possible to compensate for the heat of the building net load. Based on this idea, it is necessary not only to consider the largest sunshine in winter heat, but also to avoid excessive heat radiation in summer. In other words, the heat radiation should be the primary consideration factor.

(2) Appropriate orientation.

From the perspective of the use of solar energy, the radiation heat at 9:00 am ~ 15:00 pm in winter accounted for about 90% of all day. In this regard, it is very important to ensure that buildings in this period of time get enough sunshine.

(3) Basic measures for thermal insulation in winter:

- Taking full advantage of solar energy.
- Preventing cold air infiltration.
- Appropriate form and plane of buildings.
- Good thermal performance and appropriate heating system for rooms

(4) Basic measures on thermal insulation in summer:

- Reducing thermal effect outside.
- Thermal insulation and dissipation for exterior envelope.
- Well natural ventilation.
- Shading design.

In addition, the methods about renewable energy usage including passive solar energy heating and design strategies of nature ventilation were also concluded and summarized.

By this chapter study, the theories and strategies about passive energy efficient technologies help to provide the reference for the further design research on rural houses of Hangzhou area.

Reference

[1] Chen, H.J. Li, B.J. Dong, Z.F. Discussion on passive energy saving design of building. Building Energy Efficiency. 2007, 35(3): 29~31

[2] Ministry of Construction of the People's Republic of China. Thermal Design Code for Civil Building. China Planning Press, 1993.

[3] Olgyay V G, Olgyay A. Design with Climate: Bioclimatic Approach to Architectural Regionalism[J]. Journal of Architectural Education (1947-1974), 1963, 18(3).

[4] Sopia & Stenfan Behling. Sol Power. New York: A Publication for READ Group. 1996: 233

[5] China Meteorological Administration. Assessment Method for Solar Energy Resources. QX/T 89-2008. People 's Republic of China Meteorological Industry Standard. 2008

[6] Manfredi Nicoletti, Passive system and architectural expression, PLEA’98, Lisbon, Potugal,1998, 13-21

[7] Zhao, Q. Strategy research on solar architecture integrated design. Harbin Institute of Technology, 2008.

[8] Li, B.F. The Research on Climatic-active Design strategy of Building Skin in Hot-summer and Cold-winter Zone. Dr. Thesis. Beijing: Tsinghua University, 2004(4)

[9] Li, J.N.Exploration and practice of low - energy eco -small dwelling in hot summer and cold winter area. Architectural Journal, 2007(11):16-18.

[10] Fu, Z.X. Building Energy Efficiency Technology in Hot Summer and Cold Winter Area,China Architecture & Building Press, 2002

Chapter Three: Survey on Rural Residential Buildings in Hangzhou Area

Chapter Three: Survey on rural residential buildings in Hangzhou Area

Chapter Three

3-1 Introduction

According to the reference[1], there are more than 30,000 administrative villages in Zhejiang province, and the rural area occupies 1.5 billion square meters. As the capital of Zhejiang province, Hangzhou city has a relatively developed economy in rural area. According to the figures reported by the Hangzhou city bureau of statistics (NBS), the rural per capita net income had broken through 10,000 RMB in 2008[2] (see Fig.3-1). With the gradually increased income, rural residents have commonly used air conditioners (see Fig.3-2). to deal with the weather of hot summer and cold winter, for the comfortable indoor thermal environment, which would cause the yearly growth of electricity consumption.

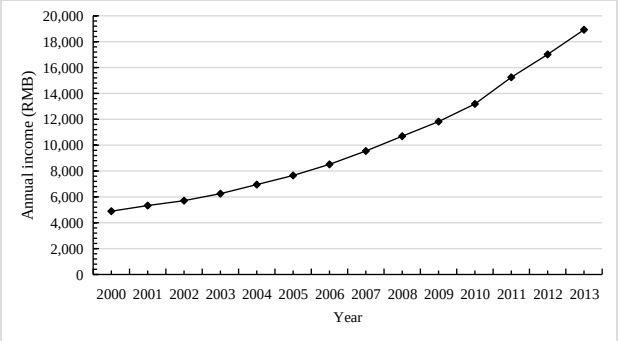

Fig.3-1 Annual income per rural resident from 2000~2013.

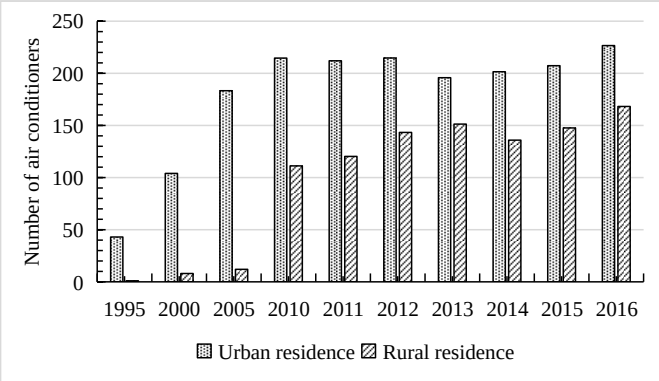

Fig.3-2 The ownership of air conditioners for every 100 households (1995~2016).

Thus, it was necessary to learn about the basic information about the rural residential buildings in Hangzhou, including design characteristics, materials, construction and indoor thermal environment. In this chapter, the survey and field measurement carried out in the villages belong to Hangzhou rural area and one of which is belong to Anji county closing to Hangzhou. It is hereby declared that the questionnaire survey and results are shared from Dr. Wang Meiyan, and the field measurement was taken by the author herself.

3-2 Survey Objects and Content

3-2-1 Survey Objects

From 2009 to 2015, under the leadership of the team member Dr. Wang Meiyan, a field survey was successively carried out on rural areas of Hangzhou and the surrounding villages, including Pu'er village of Linpu town in Xiaoshan district, Shiqiao village in Lin'an county, Ligeng village and Zhangwu village in Anji county. The following

(1) Pu'er Village

Pu'er village is located in the south of Linpu town, merged by three villages, namely Zhongjiatan, Qiaoli and Pushanhan. This village has a total of 446 households, 1531 villagers, 890 acres of arable land. To take the construction of new socialist countryside as the goal, Pu'er village has been awarded the titles of provincial "Health Village", Hangzhou "Civilized Village", "Clean Village", district "Remediation Village", district-level "Ecological Village" and so on. In this survey, there were 200 households selected as samples, among which 61% of all the samples were built before 2000, 39% built after 2000.

(2) Shiqiao Village

Shiqiao village is located in the north of Lin'an county, presenting a narrow striped distribution with total areas of 4.3 square kilometers, among which the cultivated area is 6667 acres, the bamboo area is 2000 acres. There are 4 nature villages and 575 residents. In 2006, the annual income per capita was 9000 CNY. The residents' houses are arranged on the west side of the main road with convenient traffic. This village has more mountain and less farmland, relatively rich forest resources, and being well-developed. In recent years, Shiqiao village took a rapid development and the villagers have more income to build new houses. Corresponding to the construction requirements of demonstration villages and the new village planning, the village committee carried out the new ecological construction based on the clean energy. In this survey, there were 205 household selected as samples, among which 76% of all the samples were built before 2000, 24% built after 2000.

(3) Ligeng Village

Ligeng village is located in Anji county, near to Hangzhou area, consisting of Ligeng, Limin and Licun, 120 households and 400 residents. It has beautiful environmental resources with mountains surround. In these years, its economic development has been dominated by rural tourism. In this survey, there were 50 household selected as samples, among which 70% of all the samples were built before 2000, 30% built after 2000.

3-2-2 Survey Content

(1) The following contents were carried out by questionnaire survey:

● Basic information of rural households

Including the number of family, the permanent residential population. These questions were mainly indicated in the survey on Ligeng village.

● Basic information of rural residential buildings

Including building style and features, construction quality, build time.

● Building material and construction of envelopes

Including the details of building structure, material and construction of envelopes.

(2) The following contents were carried out by field measurement

● Indoor thermal environment

Including indoor temperature, humidity and PMV value calculation. This measurement was carried out on a typical rural house located in Ligeng village.

3-3 Questionnaire Survey results

3-3-1 Features of Households

In Ligeng village, most frequent size is 5 people per household, consisting of two older couples, two young couples, and a child, accounting for 25.5% of the households surveyed. A large amount of the labor force goes out for work in ordinary villages, and only return home on holidays or Spring Festival. The migrant workers take up a high proportion of the total population in a family. The permanent residential population of ordinary households is about two people per household, accounting for 50.3% of the house surveyed. Most of them are older couples.

3-3-2 Family Income

In Ligeng village, for ordinary households, the main source of family income was from migrant laborers working in big cities. Ligeng village which is close to the big cities, the primary industry accounts for 65% of total family income sources, including the production and processing of traditional primary industry, such as high mountain tea, Chinese chestnut, bamboo and bamboo products. For tourism households, rural tourism business has replaced the primary industry, becoming the main income source. For ordinary households, 9% of them was below 50,000; for tourism households, there is no households below 50,000Yuan in surveyed objects.

3-3-3 Built Time

In these surveyed samples, most of rural houses were built before 2000, among which a small part was built before 1990. Fig.3-3 shows the built time distribution of Pu’er village and Shiqiao village. Fig.3-4~6 present the typical rural houses built in different time in these three villages.

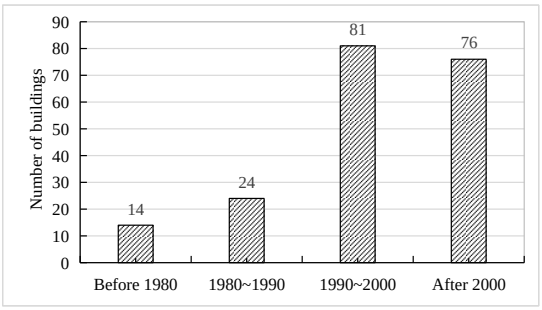

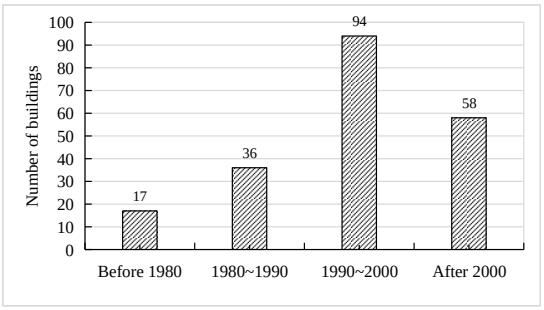

(a) (b)

Fig.3-3 Built time distribution: (a) Pu'er village; (b) Shiqiao village.

(a) Built before 1980 (b) Built in 1980s~1990s (c) Built after 2000

Fig.3-4 Rural houses of Pu'er village.

(a) Built before 1980 (b) Built in 1980s~1990s (c) Built after 2000

Fig.3-5 Rural houses of Shiqiao village.

(a) Built before 1980 (b) Built in 1980s~1990s (c) Built after 2000

Fig.3-6 Rural houses of Ligeng village.

The features of the above three types of rural houses are summarized and introduced as follows.

(1) Traditional vernacular buildings before 1980s

Chinese traditional buildings use "Jian" (the space surrounded by four pillars) as the basic unit. Normally there are more than three “Jian” in historical and cultural buildings. Villagers usually use local materials to construct their house, such as clay and stone. In this stage, the traditional vernacular building was only one story tall too, about 2.6-3m. Traditional vernacular building plane is relatively simple. The number of “Jian” is always more than three, some are more than ten.

(2) Traditional vernacular buildings in 1980s to 1990s

In this stage, these buildings were made of red solid bricks, a popular material. In addition, modern materials appeared in the countryside gradually, such as steel and concrete. As a result, the architectural form is also changed. Similar to the buildings built before 1980s, the interior facilities are not perfect, and do not have sanitary facilities. The building plans still keep the traditional "Jian" as unit, and the hall (living room) is still the center of the whole building. The common plan has several types, including "line" type, "L" type, "bracket" type and so on. Among them, "—" type is the most common. More floors are included, usually two or three stories, with two stories being more common. The first floor is higher than others for the sake of sacrificial activities in the hall, with a height of 3.2m ~ 3.9m. In addition, there are a kitchen, a bedroom for older family members and production houses on the first floor. The attic on the second floor has evolved into a living space, the height from floor to roof about 3.0m ~ 3.5m. Besides the pitched roof, there are also flat roofs. The houses often include a corridor, which is used for airing clothes and for passage.

(3) Modern buildings after 2000

After the 2000s, with the further development of the rural economy, urban buildings have had a great influence on rural buildings. Migrant workers and rural construction teams have brought new building designs to the villages, so rural residential buildings are more diverse, functional and complete to meet the needs of modern life.

Modern rural residential buildings present the trend to multi-layer, but due to the control of the government planning, the rural residence is usually 2~4 stories. The height of the first and second floor is about 3.0 ~ 3.5 m; the third floor is 2.9 m; the height of the ridge is about 2.8 m. The first floor is mainly the public space, including dining-room, living room, kitchen, garage and bedroom for the older. On the second floor, there are bedrooms, study room, guestroom and living room.

3-3-4 Construction and materials

(1) Pu’er village

In terms of Pu’er village, 13% of the houses were timber or half-timber construction, 50% were brick and concrete structure, and 38% were frame structure.

- The wall materials: 4% were made by rammed earth or wood; 87% were made by solid clay

brick; only 3% were made by light and porous new material.

- The thickness of outer wall: 64% was 200mm, 30% was 120mm, and 6% was 240mm.
- The roof style: 11% was flat roof, 37% was pitched roof, 51% was composed of flat and pitched roof.
- The roof materials: 35% of pitched roof were made of insulation panel; 24% were made of concrete or glazed tiles.
- Insulation design: 12% of the external walls had insulation materials, and the proportion of the pitched roofs with insulation was 73%.

(2) Shiqiao village

In terms of Shiqiao village, 10% of the houses were timber or half-timber construction, 72% were brick and concrete structure, and others were frame structure. For the materials, 11% were made by rammed earth, bamboo or wood, 85% were made by solid clay brick, and only 4% were made by concrete block, and no houses used new materials.

- The wall materials: 11% were made by rammed earth, bamboo or wood; 85% were made by solid clay brick; only 4% were made by concrete block, and no houses used new materials.
- The thickness of outer wall: 85% was 240mm, 15% was 120mm.
- The roof style: 7% was flat roof, 84% was pitched roof, 9% was composed of flat and pitched roof.
- The roof materials: 68% of pitched roof were made of Chinese-style tile; 31% were made of concrete and 1% was asphalt shingle.
- Insulation design: all the external walls had no insulation materials, and the proportion of the pitched roofs with insulation was 44%.

3-3-5 Window to Wall Ratio, Form Coefficient of Building

(1) Window to Wall Ratio (WWR)

Window-to-wall ratio (WWR) refers to the ratio of the transparent part of the window and balcony door on the outside wall toward the same direction in the building to the total area of the outside walls in the same direction Wall (including the area of the transparent part of the window and balcony doors on the wall)[3].

For the dwelling built before 1980s, the WWR is normally small. In the east, west and north orientation, the average WWR is only about 0.03. The WWR is larger in south, where it is about 0.07. In terms of traditional vernacular buildings built in 1980s to 1990s, the average WWR of south and north window is no more than 0.2, and that of east/west is no more than 0.1. For the newly built buildings. tend to be symmetrical along a middle axis with the courtyard and central room. However, the forms of modern buildings are various, and window forms are more diverse. In order to get better lighting, the WWR is larger than traditional buildings, especially in the west. The average WWR of east and west is 0.05 and 0.08 respectively. The average WWR of south and north is larger, which is 0.12 and 0.14 respectively.

(2) Form Coefficient

Shape coefficient of building refers to the ratio of the building surface F0 in contact with the outdoor atmosphere to the building's volume surrounded by the outdoor atmosphere V0.

3-4 Field Measurement

3-4-1 Building description

This building was newly built in 2008 (see Fig.3-7). Most of the residential buildings constructed at this time were built by the villagers who went to work in urban areas with higher income. The basic features living information of this building is:

- Layout: on the first floor, the center space was the hall connecting the bedrooms, living room, toilet and kitchen; two bedrooms were arranged facing to north and south respectively; the balcony was adjacent to living room, lying in the south.
- Occupants: 1 elder, 1 couple and 1 child (undergraduate, not at home when taking measurement).
- Measurement conditions: the bedroom was unoccupied and door closed all day; the living room was occupied with door opened from 8:00 to 13:00.
- Construction and materials: concrete frame structure; empty clay brick wall (see Fig.3-8).
  - Wall: 240mm hollow clay block, U=1.64 kWh/m^2•k.
  - Roof: slop roof with cement tiles (see Fig.3-9);
  - Window: aluminum alloy window frame; one layer glazing; U=4.6 kWh/m^2•k.
  - Base： the first floor was constructed by gravels and cobblestones, paved with cement; precast slabs were used as empty space for the purpose of dam proof.

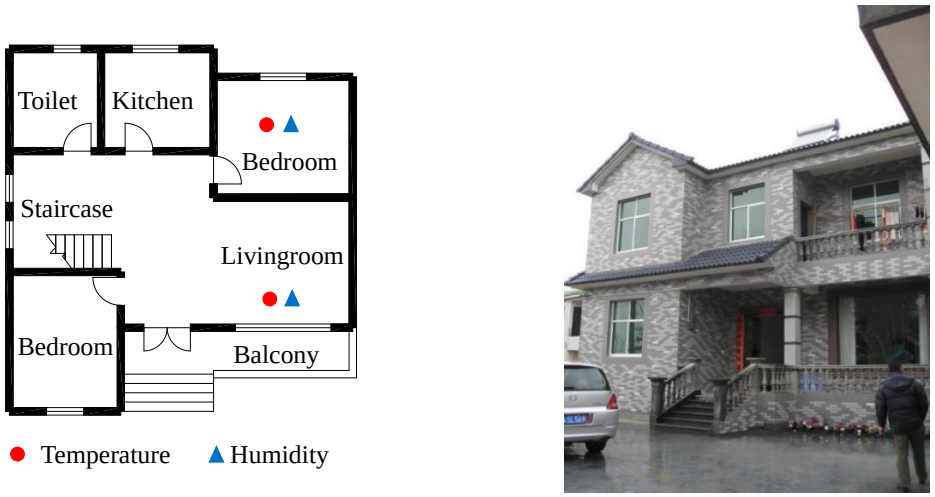

(a) (b)

Fig.3- 7 Photos of the tested dwelling: (a) Plan; (b) Overview

Fig.3-8. Hollow clay block

Fig.3-9.Cement roof.

3-4-2 Experimental setup

The thermal environment monitoring was carried-out in winter (20th January, 2011), and the monitored data includes the air temperature, relative humidity, radiation temperature, and wind speed, were recorded automatically with a 10 min sampling time. The meters are shown in Fig.3-10 ~ 3-12, and the technical specifications of the instrument including the accuracy, resolution and response time are shown in

Table.3- .

Fig.3-10 TES 1361C meter

Fig.3-11 JTR07 meter

Fig.3-12 JTR04 meter

Table.3- 1 Monitored data and technical specifications of measuring instrument.

Monitored parameters	Instrument name	Measurement range	Accuracy	Resolution
Air temperature	TES 1361C	-20℃ ~ 60℃	±0.8℃	0.1 ℃
Relative humidity	TES 1361C	10% ~ 95%	± 3% RH	0.1% RH
Wind speed	JTR07 meter	0.05 ~ 5m/s	±0.04m/s	0.01 m/s
Radiation temperature	JTR04 meter	-20℃ ~ 125℃	±0.5℃	0.1 ℃

3-4-3 Measurement Field

Fig.3-13 shows the 2 monitored points placed in the north bedroom and the living room respectively; all points of measurements points were set at 1.5 m above the ground level. The outdoor data logger was shaded using appropriate devices during the whole measurement.

(a) (b)

Fig.3-13 View of the rooms showing the data monitoring locations:
(a) bedroom facing north; (b) living room

3-4-4 Monitoring Results

Fig.3- 14 illustrates the air temperature profiles in the studied house. It can be observed that the outdoor temperature fluctuated widely in the whole day due to the rainy-sunny day. It increased from 1.1 ℃ at 6:00 to 19.4 ℃ at 12:00, while the living room temperature simultaneously rose from 6.8 ℃ to 11.1 ℃. Because the door opened during 8:00 ~ 13:00, temperatures in living room presented an obvious fluctuation. In terms of bedroom, the temperatures were relative steady and influenced a little when door open, which were slightly warmer than living room. In addition, the biggest temperature difference between bedroom and outdoor was 8.2℃, occurring at 6:00, when the outdoor temperature was only 1.1℃. At 13:00, the outdoor temperature was increased for the sunny time, 7.5℃ higher than living room.

Fig.3- 5 confirms the fact that the outdoor relative humidity varied from 24.4% to 99.9% with a range of 75.5% during monitoring time, due to the weather changing - from rainy day to sunny day. While for the bedroom, it only varied from 49.5% to 83.2% (33.7% variation range). The relative humidity of the living-room varied in the same range.

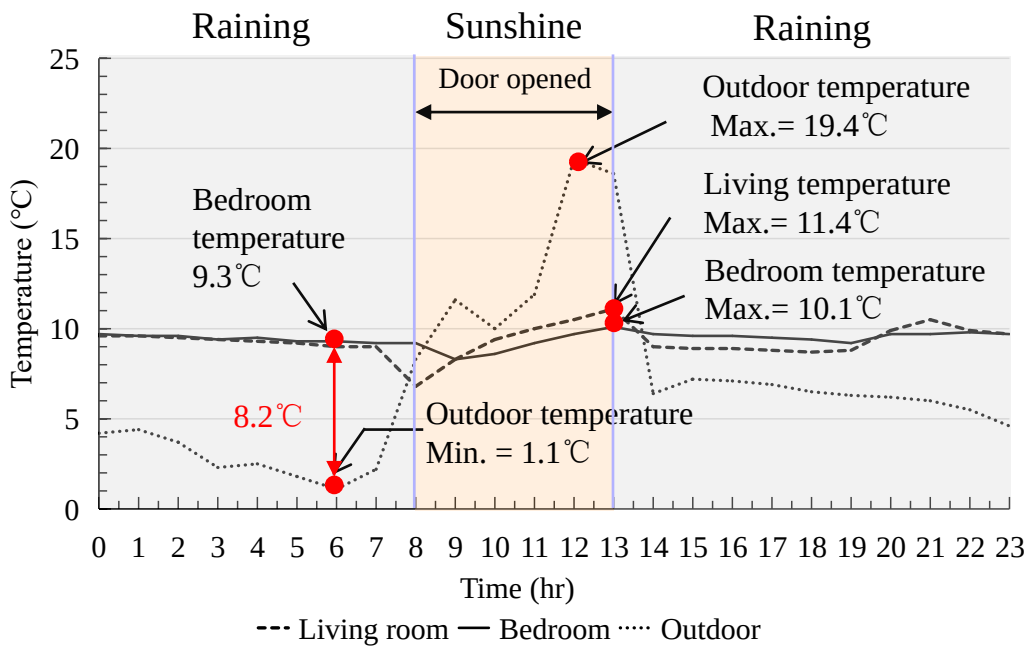

Fig.3- 14 Variation of air temperature at different monitoring points during wintertime.

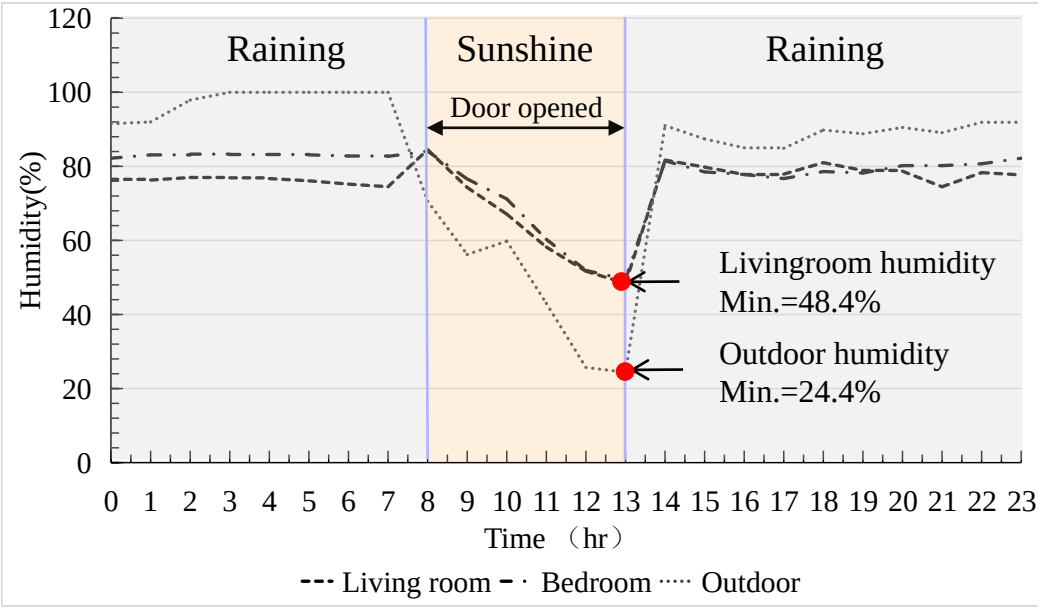

Fig.3- 15 Variation of air relative humidity at different monitoring points during wintertime.

Fig.3-16 shows the PMV (Predicted Mean Vote) values by calculation according to the monitoring results. During monitoring time, the PMV values of bedroom were in the range of -1.32~-1.57. In the two hours of from 19:00 to 21:00, PMV values were below -1.5. It could be found that the residents living in bedroom would feel cool in 8% time of the whole day.

Fig.3-17 shows the PMV (Predicted Mean Vote) values by calculation according to the monitoring results. During monitoring time, the PMV values were in the range of -1.19~-1.84. In the two hours of from 7:00 to 9:00, PMV values were below -1.5 due to the door opened. It could be found that the residents would feel cold in 8% time of the whole day in living room.

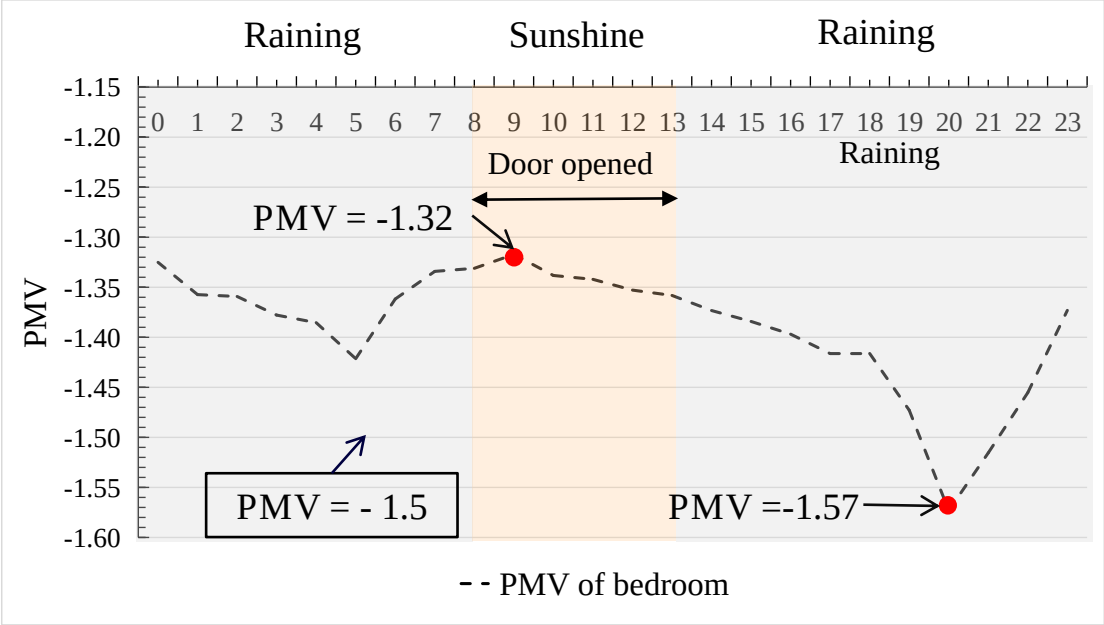

Fig. 3-16 PMV value of bedroom

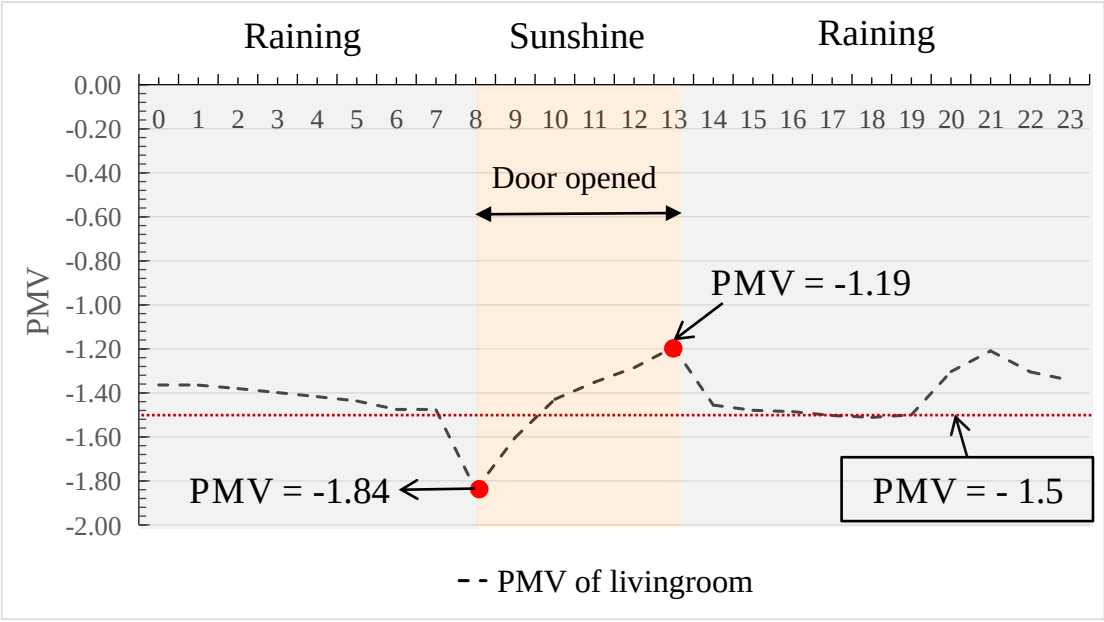

Fig.3-17 PMV value of living room

According to the results, the living room facing to south was not warmer than the bedroom, firstly due to the reason that the living room is an open space, not easy to keep warm inside, secondly for the door opened for 5 hours. And the thermal comfortable value of bedroom was not high although the door closed all along, attributed to the none of insulation design for the envelope. By the way, the plane layout of this building was not quite reasonable, should be arranged for the consideration of solar energy usage.

3-5 Summaries

Based on the electricity energy situation in Hangzhou rural residences with a close relationship of more and more air conditioners used for heating and cooling, a survey on the basic construction information and field measurement on thermal environment about rural houses were carried out from 2009 to 2015 in the villages of Hangzhou rural area.

From the survey results, the rural residential buildings of Hangzhou have the following situation and characteristics:

(1) 58% of the surveyed rural houses were built in 1980s ~1990s; modern buildings were usually built after 2000, occupied 33%

(2) For the building construction, 63% were brick and concrete construction, and the proportion of frame construction was 23%.

(3) For the wall materials, 86% were made by solid clay brick; 57% had a thickness of 240mm, the others thickness was 200mm or 120mm; 94% in the house had no insulation consideration for the walls.

(4) For the roof style, 62% were pitched roof, and 29% were flat-pitched.

(5) For the roof materials, 60% were considered with insulation method, and 40% were not.

(6) The measurement results in a newly built dwelling indicated that when the outdoor temperature was at the lowest value, the temperature difference between bedroom and outdoor was about 8.2℃; when outdoor temp. reached a maximum value, the indoor temperatures were still at a lower level. By calculation, the PMV value presented that it was a little cool during the whole monitoring day in winter time.

Reference

[1] Wang, M.Y. Gao, W.J. Survey on rural housing and new materials application in Zhejiang,

[2] http://www.hzstats.gov.cn

[3] The Architectural Design & Research Institute of Zhejiang University, Zhejiang province Institute of Architectural Design and Research, Zhejiang Institute of Meteorological Science etc. Design standard for energy efficiency of residential building in Zhejiang province (DB 33/1015-2015). China Planning Press, Beijing, 2015.

Chapter Four: Passive design and optimization on an experimental house

4-1 Introduction

In the Chapter Three, a survey on the rural residences in Hangzhou area were carried out and the situation and problems were summarized. It can be found in the results that Hangzhou is economically developed, but the standard and construction of rural housing is still backward. Almost all the dwellings were built by the villagers spontaneously, lacking of reasonable design and scientific guidance. Furthermore, more and more new buildings are under construction which will lead to huge energy and environment problems. Thus, it is quite necessary and urgent to promote the energy efficient technologies in rural area.

In 2002, the *Design Standard for Energy Efficiency of Residential Building in Hot Summer and Cold Winter Zone - Implementing Rules of Hangzhou Area* was issued by Hangzhou government as the first energy efficiency standard. Then, the first public building design standard for energy efficiency in this area was issued in 2005. The latest standard for hot/summer & cold/winter zone was published in 2010, namely JGJ 134-2010; and the latest one for Zhejiang province was issued in 2015. Comparing the main indicators in new standards of China and other counties (see Table 4-1), it can be seen that the gap between the current standard and the developed countries is relative large.

Table.4-1 Comparison of U-values for envelope in different countries.

Country	U-Value ($W/m^2 \cdot k$)		
	Wall	Roof	Window
China-HSCW (JGJ 134-2010)	0.8~1.5	0.5~1.0	2.3~4.7
China-Zhejiang (DB 33/1015-2015)	0.8~1.5	0.5~0.8	1.9~2.8
America (IECC2015)	0.34~0.77	0.17	1.99
Germany (ENEV2001)	0.35	0.25	1.5
Germany (ENEV2009)	0.28	0.2	1.3
Passive House	0.15	0.15	1.3

In this study, combining the features of Hangzhou rural house, the passive design strategies incorporated in an experimental building was put forward firstly. By using Ecotect software, the insulation thickness of building's envelope and the optimum U-value of windows were optimized and determined. In addition, the effect to energy consumption in the building with shading devices was to be compared. Finally, the construction of the building was introduced.

4-2 Passive design strategies

Hangzhou is a typical city in the hot-summer and cold-winter zone. According to the statistic[1], the average temperature in July was about 30.6℃ in 2006. Especially in July and August, the solar radiation is at the peak, while the maximum temperature occasionally exceeded 40℃ and the minimum was commonly about 28℃ in the view of history after the rainy season, which is an important factor causing the extreme clear and hot high temperature event, leading to the poor indoor thermal environment in the summer of Hangzhou. On the other hand, the average temperature in January is about 4℃ and the relative humidity was about 80%, resulting in the wet and cold indoor environment in winter.

Based on the above analysis, the design strategies response to the Hangzhou climate should be concluded as following:

1) to largely gain solar radiation energy and highly enhance envelope insulation in winter;

2) to induce nature ventilation efficiently and control the amount of solar radiation admitted into the room by using appropriate shading devices in summer.

For the reason of small temperature difference between indoor and outdoor of Hangzhou, the basic design strategies for buildings should be as the following: appropriate shape, not too tight; striving for solar energy as far as possible, avoiding negative orientation; considering natural ventilation and shading design in summer.

Thus, a small single-floor house with experimental nature was designed. The plane, side elevation and design sketch are shown in Fig.4- ~ Fig.4-3: there were three rooms facing to the south, named as Room 1, Room 2, and Room 3, which were set to the main rooms who have comfortable requirement, such as living room, bedroom or study room. The other two rooms were named as Room 4 and Room 5, set to the auxiliary rooms without comfortable requirement, such as kitchen and storeroom.

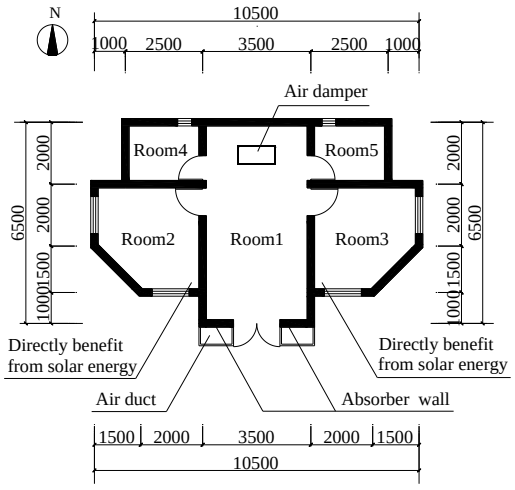

In Room 1, the external wall was designed with Trombe wall system (see Fig.4-5 & Fig.4-6), introduced in section 2-3-3-2 of Chapter Two. The other internal and external walls were made by aerated concrete block (see Fig.4-7). In Room 2 and 3, bigger size windows were designed for gaining more solar energy directly in winter. For the roof, Room 1 was designed with pitched roof, with the best angle of gaining solar energy in Hangzhou areas, namely 30°, and Room 2 & 3 used

horizontal roof. The structure method of the roof is shown in Fig.4-8.

Otherwise, an underground wind tunnel was set below the floor of Room 1, connected to Room 1 with six holes in the floor. Above the roof of Room 1, a towering device just like “solar chimney”, introduced in section 2-3-4-2 of Chapter Two, was allocated for inducing the indoor air flow, seen in

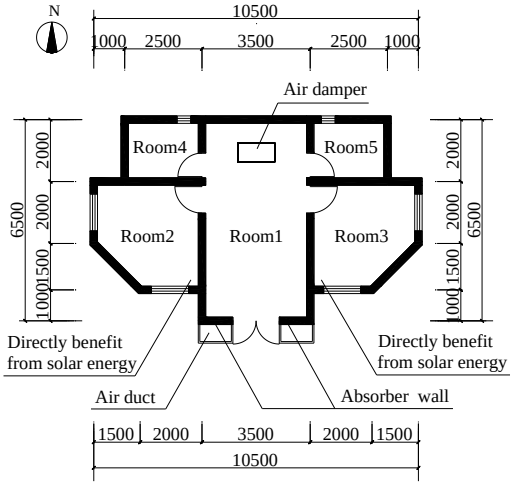

Fig.4-: when the air surrounding the vent set on the top of “solar chimney” was heated enough in summer, the indoor air flow inside the room will rise up, inducing the cool air outflow from underground tunnel. Thus, passive ventilation will be realized combining use of solar chimney and wind tunnel system.

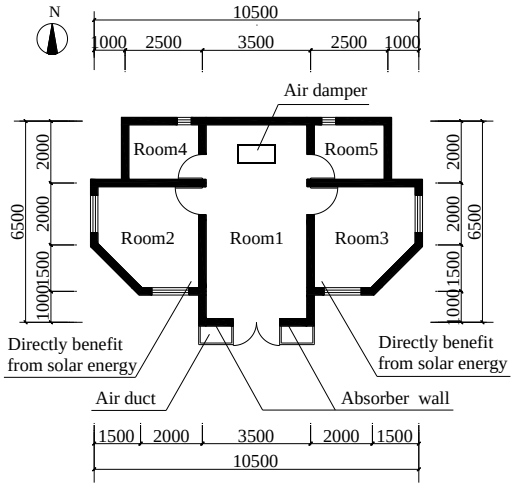

Fig.4-1. Plane

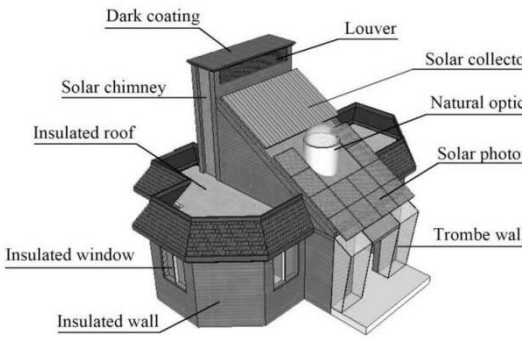

Fig.4-2. Design sketch

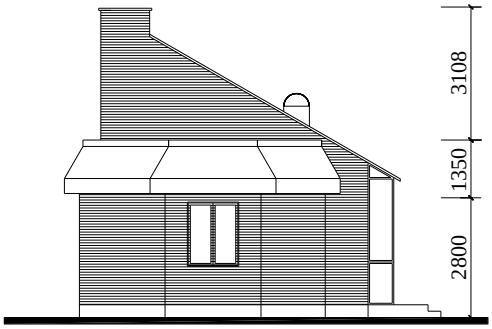

Fig.4-3. Side Elevation

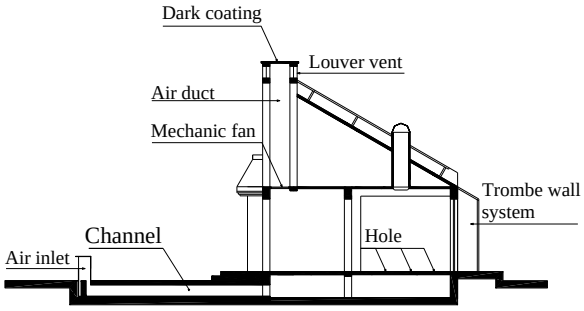

Fig.4-4. The section sketch of the passive ventilation system

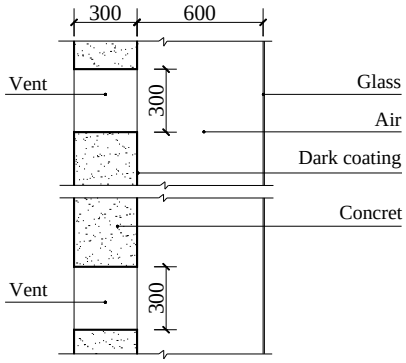

Fig.4-5. The section of the Trombe wall

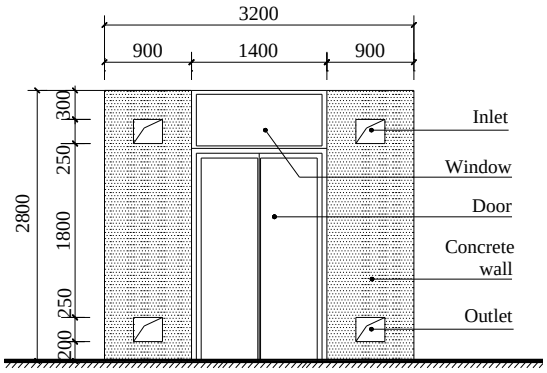

Fig.4-6. The facade of the Trombe wall

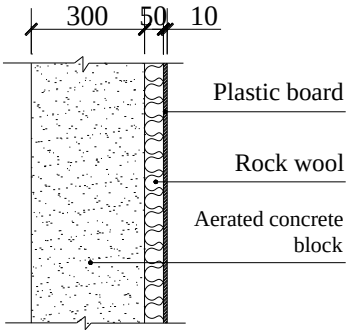

Fig.4-7. The construction details of the insulation system of the wall.

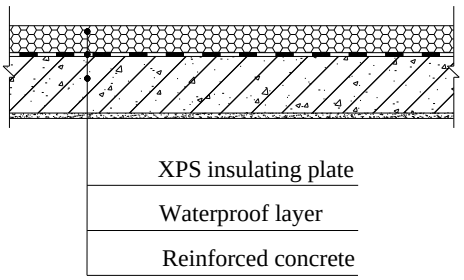

Fig.4-8. The construction details of the insulation system of the roof.

4-3. Tool and Methodology

Computer simulation is a useful method for architects and engineers to simulate and analyze building performance earlier in the design process. The indoor thermal environment of the

residences in Turpan District of Xinjiang was simulated and analyzed by using Ecotect software in the reference[2] to evaluate the thermal performance of primary scheme related to the solar radiation, heating consumption and indoor comfort level. Reference[3] carried out a simulation analysis of indoor hourly temperature towards a library building for the insulation material optimization.

The Ecotect software is a useful tool to analyze the variable physical environment and predict the energy consumption through simulating the building, for the further research and optimization on the preliminary scheme. This software was developed for architects and engineers to carry out sustainable analysis on variable physical environment during the conceptual design, including: thermal environment (heating/cooling load, energy consumption simulation, hourly temperature analysis and so on); wind environment (nature ventilation, solar heating and so on); lighting environment (sky illumination, mechanical lighting, nature lighting); sound environment (noise analysis, acoustical design); sunlight environment (sunlight reflector design, shading devices design); economic analysis (cost estimating, resources consumption analysis); environmental impact and visibility analysis[4].

The simulation method is illustrated in Fig.4-9. Firstly, establish the building model (see Fig.4-) by Ecotect software according to the building information listed in Table.4-2. Then, call for the Hangzhou weather data in typical year (database in software), and set air conditioning parameters of Room1~3 (see Table.4-3). Next, input the assumed thermal performance parameters for the building structures (see Table.4-4). The last step, enable the thermal load simulation module to calculate annual heating and cooling load. Through adjusting variables values, including insulation thickness, U-value of window, and shading device style, to determine the optimum design corresponding to relatively lower annual thermal load.

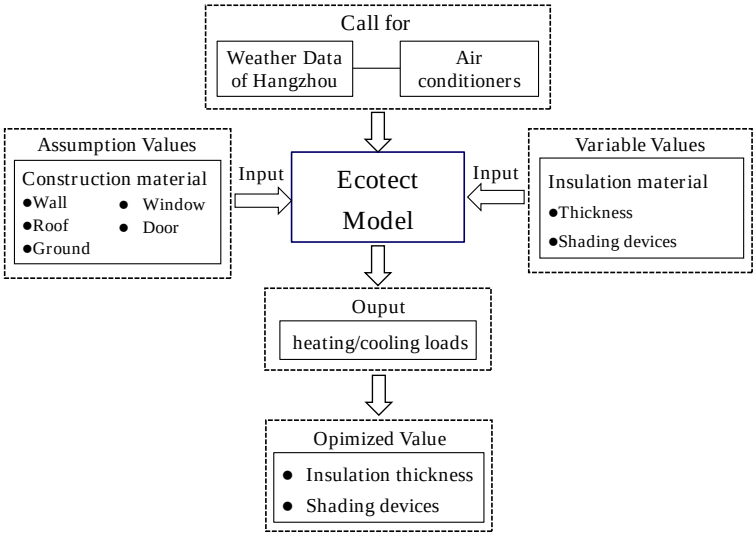

Fig.4-9. Simulation flow

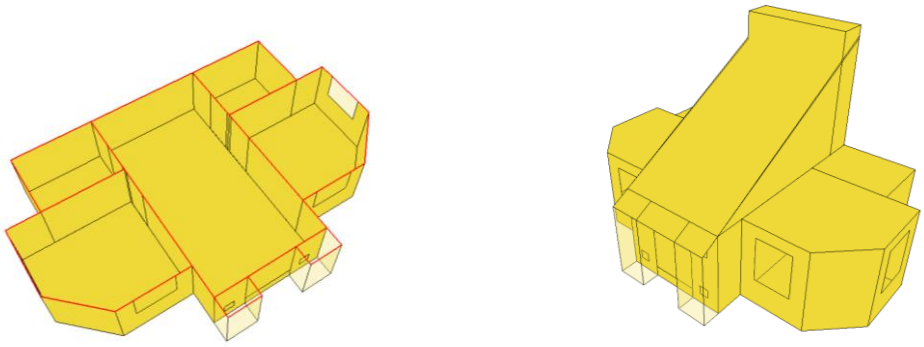

a. b.

Fig.4-10. Simplified model:（a）interior;（b）overview

Table.4-2. Design information

Floor area (m^2)		58.9
Net height (m)		2.7
Construction height (m)		7.2
Room1 (m^2)		22
Room2 (m^2)		9.6
Room3 (m^2)		9.6
Room4 (m^2)		4.9
Room5 (m^2)		4.9
Window size (height x width)	South	1.5 x 1.2
	North	0.6 x 0.6
	East	1.5 x 1.2
	West	1.5 x 1.2
Window-wall ratio	South	0.14
	North	0.02
	East	0.09
	West	0.09

Table.4-3. Operational parameters of equipment.

Room	Active System	Efficiency	Comfort band		Hours of operation	
			Lower band	Upper band	Week days	Week ends
Room1	Full air conditioning	95%	16℃	26℃	22:00 - 8:00	24h
Room2,3	Full air conditioning	95%	16℃	26℃	22:00 - 8:00	24h
Room4	Nature ventilation	——	——	——	——	——
Room5	Nature ventilation	——	——	——	——	——

Table.4-4. Characteristics and thermal properties of materials used in the design building.

Structural element	Structure and construction method (from outside to inside)	U-value ($W/m^2 \cdot k$) / Solar Heat Gain Coefficient
Wall 1	plastic board（10mm）+ rock wool（__mm）+ aerated concrete block（300mm）+ cement-lime mortar（8mm）	0.62
Wall 2	plain concrete（300mm）	2.60
Roof	XPS board（50mm）+ reinforced concrete（100mm）+cement-lime mortar（8mm）	1.23
Ground	packed soil（300mm）+ gravel pebble（400mm）+air layer（500mm）+ fine aggregate concrete（100mm）+ cement mortar（20mm）	0.47
Window	Single pane of glass with aluminium frame (no thermal break).	5.4 / 0.75
Door	solid wood door (40mm)	2.7

4-4 Results and discussion

4-4-1 Optimization of envelope insulation system

The main envelope insulation system including external wall，roof and windows plays the important role on reducing thermal energy and improving indoor thermal environment. For the purpose of obtaining the minimum energy demand by relative lower construction cost, use the Ecotect software to simulate the annual thermal loads under variable design conditions, then to determine the optimum insulation thickness of wall and roof, whose input variables are listed in Table.4-1. By the same way, the best U-value ($kWh/m^2 \cdot k$) of window was got when it decreasing from 5.4 to 1.0. It was assumed that the thermal performance of other components remained unchanged while the any one of the components was investigated on influencing the energy loads during the process of simulation.

Table.4-1. The calculated results of different U-value for external wall and roof.

External wall Structure (from outside to inside)	Insulation layer thickness (mm)	U value ($W/m^2 \cdot k$)	Roof structure (from outside to inside)	Insulation layer thickness (mm)	U value ($W/m^2 \cdot k$)
Plastic board (10mm) + rock wool (d mm) + aerated concrete block (300mm) + cement-lime mortar (8mm)	0	0.62	XPS board (d mm) + concrete weight (100mm) +cement-lime mortar (8mm)	0	1.23
	10	0.53		10	0.96
	20	0.46		20	0.71
	30	0.40		30	0.56
	40	0.36		40	0.46
	50	0.33		50	0.40
	60	0.30		60	0.35
	70	0.27		70	0.31
	80	0.25		80	0.27

90	0.24	90	0.25
10	0.22	100	0.23

4-4-1-1 Insulation thickness of the wall and the roof

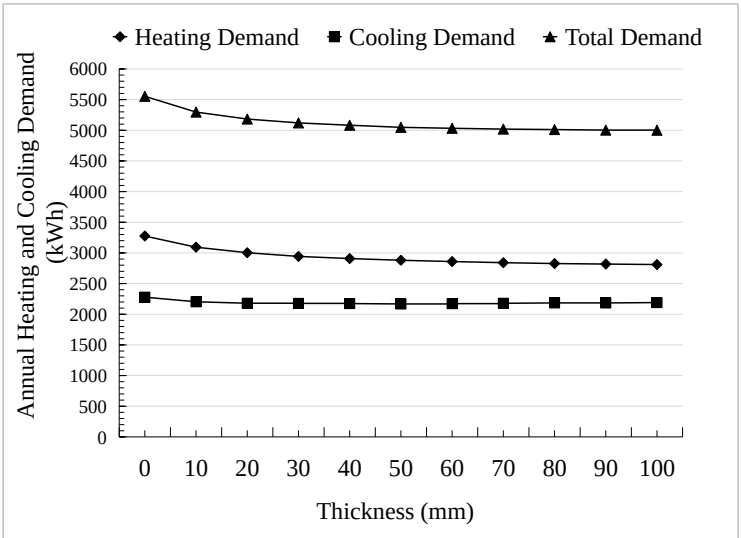

0 (a) shows that the energy consumption presents roughly decreasing tendency as the thicknesses of insulation layer constructed on the wall changing from 0mm to 100mm respectively: the heating demand of the external wall insulated by rock wool materials declines significantly by 14.2% (i.e. from 3275.7 kWh to 2810.3 kWh) compared to the cooling demand from 2278.5 kWh to 2190.5 kWh, only by 3.9%. It can be observed that total annual energy consumption mainly influenced by heating demand has a general reduction of 10% (i.e. from 5554.2 kWh to 5000.9 kWh), the profile of which is relatively obvious from 0 mm to 50 mm, but begins to level off after that.

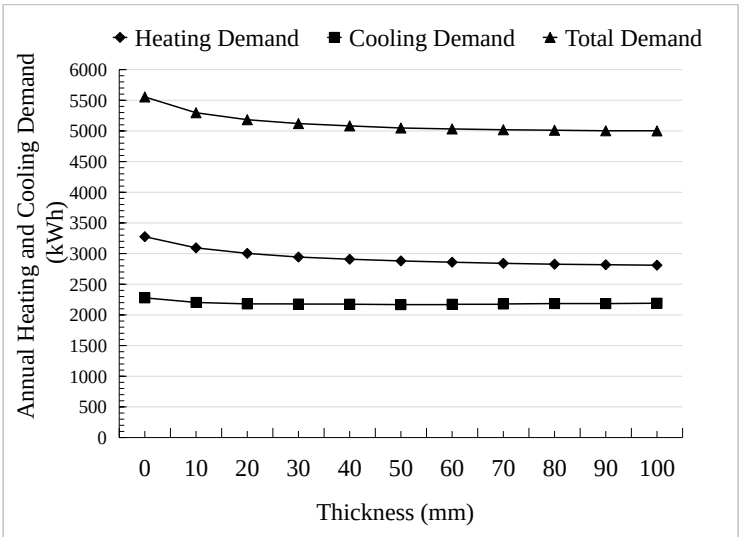

(a) the different insulation thickness of the wall

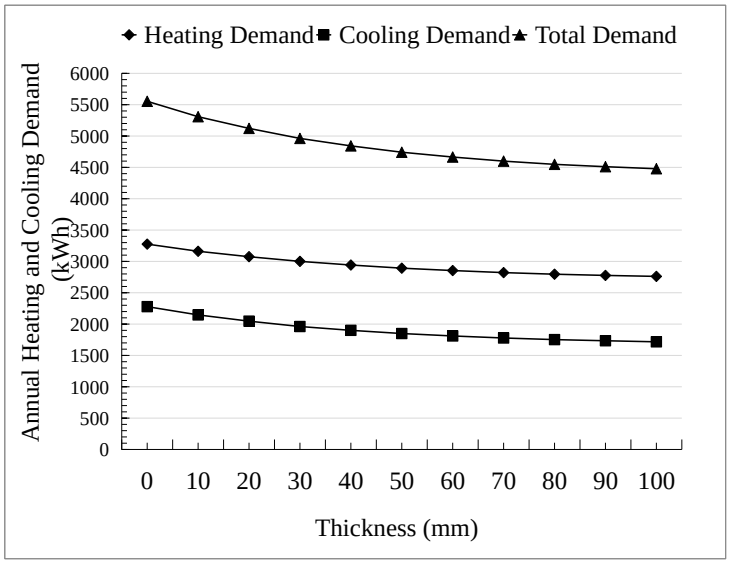

Fig.4-10. The profile of the annual energy demand changing with:
(b) the different insulation thickness of the roof

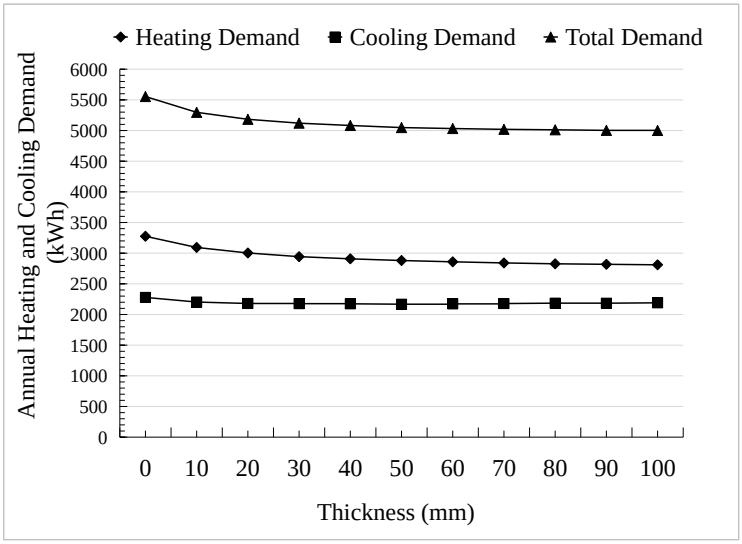

From the simulation result (see

0 (b)) about roof insulated by XPS board, the cooling demand changes obviously with a 24.6% reduction from 2278.5 kWh to 1717.3 kWh, relative to the heating energy consumption dropping down by 15.7% (i.e. from 3275. 7 kWh to 2761.0 kWh); it can also be seen that the annual total demand decreasing by 19.4% from 5554.2 kWh to 4478.3 kWh is influenced greatly by the cooling demand change, and the value begins to drop slowly when the insulation lay reaches to the thickness of 70mm. According to the result, roof insulation is the main factor considered to defend solar radiation in summer, which can be explained by the fact that the most solar radiation access is accepted by horizontal plane in Hangzhou area.

4-4-1-2 U-value of the window

The U-value changing profile of window, illustrated in

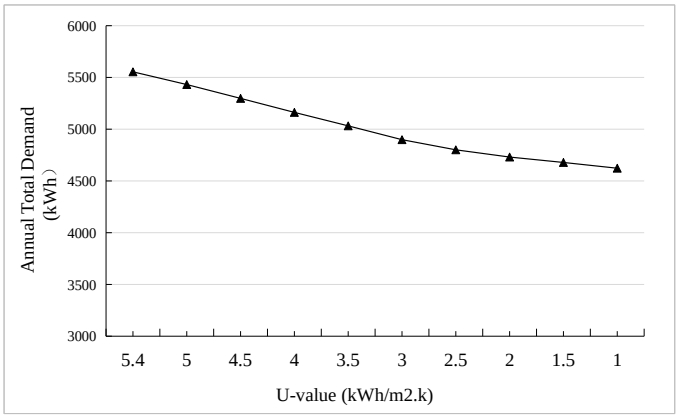

Fig.4-1, show that: as the U-value changing from 5.4 to 1.0, the annual energy demand has an over declination by 16.8%. When the U-value changing from 5.4 to 2.5, the total energy demand drops by 13.6%, and after that the decreasing tendency become slow down, with a reduction of 3.7% from 2.5 to 1.0. Considering the technical economy, the optimum U-value of window was determined as 2.5 kWh/m^2·k.

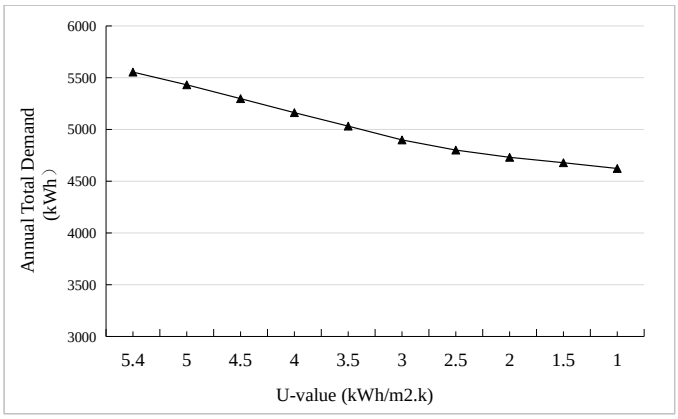

Fig.4-11. The profile of the annual energy demand changing with different U-value of the window

According to the above analysis, the optimal thicknesses of insulation layer for wall and roof were decided as 50 mm and 70 mm respectively. In terms of windows, the U-value was finally considered as 2.5 (processed by double-glazing sandwich-type coated Low-E film, a 9 mm air gap layer enclosed between two 6 mm clear glass sheets and insulating aluminum profile) for the reason that has exceeded the standard of China[错误!未定义书签。], and cost economically.

4-4-1-3 Energy consumption comparison

In Hangzhou area, the energy-saving design of residential buildings are required to conform to the mandatory standard, namely *Design Standard for Energy Efficiency of Residential Buildings in Hot Summer and Cold Winter Zone* (JGJ 134-2010) [5]. Thus, it is necessary to compare the energy-saving level between the design building and the regulated building (named standard building).

According to the simulated results, the design building model was assigned with the optimum values (see **错误!未找到引用源。**). For the standard building model, its form and orientation were set the same with the design building and the thermal properties for construction materials

were assigned with the regulated values in the standard[5], indicated in Table.4-6.

Table.4-2. The optimum values for design building and the regulated values for standard building

Component		Design building		Standard building[错误!未定义书签。]	
		U-value ($W/m^2 \cdot K$) / Shading coefficient of glasses (SC_B)	Window-wall ratio	U-value ($W/m^2 \cdot K$) / Shading coefficient of glasses (SC_B)	Window-wall ratio
Roof		0.31	——	0.5	——
Wall		0.33	——	0.8	——
Window	South	2.5 / 0.75	0.14	4.0 / 0.94	0.14
	North	2.5 / 0.75	0.02	4.0 / 0.94	0.02
	East	2.5 / 0.75	0.09	4.0 / 0.94	0.09
	West	2.5 / 0.75	0.09	4.0 / 0.94	0.09

Fig.4-2 indicates that the total energy demand of design building insulated by highly efficient materials is obviously lower than that of standard building, falling down by 18.8% relatively (i.e. from 3760.7 kWh to 3054.9 kWh). The heating demand profile represents a clear decreasing tendency with 19.9% from 2156.3 kWh to 1727.5 kWh, while the cooling demand has a change from 1604.4 kWh to 1327.4 kWh, only by 17.3%. The result determined that the amount of energy reduction was made in the design building compared with the current regulation.

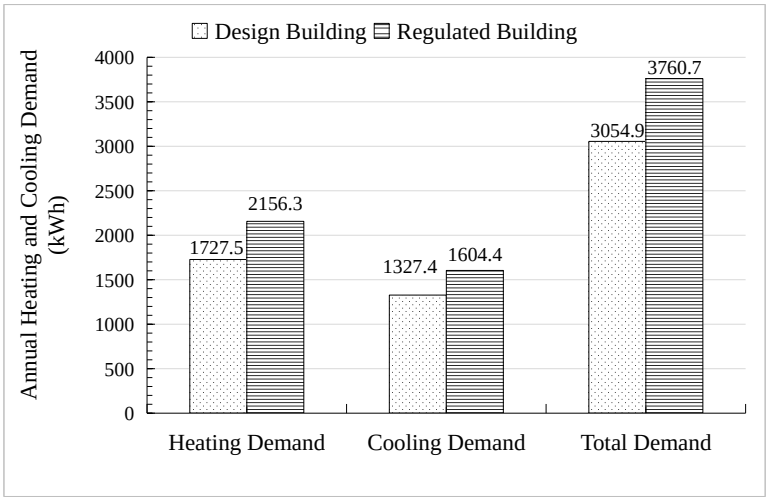

Fig.4-12. The comparison of annual energy demand of design building and standard building

4-4-2 Optimization of shading devices for windows

4-4-2-1 Shading design and calculation

Shading design is the important strategy on heat defending in summer of Hangzhou. Different

directions should have corresponding shading measures, such as baffle devices for east or west windows, horizontal rectangular devices for south windows and surrounding shade with verticals for southeast or southwest windows.

In this project, the metal baffle shading devices made of adjustable horizontal shutters were designed for the east and west external window, as shown in Fig.4-3. For the south window, the best shading devices should be the horizon sun shield due to the reason of Hangzhou location which is on the north of Tropic of Cancer. The size of shading shield can be calculated on the base of the solar altitude and azimuth angles. It is commonly thought that the horizontal size is at its the largest value when the sun moves at 12:00 in summer time. While, the wing size of the shield is decided by the azimuth angles of the sun, so the largest size should be at the sun-set time when the azimuth angle is biggest.

In Hangzhou area, much solar radiation occur at the range of 10:00 a.m. to 4:00 p.m. on each day in the period from May to September[错误!未定义书签。], which was taken as simulation conditions to be put into the Ecotect software. Then, call for the shading design module with solar database of Hangzhou, select horizontal shading device. It would be found the optimum size of shield for the south window was created automatically according to the input information, shown in Fig.4-14. Based upon the simulation result, the horizontal cantilever was decided as 450 mm. Considering the architecture style, remove the part of horizontal panel beyond the window, or change the flat shield into complex style, namely horizontal-vertical shading device (see Fig.4-15).

Based upon the above analysis, five model cases were established in software, described in Table.4-7 and Fig.4-16, to be investigated by simulation for the purpose of comparing and evaluating their effectiveness to thermal energy demand.

Table.4-7 Description of five model cases.

Case I	No shield for all windows
Case II	Horizontal shield for south window
Case III	Integrated (horizontal-vertical) shield for south windows
Case IV	Horizontal shutters for east and west windows
Case V	Integrated shield for south windows and horizontal shutters for east and west windows

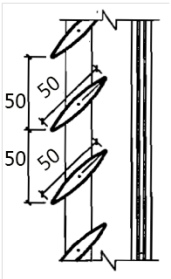

Fig.4-13. Size of metal baffle shading devices for east/west window.

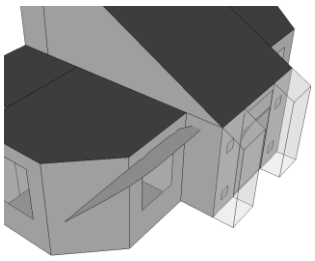

Fig.4-14. Created horizontal shading device automatically in Ecotect

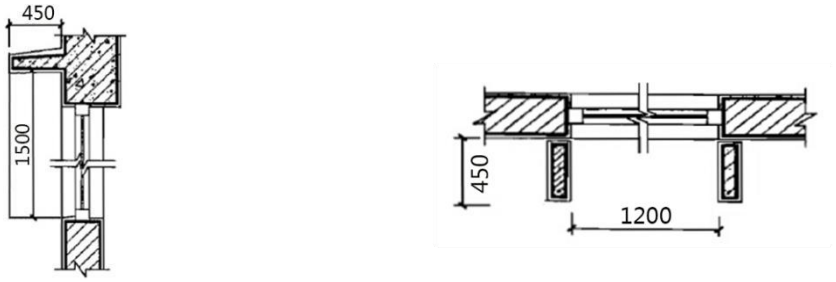

a. b.

Fig.4-15. The characteristic of surrounding shade with verticals:
(a) the cross section; (b) the flat section

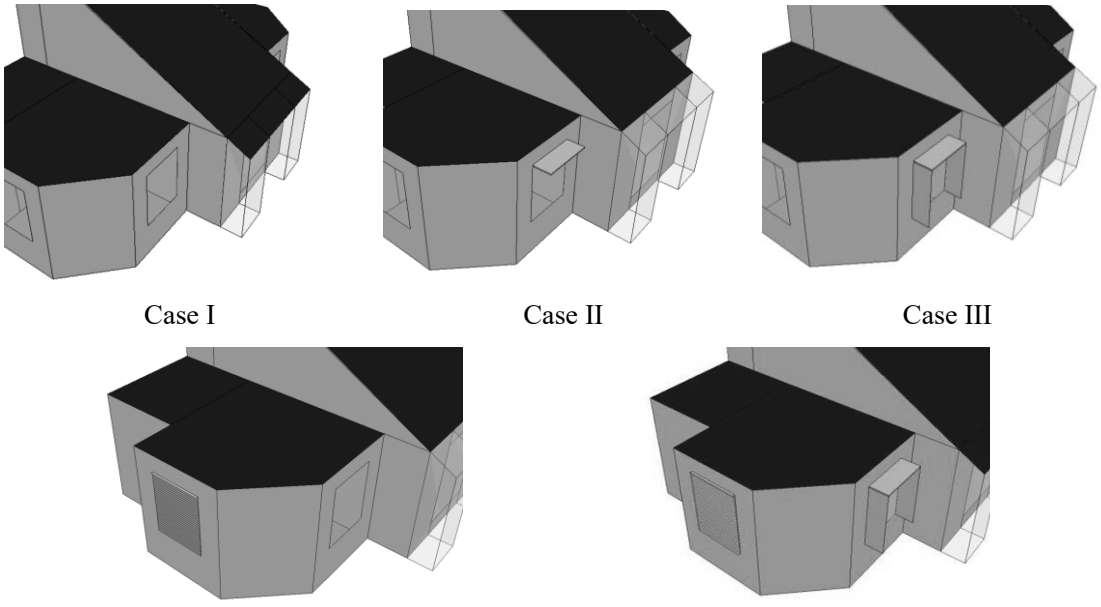

Case I Case II Case III

Case IV Case V

Fig.4-16. Three model cases

Before simulation, it should calculate the value of integrated shading coefficient (SC), which is an important indicator to evaluate the shading effectiveness including the following factors: shading coefficient of external devices (SD), shading coefficient of glasses (SC_B) and the frame-window area ratio (F_K/F_C). Formula (1)[5] indicates the calculating methods about the SC and SD. The calculating results are shown in Table.4-3~ 4-10 .

$$SC = SCc \times SD = SC_B \times (1 - F_K / F_C) \times SD \quad (1)$$

$SD = ax^2 + bx + 1$

$x = A/B$, if $x > 1$, the value is 1;

a, b — fitting coefficient;

SC — integrated shading coefficient of external window;

SD — external shading coefficient;

SCc — shading coefficient of window;

SC_B — shading coefficient of glass;

F_K — the area of the window fram;

F_C — the area of the glass;

F_K / F_C — fram and window area ratio; for the plastic steel fram, the value is 0.30, for the aluminum alloy fram, the value is 0.20

Table.4-3. Fitting coefficient (FC).

Shading type	Fitting coefficient	East	West	South

Adjustable horizontal shutters	Summer	a	0.56	0.57	—
		b	-1.30	-1.30	—
	Winter	a	0.23	0.23	
		b	-0.66	-0.69	
Fixed horizontal shield	a		—	—	0.5
	b		—	—	-0.8
Fixed vertical shield	a		—	—	0.33
	b		—	—	-0.72

Table.4-4. Calculated results of SD for east/west window

Season	SD [a]	
	East	West
Summer	0.26	0.27
Winter	0.57	0.54

(a. SD=ax2+bx+1, x=A/B; A=B=50mm)

Table.4-5. Calculated results of SD for south windows

Shading type			SD [a]
Fixed horizontal shield	A	450	0.98
	B	1580	
Fixed vertical shield	A	450	0.78
	B	1200	
Integrated shading device [b]			0.76

a. $SD=ax^2+bx+1$, x=A/B;

b. the product of SD calculated for horizontal shield and for vertical shield respectively

Table.4-6. Calculated results of SC for south windows

SC [a]	East	West	South (horizontal-vertical shield)	South (horizontal shield)
Summer	0.156	0.162	0.46	0.60
Winter	0.342	0.324	0.46	0.60

a. SC=SD×SCC, SCC=SCB×(1- FK/FC); SCB=0.75，FK/FC=0.2, then SCC=0.6

4-4-2-2 Results and analysis

(1) Shading effect of external shield for south windows

Ecotect software was used to test the shading effect of Case I ~ III. The calculated result of SD value is listed in Table.4-7, put into the software for simulation respectively. Fig.4-17 shows the energy demand simulated in three model cases. It can be seen that the cooling energy consumed by three cases has obvious difference, among which Case III with integrated shield presented a better shading effect. While in the results of annul heating demand simulation, Case I with no shading devices help to saving energy more than other cases. For the total energy demand, both

Case II and Case III showed a reduction of 2.4% relative to Case I, but still no significant effect.

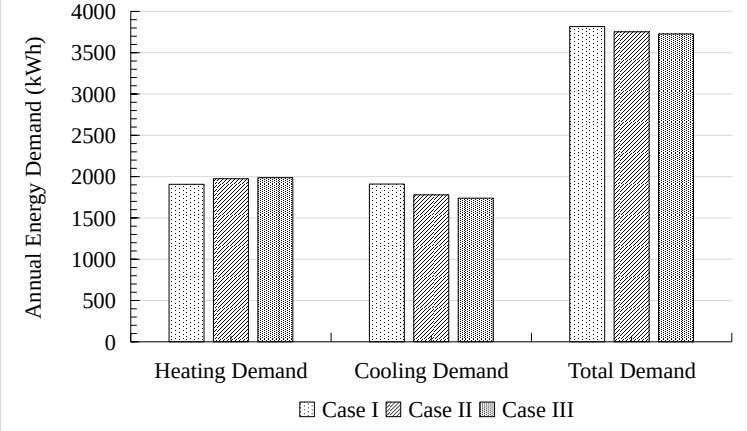

Fig.4-17 Energy demand of simulated in Case I ~ III.

(2) Shading effect of external shield for east and west windows

Ecotect software was used to test the shading effect of Case IV, taking Case I as a reference object. The calculated result of SD value is listed in Table.4-8, put into the software for simulation respectively. Fig.4-18 shows the energy demand simulated in Case I and Case IV. It can be seen that the cooling demand in Case IV decreased obviously by 11.2% relative to Case I. In terms of total energy demand, Case IV showed a reduction of 5.6%, more effective than Case II and III.

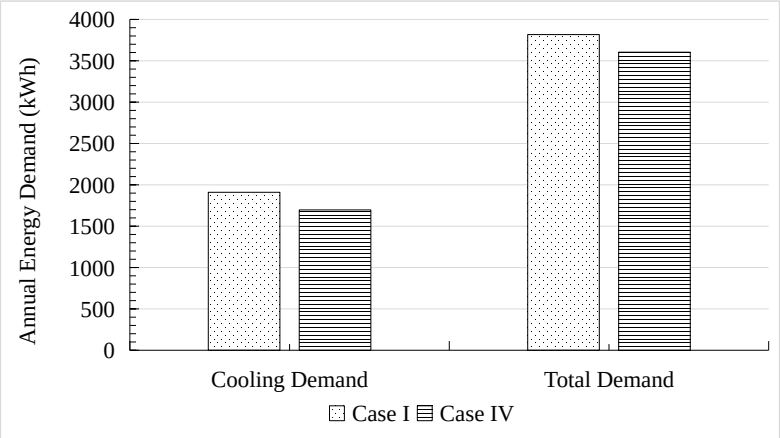

Fig.4-18 Energy demand of simulated in Case I and IV.

(3) Shading effect of external shield for all the windows

Ecotect software was used to test the shading effect of Case V, taking Case I as a reference object. The calculated result of SD value are listed in Table.4-9, put into the software for simulation respectively. Fig.4-19 shows the energy demand simulated in Case I and Case V. It can be seen that the cooling demand in Case V decreased obviously by 16% relative to Case I, and the heating demand increased by 4.2% due to the fixed external shading on south windows. In terms of total energy demand, Case V only showed a reduction of 5.9%.

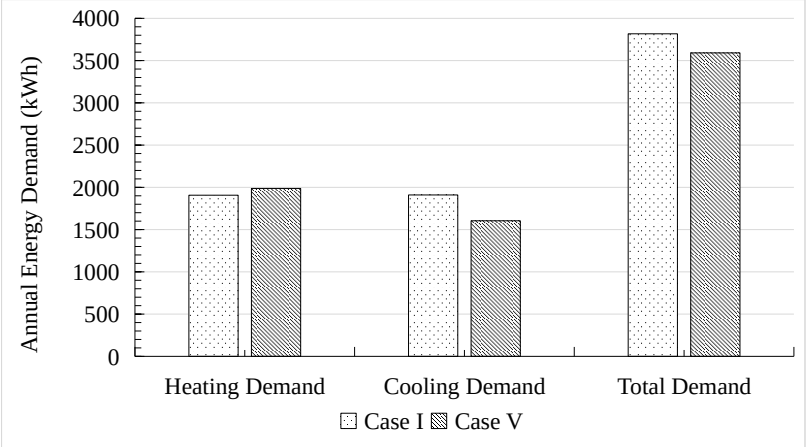

Fig.4-19 Energy demand of simulated in Case I and V.

Based upon those findings, it can be found that for the east and west window in this building, when using the adjustable horizon shutters, the cooling demand could be reduced by over 10%, showing a perfect shading effect. While in winter time, the shutters would be open for gaining solar energy directly. On the other hand, the fixed shading shield onto south windows would cause heating demand increasing, not contribute to saving total energy consumption.

Thus, in this project, shading design strategies was finally decided as the following: east and west windows were used with adjustable horizon shutters; south windows were not designed with fixed external shield, but used curtains with thermal-protective coating, which can be open in winter for obtaining solar energy and closed in summer for heat preventing.

4-5 Construction

According to the design patterns proposed in the above section , the experimental building was constructed in the campus of Zhejiang University of Hangzhou. The following presentation is the construction procedure and the main technologies are introduced.

4-5-1 Site construction

Firstly, the site was stripped and the ground was excavated after the preparation, rough and finishing grading. Then, the soil was back filled and compacted (see Fig.4-0). Next step, the ground was constructed with cement (see Fig.4-1).

a.

b.

c.

d.

Fig.4-20. Site construction I.

a.

b.

Fig.4-21. Site construction II

4-5-2 Wall construction

The exterior walls and internal partitions used aerated concrete block, with thickness of 300mm in outer walls and 200mm in inter walls (see Fig.4-2). As a new type of filling materials, the aerated concrete has the features of low density, low strength, good absorption of water and great contraction, to replace non-burning and cement brick building block for building wall body.

a.

b.

c.

d.

e.

f.

Fig.4-22. Walls construction (a~f).

4-5-3 External insulation system construction

The rock wool was chosen as insulation layer to be filled between wooden keels paved on the walls (see Fig.4-23), which has low thermal conductivity of a high-quality thermal insulating materials and is applicable to fire prevention, waterproof, heat preservation, refractory, fight fire on environment requires some occasions.

a.

b.

c.

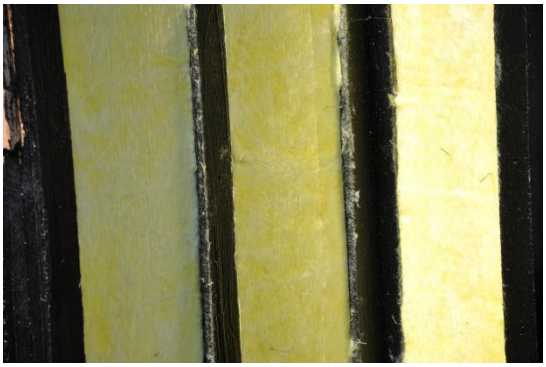

d.

e.

f.

Fig.4-23. External insulatioin system construction

4-5-4 Exterior decoration construction

The external decoration used a new type of synthesizing wood-plastic composite board with low cost, produced by local factory of Hangzhou. This material has the same processing performance with wood but better dimensional stability. Wood-plastic composite board also does not produce cracks, warping, has no wood knots and twill, and can be made of colorful products if adding coloring, coating or composite surface (see Fig.4-4).

a.

b.

c.

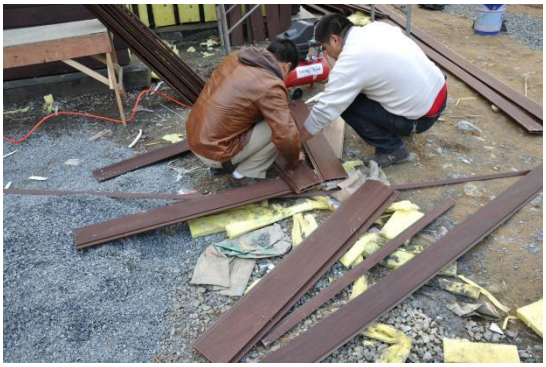

d.

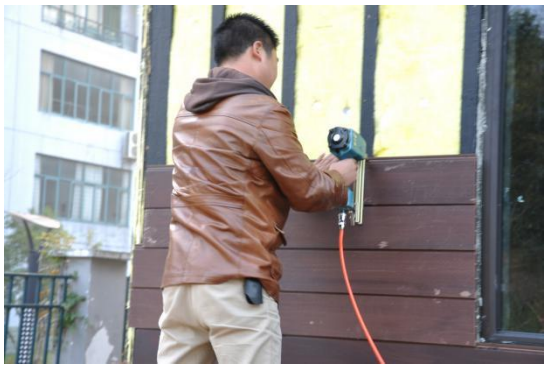

e.

f.

Fig.4-24. Exterior decoration construction (a ~ f)

4-5-5 Trombe wall construction

The Trombe wall system consist of absorber walls, air cap, upper and lower vents as well as glass cover. Specifically, there were two pieces of absorber wall made of concrete material lying on each side of the middle door, with 2.8 m high, 0.9 m wide and 0.3 m thick. The cast-in-situ concrete construction technique was applied in this building, thus the formwork shores could be seen as the transitory bearing structure in Fig.4-5 (a). After that, the absorber wall was painted

with black color and covered by glass seen in Fig.4-5 (f).

a.

b.

c.

d.

e.

f.

Fig.4-25. Trombe wall construction.

4-5-6 Solar chimney construction

Solar chimney configuration (see Fig.4-6) has about 3.0 m height above the roof of this building, equipped with equal size top and bottom rectangular air-damper. Two outlets were located on the top of the chimney facing to opposite directions. Otherwise, the body of the chimney was made of aerated concrete block with thickness of 200mm.

a. b.

Fig.4-26. Solar chimney construction

4-6 Summaries

As a whole, building construction elements play a significant role in terms of energy consumption. By using computer simulating method, the optimized passive design technologies for such an experimental building were summarized as following:

(1) Through simulating the annual energy demand, the best thick of insulation layer for the wall

and roof, as well as the optical U-value for the window were determined. It could be found that the annual total energy demand resulted from the design building had a 18.8% reduction compared with the standard building regulated in the current energy-saving design criteria.

(2) Through simulating the annual energy demand based on five shading design models, it could be found that for the east and west window in this building, when using the adjustable horizon shutters, the cooling demand could be reduced by over 10%, showing a perfect shading effect. While in winter time, the shutters would be open for gaining solar energy directly. On the other hand, the fixed shading shield onto south windows would cause heating demand increasing, not contribute to saving total energy consumption. Thus, in this project, shading design strategies was finally decided as the following: east and west windows were used with adjustable horizon shutters; south windows were not designed with fixed external shield, but used curtains with thermal-protective coating, which can be open in winter for obtaining solar energy and closed in summer for heat preventing.

Generally, simulation method is an effective way to improve the working efficiency when the passive design strategies were considered ahead of time. Through research and analysis of pre-design, an optimized experimental building was determined and constructed, contribute to the further study.

Reference

[1] Website: http://www.hzqx.gov.cn/

[2] Ren J., Wang W.J. Using Ecotect software to simulation and analysis on indoor thermal environment of herders' residential houses in Turpan area of Xinjiang, Sichuan Building Science, 2015; 41(1): 295~299

[3] Sun S., Liang J., Sun C. The research of digital simulation technique applied in the simulation of energy-saving in library exterior-protected construction, Digital Tectonic Culture, Beijing, 2015
[4] Shou L.L. Comparative research on building energy consumption analysis based on BIM with traditional building energy consumption analysis of China, Chongqing University, Chongqing, China, 2013
[5] Ministry of Construction of the People's Republic of China, *Design Standard for Energy Efficiency of Residential Buildings in Hot Summer and Cold Winter Zone* (JGJ 234-2010), Beijing, 2010

Chapter Five: Field-measurement on thermal performance of experimental house in winter time

5-1 Introduction

What about the indoor thermal environment when using passive energy efficiency technologies in the experimental building during the winter period in Hangzhou area? What is the effect of the Trombe wall heating system applied on improving the indoor thermal environment? Whether for popularization? All the above should be confirmed by experimental verification. Thus, the only method for scientific study is to carry out field measurement by using relative instruments and meters to obtain the data monitored continually in real climatic conditions.

Many in-situ measurements on ventilation performance were found in the literature in the past year. Reference[1] selected Shanghai International Gymnastics Stadium as object for site-measurement. It was found that temperature stratification in winter with air-conditioning was most obvious. The maximum difference of vertical temperature was 15.1℃ in winter. The second largest one was 12.1℃ in summer, and less than 21℃ in the transitional season. The results of measurements indicated that it was different in the characteristics on energy saving of upper openings during the different seasons. With heat balance measurements, it was discovered that the roof load and ventilated and infiltrated load account for larger percentages in terms of cooling and heating load. In this paper, many discussions on the results of site measurements showed some characteristics and regulations of indoor thermal environment in large space building. The paper[2] present experiences from a recently built area with passive houses in Linköping, Sweden and compared them with conventional buildings, mainly from an indoor environment perspective, but also based on energy use. It was found that the thermal comfort for these newly built passive houses was well within the limits in the local building code. However, some interesting findings related to local comfort such as cold floors are found in the post-occupancy evaluation as well as in the predictions. In this study[3], two field surveys had been conducted in three residences in Dalian of Northeast China to investigate the thermal environments of rural residences with a coupled Chinese elevated kang and passive solar collecting wall heating system. Indoor thermal environments were evaluated with parameters of indoor air temperature and relative humidity, surface temperature of the kang plates, air temperature of the upper/lower vents in passive solar wall and human activities, etc. The description of this survey and the methodology of data analysis were described in details in this paper. The survey results objectively provide the preliminary information regarding the indoor thermal environment of new rural energy-saving residences in winter in Northeast China.

S.A.M. Burek[4] report an experimental investigation into heat transfer and mass flow in thermosyphoning air heaters, such as solar chimneys and Trombe Walls. The test rig comprised a vertical open-ended channel with closed sides, resembling a solar collector or solar chimney approximately. Close control of the heat input was achieved by using an electrical heating mat—steady-state heat inputs ranged from 200 to 1000 W, and the channel depth was varied between 20 and 110 mm.Temperatures were recorded through out the test rig, as was the air velocity. The principal results from the data showed the function about the mass flow rate and the

thermal efficiency of the system. In the winter of 1976, Trombe[5] in the initial experiments in this field, at Odeillo, found the solar contribution to be 60-70 per cent for a house with its temperature maintained above 20°C. In this experimental investigation[6], flow visualization studies have given a deeper insight into the fundamental flow mechanisms; whilst air velocity and temperature measurements have been used to explore the natural convection heat transfer processes involved in the thermocirculation flow. Particular attention has been paid to the effects on operational performance of the wall parameters such as wall/glazing distance and vent size. The thermal performance of a passive solar heating system has been investigated in the study[7] via simultaneous temperature, velocity and flux measurements and their acquisition. The sensor locations inserted on the full-scale model of a passive heating system, a single zone with a thermal wall, were on the walls and at the vents. Experimental data showed that the wall black surface was sensitive to fluctuations in the solar intensity rate. Based on the full-scale passive solar experimental building, Sun P. analyzed the indoor thermal environment and humidity performance of passive solar building with Trombe wall, and the different ventilation patterns in different seasons, by monitoring indoor/outdoor temperature, solar radiation, surface temperature of heat collector wall and vent temperature & velocity[8].

Based upon these literature, in-situ measurements are a normal and effective methods for research. In this Chapter, field measurement was carried out on the insulated rooms and the room set with Trombe wall heating system Under the real climatic condition of Hangzhou, the following indicators are verified:

- Indoor temperatures of the rooms with insulation;
- For the room with Trombe wall, indoor temperature, surface temperature, solar radiation, vent temperature;

Through analyzing the tested data, the effectiveness of the passive technology was evaluated, and the heating level of the Trombe wall was assessed.

5-2 Measurement and analysis on indoor thermal environment of south rooms

5-2-1 Experiment set-up

The thermal environment test on the south rooms was carried out in winter (from 22nd December, 2015 to 10th February, 2016), continuing 50 days in all. The monitored data on the air temperatures and relative humidity were recorded automatically with a 15-min sampling time using an Testo 174H data logger (see 错误!未找到引用源。). The technical specifications including the accuracy, and resolution are shown in Table.5-1.

Table.5-1. Monitored data and technical specifications of measuring instruments.

Monitored parameters	Instrument name	Measurement range	Accuracy	Resolution
Air temperature	Testo 174H	-20 to 70℃	±0.35℃	0.1℃
Relative humidity	Testo 174H	0 to 100%RH	±3.0%RH	0.1%RH

Fig.5- 2 shows the measuring-point locations, named $T_{1,i}$, $T_{2,i}$ and $T_{3,i}$ considered for the monitoring of the air temperature, as well as $H_{1,i}$, $H_{2,i}$ and $H_{3,i}$ considered for the monitoring of the relative humidity placed in the south rooms separately. All points were set at 1.5 m above the ground level. The outdoor data loggers were shaded using appropriate devices during the whole measurement for recording the outdoor air temperature T_e and relative humidity H_e.

Fig.5- 1 Testo 174H data logger （Source：http://www.bjjttec.com ）

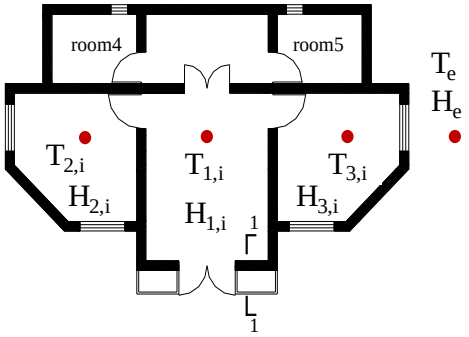

Fig.5- 2 Schematic diagram of measuring-point locations

5-2-2 Results and discussion

5-2-2-1 During the whole monitoring time

The monitoring period was from 22nd December, 2015 to 10th February 2016, spanning the most coldest three months in the year, 50 days in all, and 4800 groups of data were recorded. The variation of mean outdoor temperature $\overline{T_e}$ is shown in Fig.5- 3. It can be noticed that the mean outdoor temperature started to decrease from the first measuring day, and then dropped to 5.0℃ on the day of 1st January 2016. After that, the mean temperature suddenly rose up to 10℃, and declined continually to the lowest temperature of -5.7℃ on the day of 24th January. Afterwards, the temperature turned to increase all along.

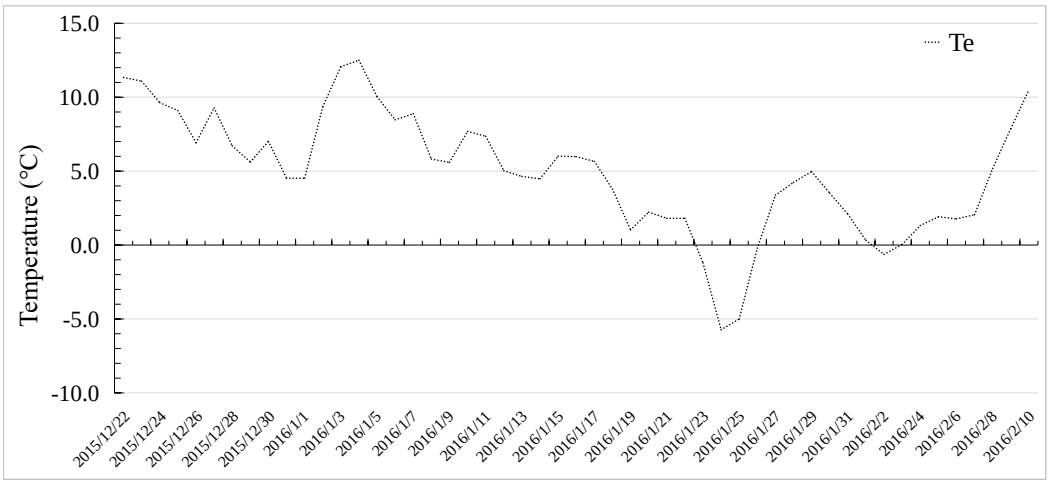

Fig.5- 3 Variation of daily mean outdoor temperature $\overline{T_e}$

（22nd December, 2015 to 10th February, 2016 ）

The daily mean indoor temperatures $\overline{T_{1,i}}$ of the middle south room with Trombe wall was compared with the mean outdoor environment temperature $\overline{T_e}$, illustrated in Fig.5- 4. It can be noticed that daily indoor temperatures were always higher than the outdoor during monitoring period. There were only five days when the value of $\overline{T_{1,i}}$ was below 5.0℃. On the day of 4th January, both of indoor and outdoor temperature reached their maximum value, and were all very close to 13.0℃. On the coldest day of 24th January, the mean temperature in the room was much higher by about 9.3℃ than the outdoor environment. In a word, the mean outdoor temperature $\overline{T_e}$ had a variation of 18.2℃ (i.e. from -5.7℃ to 12.9℃) during the fifty monitoring days, while the mean indoor temperature $\overline{T_{1,i}}$ varying from 3.3℃ to 12.9℃, showing a variation of 9.6℃ during the same time. It can be seen that the heating effectiveness of Trombe wall system was not so obvious, probably due to the reason that the airtight and insulation of the outer door were not so perfect.

Fig.5- 4. Comparison of daily mean indoor temperature $\overline{T_{1,i}}$ and mean outdoor temperature $\overline{T_e}$

（23rd December 2015 to 10th February 2016 ）

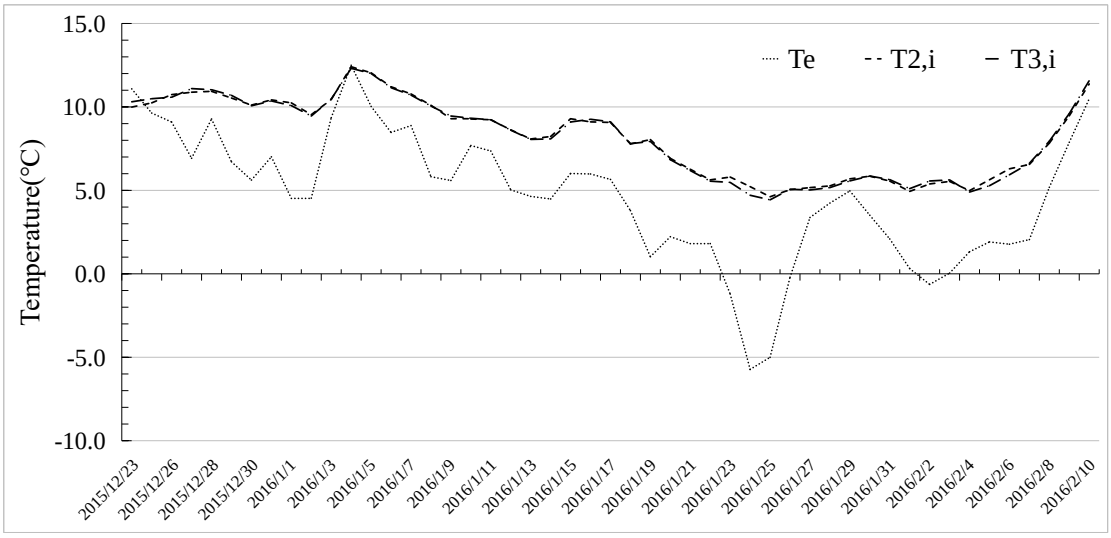

Fig.5- 5 illustrates the changing of daily mean indoor temperature of two south rooms with insulation layers, to be named $\overline{T_{2,i}}$ and $\overline{T_{3,i}}$. It can be compared that daily indoor temperatures of two rooms are very close and always higher than the outdoor during monitoring period. The temperature difference between indoor and outdoor reach the maximum values, of 10.9℃ and 10.4℃ separately. Generally, indoor temperature fluctuated slightly with the outdoor temperature changing. That is to say the insulation layers for the rooms take effect during the cold winter time.

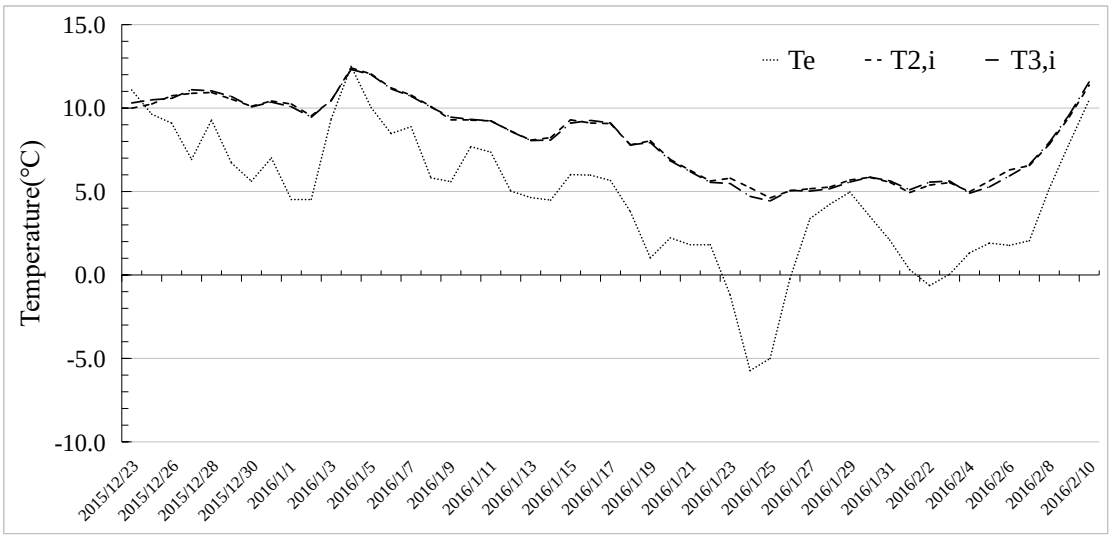

Fig.5- 5. Comparison of daily mean indoor and outdoor temperature of two south rooms with insulation layers（23rd December 2015 to 10th February 2016）

5-2-2-2 On 24th January

The coldest day of 24th January was selected as the typical climatic condition of Hangzhou area for the indoor temperature analysis of two south insulated rooms, as shown in Fig.5- 6. It can be seen that the hourly temperatures of this day were below -4℃ all along, and the minimum value was -9.5℃ tested in the night of about 23:00 p.m. to 24:00 p.m., which was the extreme low temperature rarely seen in Hangzhou. At the same time, indoor temperatures monitored in the two rooms are about 4℃, 13.5℃ higher than that of outdoor, and the temperature variations were relative steady in the whole day. For the room on the east side, its maximum temperature value was 6.6℃ appearing at the noon of about 12:00 p.m. to 13:00 p.m. Two hours later, the room on the west side also presented the biggest temperature of 7.6℃, due to the time delay of solar radiation.

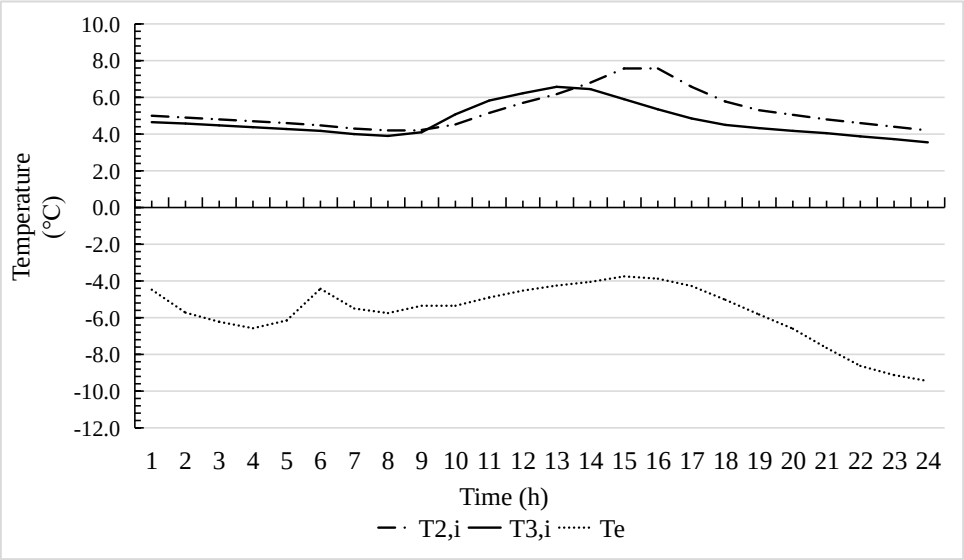

Fig.5- 6. Comparison of hourly indoor and outdoor temperature of two south rooms with insulation layers on 24th January

In terms of humidity, as shown in Fig.5-7, the outdoor value fluctuated obviously, from 35.8% to 94.6%, and the average was 62.9%. For the indoor humidity, the values of both two rooms were kept in the range of 60% to 80% all day: the minimum of west room was about 69%, and the average was 75.2%. The minimum of east room was about 64.2%, and the average was 69.3%. That could be seen that indoor humidity facing to west was higher than that facing to east.

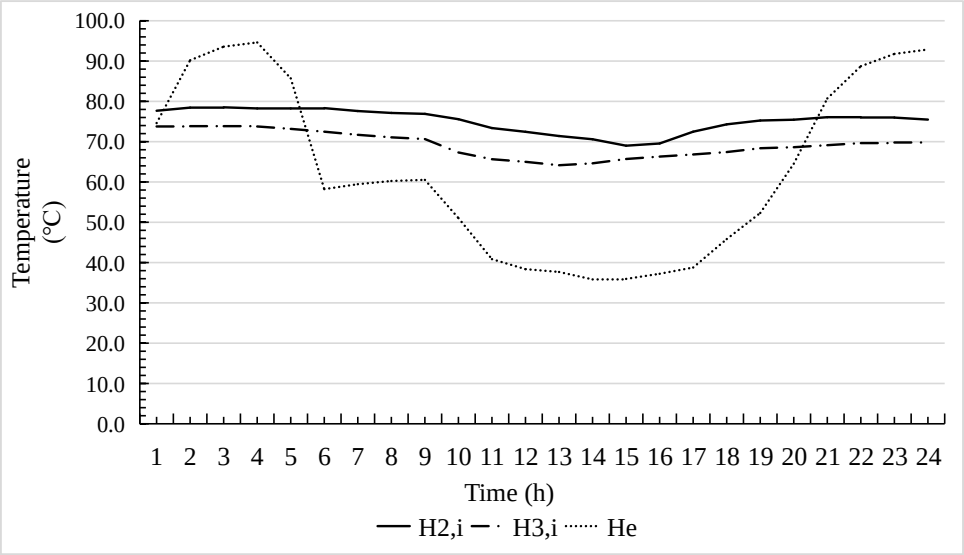

Fig.5- 7. Comparison of hourly indoor and outdoor humidity of two south rooms with insulation layers on 24th January

Fig.5-8 and Fig.5-9 shows the hourly temperature and humidity changing of middle room with Trombe wall on 24th January. It can be seen in Fig.5-8 that indoor temperatures monitored in the middle room were about 2℃, 11.5℃ higher than that of outdoor. The temperatures were relative steady in the whole day, which maximum temperature value was 5.7℃ appearing at 15:00 p.m., 3 hours later than the east room, and 1 hour later than the west room. In terms of humidity, it fluctuated from 52.4% to 64.1%, and the average was about 58.7%, lower than average outdoor humidity.

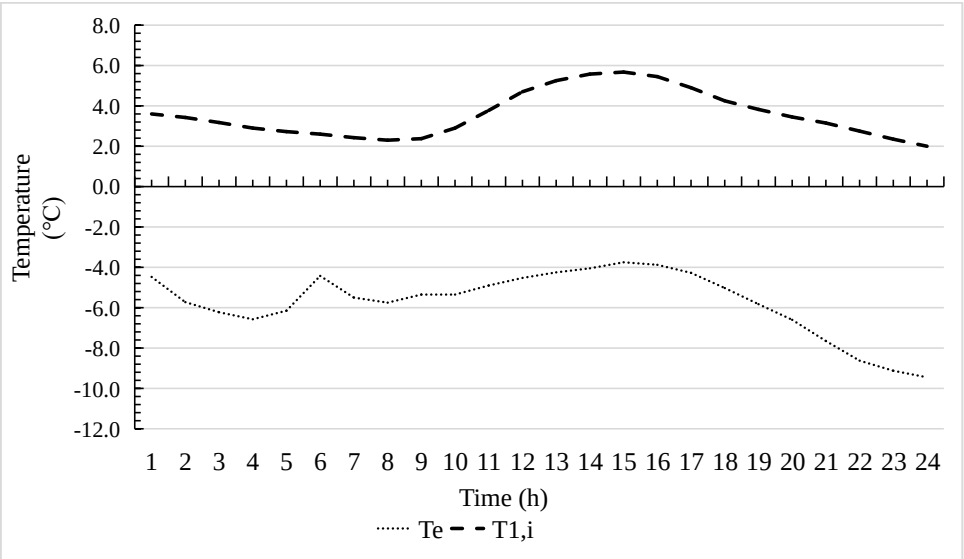

Fig.5- 8. Comparison of hourly indoor and outdoor temperature of middle room with Trombe wall

on 24th January

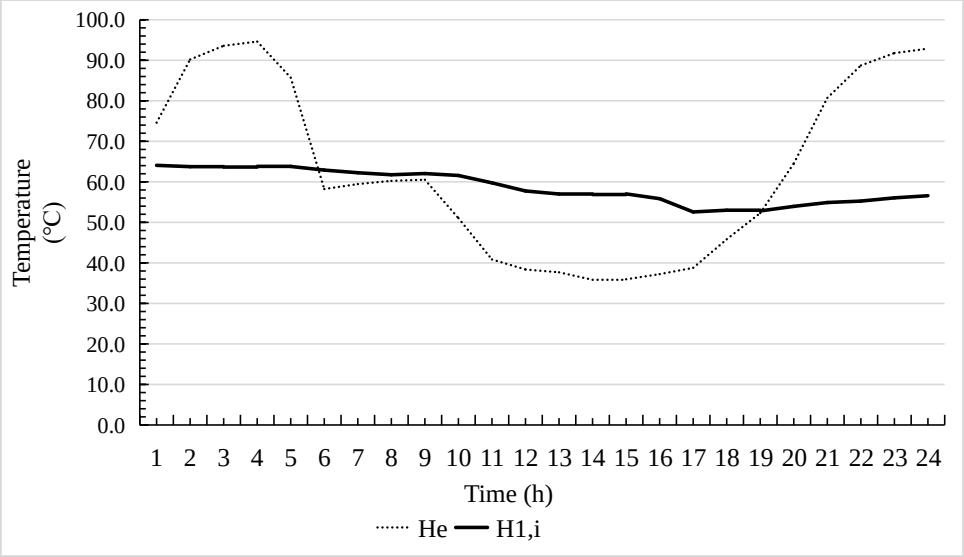

Fig.5- 9. Comparison of hourly indoor and outdoor humidity of middle room with Trombe wall on 24th January

5-3 Measurement and analysis on Trombe wall system

The monitoring work started from 15th January 2016 to 13th February 2016, lasting 30 days in all. The following indicators were continuously tested for 24 hours a day, including: external and internal surface temperature of concrete collector wall, solar radiation and air temperature in the air duct outside the Trombe wall, ambient temperature and so on. During the test, the air duct was closed all day. The experiment set-up and monitoring results are presented and analyzed in the following section.

5-3-1 Experimental set-up

5-3-1-1 Schematic description

As shown in **错误!未找到引用源。**0, Fig.5-111 and Fig.5- 122, a section of concrete collector wall was selected as research object, with 2800mm high, 900mm wide and 300mm thick. Located outside the wall, the air duct is 600mm width, and the glass cover has two layers of 6mm thick separately with air gap of 9mm thick in the middle. A lattice panel at the air inlet and outlet in the wall was used to protect it from rodents.

错误!未找到引用源。0 shows three locations with interval of 300mm considered for the monitoring of internal surface temperatures, named $\theta_{i,1}$ $\theta_{i,2}$ $\theta_{i,3}$, and two locations considered for the vent temperature testing, named T_{in} and T_{out}. Correspondingly, there also were three points located on the external surface temperature, named $\theta_{e,1}$ $\theta_{e,2}$ $\theta_{e,3}$ for the measurement, seen in Fig.5-111.

Two points were set in the air duct, 1.2m away from the ground, considered for the monitoring of

solar radiation I_0 and ambient temperature T_a, seen in Fig.5- 122.

3 ~ Fig.5- present the overview of the field measurement.

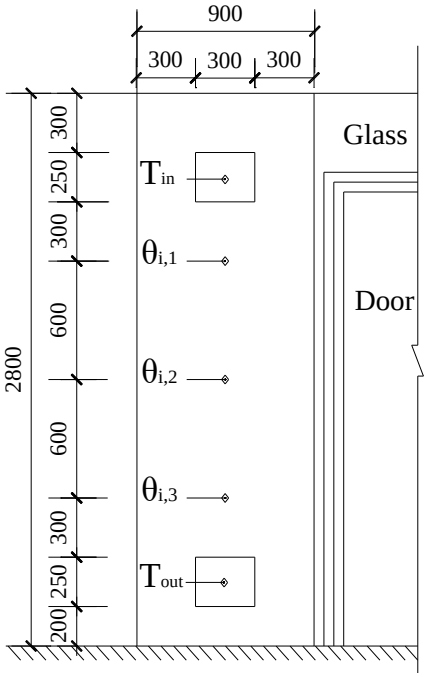

Fig.5-10. Schematic diagram of internal surface of the concrete collector wall.

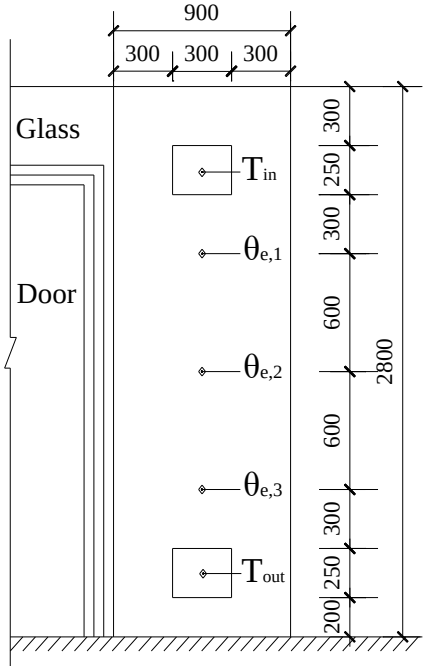

Fig.5-11. Schematic diagram of external surface of the concrete collector wall.

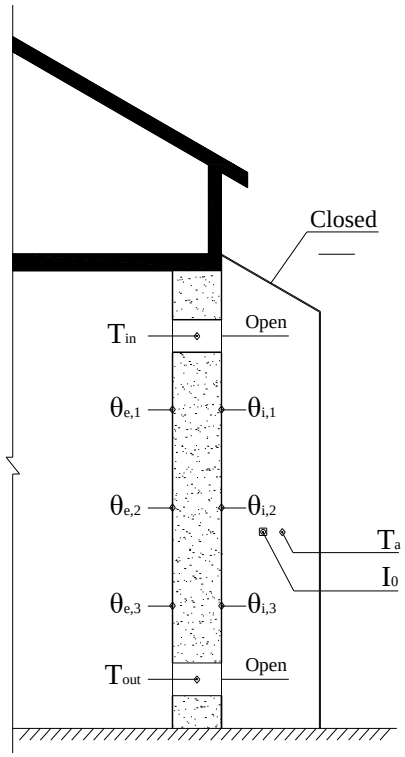

Fig.5- 12. Schematic diagram of the section of the concrete collector wall.

Fig.5- 13. Photo of field measurement (1)

Fig.5-14 Photo of field measurement (2)

Fig.5-15 Photo of field measurement (3)

Fig.5-16. Photo of field measurement (4)

Fig.5-17. Photo of field measurement (5)

5-3-1-2 Instrumentation

Surface temperature and vent temperature were collected using a data acquisition system, named JTRG-II automatic test system (see Fig.5-7). The data acquisition system consists of interconnected data loggers as a local network RS485, which is connected to a personal computer through a RS232 serial port.

The locations of each sensors are shown in 错误!未找到引用源。0, Fig.5-111. Eight platinum thermos resistance PT100 (testing range: -40℃～50℃) were employed to measure the surface and vent air temperature, which were recorded automatically with a 10 min sampling time.

Ambient temperature and solar radiation in the air duct were monitored by using JTR05 meter (see Fig.5-8). This instrument consists of a total solar radiation sensor calibrated precisely and an imported digital temperature sensor, measuring solar radiation while monitoring the ambient temperature in the air duct formed by concrete wall and glass cover. Temperature sensor has high precision and stable performance by using a sealed package with stainless steel, simple to be connected with the standard 3.5mm plug form (testing range: -20～85℃; precision: <±0.5℃) . The data were recorded automatically with a 10-min sampling time. The technical specifications of solar radiation sensor are shown in

Table.5- 2.

Fig.5-7. JTRG-II Automatic test system
(Source: http://www.bjjttec.com)

Fig.5-8. JTR05 Solar radiation meter
(Source: http://www.bjjttec.com)

Table.5- 2 Technical specifications of solar radiation sensor.

Parameter	Range	Remark
Spectrum	0.3～3.2 μm	
Radiation	0～2000 W/m^2	
Temperature coefficient	≤±2%	(-10℃ ～+40℃)
Non-linearity	±2%	
Cosine response	≤±7%	(solar altitude angle is 10°)
Sensitivity	7～14 mv / kw•m^{-2}	
Response time	< 35 s	(99%)
Stability	≤±2%	Annual average
Operating temperature	-50℃～+50℃	

The indoor and outdoor temperature were recorded automatically with a 15-min sampling time using an Testo 174H data logger (see 错误!未找到引用源。). The technical specifications including the accuracy, and resolution are shown in Table.5-1.

5-3-2 Weather conditions during the monitoring period

The monitoring work started from 15th January 2016 to 13th February 2016, lasting 30 days in all. The statistics on weather conditions during monitoring period are shown in

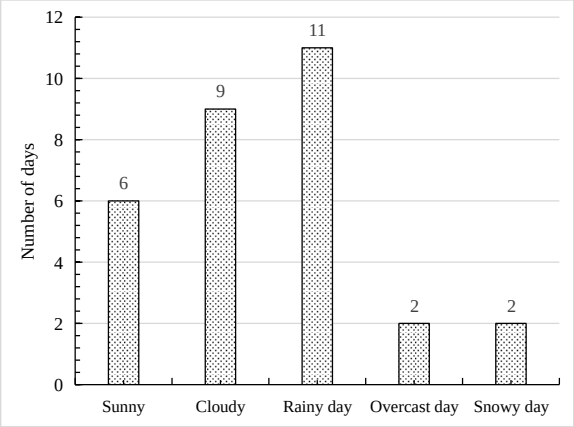

Fig. 5-0. It can be illustrated that cloudy and rainy days were on the vast majority of testing days, accounting for two third of measurement time. Only six days were sunny, accounting for one fifth. One half of the rest time were snowy days, and the other were overcast sky. Furthermore, Fig.5- 3 indicates that the monitored outer temperatures in this period were the coldest in the whole testing time. Thus, the Trombe wall heating level can be examined better in these more severe weather conditions in winter time of Hangzhou.

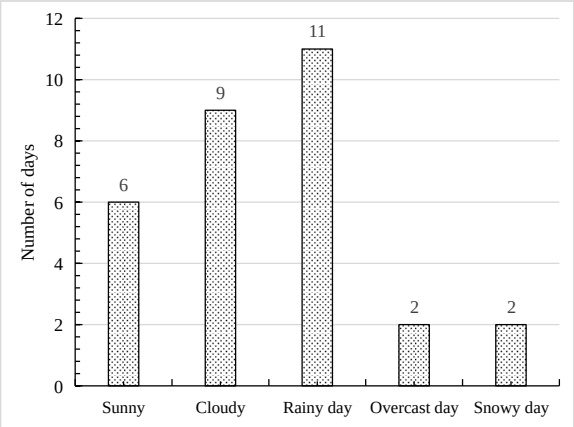

Fig. 5-20 Statistics on weather conditions from 15th January 2016 to 13th February 2016.

In order to study and master the thermal-circulation characteristic of the Trombe wall and the dynamic changing of indoor thermal environment, five testing dates as representative of typical weather conditions were selected shown in Table.5-3.

Table.5-3. Selected testing date under typical weather conditions

January 19th	January 22nd	January 28th	February 1st	February 6th
Cloudy	Snowy day	Rainy day	Overcast day	Sunny day

5-3-3 Variation of ambient temperature and solar radiation in the air duct on typical days

The following indicators were continuously tested for 24 hours on typical days, including: solar radiation I_0 , ambient temperature T_a in the air duct and outdoor ambient temperature T_e . Monitoring results and analysis are in the following sections.

(1) 19th January, 2016, Cloudy

The data of global solar irradiance I_0 and ambient temperature T_a in the air duct were recorded for 24 hours on 19th January 2016. In the Fig.5- 1, it can be found that the solar irradiance I_0 began to increase at 9:00 a.m., reaching its peaking value of 451.5W/m^2 in the time of

12:00~13:00 p.m. The changing of ambient temperature T_a had a similar profile with solar irradiance I_0, which fluctuated obviously with s maximum value of 21.7℃ in the time of 13:00~14:00 p.m., one hour later than the occurrence time of the maximum irradiance value. The minimum value of T_a is 1.0℃, and the diary variation was 20.7℃. On the other hand, the outdoor temperature T_e had its biggest value of 4.9℃, three hours later than the peak time of solar irradiance.

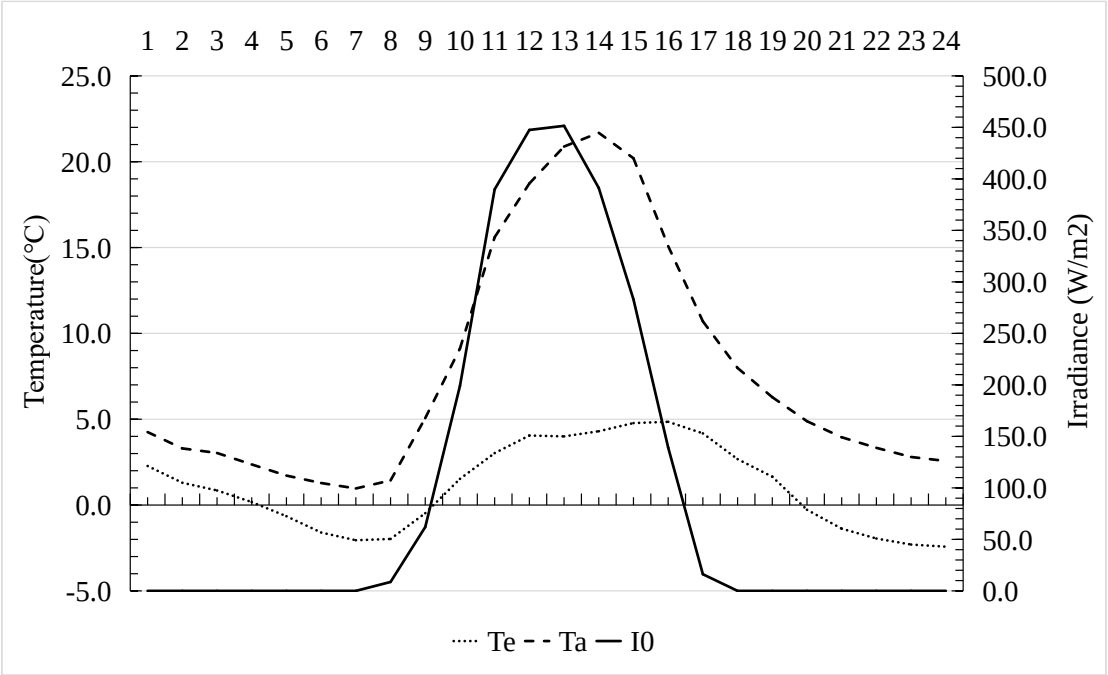

Fig.5- 21 Variation of solar radiation and ambient temperature in the air duct on 19th January.

According to the monitoring results, solar radiation had a relatively good level in cloudy weather condition, and the ambient temperature in the closed transparent air duct was mainly affected by solar radiation. It can be explained by the fact that the air duct with glass cover absorbed much solar energy, acting as a greenhouse to keep thermal inside and help to heat Thromb wall.

(2) 22nd January, 2016, Snowy day

The data of global solar irradiance I_0 and ambient temperature T_a in the air duct were recorded for 24 hours on 22nd January 2016. It can be found in Fig.5-9 the solar radiation shows a very low level in this snowy day, and the maximum irradiance value is not more than 15W/m^2. The change of outdoor temperature T_e was relatively steady with a small daily range. The maximum temperature was 3.1℃, occurring in the time of 13:00 p.m.~14:00 p.m., and the minimum is 0.3℃. The daily range was about 2.8℃. In the air duct, the maximum air temperature T_a obtained approximately at the same time with the outdoor temperature was 3.7℃, the minimum was 2.2℃, and the daily temperature difference was only 1.5℃.

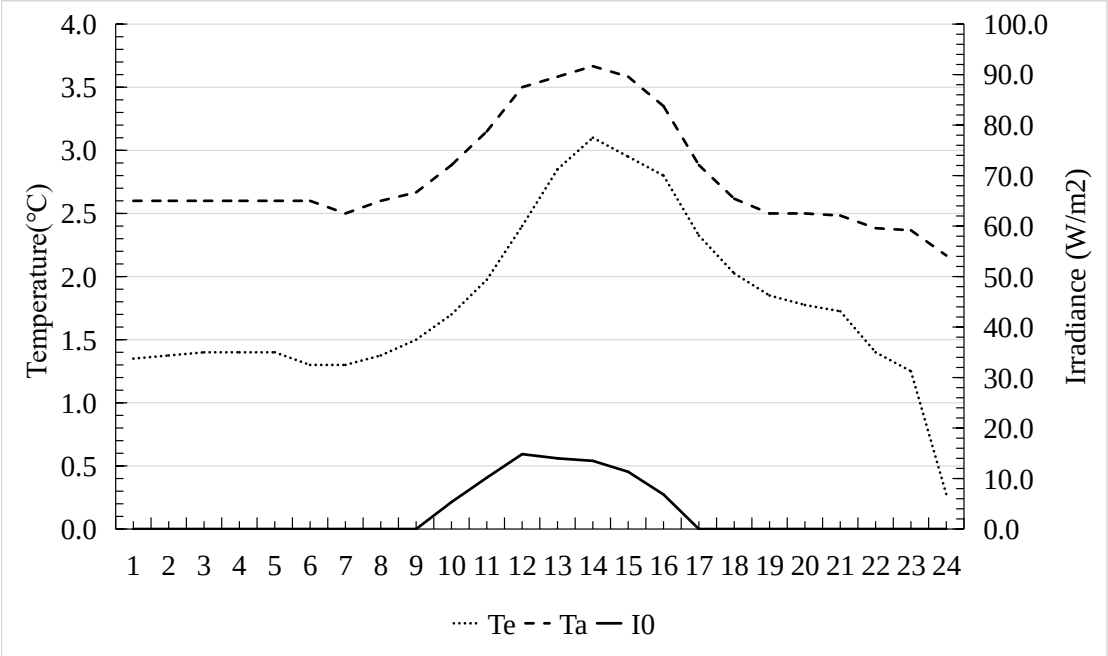

Fig.5-9 Variation of solar radiation and ambient temperature in the air duct on 22nd January.

According to the monitoring results, solar radiation had a relatively low level in snowy weather condition, and the ambient temperature in the closed transparent air duct mainly depend on outdoor temperature. It can be concluded that the Thromb wall system cannot work very well due to the reason of less solar radiation.

(3) 28th January, 2016, Rainy day

The data of global solar irradiance I_0 and ambient temperature T_a in the air duct were recorded for 24 hours on 28th January 2016. It can be found in Fig.5- 10 that the solar radiation shows a very low level in this rainy day, and the maximum irradiance value is only 10.7W/m^2. The change of outdoor temperature T_e was relatively steady with a small daily range of 2.6℃, the maximum temperature was 5.6℃, and the minimum was 3.0℃. In the air duct, the maximum air temperature T_a obtained approximately at the same time with the outdoor temperature was 6.7℃, the minimum was 4.9℃, and the daily temperature difference was only 1.8℃.

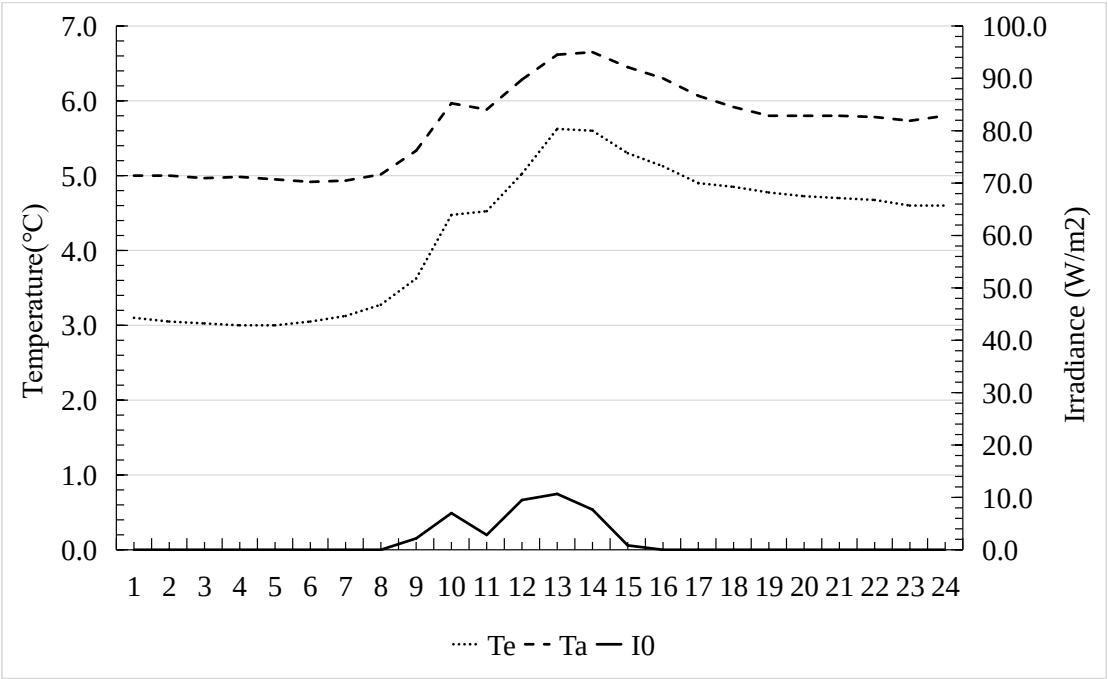

Fig.5- 10 Variation of solar radiation and ambient temperature in the air duct on 28th January.

According to the monitoring results, solar radiation had a relatively low level in rainy weather condition, and the ambient temperature in the closed transparent air duct mainly depend on outdoor temperature. It can be concluded that the Thromb wall system cannot work very well due to the reason of less solar radiation. The situation was the same with the snowy day.

(4) 30th January, 2016, Overcast day

The data of global solar irradiance I_0 and ambient temperature T_a in the air duct were recorded for 24 hours on 30th January 2016. It can be found in Fig.5- 11 that the solar radiation shows a very low level in overcast day, and the maximum irradiance value is only 14.5W/m^2, occurring in the time of 15:00~16:00 p.m. The change of outdoor temperature T_e was relatively steady with a small daily range of 2.7℃, the maximum temperature was 5.3℃, and the minimum was 2.6℃. In the air duct, the maximum air temperature T_a obtained approximately at the same time with the outdoor temperature was 6.5℃, the minimum was 4.3℃, and the daily temperature difference was only 2.2℃.

According to the monitoring results, solar radiation had a relatively low level in overcast weather condition, and the ambient temperature in the closed transparent air duct mainly depend on outdoor temperature. It can be concluded that the Thromb wall system cannot work very well due to the reason of less solar radiation. The situation was the same with the snowy and rainy day.

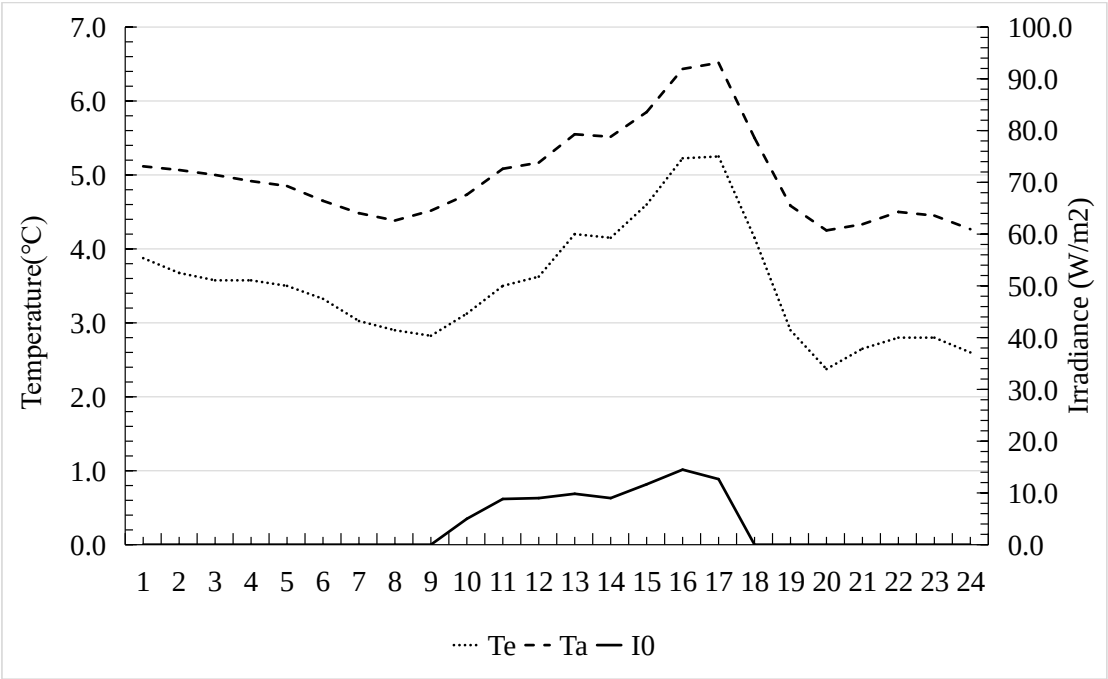

Fig.5- 11 Variation of solar radiation and ambient temperature in the air duct on 30th January.

(5) 6th February, 2016, Sunny day

The data of global solar irradiance I_0 and ambient temperature T_a in the air duct were recorded for 24 hours on 6th February 2016. In the Fig.5-12, it can be found that the solar irradiance I_0 began to increase at 9:00 a.m., reaching its peaking value of 326.3 W/m^2 in the time of 13:00~14:00 p.m. The changing of ambient temperature T_a had a similar profile with solar irradiance I_0, which fluctuated obviously with s maximum value of 20.2℃ in the time of 14:00~15:00 p.m., one hour later than the occurrence time of the maximum irradiance value. The minimum value of T_a was 1.5℃, and the diary variation was 18.7℃. On the other hand, the outdoor temperature T_e had its biggest value of 7.3℃, one hours later than the peak time of solar irradiance.

According to the monitoring results, solar radiation had a relatively good level in sunny weather condition, and the ambient temperature in the closed transparent air duct was mainly affected by solar radiation. It can be explained by the fact that the air duct with glass cover absorb much solar energy, acting as a greenhouse to keep thermal inside and help to heat Thromb wall.

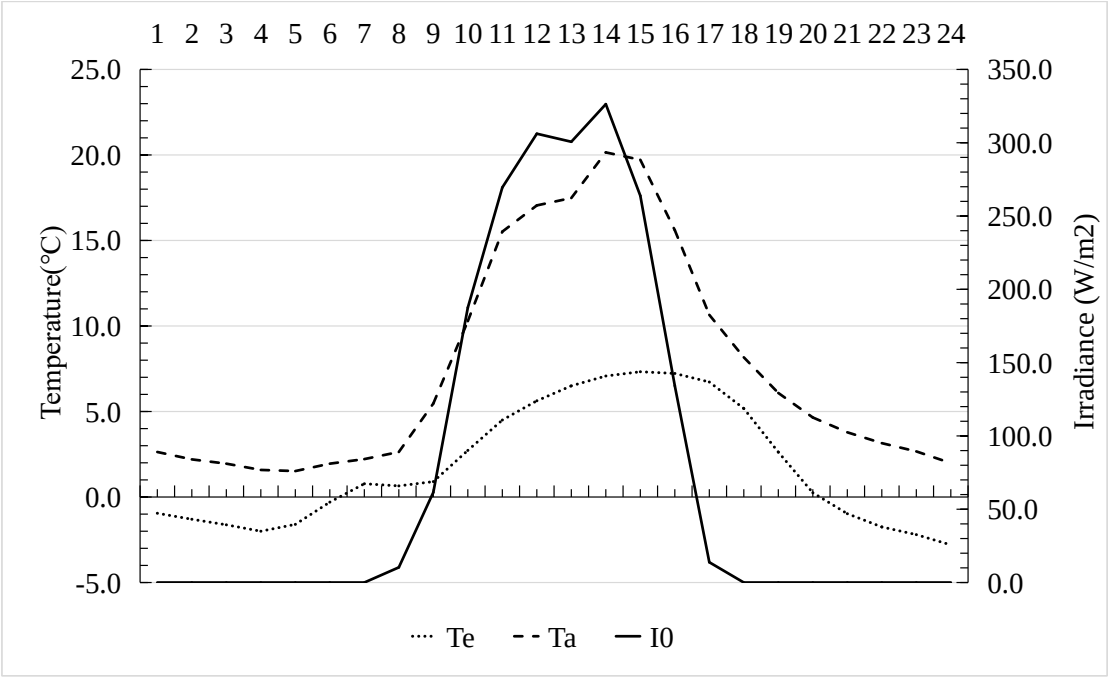

Fig.5-12. Variation of solar radiation and ambient temperature in the air duct on 6th February.

5-3-4 Dynamic changing of thermal performance of Trombe wall system on typical days

The following indicators were continuously tested for 24 hours with a 10 min sampling time on sunny day and overcast day, including: external surface temperature $\theta_{e,1}$, $\theta_{e,2}$ and $\theta_{e,3}$; internal surface temperature $\theta_{i,1}$, $\theta_{i,2}$ and $\theta_{i,3}$. Indoor temperature T_i, outdoor temperature T_e and global soar radiation I_0 were also recorded synchronously, compared together with the average surface temperature $A_{\theta,e}$ and $A_{\theta,i}$. Results and analysis are indicated in the following sections.

(1) 24th January, 2016, Sunny day

Fig.5- 13 shows the variation of the average surface temperature $A_{\theta,e}$, $A_{\theta,i}$, indoor temperature T_i, outdoor temperature T_e, and global soar radiation I_0. The profiles in the Fig.5-13 illustrate that the average external surface temperature $A_{\theta,e}$ began to increase with the solar irradiance rising from the time of 9:00~10:00 a.m. At 13:00 p.m., it can be observed that the surface temperature $A_{\theta,e}$ reached its maximum value of 19.4℃, one hour later than with the peak value time of solar radiation, with 14.2℃ higher than that obtained in the morning time. After that, solar radiation I_0 started to decline, while the external surface temperature $A_{\theta,e}$ remained 18℃ ~ 19℃, and dropped to 15℃ at the time of 16:00~17:00 p.m.

Relative to the external surface, the internal surface temperature $A_{\theta,i}$ showed a small fluctuation. From the early morning, it began to rise up slowly, exceeded indoor temperature T_i when the time was about 14:00~15:00 p.m., and achieved the value of 6.1℃. After that, it continued to increase and reached its maximum value of 8.2℃ in the time of 18:00~19:00 p.m., 6 hours later than the peak time of external surface temperature $A_{\theta,e}$, while 0.3℃ higher than $A_{\theta,e}$ at the same time.

For the indoor temperature T_i, it had a daily variation of 3.7℃. The maximum of T_i was 5.7℃, occurring in the time of 14:00~15:00 p.m. After that time, indoor temperature was always lower than the inner surface temperature.

According to the above analysis, the external surface of the concrete wall was stimulated greatly by the solar radiation in the sunny day, and concrete wall had the obvious time-lag effect due to the heat storage characteristic. While, the inner surface has a higher temperature in the night, enhancing the heating effect of Trombe wall.

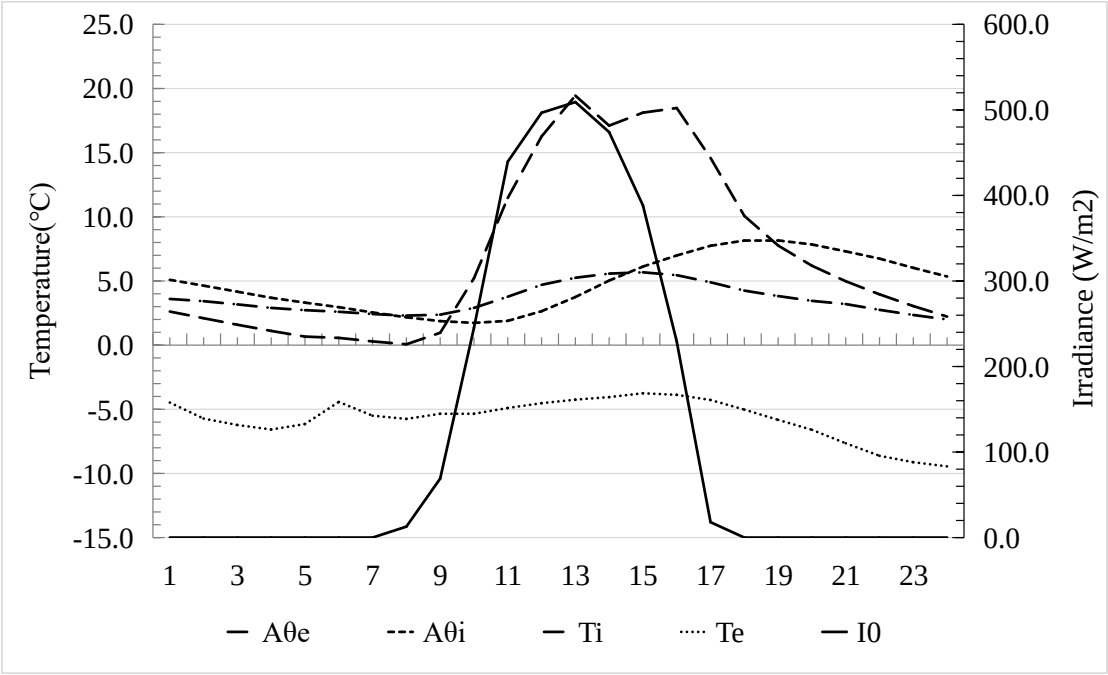

Fig.5- 13. Dynamic changing of thermal performance on 24th January.

(2) 30th January, 2016, Overcast day

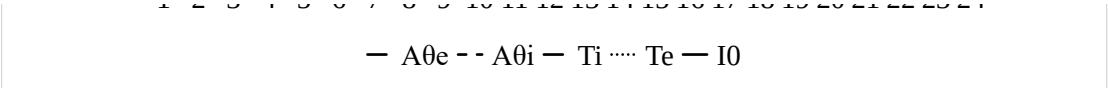

Fig.5-14 shows the variation of the average surface temperature $A_{\theta,e}$, $A_{\theta,i}$, indoor temperature T_i, outdoor temperature T_e, and global soar radiation I_0.

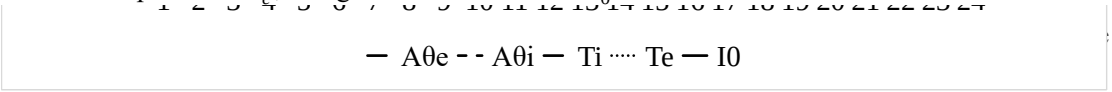

Fig.5-14 illustrate that the the global solar radiation I_0 had a low level in whole day resulting that both of surface temperatures had a slight variation, and external surface temperature $A_{\theta,e}$ was lower than internal $A_{\theta,i}$ in most of time. When the solar irradiance reached its peak value at 15:00 p.m., the external surface temperature $A_{\theta,e}$ began to increase and exceed the internal $A_{\theta,i}$ with obtaining its biggest value one hours later. After that, solar radiation I_0 started to decline rapidly, at the same time, surface temperature $A_{\theta,e}$ also presented a downward trend obviously.

For the indoor temperature T_i, it was slightly higher than the outdoor T_e, and also higher than

both of the surface temperatures.

According to the above analysis, the external surface of the concrete wall was almost not stimulated by the solar radiation on the overcast day, and the indoor temperature was always higher than the surface temperature. It can be concluded that Trombe wall heating system had no significant effect on the day with no sun.

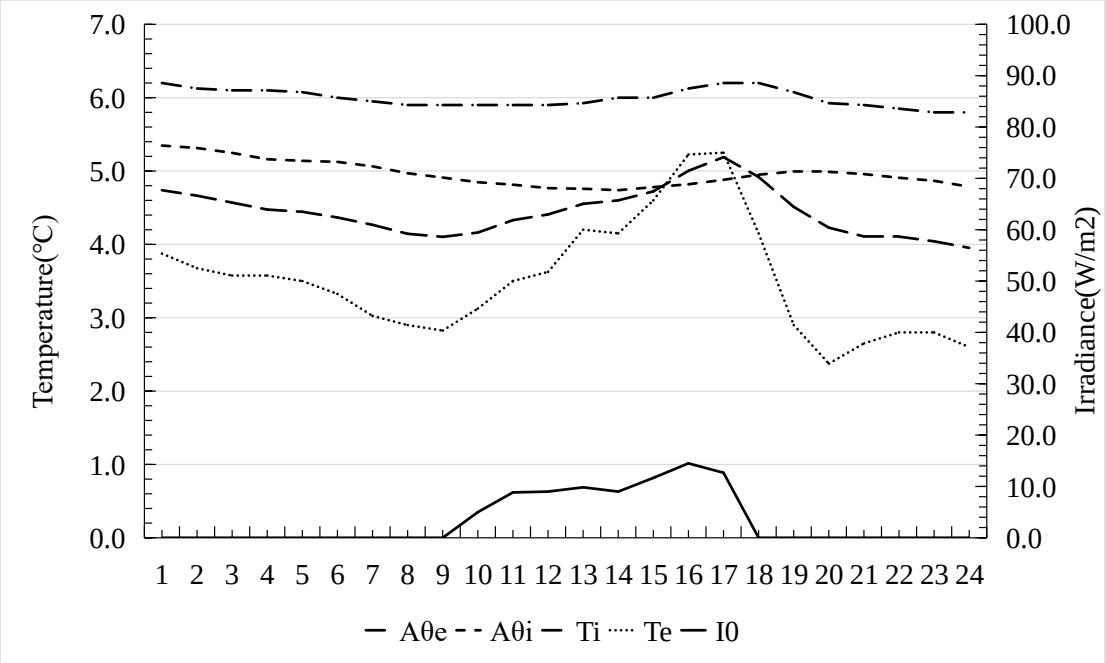

Fig.5-14. Dynamic changing of thermal performance on 30th January.

5-3-5 Variation of surface temperature on the Trombe wall on typical days

The following indicators were continuously tested for 24 hours with a 10-min. sampling time on sunny day and overcast day, including: external surface temperature at different height, named $\theta_{e,1}$, $\theta_{e,2}$ and $\theta_{e,3}$. All of the above were compared together with the changing of the solar radiation I_0 synchronously. Results and analysis are indicated in the following sections.

(1) 24th January, 2016, Sunny day

Fig.5-15 shows the variation of the external surface temperature at different height named $\theta_{e,1}$, $\theta_{e,2}$ and $\theta_{e,3}$. It can be illustrated from Fig.5-15 that the surface temperature fluctuation of collector wall was very similar to that of solar radiation. The tested temperature of the external surface were changing with the height of location on the wall, and the sequence was $\theta_{e,1} > \theta_{e,2} > \theta_{e,3}$ from big to small. From 10:00 a.m., the temperature difference between $\theta_{e,1}$ located at the top of the wall and $\theta_{e,3}$ at the lowest becomes obvious, and reached its biggest value of 3.7℃ at 12:00. It was at 17:00 p.m.when the difference between them started to decline.

The above analysis explains that the air in the central core of the duct heat up when stimulated by solar thermal energy. Then the warm flow will rise up with density decreasing, which made

convention heat transfer increasing between the upward air and the top surface of the wall, resulting a temperature gradient observed on the different height of the wall, and that more obvious when solar radiation more high.

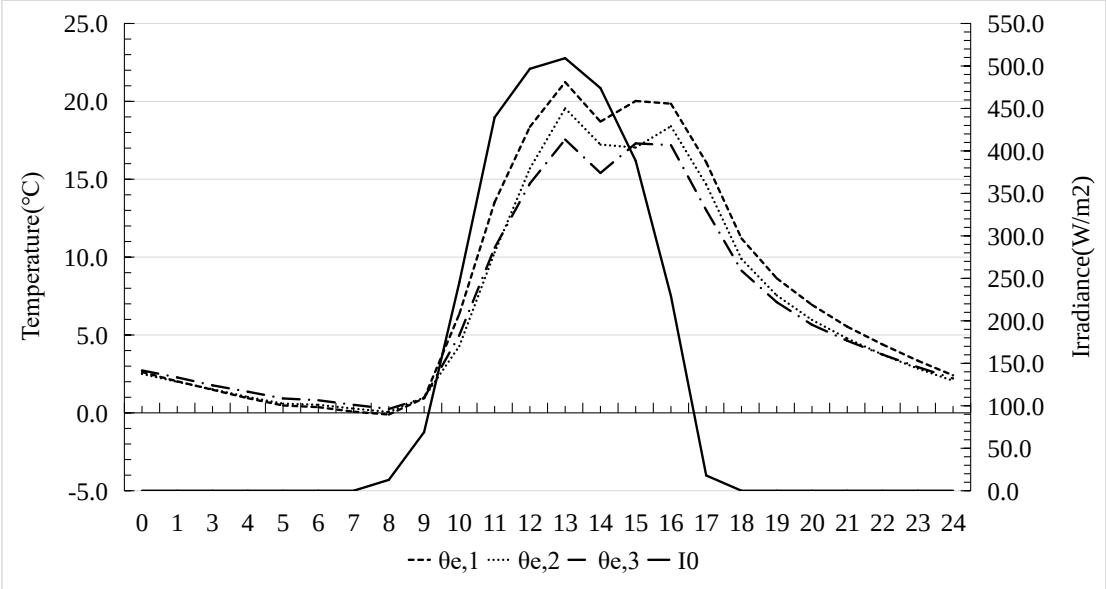

Fig.5-15 Variation of surface temperature on the Trombe wall on 24th January.

(2) 30th January, 2016, Overcast day

Fig.5- 16 shows the variation of the external surface temperature at different height named $\theta_{e,1}$, $\theta_{e,2}$ and $\theta_{e,3}$. It can be illustrated from Fig.5- 16 that the global solar radiation I_0 had a low level in whole day resulting that the surface temperature at middle height $\theta_{e,2}$ was very close to that at the top $\theta_{e,1}$ all along. At the time of 15:00 p.m., solar radiation reached its peak value, when there was a little temperature difference between the upper surface and the middle surface, and that obtained biggest value of 0.3℃ at 16:00 p.m.

The above analysis explains that the external surface temperature of the concrete wall had no obvious gradient on the overcast day, due to the less solar radiation.

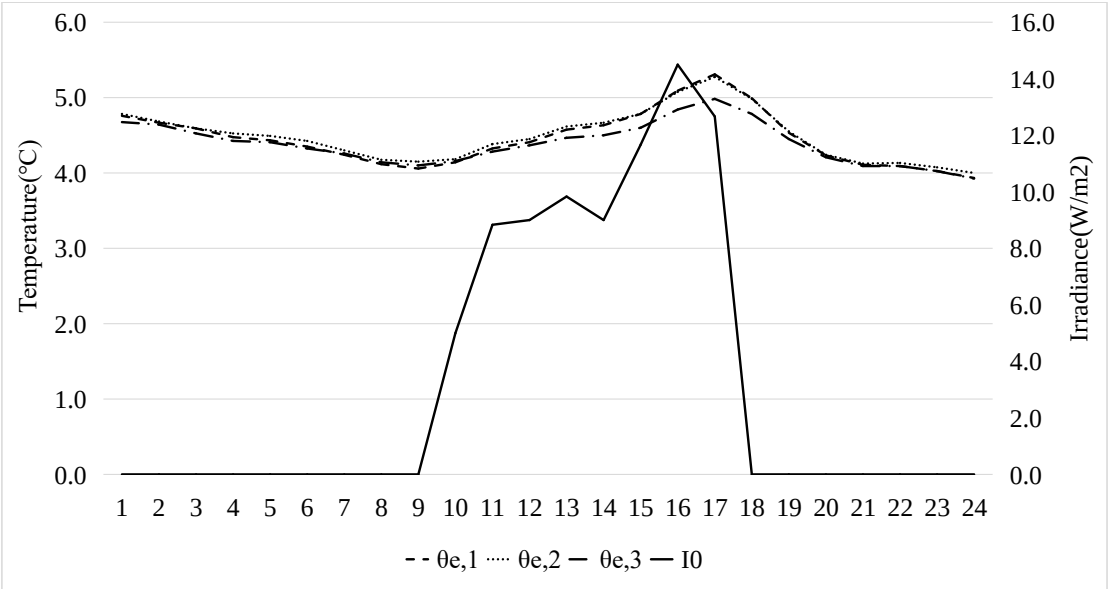

Fig.5- 16. Variation of surface temperature on the Trombe wall on 30th January.

5-3-6 Variation of temperature of inlet air and outlet air on typical days

The following indicators were continuously tested for 24 hours with a 10-min sampling time on sunny day and overcast day, including inlet air temperature T_{in} and outlet air temperature T_{out}. Both of the temperatures are compared with the changing of the solar radiation I_0 synchronously. Results and analysis are indicated in the following sections.

(1) 24th January, 2016, Sunny day

错误!未找到引用源。0 shows the variation of inlet air temperature T_{in} and outlet air temperature T_{out}. It can be illustrated from **错误!未找到引用源。**0 that the air temperature difference between inlet T_{in} and outlet T_{out} was in the range of 2℃~3℃ from 8:00 a.m. to 13:00 p.m., not so obvious. At noon, the solar radiation obtained the peak value. Two hours later, the inlet air temperature T_{in} reached its maximum value of 9.3℃, but much lower than the top of external surface temperature $\theta_{e,1}$ (see Fig.5-15) at the same time. Then, the air temperature difference between T_{in} and T_{out} began to increase till to the time around 20:00 p.m., when achieving its maximum value of 5.1℃, after that decreasing gradually.

The above analysis explains that the inlet air temperature was effected obviously by solar radiation on the sunny day. The air temperature difference between the two vents had a time-lag compared with the peak time of solar radiation. A maximum increment of 5.1℃ of air temperature was reached through the Trombe system.

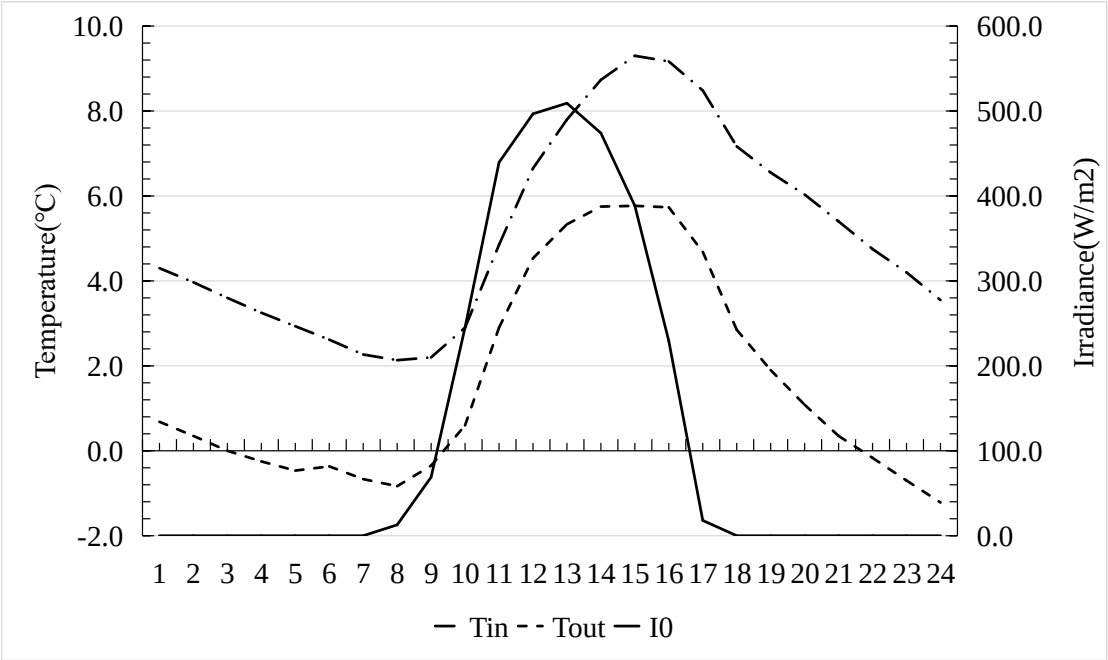

Fig.5- 30 Variation of air temperature of inlet and outlet on 24th January.

(2) 30th January, 2016, Overcast day

Fig.5-1 shows the variation of inlet air temperature T_{in} and outlet air temperature T_{out} . It can be illustrated from Fig.5- that the inlet air temperature T_{in} was not much higher than the outlet T_{out} . The maximum temperature difference was lower than 1℃ all along. At the time of 15:00 p.m., solar radiation reached its peak value, and two hours later, the temperature difference began to rise up to obtain its biggest value of 0.9℃ at 19:00 p.m. After that, the value of temperature difference declined gradually.

The above analysis explains that the increment of inlet air temperature was very small on the overcast day, due to the less solar radiation. Thus, the Trombe wall heating system has no obvious effect under such weather conditions.

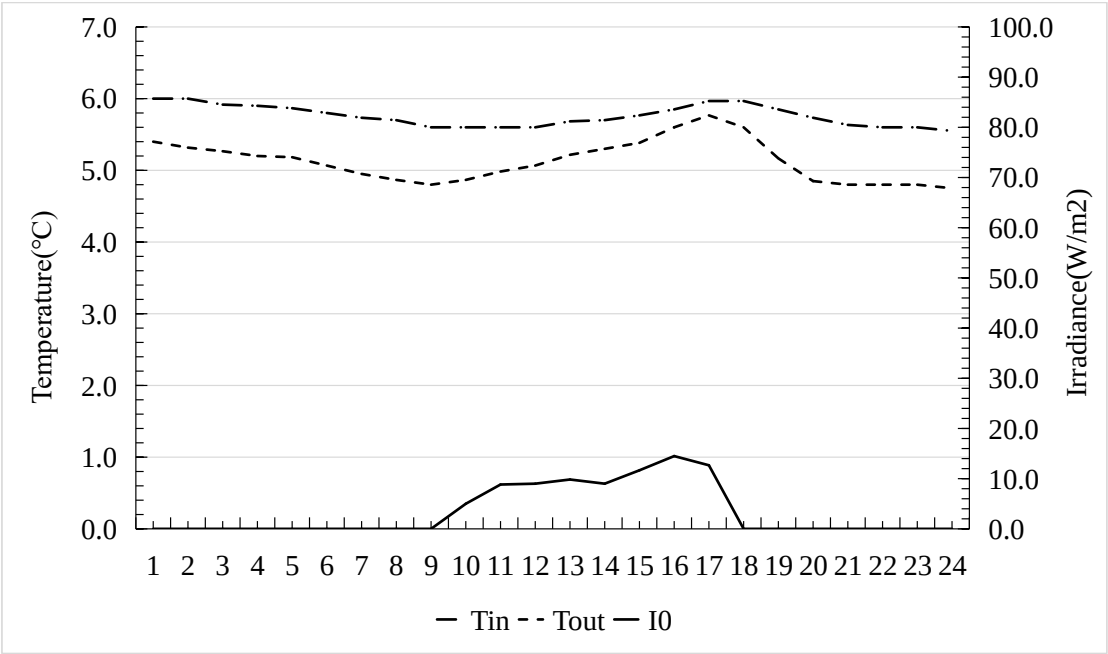

Fig.5-31 Variation of air temperature of inlet and outlet on 30th January.

5-4 Summaries

In this Chapter, field measurement was carried out on the South rooms under the real climatic condition of Hangzhou city. The monitoring period was from 22nd December, 2015 to 10th February, 2016, spanning the most coldest three months in the year, 50 days in all. the following indicators were observed and studied on different weather conditions:

- Indoor and outdoor temperatures of the rooms with insulation and with Trombe wall system separately;
- Solar radiation in the air duct of Trombe wall system;
- For the room with Trombe wall system, indoor temperature, external/internal surface temperature of the wall, inlet/outlet air temperature in the wall.

Through analyzing the monitored data, the thermal characteristics and effectiveness of these passive technologies were verified and determined as following:

(1) During the coldest wintertime of Hangzhou, indoor temperature fluctuate slightly with the outdoor temperature changing. When outdoor temperature reached the minimum value, indoor temperatures were at a higher level with maximum difference of 13.5℃. That was to say the insulation design for envelope played a certain role on improving indoor thermal environment.

(2) For the room with Trombe wall system, in most time of the coldest day, the inner surface temperature was kept at a higher level than indoor temperature, which proved a good heating effect of Trombe wall.

(3) In the sunny days, a maximum air temperature difference between the inlet and outlet was obtained by 5℃.

Reference

[1] Huang C, Zou Z, Li M, et al. Measurements of indoor thermal environment and energy analysis in a large space building in typical seasons[J]. Building & Environment, 2007, 42(5):1869-1877.
[2] Rohdin P, Molin A, Moshfegh B. Experiences from nine passive houses in Sweden – Indoor thermal environment and energy use[J]. Building & Environment, 2014, 71(71):176-185.
[3] Chen B, Zhuang Z, Chen X, et al. Field survey on indoor thermal environment of rural residences with coupled Chinese kang and passive solar collecting wall heating in Northeast China[J]. Solar Energy, 2007, 81(6):781-790.
[4] S.A.M. Bureka, A. Habeb, Air flow and thermal efficiency characteristics in solar chimneys

and Trombe Walls, Energy and Buildings 39 (2007) 128–135.
[5] F. Trombe, J. F. Robert, M. Cabanat and B. Sesolis, Some performance characteristics of the C.N.R.S. solar house collectors. Passive Solar Heating and Cooling Conf. Workshop.and Proc., Alberquerque, New Mexico, 18-19th May 1976: 201-202.
[6] A. Akbarzadeh, W.W.S. Charters, D.A. Lesslie, Thermocirculation characteristics of a Trombe wall passive test cell, Solar Energy, Volume 28, Issue 6, 1982, Pages 461-468
[7] Onbasioglu H, Egrican A N. Experimental approach to the thermal response of passive systems[J]. Energy Conversion & Management, 2002, 43(15):2053-2065.
[8] Sun P. Chen B. Liu YW. Experimental studies of passive solar house on indoor thermal performance in winter in Dalian. Building Energy & Environment, 2005, 24(1):22-27.

Chapter Six：Field-measurement on thermal performance of experimental building in summer time

6-1 Introduction

For the purpose on studying the indoor thermal environment when using passive energy efficiency technologies in the experimental building during the summer period in Hangzhou area, experimental verification was necessary to be applied. Thus, the only method for scientific study is to carry out field measurement by using relative instruments and meters to obtain the data monitored continually in real climatic conditions.

Many in-situ measurements on ventilation performance were found in the literature in the past year. This study[1] reports on an experimental investigation into heat transfer and mass flow in thermosyphoning air heaters, such as solar chimneys and Trombe Walls. In the reference[2], an extensive investigation was made and seven passive ventilation strategies, including: window openings, atria and courtyards, wing walls, chimney cowls/exhaust cowls, wind towers, wind catchers and wind floor e air inlet system. Solar chimneys and underground ventilation ducts were also assumed in the paper[3].

In this Chapter, field measurement was carried out on the South rooms, of which two rooms were installed with insulation materials, the other was set with Trombe wall system and solar chimney ventilation system. Under the real climatic conditions of Hangzhou, the following are investigated:

- Indoor temperatures of the south rooms;
- Indoor temperature, surface temperature, solar radiation and duct air temperature on the Trombe wall system;
- Air temperature and velocity of inlets and outlets located in the outer and inner room on solar chimney ventilation system.

Through analyzing the tested data, the effectiveness of the passive technologies are evaluated, and indoor environment of rooms are assessed.

6-2 Measurement and analysis on indoor thermal environment of South rooms

6-2-1 Experiment set-up

The thermal environment test on South rooms was carried out in summer (from 23rd June, 2016 to 4th August, 2016), continuing 43 days in all. The monitored data on the air temperature were recorded automatically with a 15-min sampling time using an Testo 174H data logger (see Fig.6-1). The technical specifications including the accuracy, and resolution are shown in Table.6-1.

Table.6- 1. Monitored data and technical specifications of measuring instruments.

Monitored parameters	Instrument name	Measurement range	Accuracy	Resolution
Air temperature	Testo 174H	-20 to 70℃	±0.35℃	0.1℃
Relative humidity	Testo 174H	0 to 100%RH	±3.0%RH	0.1%RH

Fig.6-2 shows the measuring-point locations, named $T_{1,i}$, $T_{2,i}$ and $T_{3,i}$ considered for the monitoring of the air temperature, as well as $H_{1,i}$, $H_{2,i}$ and $H_{3,i}$ considered for the monitoring of the relative humidity placed in the south rooms separately. All points were set at 1.5 m above the ground level. The outdoor data loggers were shaded using appropriate devices during the whole measurement for recording the outdoor air temperature T_e and relative humidity H_e.

Fig.6-1 Testo 174H data logger （Source：http://www.bjjttec.com ）

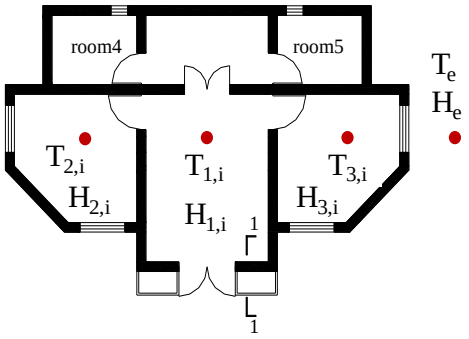

Fig.6-2 Schematic diagram of measuring-point locations

6-2-2 Results and discussion

6-2-2-1 During the whole monitoring time

According to the historical data recorded on the Hangzhou Meteorological website, from the monitoring day of 23rd June to 19th July, there were many thunderstorms and cloudy weather. After the end of July, there were all the high temperature clear and hot days till to early of August. It can be seen in Fig.6-3 that the mean outdoor temperature $\overline{T_e}$ dropped to 21℃ rapidly, and then began to increase. In spite of the effects of the thunderstorms weather condition, the temperature still presented a overall upward trend. In addition, the mean outdoor temperature $\overline{T_e}$ was above 30 ℃ from 20th July to 3rd August, continuing for 15 days, when were the hottest time during the entire monitoring period.

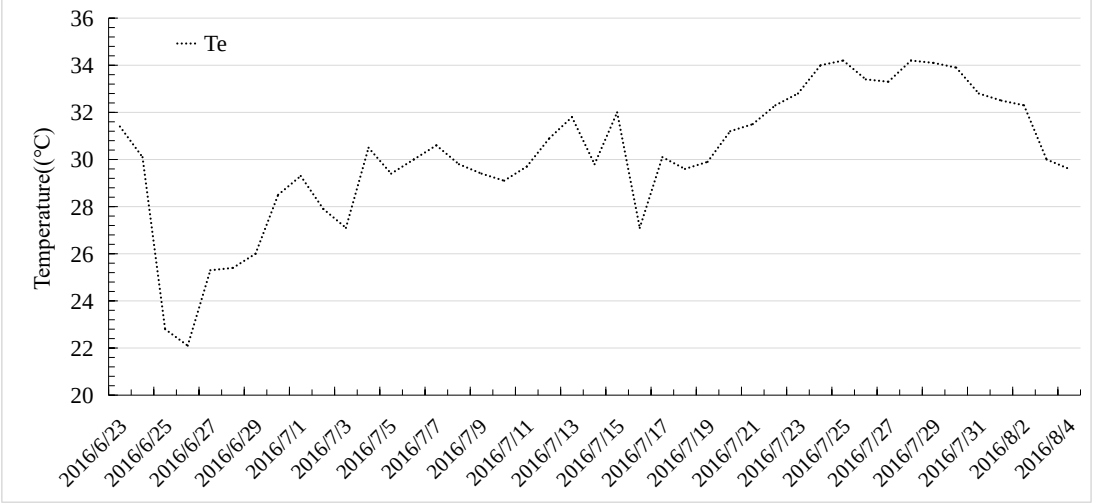

Fig.6-3 Variation of daily mean outdoor environment temperature
（23rd June, 2016 to 4th August, 2016）

The daily mean indoor temperatures $\overline{T_{1,i}}$, $\overline{T_{2,i}}$ and $\overline{T_{3,i}}$ are compared with the mean outdoor environment temperature $\overline{T_e}$, illustrated in Fig.6- 4. It can be noticed that daily indoor temperature $\overline{T_{1,i}}$ were always lower than that of the other rooms on the both side of it during whole monitoring period, and also had a slight variation. This was because of that the measuring point $T_{1,i}$ was located in the middle room with only one side wall facing to the south, while the other two rooms had three exterior walls influenced by the outdoor hot environment more easily. On the day of 26th June, both outdoor and indoor temperature had the lowest value, 23.8℃，25.1℃and 25.1℃ for $\overline{T_{1,i}}$, $\overline{T_{2,i}}$ and $\overline{T_{3,i}}$ separately, higher than the outdoor T_e of 22.1℃. On the day of 25th July, mean outdoor temperature $\overline{T_e}$ reached its peak value of 34.2℃, compared with that $\overline{T_{1,i}}$, $\overline{T_{2,i}}$ and $\overline{T_{3,i}}$ had the smaller value with 31.7℃，32.8℃ and 33.5℃ separately.

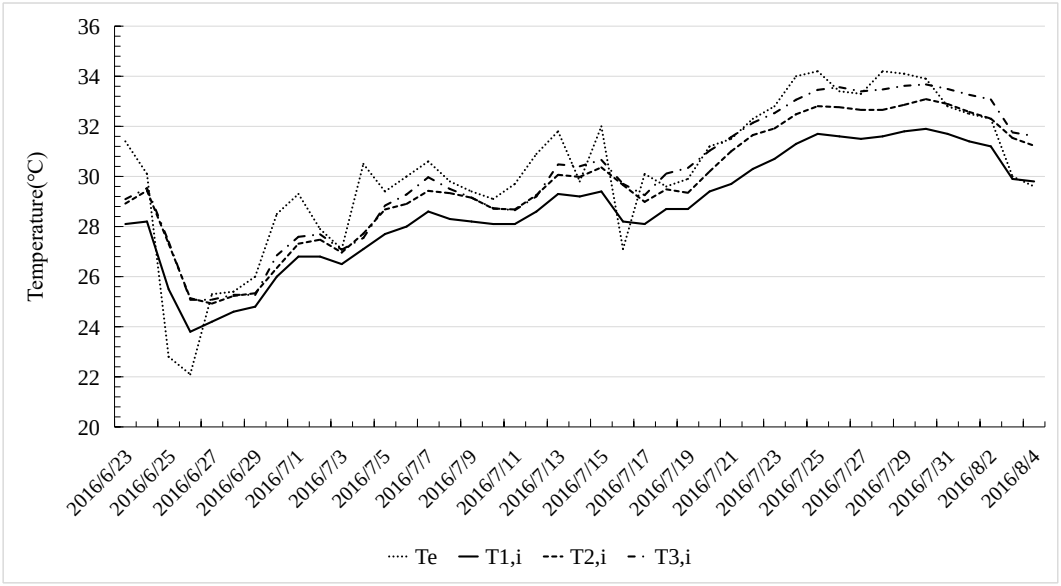

Fig.6- 4 Comparison of daily mean indoor and outdoor temperature of south rooms
（23rd June, 2016 to 4th August, 2016）

6-2-2-2 On 22nd July

The hottest day of 22nd July was selected as the typical climatic condition of Hangzhou area for the indoor temperature analysis of two south insulated rooms, as shown in Fig.6- 5. It can be seen that the hourly outdoor temperatures T_e of this day had been above 30℃ from 7:00 a.m. to 21:00 p.m., with the extreme value 39.4℃ occurring around 15:00~16:00 p.m. The daily outdoor temperature difference was about 12.6℃, that was a typical weather in Hangzhou, named high-temperature and clear-hot day. At the same time, indoor temperatures $T_{2,i}$ and $T_{3,i}$ monitored in the two rooms located on the both side had a relative steady variation in the whole day, and all higher than 30℃. For the room on the east side, its maximum temperature was 33.3℃, appearing at 16:00~17:00 p.m., one hour later than the outdoor; while, the value of the room on the west was bigger than the east one, and presented the biggest temperature of 34.7℃, at the time of 17:00~18:00 p.m., two hours later delayed. The daily temperature difference of the east room was 2.8℃, and that of the west one was 4.1℃. Fig.6-6 shows the indoor and outdoor humidity changing of two south rooms. It can be seen that the average humidity was relative high in the two rooms in the range of 80% to 83%, much higher than outdoor average value of 68%.

What's more, the doors and windows were closed at day and night during monitoring time, the heat accumulated in the room could not be distributed resulting higher indoor temperature than the outdoor at night. For the west room, long-term hot indoor condition in the whole day could be observed due to the direction influence. It must be suggested that natural ventilation by opening windows at night in summer of Hangzhou is an effective method for cooling. In addition, using heat protection or shading devices on the west side of buildings are quite necessary in spite of insulation layer.

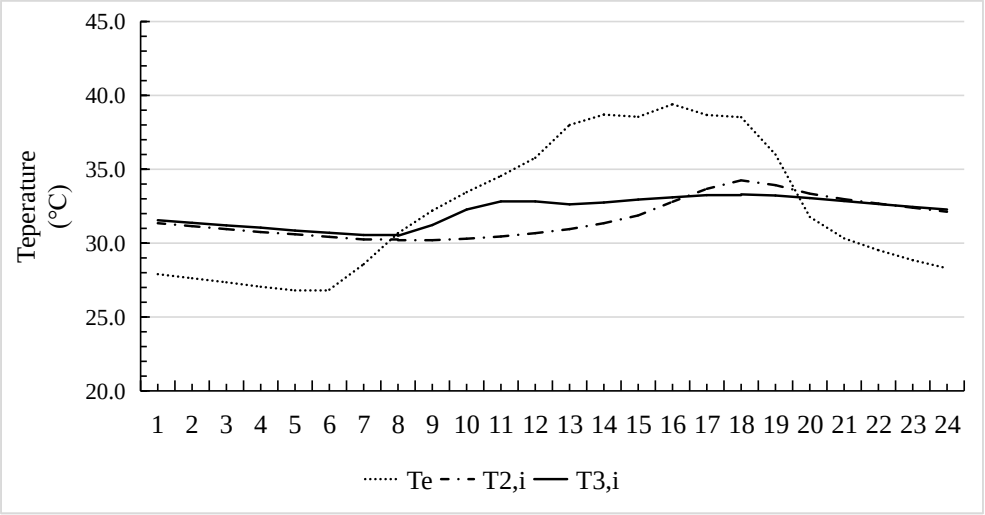

Fig.6- 5 Comparison of hourly indoor and outdoor temperature of two south rooms with insulation layers on 22nd July.

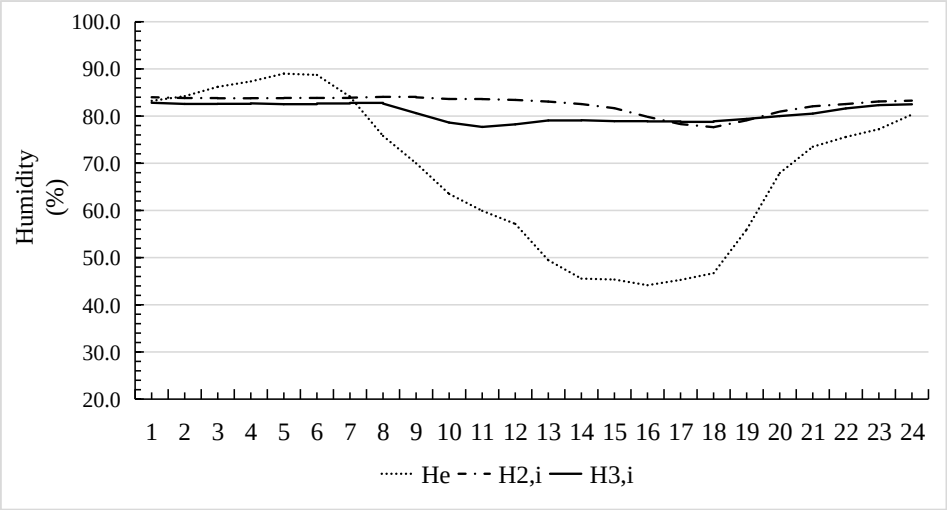

Fig.6- 6 Comparison of hourly indoor and outdoor humidity of two south rooms with insulation layers on 22nd July.

The hottest day of 22nd July was selected as the indoor temperature analysis of room with Trombe wall, as shown in Fig.6-. It can be seen that the indoor temperature $T_{1,i}$ had a slight fluctuation of 3.3℃. The biggest value of $T_{1,i}$ was 32℃ tested in the time of 16:00~17:00 p.m., 7.4℃ smaller than the peak value of outdoor temperature T_e occurring one hour earlier.

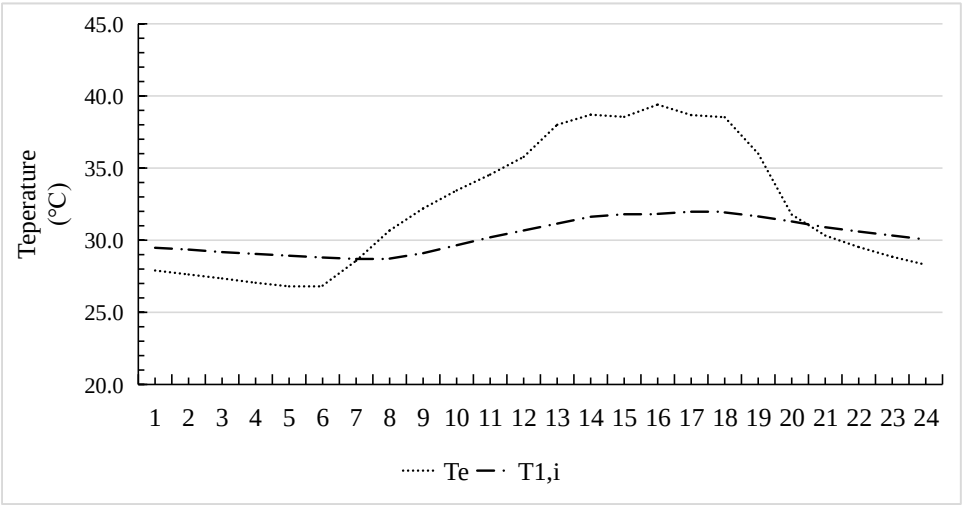

Fig.6-7 Comparison of hourly indoor and outdoor temperature of room with Trombe wall on 22nd July.

Fig.6-8 shows the indoor and outdoor humidity changing of room with Trombe wall. It can be seen that the average humidity was relative high with the value of 82%, much higher than outdoor average value of 68%.

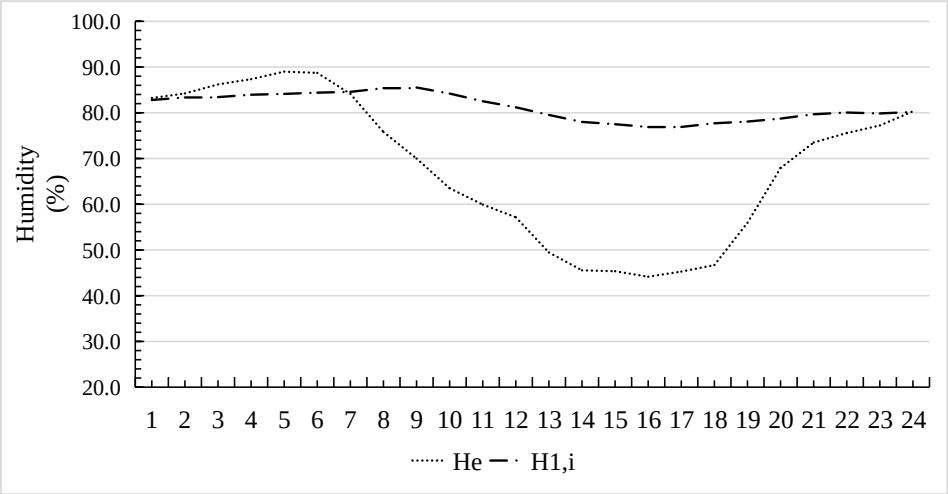

Fig.6-8 Comparison of hourly indoor and outdoor humidity of room with Trombe wall on 22nd July.

Based on the results, the air duct outside of the Trombe wall was open all along, in order to cooling the external surface by convention method. No other windows were provided except some vents located inside the room. One rectangle vent was set horizontally on the ceiling used to separate the upper rectangle chimney space and lower room, and three circle vents were on the ground floor, combined with an outdoor vent constructed on the outside ground into a thermal pressure system. From this figure, the thermal environment of the middle room with Trombe wall system was not desirable. Thus, the ventilation effect will be verified and discussed in the next section.

6-3 Measurement and analysis on Trombe wall system and solar chimney ventilation system

The monitoring work started from 23rd June 2016 to 4th August 2016, lasting 43 days in all. The following indicators were continuously tested for 24 hours a day, including:

- Indoor temperature, surface temperature, solar radiation and duct air temperature on the Trombe wall system;
- Air temperature and velocity of inlets and outlets located in the outer and inner room on solar chimney ventilation system.

The experiment set-up and monitoring results are presented and analyzed in the following section.

6-3-1 Experimental set-up

6-3-1-1 Schematic description

(1) Schematic description on Trombe wall system

As shown in Fig.6-, Fig.6-100 and Fig.6-1, a section of concrete collector wall was selected as research object, with 2800mm high,

900mm wide and 300mm thick. Located outside the wall, the air duct was 600mm deep, and the glass cover had two layers of 6mm thick separately with air gap of 9mm thick in the middle. A lattice panel at the air inlet and outlet in the wall was used to protect it from rodents.

Fig.6- shows the location for the monitoring of internal surface temperatures, named θ_i, and two locations considered for the vent temperature testing, named T_{in} and T_{out}. Correspondingly, there was also the other point θ_e located on the external surface for the temperature measurement, seen in Fig.6-100.

Two points were set in the air duct, 1.2m high above the ground, considered for the monitoring of solar radiation I_0 and ambient temperature T_a, seen in Fig.6-1.

Fig.6-6 present the overview of the field measurement.

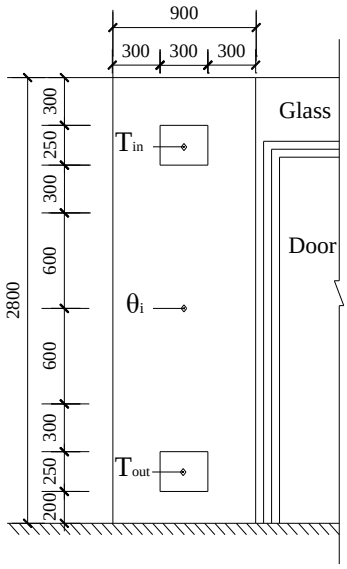

Fig.6-9. Schematic diagram of internal surface of the concrete collector wall.

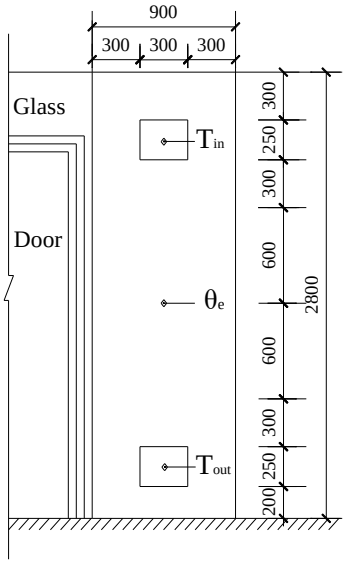

Fig.6-10. Schematic diagram of external surface of the concrete collector wall.

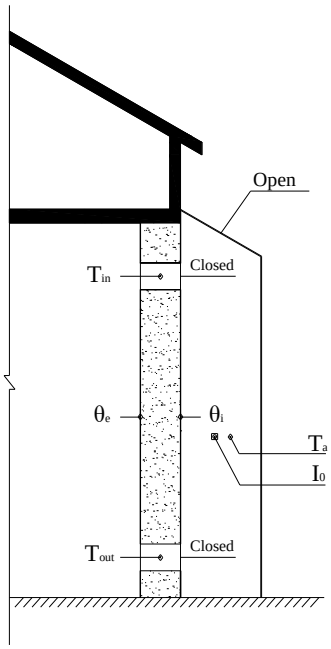

Fig.6-11. Schematic diagram of the section of the concrete collector wall.

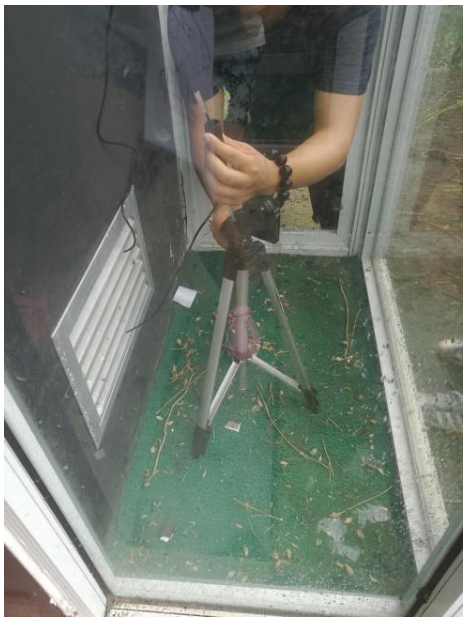

Fig.6-6. Photo of field measurement

(2) Schematic description on solar chimney ventilation system

In order to investigate the cooling effect of the tunnel ventilation enhanced by solar chimney, the measuring points for testing temperature and wind speed were arranged at the typical locations.

The temperature monitoring locations are shown in Fig.6-7 and Fig.6-8, including: outdoor inlet t_1, indoor space directly below the ceiling t_2, indoor inlet in the floor t_3, the middle of the room t_4, every 1.2 m in the air duct of the chimney from bottom to top t_5, t_6, t_7 and t_8. All the points inside the room were at 1.5 m above the floor.

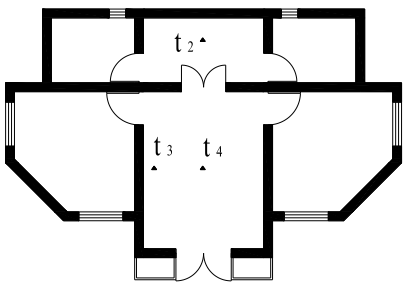

Fig.6-7. Plan view of the temperature monitoring locations

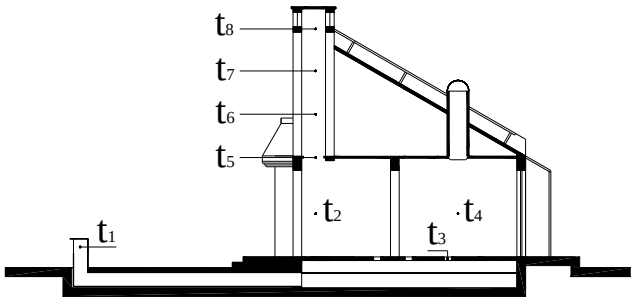

Fig.6-8. Section view of the temperature monitoring locations.

The wind speed locations were shown in Fig.6- 9 and Fig.6- 10, including: outdoor inlet v_1, indoor space directly below the ceiling v_2, indoor inlet in the floor v_3, the middle of the room

v_4 , every 1.2 m in the air duct of the chimney from bottom to top v_5, v_6, v_7 and v_8. All the points inside the room were at 1.5 m above the floor.

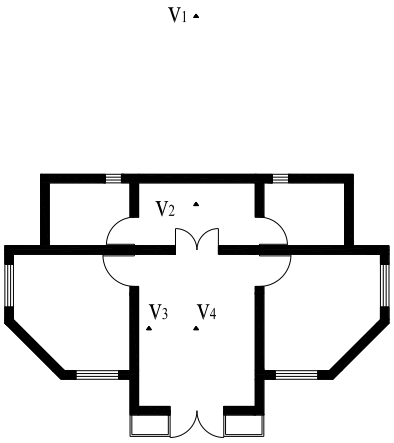

Fig.6- 9. Plan view of wind speed monitoring locations

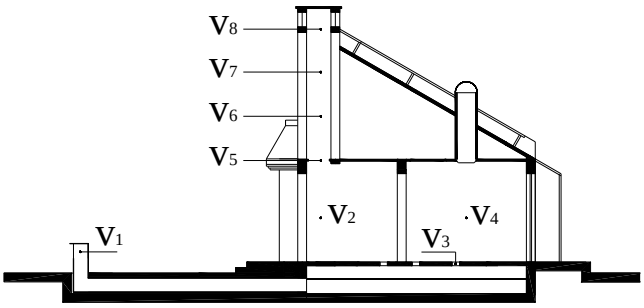

Fig.6- 10. Section view of wind speed monitoring locations.

6-3-1-2 Instrumentation

Surface temperature and vent temperature were collected using a data acquisition system, named JTR01 automatic test meter (see Fig.6- 11). The measurement range is -20℃~85℃, accuracy is ±0.5℃ (±0.2℃ at normal temperature).

Ambient temperature and solar radiation in the air duct were monitored by using JTR05 meter (see **错误!未找到引用源。**). This instrument consists of a total solar radiation sensor calibrated precisely and an imported digital temperature sensor, measuring solar radiation while monitoring the ambient temperature in the air duct formed by concrete wall and glass cover. Temperature sensor has high precision and stable performance by using a sealed package with stainless steel, simple to be connected with the standard 3.5mm plug form (testing range: -20～85℃; precision: <±0.5℃) . The data were recorded automatically with a 10-min sampling time. The technical specifications of solar radiation sensor are shown in **错误!未找到引用源。**.

(a)

(b)

Fig.6- 11. JTR01 temperature testing meter: (a) Front view; (b) Back view.

Wind speed was monitored by using JTR07 Multi-channel wind speed meter (see Fig.6-12). The measurement range is 0.05-5m/s, accuracy is ±0.04m/s and resolution is 0.01 m/s. Fig.6-13 presents the overview of the field measurement.

The monitored data on the air temperature were recorded automatically with a 15-min sampling time using an Testo 174H data logger (see Fig.6-1). The technical specifications including the accuracy, and resolution are shown in Table.6- 1.

Fig.6-12. JTR07 Multi-channel wind speed meter.

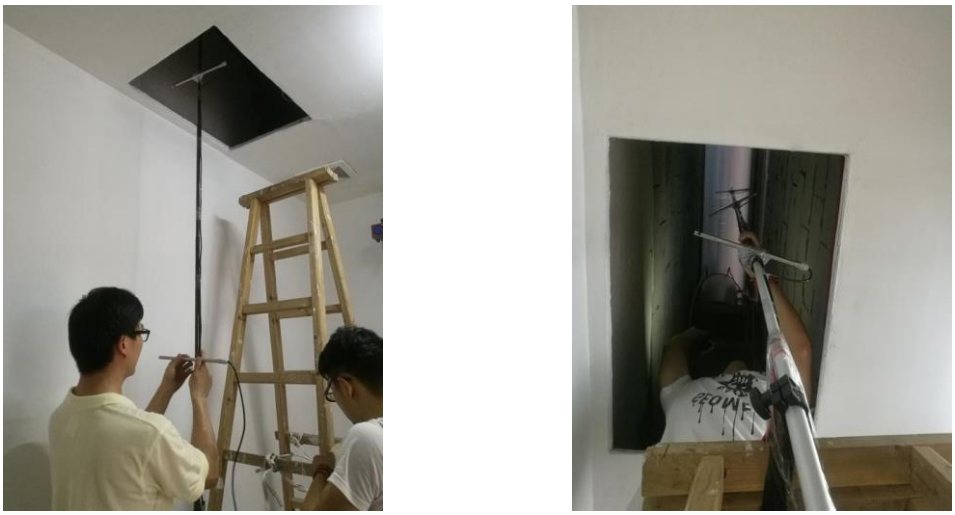

Fig.6-13. Photo of field measurement

6-3-2 Weather conditions during the monitoring period

The monitoring work started from 23rd June 2016 to 4th August 2016, lasting 43 days in all. The statistics on weather conditions during monitoring period are shown in Fig.6- 14. It can be illustrated that cloudy and rainy days are on the vast majority of testing days, accounting for 70% of the measurement time. Fig.6-3 indicated that the monitored outer temperatures in this period were the hottest in summer time of Hangzhou. Thus, the thermal environmental conditioning capacity of Trombe wall and solar chimney ventilation system can be examined and studied better in these typical weather conditions.

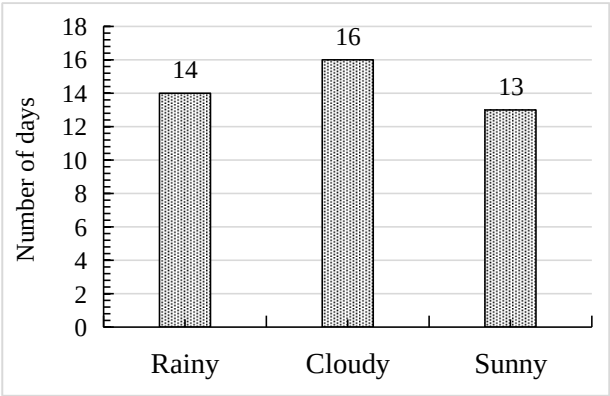

Fig.6- 14 Statistics on weather conditions from 23rd June 2016 to 4th August 2016

In order to observe and study the thermal-circulation characteristic of the Trombe wall and solar chimney system, three testing dates as representative of typical weather conditions are selected shown in Table.6-2.

Table.6-2 Selected testing date under typical weather conditions

June 23th	July 16th	July 22nd
Cloudy	Rainy day	Sunny day

6-3-3 Results and discussion on Trombe wall system

6-3-3-1 Variation of ambient temperature and solar radiation in the air duct on typical days

The following indicators were continuously tested for 24 hours on typical days, including: solar radiation I_0 , ambient temperature T_a in the air duct and outdoor ambient temperature T_e . Monitoring results and analysis are in the following sections.

(1) 23rd June, 2016, Cloudy

The data of global solar irradiance I_0 and ambient temperature T_a in the air duct were recorded for 24 hours on 23rd June, 2016. In the Fig.6-15, it can be found that：the global solar irradiance I_0 stated to increase in the early morning around 6:00 a.m., and reached its peak value of 168W/m^2 in the time of 12:00~13:00 p.m. Synchronously, the ambient temperature T_a also obtained the biggest value of 41.1℃, the smallest of which was 15.7℃ tested around 4:00~5:00 a.m. with a variation of 15.4℃ in whole day. Furthermore, the outdoor temperature T_e had the peak value of 39.5℃ monitored five hours later than the time of solar radiation.

According to the monitoring results, solar radiation had a relatively high level in cloudy weather condition, and the ambient temperature in the air duct was mainly affected by solar radiation. For the air duct, it was not fully open to induce cross ventilation, so the temperature in it was quite high and not help to cool the surface of the concrete wall.

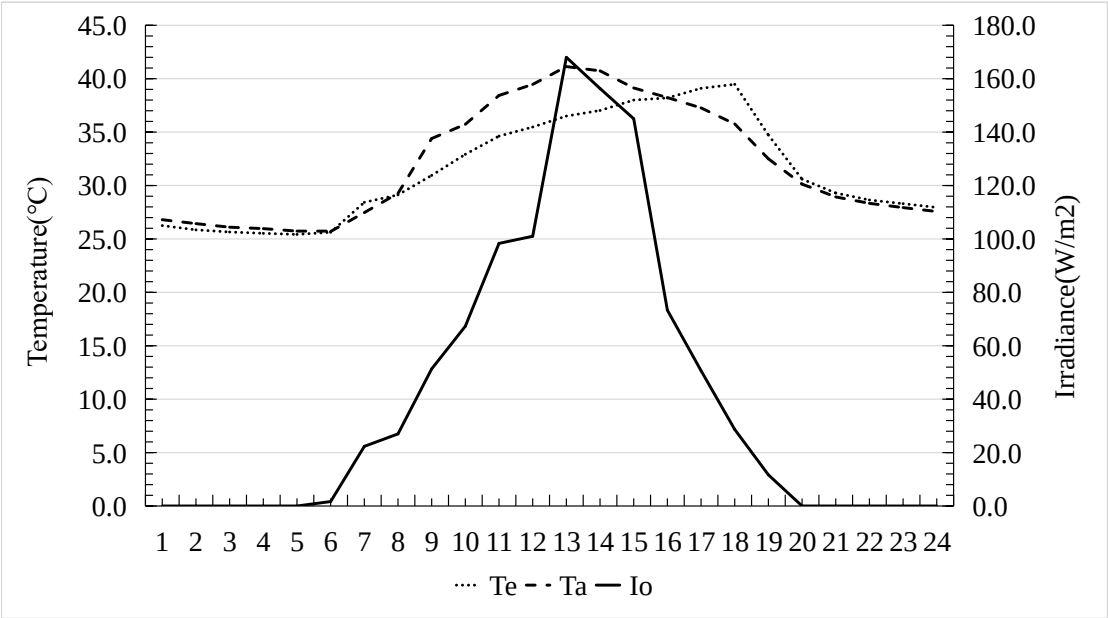

Fig.6-15. Variation of solar radiation and ambient temperature in the air duct on 23rd June.

(2) 16th July, 2016, Rainy day

The data of global solar irradiance I_0 and ambient temperature T_a in the air duct were recorded for 24 hours on 16th July, 2016. In the Fig.6-16, it can be found that the global solar radiation I_0 had a very low level in the whole day, and the maximum value of it was not more than 46.3W/m^2. The ambient temperature T_a was very similar to the out door temperature T_e, which had a slight fluctuation of 5℃, with the maximum of no more than 30℃ and the minimum of about 25.5℃.

According to the monitoring results, solar radiation had a relatively low level in rainy weather condition, and the ambient temperature in the open transparent air duct mainly depend on outdoor temperature.

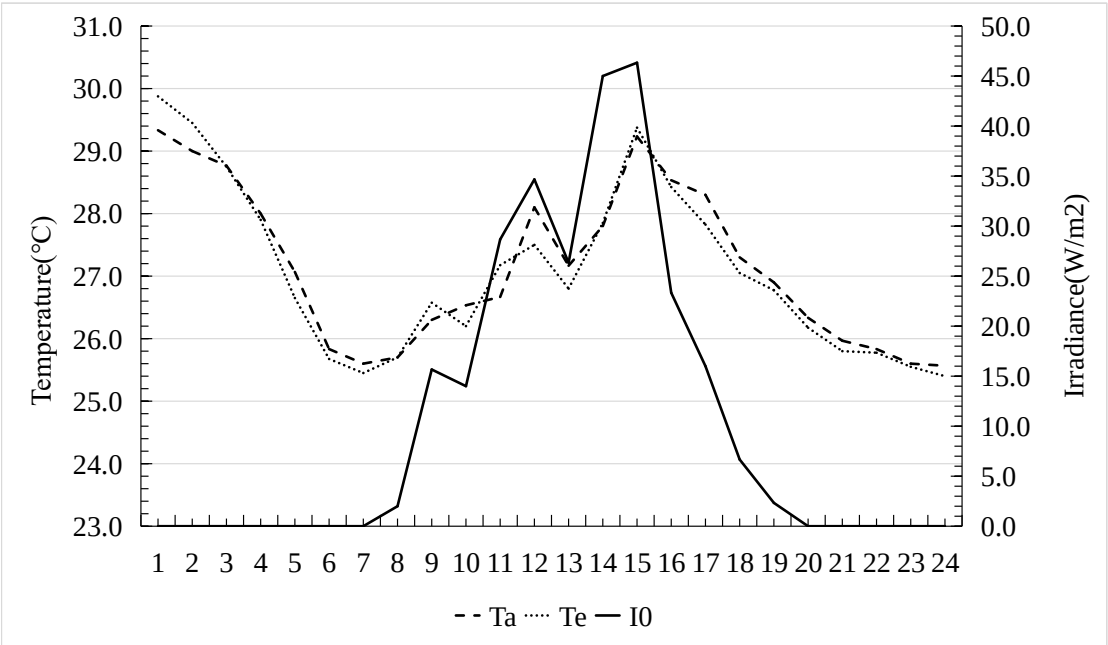

Fig.6-16. Variation of solar radiation and ambient temperature in the air duct on 16th July.

(3) 22nd July, 2016, Sunny day

The data of global solar irradiance I_0 and ambient temperature T_a in the air duct were recorded for 24 hours on 22nd July 2016. In the Fig.6-17, it can be found that the solar irradiance I_0 began to increase at 7:00 a.m., reaching its peaking value of 216.7 W/m^2 in the time of 13:00~14:00 p.m. The changing of ambient temperature T_a was not influenced by solar radiation at all due to the glass cover open. The biggest value of T_a was 45.2℃, occurring at about 9:00 a.m.; while the outdoor temperature T_e reached its maximum value of 39.4℃, two hours later than the peak time of solar radiation.

According to the monitoring results, solar radiation had a relatively high level in sunny weather condition. The air duct must not be closed in case the temperature will be too high in it.

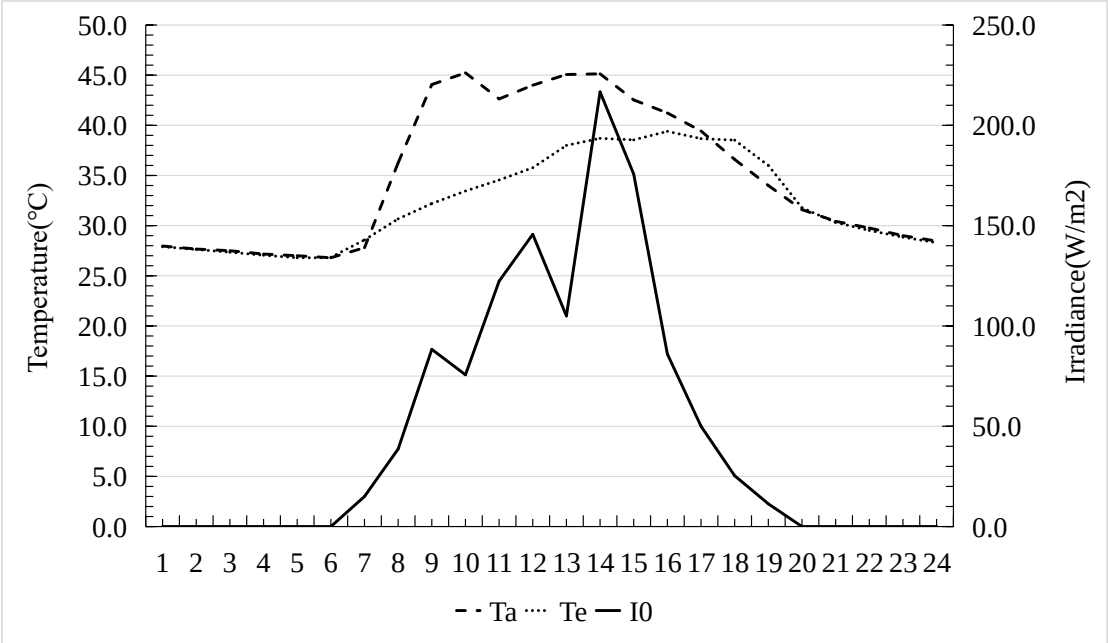

Fig.6-17 Variation of solar radiation and ambient temperature in the air duct on 22nd July

6-3-3-2 Dynamic changing of thermal performance of Trombe wall system on typical days

The following indicators were continuously tested for 24 hours with a 10 min sampling time on sunny day and rainy day, including: external and internal surface temperature θ_e and θ_i; indoor temperature T_i, outdoor temperature T_e and global soar radiation I_0 were also recorded synchronously, compared together with the surface temperature. Results and analysis are indicated in the following sections.

(1) 22nd July, 2016, Sunny day

Fig.6- shows the variation of the surface temperature θ_e and θ_i, indoor temperature T_i, outdoor temperature T_e, and global soar radiation I_0. It can be illustrated that the external surface temperature θ_e got a rapid increase by stimulation of solar radiation in sunny day. The external surface temperature θ_e showed its peak value of 41.7℃ three hours earlier than that of outdoor temperature T_e, and the average value of θ_e was 35.1℃ with a variation of 6.6℃ in a whole day.

As the thermal inertia of concrete materials, internal surface temperature θ_i fluctuated gently. At 18:00 p.m., the peak value of θ_i was about 34.5℃, and the average was 32.3℃, with a temperature amplitude of 2.2℃. In terms of indoor temperature T_i, the highest was 32℃, and the lowest was 28.7℃, less variation compared outdoor temperature T_e.

According to the above analysis, concrete wall present obvious time-lag effect due to the heat storage characteristic, which partly did work on relieving the inner thermal environment but not enough. At night of that day, indoor temperature was even higher than the outdoor, due to less ventilation.

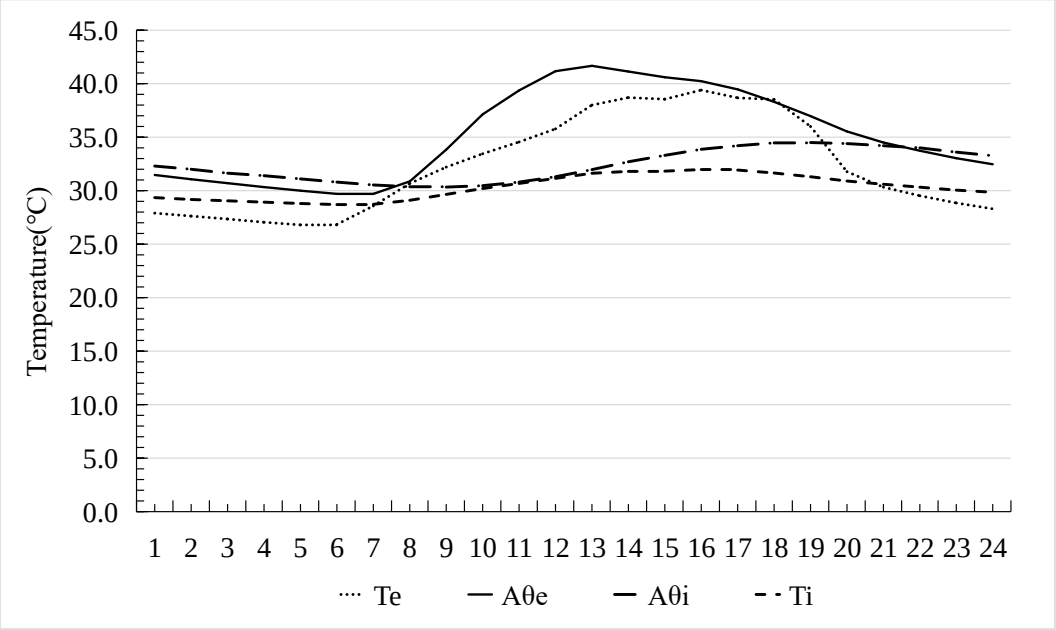

Fig.6- 24. Dynamic changing of thermal performance on 22nd July.

(2) 16th July, 2016, Rainy day

Fig.6-18 shows the variation of the surface temperature θ_e and θ_i, indoor temperature T_i, outdoor temperature T_e, and global soar radiation I_0. It can be illustrated that the external and internal surface temperature had little fluctuation, similar with the indoor air temperature T_i. Because the vents on the concrete wall were all closed at day and night, the values of T_i were always higher than the outdoor.

According to the above analysis, concrete wall does not contribute to heat dissipation inside the room in rainy weather conditions, so it is very important to enhance natural ventilation in time.

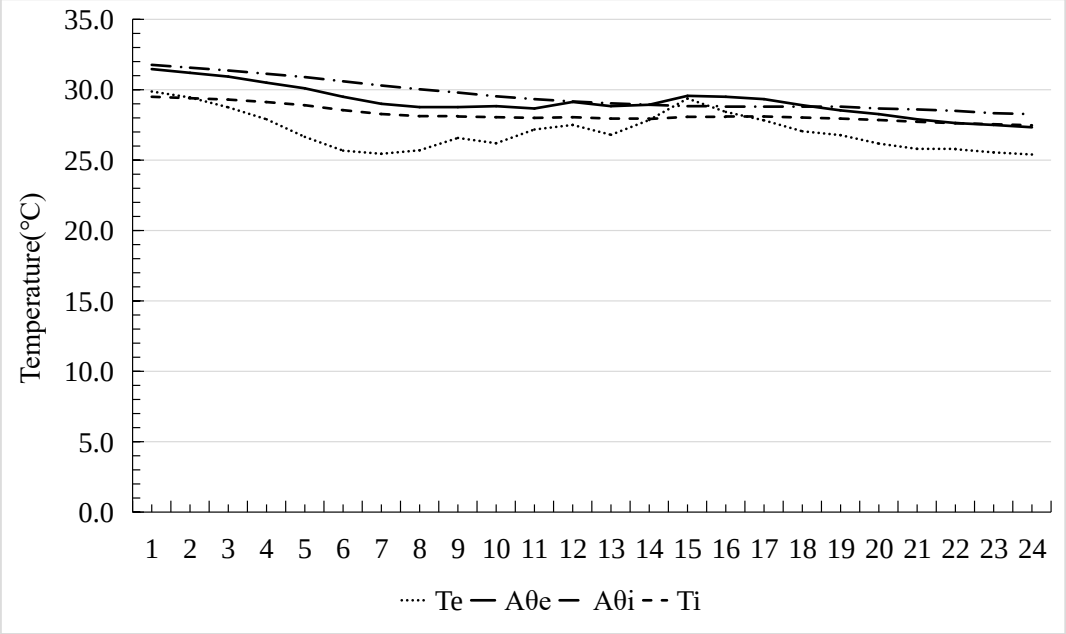

Fig.6-18 Dynamic changing of thermal performance on 16th July.

6-3-4 Results and discussion on solar chimney ventilation system.

The following temperature points were continuously tested for 24 hours with a 10 min sampling time on sunny day and rainy day, including: outdoor inlet t_1, indoor space directly below the ceiling t_2, indoor inlet in the floor t_3, the middle of the room t_4, every 1.2 m in the air duct of the chimney from bottom to top t_5, t_6, t_7 and t_8. All the points inside the room were at 1.5 m above the floor.

The following points for wind speed were continuously tested for 24 hours with a 10 min sampling time on sunny day and rainy day, including: outdoor inlet v_1, indoor space directly below the ceiling v_2, indoor inlet in the floor v_3, the middle of the room v_4, every 1.2 m in the air duct of the chimney from bottom to top v_5, v_6, v_7 and v_8. All the points inside the room were at 1.5 m above the floor.

The measured points were presented in Fig.6-13 ~ Fig.6-16, and results and analysis are indicated in the following sections.

6-3-4-1 Variation of air temperature at the different points on typical days

(1) 22nd July, 2016, Sunny day

Fig.6- 19 shows the variation of air temperature at the different points from outdoor inlet to the top of the chimney. It can be illustrated that the outdoor inlet temperature t_1 had a obvious fluctuation as well as the air temperature t_8 tested at the top of chimney, for the reason that they were influenced easily by the outdoor environment. The value of t_1 was smaller than t_8 all the time except the period of 6:00~9:00. From 5:00 ~17:00, outdoor temperature t_1 was higher than t_3 located at the floor outlet inside the room, with the maximum temperature difference of 6.4℃ occurring at about 14:00~15:00. It can be observed that indoor temperatures tested at the points

distributed from the lower space to the upper air duct had a small- to- big trend with the height changing, that was $t_3 < t_4 < t_5 < t_8$. The maximum temperature difference between t_3 and t_8 was 7.9℃, appearing at about 13:00 ~14:00.

From the above analysis, the temperature distribution complies with the principle of hot thermal pressure ventilation. At the top of the chimney, the air around obtains a higher temperature stimulated by solar heat, and the indoor air flow will rise up driven by the buoyancy resulted from small density; at the same time, outdoor airflow pass into the underground channel by the "blow-and-pull" action of the chimney, and the temperature declined through heat exchange with the soil, finally cooling the inner space.

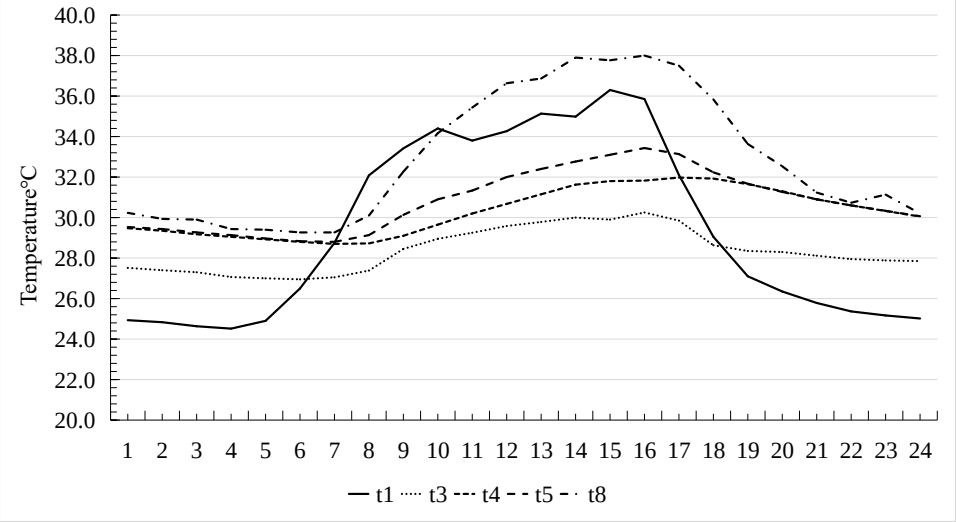

Fig.6- 19.Variation of air temperature at the different points on 22nd July.

Fig.6- 20 shows the variation of air temperature at the different points in the air duct of the chimney. It can be illustrated that the temperature began to appear gradient at different height of points, the higher points increasing obviously while the lowers fluctuating slightly. As the height changing, temperatures of points appeared a regular distribution of $t_2 < t_5 < t_6 < t_7 < t_8$

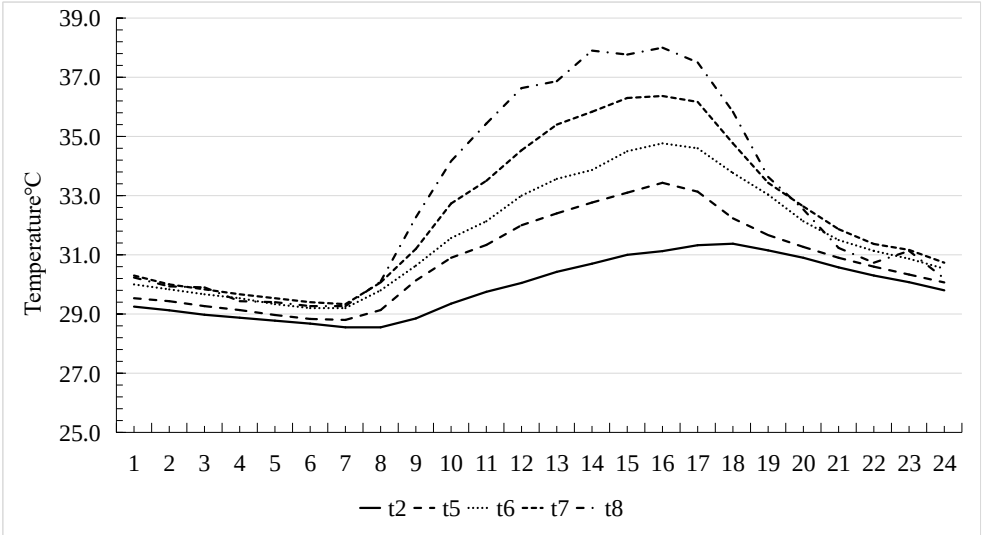

Fig.6- 20 Variation of air temperature at the different points in the chimney on 22nd July.

(2) 16th July, 2016, Rainy day

Fig.6-21 shows the variation of air temperature at the different points from outdoor inlet to the top of the chimney. It can be illustrated that the outdoor inlet temperature t_1 was at the lowest level in whole day. The results monitored at other points had no obvious difference. The value of t_5 was very closed to the highest point t_8, but stated to exceed it after 17:00 o'clock. Then, it can be confirmed that was phenomenon of air sinking.

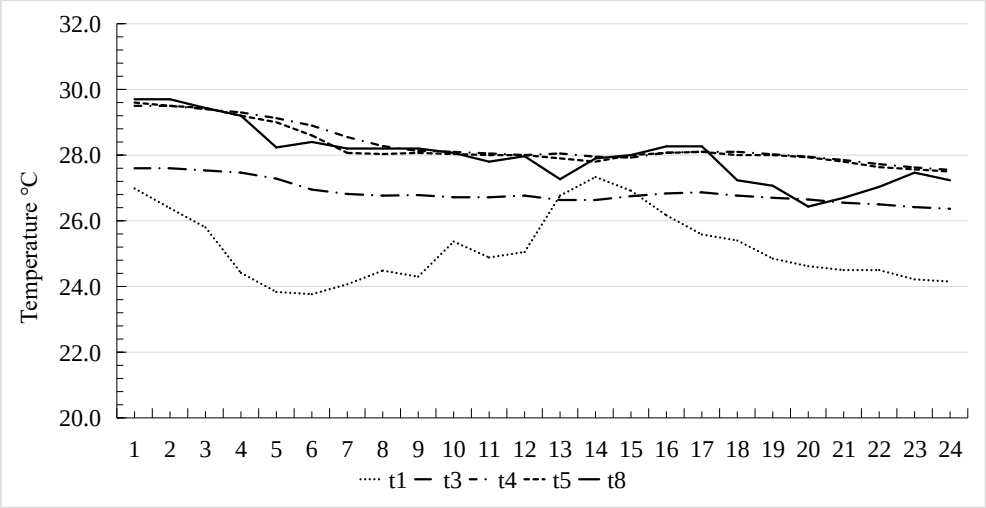

Fig.6-21. Variation of air temperature at the different points on 16th July.

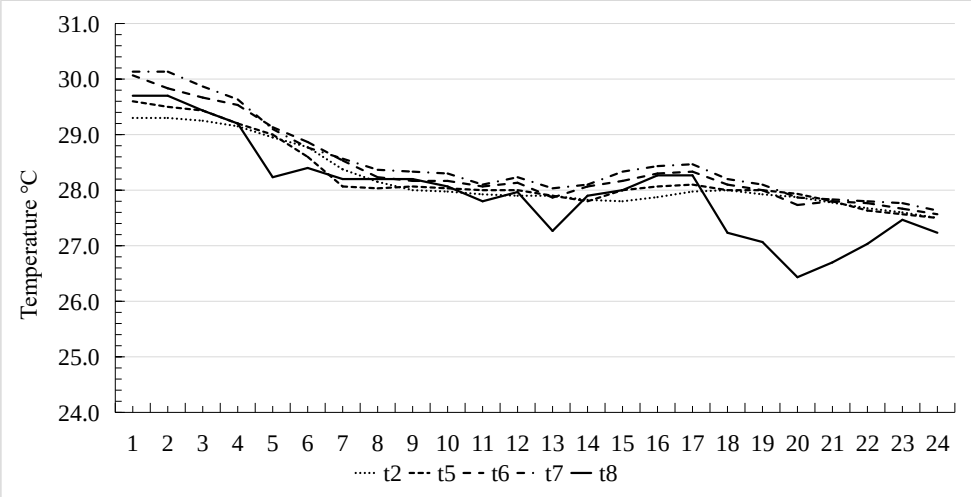

Fig.6-9 shows the variation of air temperature at the different points in the air duct of the chimney. It can be illustrated that the temperatures monitored at different points had no obvious difference as the height changing. No roles can be observed for the highest point t_8 due to the rainy weather outside. So, the natural ventilation cannot be improved by thermal pressure in days with no sun.

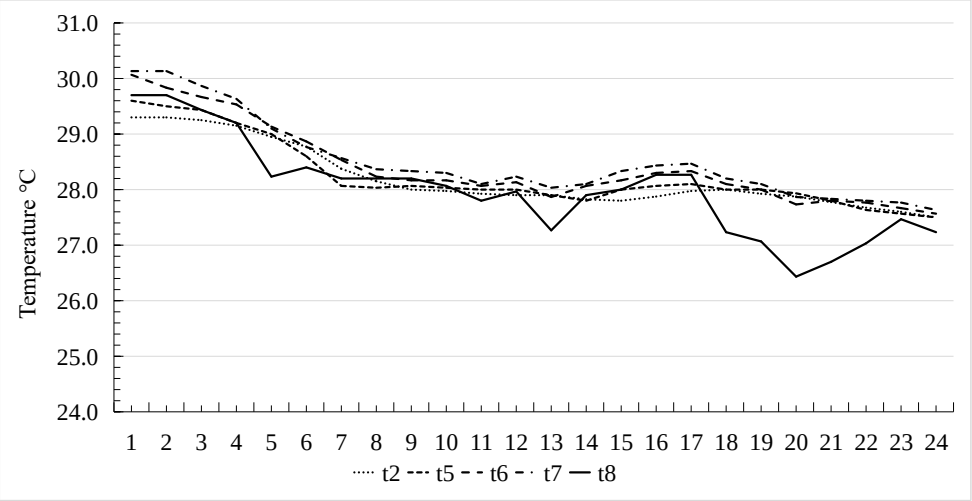

Fig.6-29. Variation of air temperature at the different points in the chimney on 16th July.

6-3-4-2 Variation of wind speed at the different points on typical days

For the reason of a high variation of wind, the speed data recorded every 20 minutes were presented and analyzed in the following figures.

Fig.6-22 shows the variation of wind speed at the different points from outdoor inlet to the top of the chimney on 22nd July, 2016, sunny day. It can be illustrated that the wind speed of point v_3 had the most obvious fluctuation and the speed values at night were relative higher than the daytime. From 12:00 to 16:00 p.m., the data of point v_3 had a synchronous changing with the point v_1. That might be considered that the airflow was more active after noon. In addition, there had almost no speed tested at other points except the outdoor inlet and inner point below the ceiling connecting the room and upper duct.

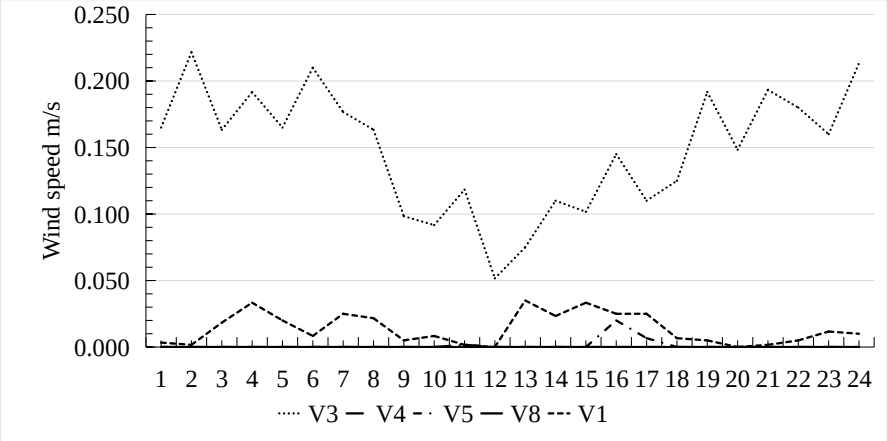

Fig.6-22. Variation of wind speed at the different points on 22nd July.

6-4 Summaries

In this Chapter, field measurement was carried out on the South rooms, of which two rooms were installed with insulation materials, the other was set with Trombe wall system and solar chimney ventilation system. Under the real climatic conditions of Hangzhou, the following were determined:

- Indoor temperatures of the south rooms;
- Indoor temperature, surface temperature, solar radiation and duct air temperature on the Trombe wall system;
- Air temperature and wind speed of vents located in the outer and inner room on solar chimney ventilation system.

Through discussing and analyzing the tested data, the following were examined and assessed:

indoor thermal environment of south rooms with insulation layers; the variation of ambient temperature and solar radiation in the air duct, as well as the dynamic changing of thermal performance for the Trombe wall system. The most importantly, the ventilation effectiveness on the solar chimney system was also verified.

It can be found that:

(1) When outdoor temperature reached its maximum value, the maximum temperature difference between the tested rooms and outdoor can be obtained by 7.6℃. It was to say that using insulation layers and Trombe wall system could protect building against heat in summer to a certain extent.

(2) Due to the thermal inertia of the concrete wall, on the hottest day, the indoor temperature had a smaller fluctuation of 3.3℃.

(3) It had no obvious ventilation effect by using such a solar chimney to induce natural ventilation. There had no obvious airflow crossing through the main space in the room. Thus, the configuration and size should be optimized in future.

Reference

[1] Burek SAM, Habeb A. Air flow and thermal efficiency characteristics in solar chimneys and Trombe Wall. Energy and Building 2007; 39: 128–35.

[2] KhanN,SuY,RiffatFB. A review on wind driven ventilation techniques. Energy and Buildings 2008; 40: 1586-604.

[3] Anh Tuan Nguyen*, Sigrid Reiter The effect of ceiling configurations on indoor air motion and ventilation flow rates Building and Environment 2011; 46: 1211-1222.

Chapter Seven: Improvement on thermal performance of Trombe Wall System by Simulation

Chapter Seven

7-1 Introduction

In the first few chapters, the passive energy efficiency technologies were studied theoretically and investigated through field-measurement method. The advantage and application limitation of the passive technologies in real operation were summarized, which provides a scientific and powerful basic data for the further research. Trombe wall heating system is a reliable passive technology that can reduce the energy requirement with low costs. According to the measurement results from Chapter IV, it is very necessary to improve the configuration of the Trombe wall system for the further optimization. But, such experimental study on a real building is normally affected by construction period, weather conditions as well as research funding, with a lower work efficiency. So, CFD (Computational Fluid Dynamics) techniques are applied very well to numerically investigate the thermal performance on Trombe wall system, for the purpose of enhancing its heating effect.

CFD (Computational Fluid Dynamics) techniques have been applied to ventilation studies for over 30 years, and many researchers are still seeking for more accurate, more reliable, and faster CFD models. Zhai[错误!未定义书签。] reviewed popular turbulence models that could be used for indoor environment modeling. They ascertained several favorable models from eight different categories. They found that the performance of the models was not always consistent for different flows. Among the RANS models tested, the RNG $k-\varepsilon$ models had the best overall performance. Many other researchers[1][2] tested various RANS models for predicting ventilation performance in buildings. These studies also concluded that one model could perform well for one flow but poorly in another. The performance of the RNG $k-\varepsilon$ model was rather stable. Due to the significant of thermal chimney systems, a number of studies have been carried out thus far. With respect to the model validation, Ong[3] developed a steady state model to simulate a thermal chimney and validated the model against experimental data. A detailed and dynamic model was developed and validated against experimental data from the literature in the study[4], taking into account relatively detailed mechanisms such as two-dimensional conduction through the absorber wall. An analytical model was also developed by Miyazaki et al.[5] and was validated against CFD data. Using the verified model, reduced fan shaft power by a thermal chimney and heating and cooling load changes by the thermal chimney were evaluated.

Based on the above literature, the reliability of CFD (Computational Fluid Dynamics) technology used in solar energy applications was to be verified. In this chapter, the Trombe wall heating system as a single researching module was separated from the building (see Fig. 7-1). Firstly, the model of Trombe wall system was validated against the monitored data for winter time by using Fluent software based on CFD (Computational Fluid Dynamics) technology. Secondly, with this validated model, the simulation on thermal performance of the Trombe wall system was carried out to investigate the effects of each operating parameters by changing each input variable one by one, and to determine the sensitivity of the thermal performance to individual parameters.

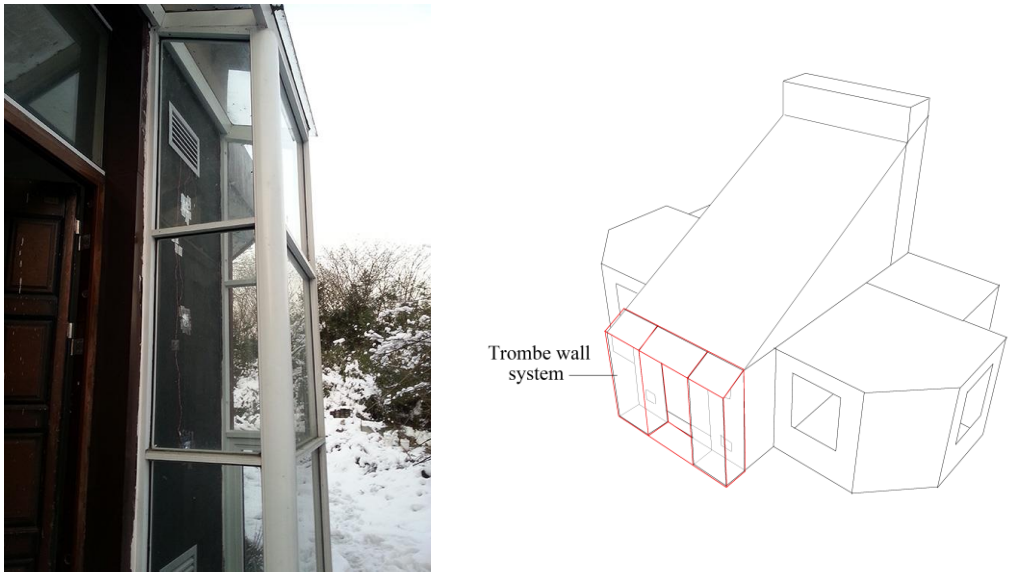

a. b.

Fig. 7-1. Trombe wall system: (a) Photo; (b) Sketch

The factors influencing thermal performance of Trombe wall mainly consist of outdoor meteorological parameters and the structure of the system itself. The fluctuation of outdoor climate is normally uncertainty and easily affected by ambient situation, so taking the structural parameters as sensitive factors to investigate and analyze the performance of the Trombe wall is necessary and scientific relatively. These input parameters are illustrated in Table.7- 1.

Table.7- 1 Variable structural parameters.

Structural parameters		
Variables	Air duct width（D）	D=0.2m, 0.3m, 0.4m, 0.5m, 0.6m
	Concrete wall height (H)	H=3m, 4m, 5m, 6m

Through simulation, the optimum size of Trombe wall can be obtained.

7-2 Model validation

7-2-1 Simulation tool and model validation procedure

7-2-1-1 Fluent software

Fluent is such a software produced in America as a universal tool for the computation of fluid dynamics and heat transfer in the engineering research field, which can solve in-compressible or compressible fluids, Newtonian or non-Newtonian fluids, single-phase or multi-phase fluid including steady or unsteady state, laminar or turbulent, as well as forced flow or natural convection in one-dimensional, two-dimensional and three-dimensional spaces, so as to determine the distribution of the mass, momentum, heat and others of fluid in spaces, solving problems involving complex equations such as flowing, chemical reactions, heat transfer, etc. In addition, it also provides a flexible grid processing capabilities, to support two-dimensional or three-dimensional triangular mesh, hexahedral, tetrahedral mesh and hybrid mesh. So, the software is widely used in building environmental engineering, power engineering, aerospace and other professional fields.

Solution steps of Fluent software are as follows: (1) create a grid; (2) select the appropriate solver; (3) grid input; (4) check the grid; (5) select the solver; (6) select the basic equation; (8) determine the boundary conditions; (9) adjust the control parameters; (10) initialize the flow field; (11) calculate; (12) check the results and save the results; (13) Correct the results.

7-2-1-2 Validation procedure

Simulation validation will be carried out in accordance with the following ideas:

Firstly, a physical model abstracted from the Trombe wall system was established by Fluent software;

Secondly, the boundary conditions including the values of outdoor and indoor temperature, solar radiation, and the thermal performance of envelope material were input to simulate the airflow distribution in the both adjacent space and on the inner/external surface of the concrete wall.

Then, the simulated temperatures distributed in the following typical positions: air temperature in the duct and in the room, inlet temperature and outer surface temperature on the Trombe wall, were compared with the monitored values, which have the advantage of being strongly linked to the heating effectiveness of the Trombe wall.

Finally, the Trombe wall system model was considered to be validated, if the residual between the simulated and the monitored values is reaching a value defined by international standards[6][7].

错误!未找到引用源。 illustrates the model validation procedure.

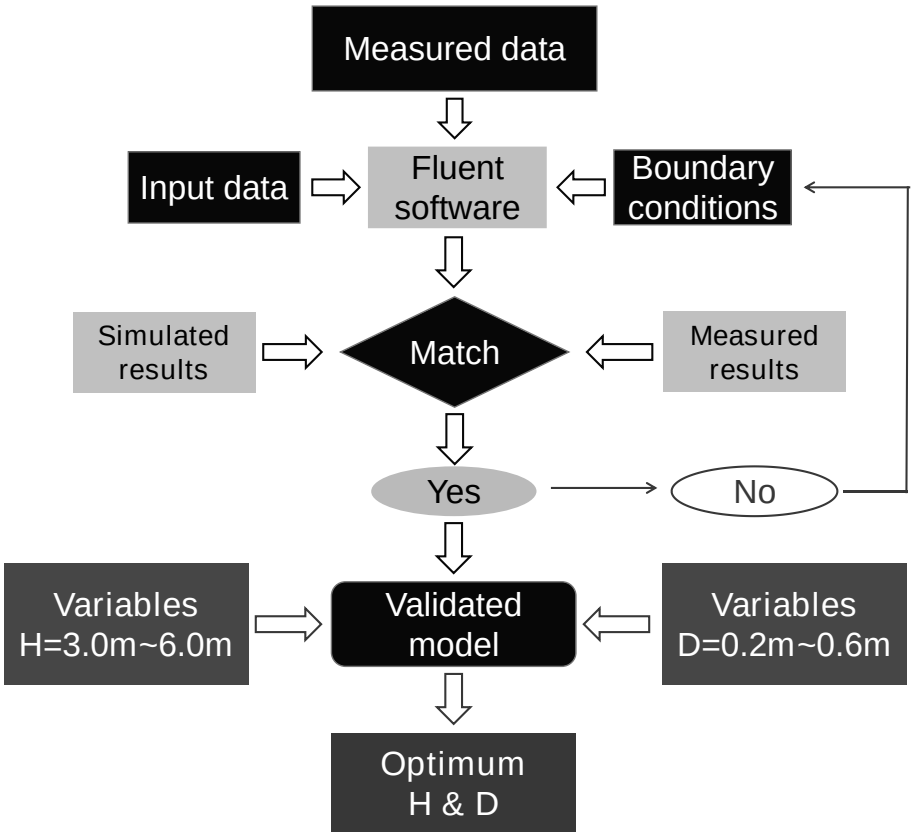

Fig.7-2 Model validation procedure

7-2-2 Model development

7-2-2-1 Physical model description

Accurate physical model is a necessary prerequisite for parameter analysis. For the sake of simplicity, the unit of Trombe wall system was modeled separately. The plane scope is shown in Fig.7- 3. Fig.7- 4 shows the section of the main element of the Trombe wall system, and the front of it is shown in Fig.7- 5. For the room part, the width W, depth L, net height H, were 3200mm、4200mm and 3000mm respectively. The concrete wall was 300 mm thick and 3000 mm high (H=3000mm), the air duct was 600 mm wide (d=600mm) and the glass cover was made of double glazed with the size of 6mm + 9mmA + 6mm. There were two vents located separately at the upper and lower of the concrete wall, with 300 mm wide (a=300mm), 250 mm high (b = 250mm) and 300 mm deep as the same as the concrete wall. It can be seen in Fig.7- 5 that a metal door, 1400 mm wide and 2200 mm high, was installed in the middle of the wall. There was a closed glass window (600 mm high and 1400 mm wide) provided above the door for natural lighting.

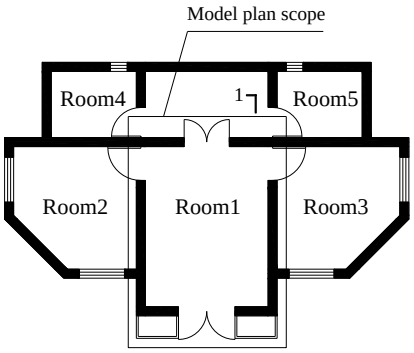

Fig.7- 3 Schematic diagram of plane

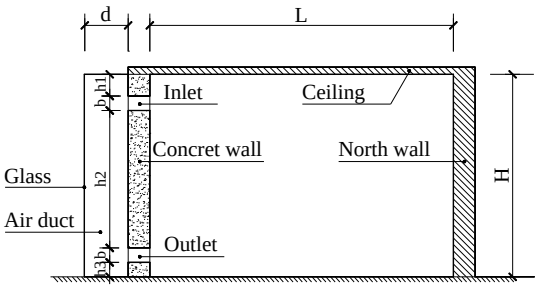

Fig.7- 4 1-1 Section

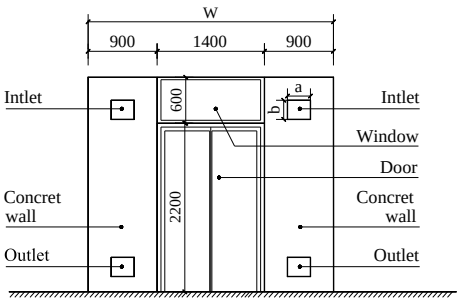

Fig.7- 5 Schematic diagram of front

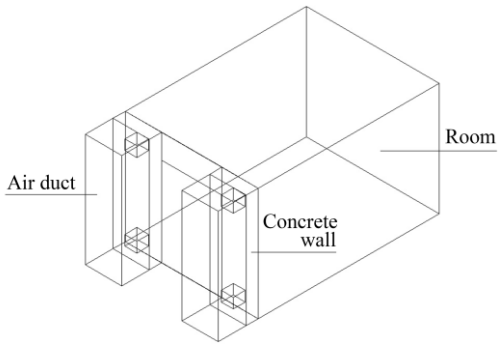

Fig.7- 6 Simplified 3D model of the Trombe wall

7-2-2-2 Numerical model description

(1) Model simplified

The heat exchange of the Trombe wall system consist of two processes:

1) Heat transfer between the collector wall and the outer glass air gap. The sun rays were projected onto the glass surface, a small part of which were absorbed by glass, and the others were transmitted into the air duct. Most of the solar radiation within the duct were absorbed by the concrete wall, causing the surface temperature of the wall increasing. Some heat absorbed by wall were conduct into the other side of the wall, the others were exchanged with the adjacent air by convention. This was achieved as a result of the fact that the solar energy caused a temperature rise as well as density drop of the air in the duct. The drop in air density caused air within the air duct to rise and went into the room through the upper vent of the wall. The air which left the duct was typically replaced by inner air from the lower vent of the wall.

2) Heat transfer between the collector wall and the inner space of Room 1. Due to the thermal conduct through concrete wall, its inner surface temperature obtained an increase. Some of the thermal energy were exchanged with the exposed surface of the room by radiation, the others were delivered into the ambient air.

Based upon the thermal transfer analysis, the heat exchanging procedure were divided into two parts: one was considered as the process of fluid-solid coupling heat transfer between the glass cover and the concrete wall; the other was considered as the heat transfer process between the concrete wall and Room 1. Thus, the simplified model is shown in Fig.7- 6, and the two parts of the Trombe wall unit are separately established as presented in Fig.7- 7.

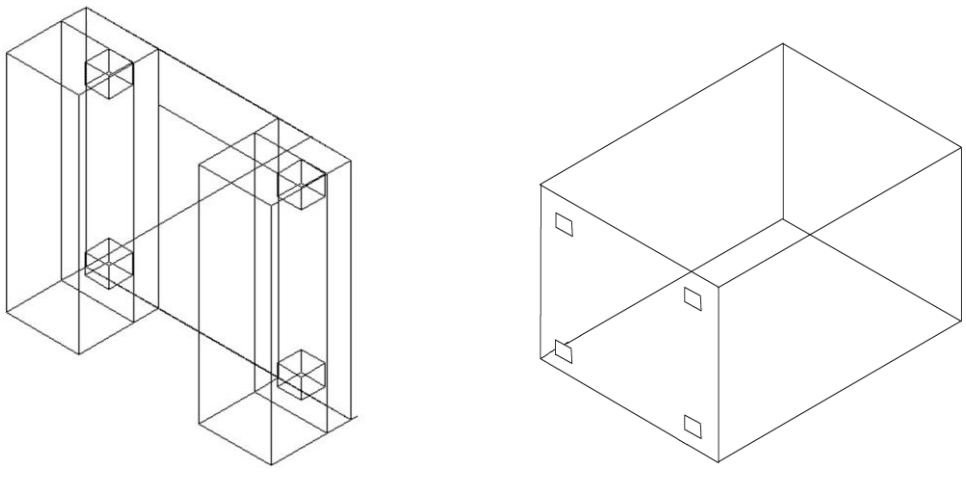

a. b.

Fig.7- 7 Schematic diagram of simplified model: (a) Model I; (b) Model II

(2) Model assumed

The following values were obtained from the simulation results of Model I, including: the inner surface temperature of the concrete wall, the inner surface temperature of the metal door, as well as the airflow velocity of upper vent on the wall, which were as the boundary conditions for the Model II.

To simplify the analysis, the air was assumed as in-compressible gas. The numerical calculations were performed for the steady-state velocity and temperature fields inside the room, and turbulent-state inside the air duct. The Boussinesq approximation was used to deal with the change of the buoyancy term due to the temperature difference in the momentum equation. RNG $k-\varepsilon$ model was applied to the numerical calculation for the turbulent state. $k-\varepsilon$ was compared with various turbulence models in the study[8], which reported that $k-\varepsilon$ was a good compromise except for natural ventilation with significant indoor thermal loads. DO model was used to radiation calculation.

The steady-state form of these equations is listed as follow

Continuity

$$\frac{\partial}{\partial_{xi}}(\rho u_i)=0, \qquad (1)$$

momentum:

$$\frac{\partial}{\partial x_j}(\rho u_i u_j)=\frac{\partial p}{\partial x_i}+\frac{\partial \tau_{ij}}{\partial x_j}+\rho g_i, \qquad (2)$$

energy:

$$\frac{\partial}{\partial x_i}(\rho u_i h)=\frac{\partial}{\partial x_i}(k\frac{\partial T}{\partial x_i})+u_i\frac{\partial p}{\partial x_j}+\tau_{ij}\frac{\partial u_i}{\partial x_j}, \qquad (3)$$

where ρ is the density, μ_i is the velocity component in the i-direction, p is the static pressure, x_i is a Cartesian coordinate, τ_{ij} is the stress tensor, g_i is the gravitational acceleration in the i-direction, h is the static enthalpy, k is the thermal conductivity, and T is the temperature.

Due to the complicated phenomena taking place in the Trombe wall system, several simplifying assumptions were made. These assumptions are listed as flows:

1) Envelope structures were regarded as insulation except the glass cover and the concrete wall;

2) The inner surface temperatures of the concrete wall in Model II were regarded as evenly distributed;

3) No compressibility effects were expected in this study， according with Boussinesq approximation；

4) No-heating devices in the room; no-penetration at all boundaries; regardless of heat loss.

(3) Solution methods

Unstructured meshes were used, and set intensively at vents and near the walls. Other solution methods are listed in Table. 7-2 ~ 7-4.

Table. 7-2 Spatial discretion

Pressure	Pressure-	Gradient	Momentum	Energy	Turbulent	Turbulent
Body	Simple	Least	Second	Second	First Order	First Order

Table. 7-3 Under-Relaxation Factors

Pressure	Density	Body	Momentum	Turbulent	Turbulent	Turbulent	Energy	DO
0.3	1	1	0.7	0.8	0.8	1	0.5	1

Table. 7-4 Convergence absolute criteria

Continuity	X-Velocity	Y-Velocity	Z-Velocity	Energy	Turbulent	Turbulent	DO
0.001	0.001	0.001	0.001	1e-6	0.001	0.001	1e-6

(4) Weather data

The sun rays were projected onto the glass surface, a small part of which were absorbed by glass, and the others were transmitted into the air duct. Most of the solar radiation within the duct were absorbed by the collector wall, causing the surface temperature of the wall increasing. Some heat absorbed by wall conduct into the other side of the wall, the others were exchanged with the adjacent air by convention.

Based upon the above analysis, it was achieved as a result of the fact that the solar radiation was the main factor causing the temperature rise in the duct. Thus, solar radiation module was necessary to be called in the simulation process[9]. Simulating time was set from 10:00 a.m. to 17:00 p.m. on 24th January, 2016. Hourly solar irradiance data was obtained from the Fluent solar module.The average of the hourly measured indoor and outdoor temperature $\overline{T_i}$ and $\overline{T_e}$ are listed in Table.7-:

Table.7-5 Hourly measured temperatures on 24th January, 2016

Time (24h)	$\overline{T_i}$ （℃）	$\overline{T_e}$ （℃）	$\overline{T_o}$ （℃）
10:00 a.m.	3.8	-4.9	2.9
11:00 a.m	4.7	-4.5	4.5
12:00 p.m	5.3	-4.3	5.3
13:00 p.m.	5.6	-4.1	5.8
14:00 p.m.	5.7	-3.8	5.8
15:00 p.m.	5.5	-3.9	5.7
16:00 p.m.	4.9	-4.3	4.7

$\overline{T_e}$ - measured average hourly outdoor temperature（℃）; $\overline{T_i}$ - measured average hourly indoor temperature（℃）; $\overline{T_o}$ - measured average outlet temperature (lower vent)（℃）.

7-2-2-3 Boundary conditions

(1) Physical properties of main materials

Physical parameters of construction materials are listed in Table.7-.

Table.7-6 Thermophysical parameters

Name	ρ	C_ρ	k	α	γ
Double-deck glazing	2500	840	0.084	150	1.5
Concrete wall	2100	920	1.28	——	——
Door	7850	480	58.2	——	——

ρ - Density (Kg/m^3)；

C_ρ - Specific Heat (J/(Kg·K))；

k - Thermal Conductivity (W/(m·K)；

α - Absorption Coefficient (1/m);

γ - Refractive Index.

(2) Boundary conditions of Model I

- The heat transfer coefficient of the material was determined by theoretical calculation；
- The temperature value of the free flow was decided by the monitored indoor or outdoor temperature；
- The radiation temperature was considered to be equal to the temperature value of the free flow;
- The free flow temperature in the air duct was determined by the simulation result;
- Lower vent: standard atmospheric pressure, the temperature was decided by the monitored value;
- Upper vent: standard atmospheric pressure, the back flow temperature was considered to be equal to free flow.

(3) Boundary conditions of Model II

- The heat transfer coefficient of the material was determined by theoretical calculation；
- Inner surface temperatures of Trombe wall and the door were determined by the simulation result;
- The surface temperature of ceiling was considered to be equal to the indoor temperature $\overline{T_i}$ (see Table.7-);
- The free flow temperature outside of the ground was assumed as the same as the outdoor temperature $\overline{T_e}$ (see Table.7-);
- Upper vent: the velocity V_{in} and the temperature T_u were simulated results from Model I;
- Lower vent: standard atmospheric pressure, natural back flow.

7-2-3 Validation results and discussion

7-2-3-1 Statistic indicators

Normalized Mean Bias Error - (NMBE) and the Coefficient of Variation of Root Square Mean Bias Error - CV(RMSE) are two well-accepted statistical indicators, which were adopted to assess the agreement between the simulation and the monitoring results. Both of them are formally defined as follows [6][7]:

$$NMBE(\%) = \frac{\sum_{i=1}^{n}(t_{ip} - t_{im})}{n-1} \times \frac{1}{\overline{t_m}} \times 100 \quad (4)$$

$$CV(RMSE)(\%) = \sqrt{\frac{\sum_{i=1}^{n}(t_{ip} - t_{im})^2}{n-1}} \times \frac{1}{\overline{t_m}} \times 100 \quad (5)$$

t_{ip} - simulated temperature of node i;

t_{im} - monitored temperature of node i;

$\overline{t_m}$ - arithmetic mean of a sample of n measured data;

n - number of monitored data (temperature) during the monitoring period.

The $NMBE$ indicator provides information on the discrepancy between the simulated and the measured temperature; a positive value indicates that the simulated temperatures are generally larger than the monitored data and vice versa (an ideal $NMBE$ value is nil). The $CV(RMSE)$ indicator expresses the relative ratio (in percent) between these discrepancies and the average of all monitored temperatures; the $CV(RMSE)$ indicator is always positive (a nil value is ideal). The $NMBE$ values indicates the presence of a systematic error or bias, while the $CV(RMSE)$ is a strong indicator of the simulation accuracy[10].

7-2-3-2 Hourly simulation results

The hourly measured average temperatures and simulated temperatures are summarized in Table.7-, followed by the corresponding NMBE and CV(RMSE) values.

Table.7-7 Summary of simulated and measured temperatures for model validation.

Date	Time (h)	Air temperature in duct （℃）		External surface temperature of the concrete wall （℃）		Upper vent temperature （℃）	
		Simulated t_a	Measured t_a'	Simulated $\bar{\theta}$	Measured $\bar{\theta}'$	Simulated t_u	Measured t_u'
24th Jan. 2016	10	11.7	11.2	16	11.5	5.7	4.9
	11	10.3	13.3	17.1	16.3	6	6.7
	12	10.7	13.8	17.2	19.4	6.3	7.8
	13	12.2	15.6	19.5	17.1	7.2	8.7
	14	14.1	15.6	21.6	18.1	7.6	9.3
	15	14.5	10.5	22.5	18.5	7.9	9.2
	16	10.3	7.7	20.7	16.6	7.4	8.5
NMBE		-9.80%		19.03%		-15.20%	
CV(RMSE)		23%		20.60%		18.40%	

It can be seen that the simulated inlet temperature fits well with the measured data during the period from 10:00 ~ 16:00, which were all remain lower than 25%, conforming to the regulation of ASHRA (American Society of Heating Refrigerating and Air-conditioning Engineers)[7].

7-2-3-3 Simulation results and discussion at typical time

The simulation results operated at 14:30 on 24th January was selected to be discussed and analyzed. In this section, Model I and II were simulated at this moment, for the sake of the validation against the measured values, and the flow distribution inside was also investigated.

The simulation procedure was carried out in two parts, one part was for Model I and the other for Model II.

Fig.7- shows the coordinate figure of Model I, front view (Z-Y plane) and lateral view (Z-X plane). The origin of the x-axis (x=0) is located in the middle of the door at the bottom of the wall showing the distance between the inner surface of the wall and the outer glass cover, the second y-axis indicates the width of the wall and the z-axis indicates the height of the wall.

Fig.7- shows the coordinate figure of Model II, front view (Z-Y plane) and lateral view (Z-X plane). The origin of the x-axis (x=0) is located at the left corner at the bottom of the wall showing the deep of the room, the second y-axis indicates the width of the wall and the z-axis indicates the height of the wall.

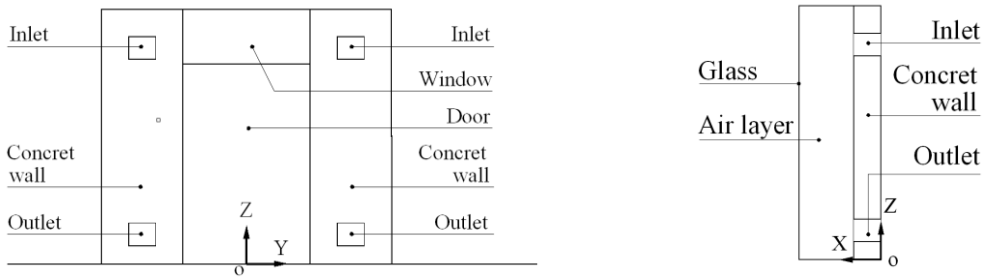

(a) (b)

Fig.7- 8 Coordinate figure of Model I: (a) front view; (b) lateral view

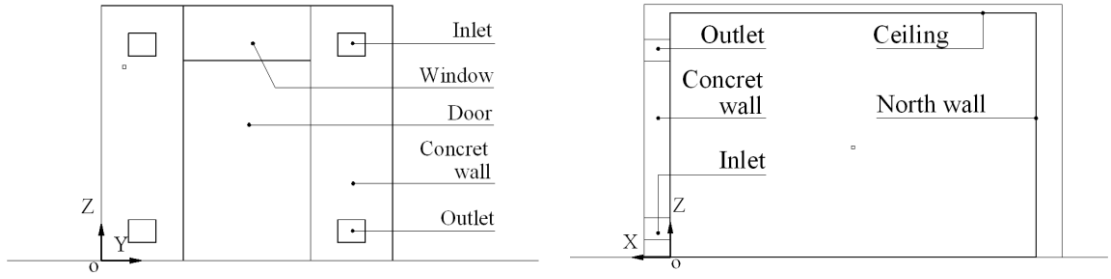

(a) (b)

Fig.7- 9 Coordinate figure of Model II: (a) front view; (b) lateral view

(1) Simulation results and discussion on Model I

Fig.7- 0 shows the simulated temperature distribution for the section of Model I (x=0, y = -1275mm, z=o). At this time, the solar radiation is relatively strong and steady, so the air temperature in the duct presents an obvious small-big trend up along the z-axis as shown the color changing in Fig.7- . The bottom average temperature was about 9℃, and the upper was 20℃. Because of the heat exchange, the temperature of wall presented a gradual deduction from outside to inside. In addition, the air close to the glass cover is much colder than that near to the wall at same level, due to the relative poor insulation of glazing.

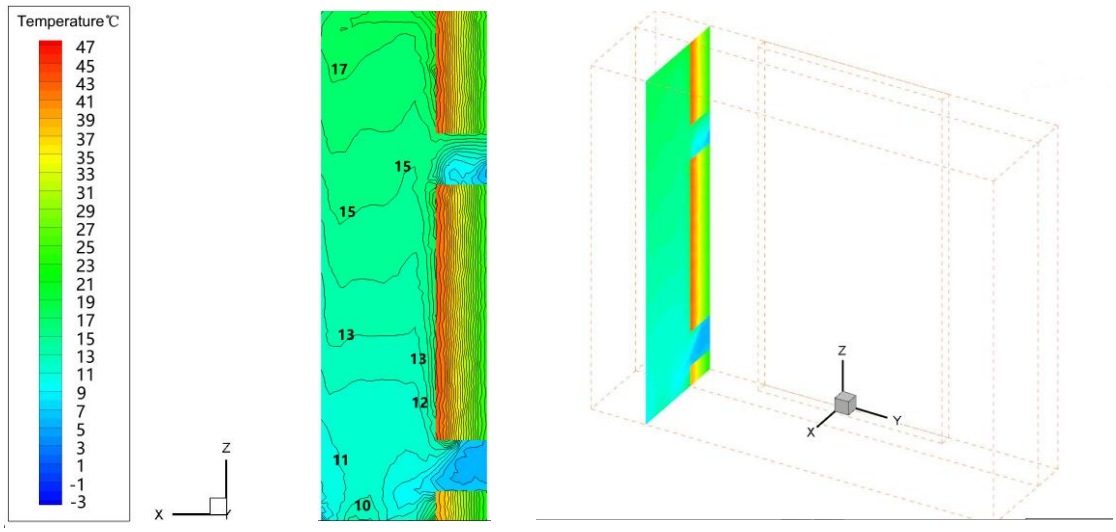

(a) Z-X Section (b) 3D view

Fig.7- 10. Simulated temperature distribution for Model I (x=0, y = -1275mm, z=o)

Fig.7- 8. Simulated air velocity distribution for the section of x=0, y = -1275mm, z=o. It can be observed that the wind speed at the inlet was greater than the lower outlet due to the warmer air heating the external surface of the concrete wall. Furthermore, decreasing air density caused the air within the duct to rise and go into the room through the upper vent of the wall. The air which left the thermal chimney was typically replaced with inner air from the lower vent of the wall.

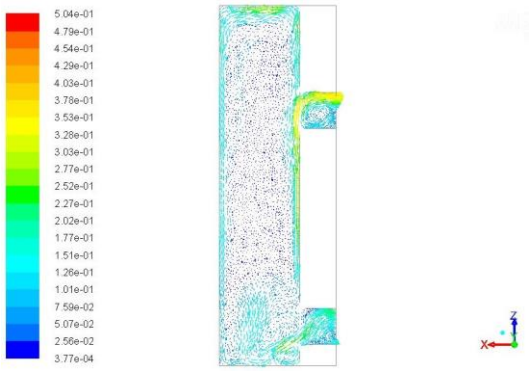

Fig.7- 8. Simulated air velocity distribution for the section of x=0, y = -1275mm, z=o

(2) Simulation results and discussion on Model II

Fig.7- 9 shows the simulated temperature distribution of the section of x=0, y=475mm, z=o, which is located at the center line of the inlet and outlet. It can be observed that along the z-axis direction (from ground to ceiling), the air temperature presented a significant stratification of 4℃ ~ 9℃. At the position nearing to upper vent on the concrete wall, the temperature was higher. Furthermore, the temperature around ground was obviously lower than that nearing the ceiling, showing a remarkable transition at 700 mm high (z=700mm).

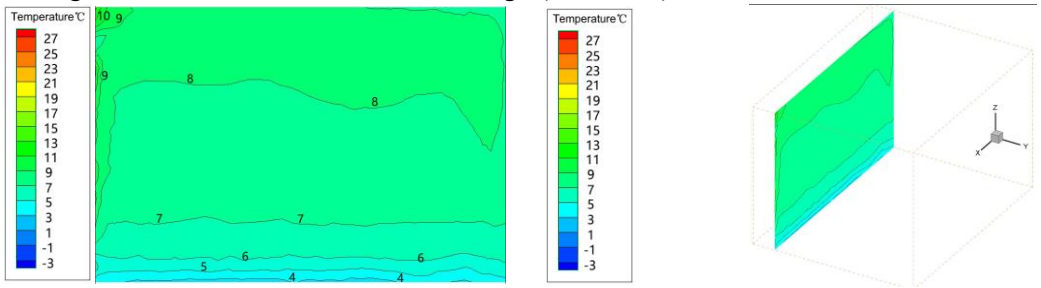

(a) (b)

Fig.7- 9. Simulated temperature distribution for Model II:
(a)/(b) view of the section of x=0, y =475mm, z=o

Fig.7- 10. Simulated temperature distribution for the section of x=0, y = 0, z =1200mm.

Comparing the air temperature profile beside the door and the concrete wall, diverse colors can be observed that the blue color is indicted as lower value and the yellow or red is shown as higher. It can be considered that a non-uniform temperature distribution along the depth of the room is produced by different heat-exchanging ability of the envelope. Thus, the higher temperature areas are mainly concentrated in the middle of the room and around interior wall. The average temperature was about 6.75℃ at 1200 mm high.

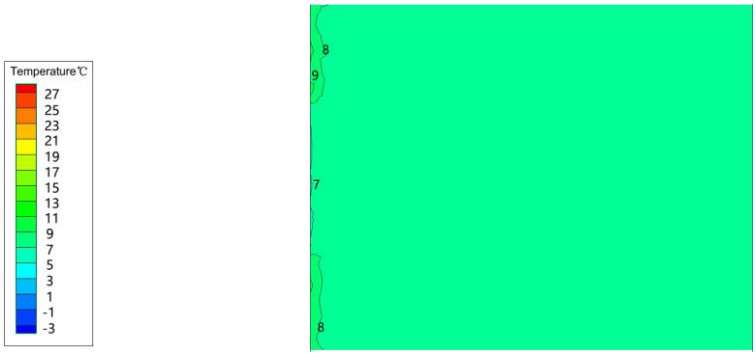

Fig.7- 10. Simulated temperature distribution for the section of x=0, y = 0, z =1200mm

(3) Validation Result

Based on the above simulation results and the measurement data, the measured average temperatures and simulated ones, including the air temperature in the air duct T_a (z = 1200 mm), indoor temperature T_i (z = 1200 mm), the average temperature on the external surface of the concrete wall $\overline{\theta}$, and the inlet temperature T_u, are summarized in Table.7, followed by the corresponding NMBE and CV(RMSE) values.

Table.7-8. Summary of simulated and measured temperatures for model validation.

Time	Air temperature in the duct		External surface temperature of the concrete wall		Inlet temperature		Air temperature in the room	
	Simulated	Measured	Simulated	Measured	Simulated	Measured	Simulated	Measured
	t_a	t_a'	$\overline{\theta}$	$\overline{\theta}'$	t_u	t_u'	t_i	t_i'
14:30	14.1	15.6	21.6	18.1	7.6	9.3	7.5	5.7
NMBE	5.7%							
CV(RMSE)	21.52%							

It can be seen from the above data that the simulated values at the typical positions are higher than the measured data, and the results in the air duct show the opposite situation. In short, the measured values are slightly higher than the simulated values.

The CV(RMSE) is calculated of 21.52%, remaining lower than 25%, which is recommended as the maximum acceptance value of an empirical validation by ASHRAE [7]

7-3 Parameters analysis

Using the newly validated model described in the section 7-2, the performance of the Trombe wall system can be predict under various parameters, for the purpose of enhancing its heating effect responding to the weather conditions of Hangzhou. Effects of each operating parameter was investigated by changing each input variable one by one to determine the sensitivity of the system performance to individual parameters.

the parametric analysis looking into the effects of two operating input variables affecting the heating rate is described. These input parameters were illustrated in Table.7- 1. The running time of 14:30 on 24th January 2016 was taken as the boundary condition, due to the "goodness of fit" between the simulated and measured temperatures, for the sake of predicting the performance of Trombe wall before building it.

7-3-1 Effect of air duct width

Model I and Model II were simulated respectively by only changing the duct width from 0.2m to 0.6m to investigate and analyze the temperature distribution in them, and then to assess the sensitivity of the thermal performance of the Trombe wall heating system to the individual parameter.

In terms of Model I, the section of x=0, y = -1275mm, z=o was still taken as the study object, and of Model II, was the section of x=0, y = 475mm, z=o. The description about the coordination was shown in **错误!未找到引用源。** and **错误!未找到引用源。**.

7-3-1-1 Variation of air temperature in air duct

Fig.7-5 ~ 19 shows air temperatures at typical position in the duct, when the duct width changing from 0.2m to 0.6m. It can be seen that the temperature difference of the bottom-top in the duct are getting less obvious as the width increasing. The external surface temperatures of the wall are becoming higher with the smaller of the width.

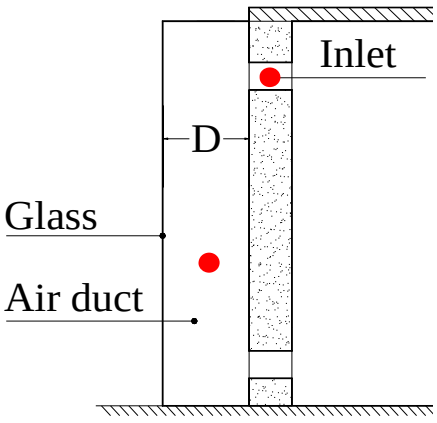

Fig.7-14. Section of air duct

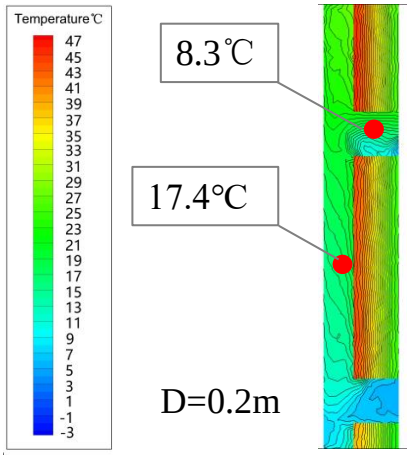

Fig.7-15. Contour of temperature in the duct (D=0.2m)

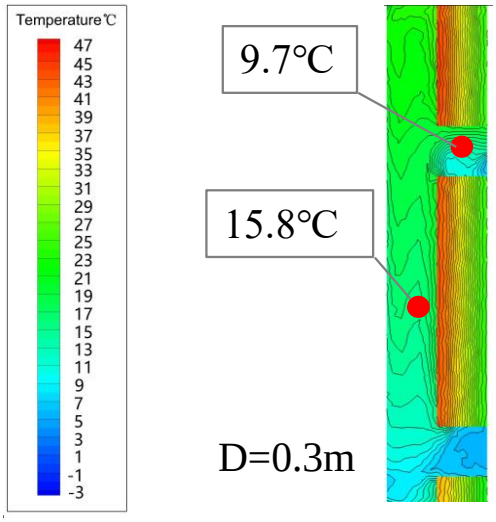

Fig.7- 16. Contour of temperature in the duct (D=0.3m)

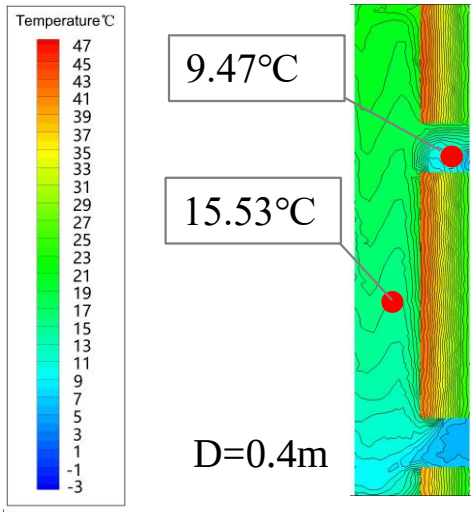

Fig.7- 17. Contour of temperature in the duct (D=0.4m)

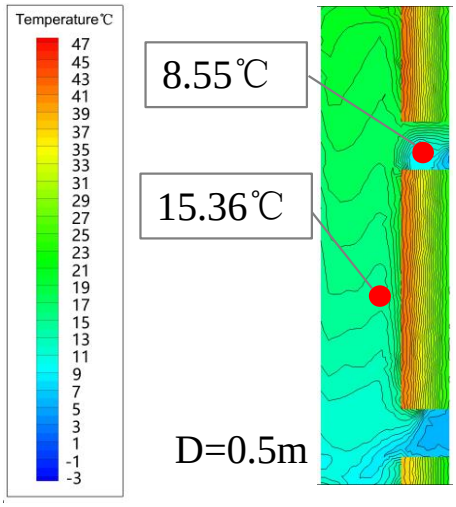

Fig.7- 18. Contour of temperature in the duct (D=0.5m)

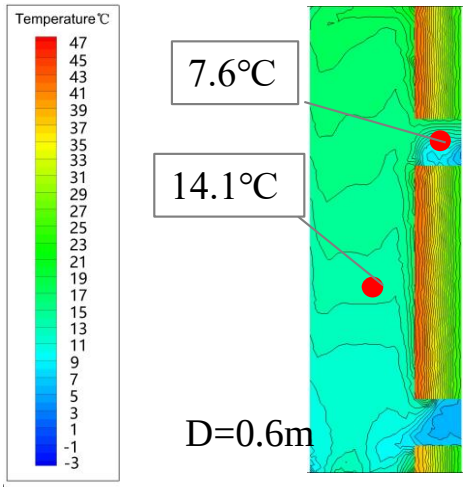

Fig.7- 19. Contour of temperature in the duct (D=0.6m)

In order to study more detailed, the analysis was also performed on seven points in the duct, named Z1 ~ Z7, being along the z-axis (x= 0.5 m, y=-1.275m) at a distance of 0.3m (see Fig.7-).

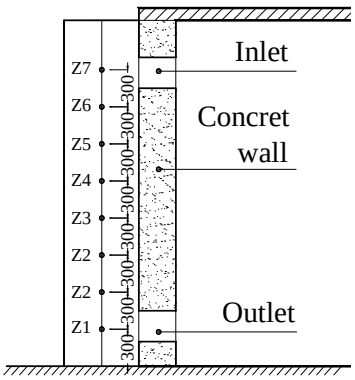

Fig.7-20. Distribution of points located at the z-axis

The simulated results for the seven points are listed in Table.7- and the profile of temperatures

are shown in

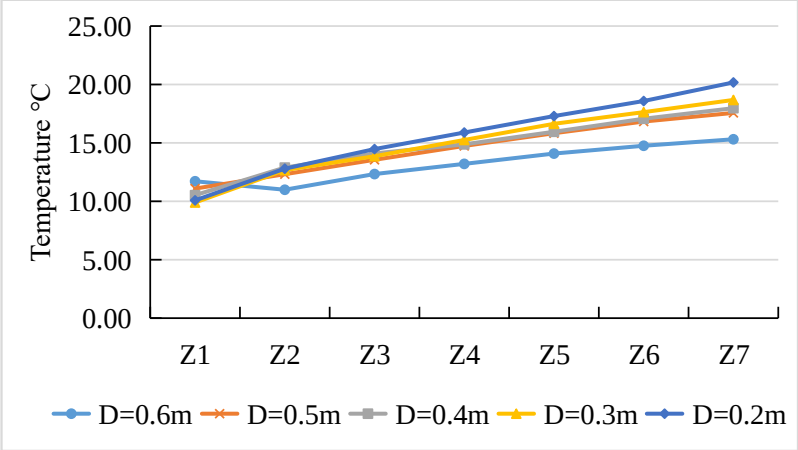

Fig.7- . As illustrated in this figure, the air temperature is obviously increased by the height changing regardless of the width variation, indicating that the warmer air is driven to rise upward by buoyancy effect. It also can be observed that the temperature increasing tendency is more prominent as the width lower. When D=0.6m, the temperature of Z7 is increased by 30.7% relative to the lowest point Z1; when D=0.5m, the percentage is 58.2%; when D=0.2m, the percentage is obtained by 100.1%. Based on the above results, it can be said that thinner duct induce more obvious temperature gradient from bottom to top.

In addition, the variation of temperature at the same height when width changing is also investigated as shown in

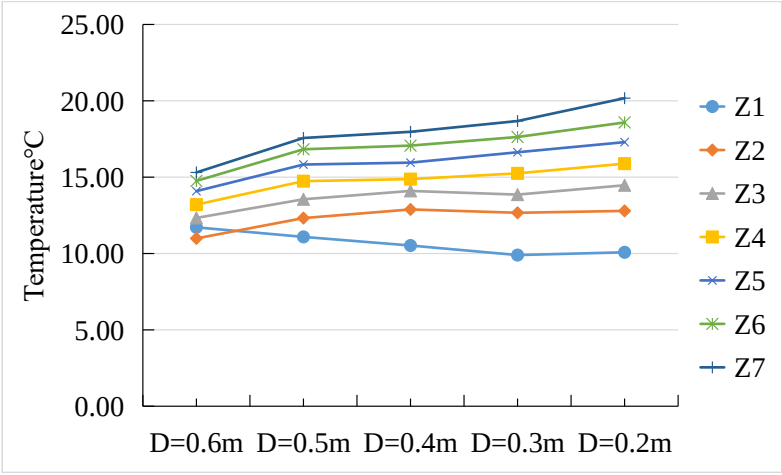

Fig.7- . As the position of the point changes from high to low, the fluctuation of the temperature is less influenced by the variation of the duct width. When the air duct width is reduced from 0.6 m into 0.2 m, the air temperature increased by 31.7% at the highest position of Z7, while declined by 13.9% at the lowest Z1. The point Z7 is closed to the inlet, contributed to enhancing the heating effect. Consistent with the above conclusions, the duct width is smaller, the thermal performance of the Trombe wall is better.

Table.7-9 Simulated results of temperatures at different height.

	D=0.6m	D=0.5m	D=0.4m	D=0.3m	D=0.2m

Z1	11.71	11.09	10.52	9.90	10.08
Z2	10.99	12.32	12.89	12.67	12.79
Z3	12.33	13.55	14.10	13.86	14.47
Z4	13.20	14.74	14.87	15.25	15.89
Z5	14.09	15.83	15.95	16.63	17.29
Z6	14.75	16.83	17.07	17.63	18.58
Z7	15.31	17.57	17.97	18.68	20.17

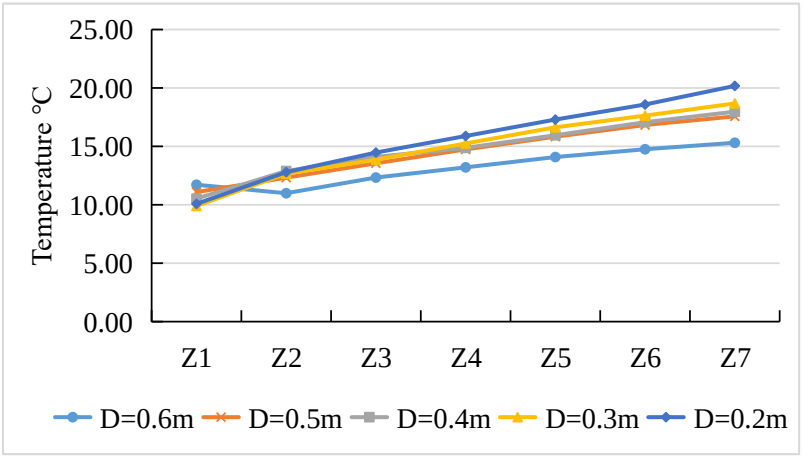

Fig.7- 21. Variation of air temperature at the same width when height changing (Z1~Z7)

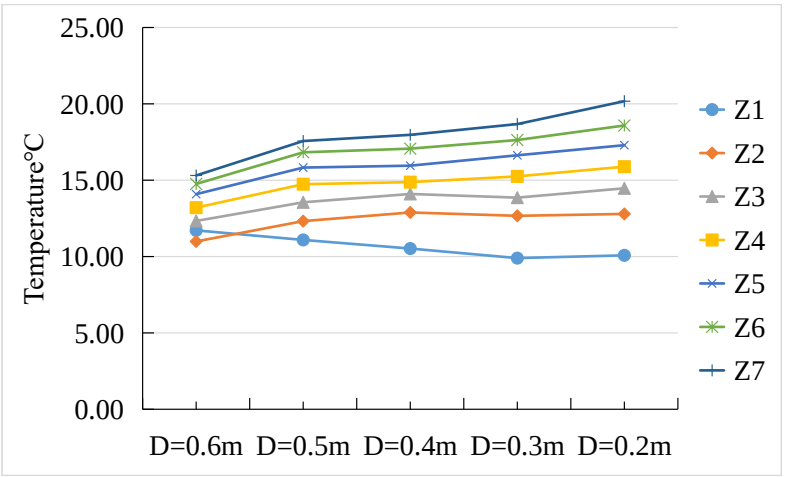

Fig.7- 22. Variation of air temperature at the same height when width changing(Z1~Z7)

7-3-1-2 Variation of temperatures at typical locations

The simulated results for the indicators are listed in Table.7- 1, including the average air temperature in the duct T_a, air temperature at inlet/outlet T_{in} / T_{out}, inner/external surface temperature of the concrete wall θ_{i} / θ_{e}, as well as the indoor temperature T_{i}.

The variation profiles of these values are shown Fig.7- . It can be seen that as the air duct width

increasing, the values of T_a and θ_e present a general decline trend. For the value T_{in}, it obtains an increase by 16.3% since the width changing from 0.2 m to 0.3 m, and then falls off as D value increasing. Accordingly, the valued θ_i shows a similar variation with T_{in}. In terms of T_i, it represents the effect of the heating system, getting its peak value of 7.86℃ at the width of 0.4 m, obtaining an increase by 8.7% relative to the value at the width of 0.2 m. The value of T_{in} and T_i all indicate the level of heating airflow into the room, so the optimum width of the duct can be determined as 0.3 m ~ 0.4 m.

In a word, the thermal performance of the Trombe wall is relative sensitive when the air duct width is small, and wider duct is not conductive to enhancing the heating effect of the Trombe wall system. The optimum size for the duct is better in the range from 0.3 m ~ 0.4 m.

Table.7- 10 Simulated results of temperatures at typical locations.

	T_a	T_i	θ_i	θ_e	T_{in}	T_{out}
D=0.2m	17.4	7.23	22.22	44.76	8.3	5.81
D=0.3m	15.81	7.58	21.93	44.1	9.646	6.16
D=0.4m	15.53	7.86	21.61	43.24	9.47	6.41
D=0.5m	15.36	7.52	21.3	42.44	8.55	6.11
D=0.6m	14.1	7.5	21.6	43.12	7.6	6.12

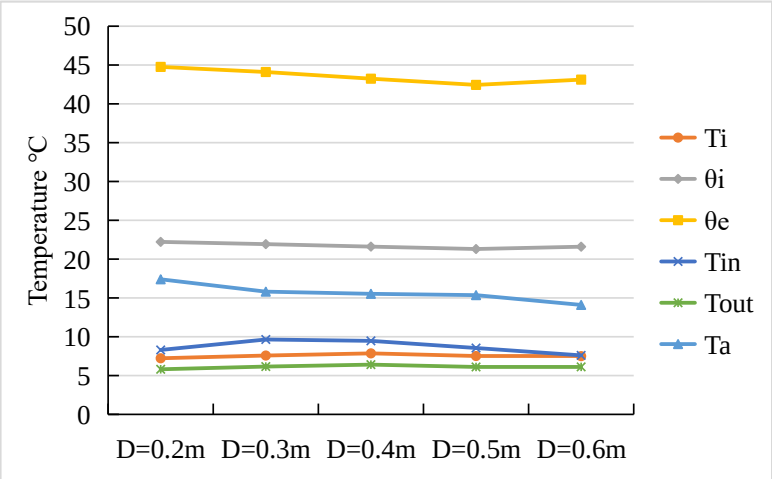

Fig.7- 23. Variation of temperatures at typical locations.

7-3-1-3 Variation of air temperature in the room

When the duct width changing, the temperature layout inside the room is influenced much accordingly. So, it is very necessary to investigate the distribution in the depth direction and height direction on the selected section of the room. In order to study more detailed, the analysis is also performed on the points at three different height and eight different depth in the section studied. The origin of x-axis (x=0) is located at the left corner at the bottom of the room, the z-axis

indicates the height of the room. All the observed points (x=0.5, 1.0, 1.5, 2.0, 2.5, 3.0, 3.5, 4.0, and z=0.325, 1.5, 2.375m) are indicated in Fig.7-4.

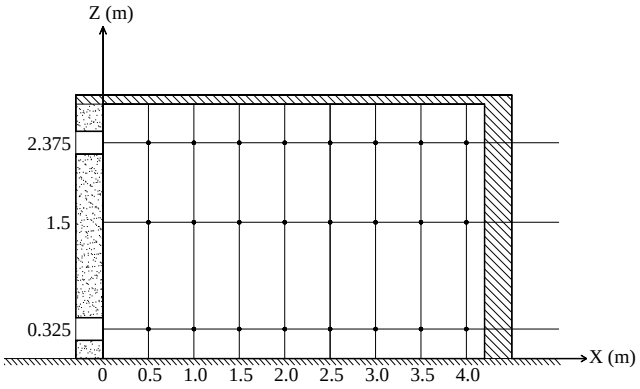

Fig.7-24. Description of the coordination for the points studied.

The simulated results at each point in the room are shown in 错误!未找到引用源。~15, the temperature variation at each width are show in 错误!未找到引用源。5 ~ 错误!未找到引用源。9. It can be seen from these figures, all the temperature values in z-axis direction show an upward trend regardless of the positions along the x-axis, as the air duct width changing. At the position of z=1.5m, the temperature is always close to the value at upper location of z=2.375m, the same height with the inlet, but bigger than the value near the ground of z = 0.325m.

Table.7- 11. Simulated results（℃）
(D=0.2m)

z / x	0.325m	1.5m	2.375m
0.5m	5.97	7.53	8.04
1m	5.67	7.54	8.04
1.5m	5.64	7.54	8.09
2m	5.80	7.55	8.09
2.5m	5.81	7.59	8.04
3m	5.88	7.58	8.03
3.5m	5.87	7.55	7.98
4m	5.79	7.55	7.97

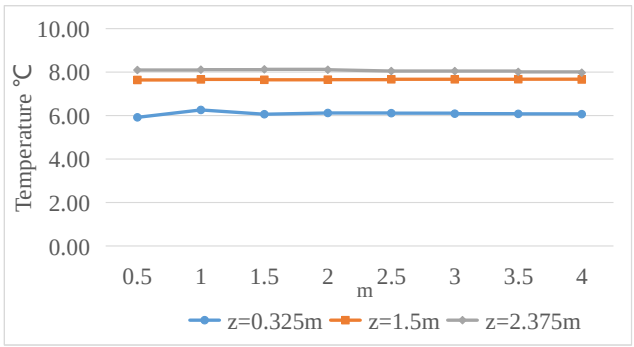

Fig.7- 25. Profiles of air temperature at different points in the room when D=0.2m

Table.7- 12. Simulated results（℃）
(D=0.3m)

z / x	0.325m	1.5m	2.375m
0.5m	5.87	7.83	8.36
1m	6.22	7.88	8.38

1.5m	6.09	47.87	8.42
2m	6.10	7.88	8.41
2.5m	6.16	7.88	8.36
3m	6.15	7.88	8.32
3.5m	6.21	7.89	8.29
4m	6.05	7.89	8.26

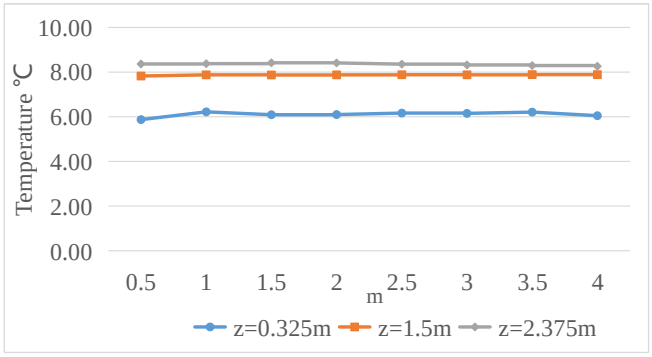

Fig.7- 26. Profiles of air temperature at different points in the room when D=0.3m

Table.7- 13. Simulated results（℃）(D=0.4m)

z / x	0.325m	1.5m	2.375m
0.5m	6.41	8.03	8.56
1m	6.43	8.07	8.58
1.5m	6.36	8.06	8.61
2m	6.40	8.05	8.60
2.5m	6.41	8.08	8.53
3m	6.40	8.07	8.51
3.5m	6.47	8.08	8.49
4m	6.31	8.08	8.43

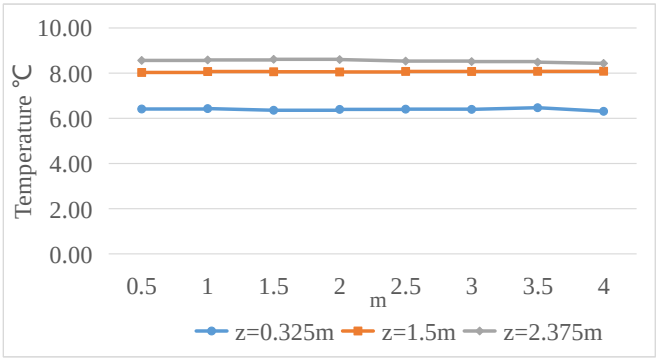

Fig.7- 27. Profiles of air temperature at different points in the room when D=0.4m

Table.7- 14. Simulated results（℃）(D=0.5m)

z / x	0.325m	1.5m	2.375m
0.5m	6.04	7.71	8.21
1m	6.27	7.74	8.22
1.5m	6.16	7.74	8.25
2m	6.10	7.76	8.23
2.5m	6.10	7.76	8.18
3m	6.14	7.75	8.16
3.5m	6.15	7.77	8.13
4m	6.04	7.76	8.09

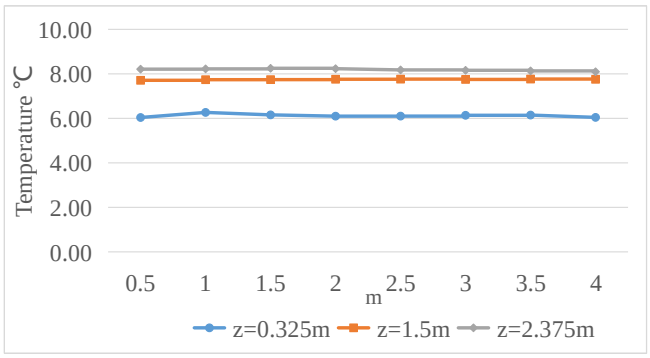

Fig.7- 28. Profiles of air temperature at different points in the room when D=0.5m

Table.7- 17. Simulated results（℃）(D=0.6m)

z / x	0.325m	1.5m	2.375m

0.5m	5.92	7.64	8.10
1m	6.26	7.66	8.11
1.5m	6.06	7.65	8.13
2m	6.12	7.65	8.11
2.5m	6.11	7.67	8.05
3m	6.09	7.67	8.05
3.5m	6.08	7.67	8.01
4m	6.06	7.66	7.97

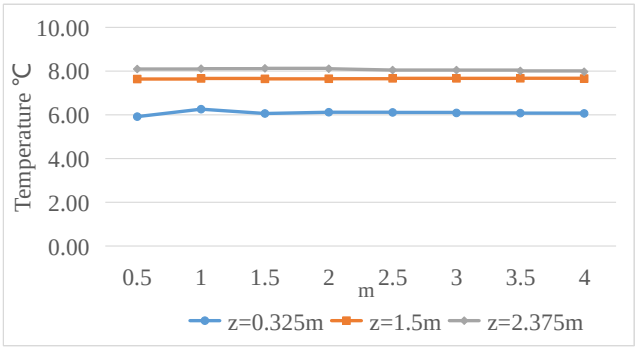

Fig.7- 29. Profiles of air temperature at different points in the room when D=0.6m

In addition, the temperature changing of the points along the x-axis at the position of 1.5m above the ground are also investigated, namely x=0.5m/1.5m/2.5m/3.5m, z=1.5m. The results are shown in Fig.7-30 ~ Fig.7-33. All the figures show that when D value changed from 0.3m to 0.4m, the temperatures would increase obviously.

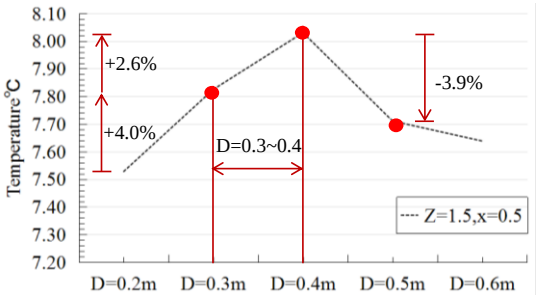

Fig.7-30. Variation of temperatures at x=0.5m, z=1.5m with D value changing.

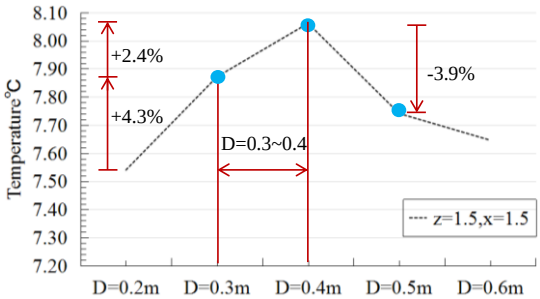

Fig.7-31. Variation of temperatures at x=1.5m, z=1.5m with D value changing.

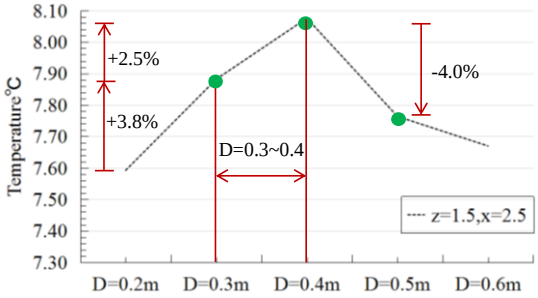

Fig.7-32. Variation of temperatures at x=2.5m, z=1.5m with D value changing.

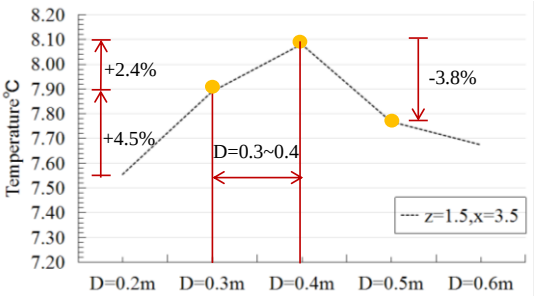

Fig.7-33. Variation of temperatures at x=3.5m, z=1.5m with D value changing.

In a word, the temperatures variation in the room are not so sensitive to the width changing of the air duct, only those of which nearing the concrete wall present a little fluctuation with the size wider and wider, especially at the range of 0.3m~0.4m. To be considered on the room configuration, wider duct is not conductive to heating for those with larger depth.

7-3-2 Effect of wall height

Model I and Model II were simulated respectively by only changing the wall height from 3.0 m to 6.0 m to investigate and analyze on the temperature distribution in them, and then to assess the sensitivity of the thermal performance of the Trombe wall heating system to the individual parameter.

In terms of Model I, the section of x=0, y = -1275mm, z=o was still taken as the study object, and of Model II, was the section of x=0, y = 475mm, z=o. The description about the coordination can be seen in 错误!未找到引用源。 and 错误!未找到引用源。.

7-3-2-1 Variation of air temperature at typical locations in the duct

Fig.7- 5 ~ Fig.7- 8 shows the contour of air temperature in the duct, when the wall height changing from 3.0 m to 6.0 m. The simulated results for the indicators are listed in Table.7-, including the average air temperature in the duct T_a, air temperature at inlet T_{in}, external surface temperature of the concrete wall θ_e. And the variation of temperatures at typical locations are shown in Fig.7- 9.

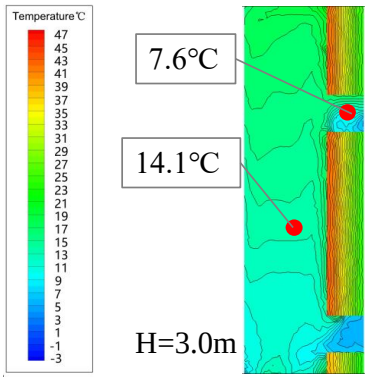

Fig.7- 34. Contour of temperature in the duct (H=3.0m).

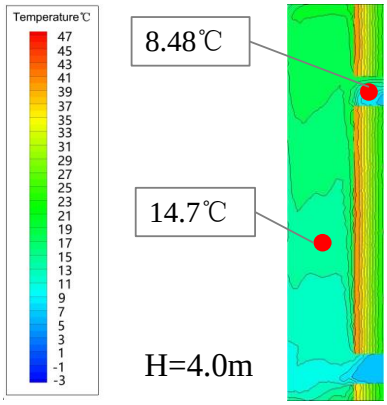

Fig.7- 35. Contour of temperature in the duct (H=4.0m).

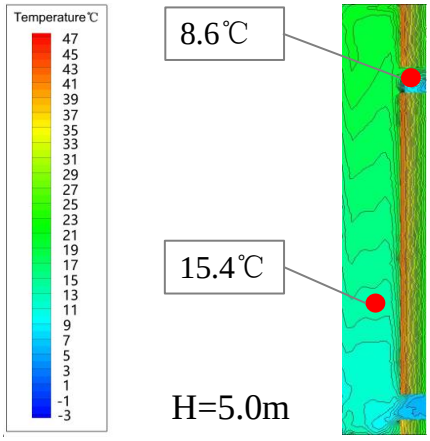

Fig.7- 36. Contour of temperature in the duct (H=5.0m).

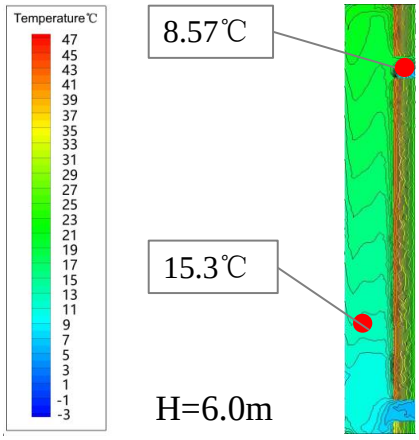

Fig.7- 37. Contour of temperature in the duct (H=6.0m).

It can be seen that as the wall height increasing, the average temperature in duct T_a shows a similar variation with the air temperature of inlet T_{in} when the height changes from 3.0m to 5.0m. For the value of T_a, it obtains an increase by 9.5% from 14.10℃ to 15.44℃, and the value of T_{in} rise up from 7.60 ℃ to 8.60 ℃, showing an increase of 13.15%. But with the height of the wall further increasing, those two indicators begin to decline slightly. In terms of the surface temperature θ_e, it falls off obviously when the wall height was increased from 3.0m to 5.0m, getting a decline by 4.5%. It can be seen from Table.7- 18 and Fig.7- 39, that the air temperature nearing the inlet had an apparent increase with the higher wall in the range of 3.0 m ~ 5.0 m, not obvious when height reached 5.0 m. The optimum size of the height should not be lower than 4.0 m, when the inlet temperature was raised significantly compared to 3.0 m.

Table.7-18. Simulated results as height changing. （℃）

	T_a	θ_e	T_{in}

H=3.0m	14.10	43.12	7.60
H=4.0m	14.73	41.4	8.48
H=5.0m	15.44	41.68	8.60
H=6.0m	15.31	41.48	8.57

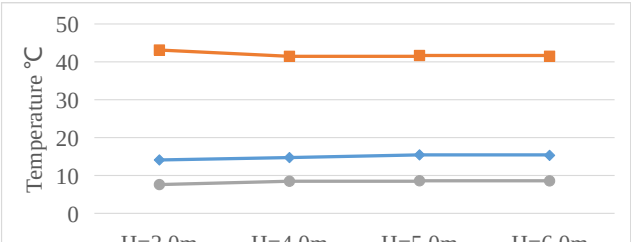

7-3-2-2 Variation of air temperature in the room

When the wall height changing, the temperature layout inside the room was influenced much accordingly. So, it was very necessary to investigate the distribution in the depth direction and height direction on the selected section of the room.

In order to study more detailed, the analysis was also performed on the points at three different height and eight different depth in the section studied. The origin of x-axis (x=0) was located at the left corner at the bottom of the room, the z-axis indicated the height of the room.

Fig.7- 0 shows the observed points (x=0.5, 1.0, 1.5, 2.0, 2.5, 3.0, 3.5, 4.0, and z=0.325, 1.5, 2.375m) when the wall is 3.0m high; Fig.7- 1 shows the observed points (x=0.5, 1.0, 1.5, 2.0, 2.5, 3.0, 3.5, 4.0, and z=0.325, 1.5, 3.575m) when the wall is 4.0m high; Fig.7-2 shows the observed points (x=0.5, 1.0, 1.5, 2.0, 2.5, 3.0, 3.5, 4.0, and z=0.325, 1.5, 4.575m) when the wall is 5.0m high; Fig.7-3 shows the observed points (x=0.5, 1.0, 1.5, 2.0, 2.5, 3.0, 3.5, 4.0, and z=0.325, 1.5, 5.575m) when the wall is 6.0m high.

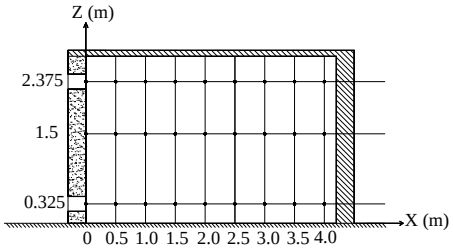

Fig.7- 40. Description of the coordination for the points studied (H=3.0m)

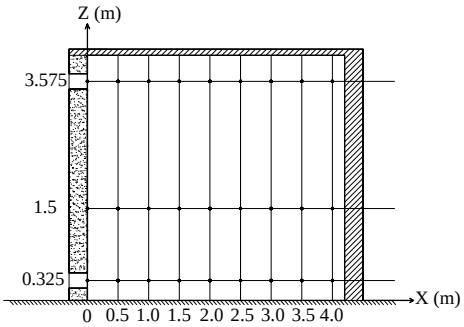

Fig.7- 41. Description of the coordination for the points studied (H=4.0m)

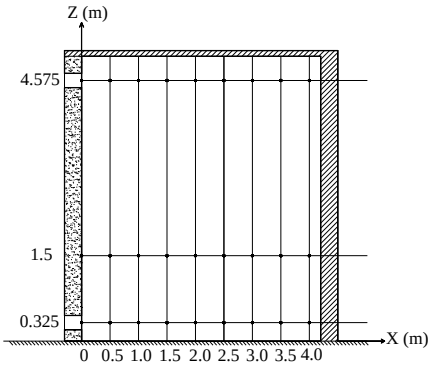

Fig.7-42. Description of the coordination for the points studied (H=5.0m)

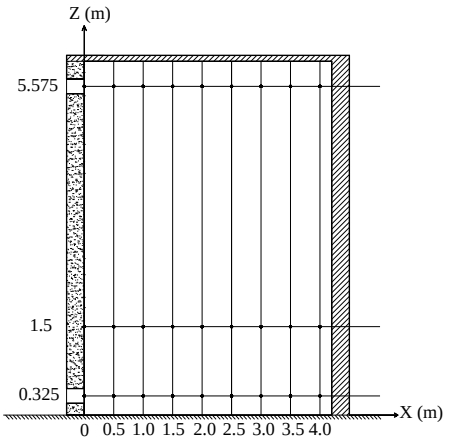

Fig.7-43. Description of the coordination for the points studied (H=6.0m)

The simulated results at each point in the room are shown in Table.7- 2 ~ Table.7- , the temperature variation at each height are show in

Fig.7-4 ~ Fig.7-7. It can be seen from these figures that the overall temperature at each point has an increase as the height of the wall increases. From the simulation results at each wall height, the temperature variation in the Z-axis direction is more significant than in the x-axis direction. At the position of z=1.5m, the temperature is close to the value of the top inlet but bigger than the value near the ground of z=0.325m, as the height of the wall changes from 3.0m to 4.0m. When the wall exceeds 4.0m high, there is almost no difference in the temperature of each point along the x-direction, but the temperature difference between the point (Z = 1.5m) and the highest point of air inlet showing becoming bigger, and showing obvious gradient of high-medium-small from top to bottom.

Table.7- 2. Simulated results（℃）

(H=3.0m)

z / x	0.325m	1.5m	2.375m
0.5m	5.92	7.64	8.10
1m	6.26	7.66	8.11
1.5m	6.06	7.65	8.13
2m	6.12	7.65	8.11
2.5m	6.11	7.67	8.05
3m	6.09	7.67	8.05
3.5m	6.08	7.67	8.01
4m	6.06	7.66	7.97

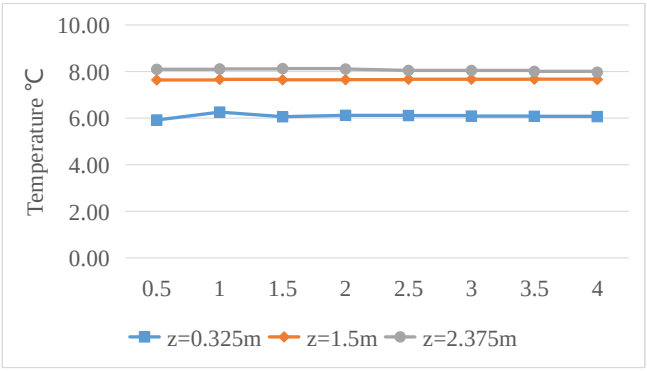

Fig.7-44. Profiles of air temperature at different points in the room when H=3.0m

Table.7- 20. Simulated results（℃）(H=4.0m)

z / x	0.325m	1.5m	3.575m
0.5m	6.44	7.65	8.30
1m	6.49	7.75	8.24
1.5m	6.39	7.74	8.22
2m	6.50	7.74	8.22
2.5m	6.61	7.75	8.22
3m	6.50	7.77	8.21
3.5m	6.53	7.74	8.21
4m	6.65	7.75	8.21

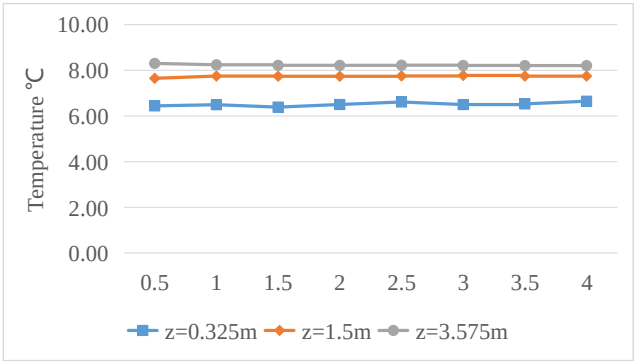

Fig.7-45. Profiles of air temperature at different points in the room when H=4.0m

Table.7- 21. Simulated results（℃）(H=5.0m)

z / x	0.325m	1.5m	4.575m
0.5m	6.41	7.67	8.69
1m	6.53	7.69	8.64
1.5m	6.40	7.70	8.61
2m	6.38	7.69	8.60
2.5m	6.41	7.71	8.60
3m	6.39	7.69	8.59
3.5m	6.42	7.69	8.60
4m	6.46	7.67	8.64

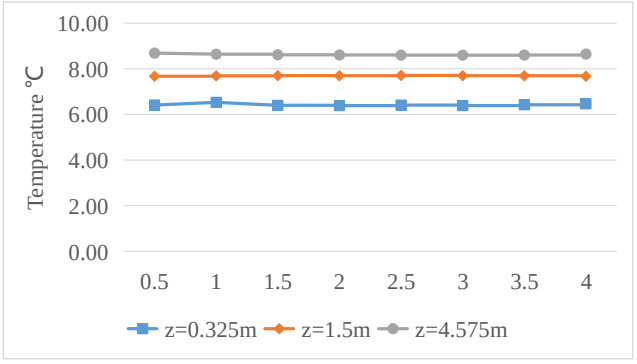

Fig.7-46. Profiles of air temperature at different points in the room when H=5.0m

Table.7- 22. Simulated results（℃）
(H=6.0m)

z / x	0.325m	1.5m	5.575m
0.5m	6.73	7.76	9.14
1m	6.67	7.76	9.11
1.5m	6.59	7.77	9.08
2m	6.61	7.77	9.04
2.5m	6.55	7.78	9.01
3m	6.58	7.76	9.01
3.5m	6.46	7.78	9.04
4m	6.60	7.76	9.06

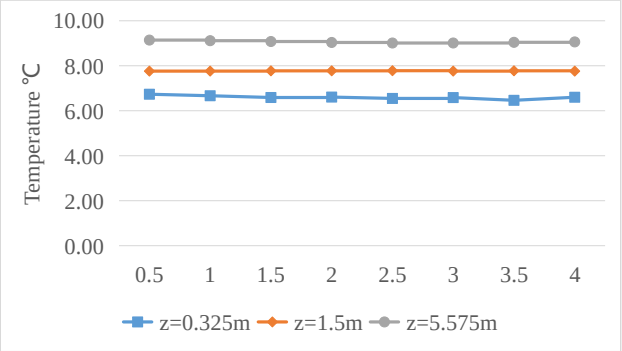

Fig.7-47. Profiles of air temperature at different points in the room when H=6.0m

The air temperature variation of the inlet (z=2.375, 3.575, 4.575, and 5.575m) at each height (H=3.0, 4.0 5.0, and 6.0m) when x-value changing are shown in Fig.7- 8. It can be seen from the figure that, with higher of the wall, the temperatures at the air inlet increase obviously, especially when the height exceeds 4.0m, the temperatures rise significantly. As the height increasing from 3.0m to 6.0m, the changing of these profiles in x-direction can be observed that the temperature at position (x=0.5m) obtains an increase by 12.8% (from 8.1℃~9.14℃) and then fall off to 11.4% at x=2.0m. With the x value increasing, the temperature increase with the wall height changing begins to rise and reaches to 13.6% until x=4.0m. This indicated that the height changing of the wall has an effect on the temperature level both at position near the wall and at a depth of more than 2.0m.

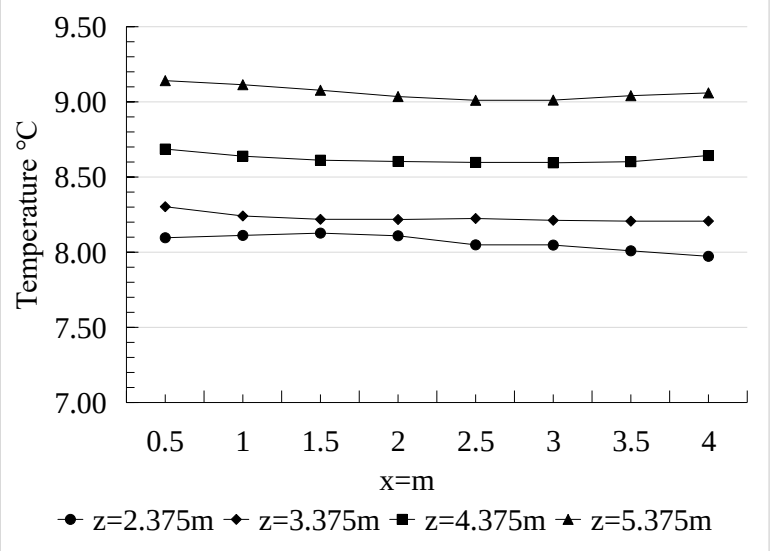

Fig.7- 48. Air temperature variation of the inlet at each height of wall when x-value changing.

At each height of the wall, the temperature difference between the positions of the highest and

the lowest along x-direction are observed in Fig.7- 9. It can be seen that the air temperature difference between inlet and outlet at x=0.5m position suddenly drops to the lowest point when height changing from 3.0m to 4.0m, and then increase when the wall exceeds 4.0m high, where is an inflection point. The temperature difference percentage when H=3.0m is similar with the value when H=6.0m, showing about 36.5%. As seen along the x-axis direction, the higher the wall, the higher the air temperature difference between the inlet and outlet. At the location of x=4.0m, the difference percentage increases in the range of 31% to 37% as the height changing from 3.0m to 6.0m.

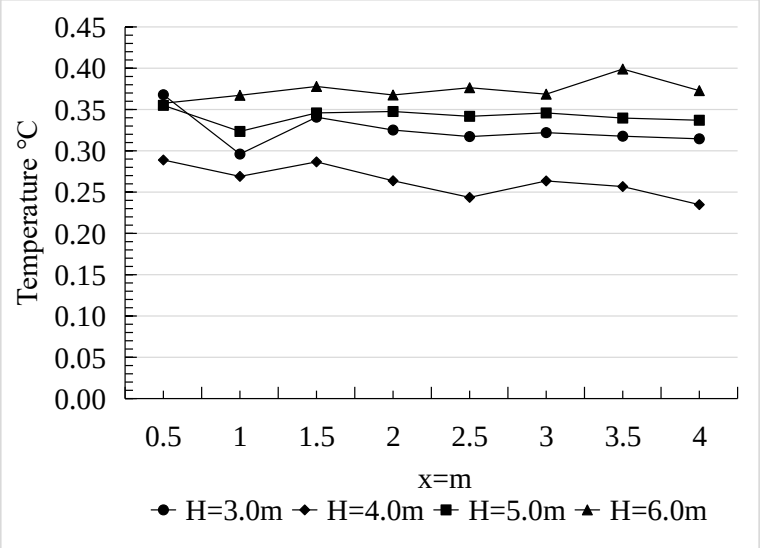

Fig.7- 49. Variation of temperature difference percentage between the inlet and outlet at each height of wall when x-value changing.

7-4 Summaries

In this chapter, CFD models were used to numerically investigate and assess the dynamic thermal behavior of the room with Trombe wall heating system, for the purpose of improving its heating effect in winter under Hangzhou weather conditions.

Firstly, through the statistical method, the hourly simulated temperatures were compared with the measured data during the period from 10:00 ~ 16:00 on 24th January 2016. The validated results indicate that the corresponding values of CV(RMSE) all remain lower than 25%, which is recommended as the maximum acceptance value of an empirical validation by ASHRAE [7].

Secondly, using the newly developed model, the performance of the Trombe wall system were predict under each operating parameter, including the width of the air gap between glass cover and the height of the concrete wall. It could be found that both the parameters of air duct width and the concrete wall height have influence on the thermal performance of Trombe wall, some conclusions and suggestions about the optimum design are as follows:

(1) In the air duct, the inlet temperature (upper vent) and air temperature in the duct were higher with the air duct width smaller. That was to say the thermal performance of the Trombe wall was relatively sensitive when the air duct width was small. In the room, the temperatures along the depth of the room at the points of 1.5m and 2.325m above the ground were obviously increased when air duct width became from 0.2 m to 0.4 m, and with a higher lever in the range of 0.3m ~ 0.4 m, which could be considered as a optimum size of air duct for heating the inside room. So, the air duct width in the range of 0.3m ~ 0.4 m can be considered as a optimum size of air duct for heating the inside room.

(2) In terms of wall height, air temperature in the air duct did not show obvious rise when wall height increasing. In the room, when the wall height exceeds 5.0m, the temperatures near the inlet would have an obvious increase, while have almost no difference with the height below 4.0m. With the wall height increasing, the position of 1.5m above the ground have no change on temperature.

Reference

[1] apsoba M, Moureh J, Flick D. Airflow patterns inside slotted obstacles in a ventilated enclosure. Computers and Fluids 2007;36(5):935–48.

[2] Rohdin P, Moshfegh B. Numerical predictions of indoor climate in large industrial premises. A comparison between different k–e models supported by field measurements. Building and Environment 2007;42(11):3872–82.

[3] K.S. Ong, A mathematical model of a solar chimney, Renewable Energy 28 (2003) 1047–1060.

[4] J. Marti-Herrero, M.R. Heras-Celemin, Dynamic physical model for a solar chimney, Solar Energy 81 (2007) 614–622.

[5] T. Miyazaki, A. Akisawa, T. Kashiwagi, The effects of solar chimneys on thermal load mitigation of office buildings under the Japanese climate, Renewable Energy 31 (2006) 987–1010.

[6] ASHRAE. ASHRAE guideline 14-2002, measurement of energy and demand savings. Atlanta: ASHRAE; 2002.

[7] ASHRAE. ASHRAE handbook of fundamentals. Atlanta: ASHRAE; 2009.

[8] Barbason M, Reiter S. About the choice of turbulence model in building physics simulation. In: 7th international conference on indoor air quality, ventilation and energy conservation in buildings, Syracuse, New York; 2010

[9] Arulanandam S J, Gterry Hollandsk, Brundrett E. A CFD transfer analysis of the transpired solar collector under no-wind conditions[J], Solar Energy, 1999, 67(1-3): 93-100

[10] Nguyen AT, Reiter S. An investigation on thermal performance of a low cost apartment in hot humid climate of Danang. Energy Build 2012; 47:237e46

Chapter Eight: Conclusions

Energy situation and ecological environment has been a crucial issues in China's rural areas. Hangzhou, as a well-developed city, whose commercial energy consumption in rural residence has experienced remarkable increase in these decade, due to the improved household income and numbers of newly built houses. Thus, passive energy efficient technology, was put forward by China's government, as a low-cost and effective way to be promoted in rural residences, for reducing the commercial energy consumption through excellent insulation design and renewable energy usage.

In this thesis, Hangzhou rural area was taken as a case study. By surveying and measuring, the basic construction information in rural area of Hangzhou was learned that there were no more than 10% in Hangzhou rural households to use insulation materials on the walls, and the indoor thermal comfort was not good with no air conditioning in winter time. Under this situation, an experimental building integrated with passive energy efficient technologies was designed and constructed, for providing a sample house in Hangzhou rural area. In order to learn about the real operation effect of passive energy efficient technology, field measurements on this building were developed during winter and summer time. According to the experimental results, the thermal environment and performance of this building were analyzed and evaluated. Next, for improving the passive heating effect, Trombe wall system was further investigated through simulation method on the thermal performance influenced by variable structural parameters.

By this study, the passive design for the sample building was proved effective to defend the extra-low and extra-high temperatures under Hangzhou climate conditions. Thus, such a building can be promoted as a demonstration in rural area of Hangzhou, and the study methods can be used for reference in passive design.

The detailed conclusions and results are summarized as follows:

Chapter1: the energy situation ans environment problems in China's rural area were introduced. The relative concept and field for study also were represented. As a solution, passive energy efficient technology was illustrated. Furthermore, the previous studies about this research were reviewed. Finally, the purpose of this study was explained, as well as the study methods were illustrated, mainly including quantitative study, experimental study and numerical simulation.

Chapter2 :the external environment and resources in hot/summer & cold/winter zone were described, and the feasibility of the application of solar energy was evaluated. In addition, the methods about renewable energy usage including passive solar energy heating and design strategies of nature ventilation were also concluded and summarized.

Chapter3: a survey on the basic construction information and field measurement on thermal environment about rural houses were carried out from 2009 to 2015 in the villages of Hangzhou rural area. It could be found that most of the surveyed rural houses were built in 1980s ~1990s, and modern buildings were usually built after 2000, occupied 33%. Over 60% of the building construction were brick and concrete construction, and the frame construction was not popular.

For the wall materials, over 90% of all had no insulation consideration, and the wall thickness of nearly 50% in all was less than 240mm. For the roof style, over 60% were pitched roof, and over 60% considered with insulation method. The measurement results in a newly built dwelling indicated that the PMV value by calculation showed that it was a little cool during the whole monitoring day in winter time.

Chapter4, an experimental building with passive design strategies was put forward and explained based on Hangzhou Climate. By simulation, the best thick of insulation layer for the wall and roof, as well as the optical U-value for the window were determined. As a result, the annual total energy demand resulted from the design building had a 18.8% reduction compared with the regulated building by the current energy-saving design standard. In addition, by further simulation, the east and west windows were decided to be used with adjustable horizon shutters; the south windows used curtains with thermal-protective coating.

Chapter5, carried out the field measurements on indoor thermal environment in winter time of Hangzhou. It was proved that during the coldest wintertime of Hangzhou, indoor temperature fluctuate slightly with the outdoor temperature changing. When outdoor temperature reached the minimum value, indoor temperatures were at a higher level with maximum difference of 13.5℃. In the sunny and cold day, a maximum air temperature difference between the inlet and outlet on Trombe wall was obtained by 5℃ during the day time.

Chapter6, carried out the field measurements on indoor thermal environment in summer time of Hangzhou. It was proved that the maximum temperature difference between the tested rooms and outdoor can be obtained by 7.6℃ on the hottest day, and the indoor temperature had a smaller fluctuation of 3.3℃. It could be proved that using insulation layers and Trombe wall system can protect building against heat in summer to a certain extent. On the other hand, it had no obvious effect to induce natural ventilation by using the “solar chimney”.

Chapter7, used the validated CFD model of Trombe wall to numerically investigate and assess the dynamic thermal behavior of the room with Trombe wall heating system. By comparing the air temperature distribution in the air duct and room under input variables, it could be concluded that when the air duct width is at the range of 0.3~0.4m, and the wall height at 4.0~ 5.0m, the better thermal performance of Trombe wall can be obtained.

Chapter8, summarized the results in every chapter.